The University of Nottingham

UNITED KINGDOM · CHINA · MALAYSIA

Xu, Tianning (2009) New hybrid cycloconverters: an evaluation of their performance. PhD thesis, University of Nottingham.

New Hybrid Cycloconverters:
An Evaluation of their Performance

Tianning Xu, MSc

Thesis submitted to the University of Nottingham
for the degree of Doctor of Philosophy

Aug, 2009

Abstract

Nowadays, power electronic converters based exclusively on IGBTs seem to have achieved excellent load side performance up to megawatt powers range in the low voltage range (200-690Vrms) and are steadily gaining good performance in the medium voltage range as well. However, the medium and high voltage/high power range remains dominated by converters using naturally commutated thyristors, such as line-commutated cycloconverters, line-commutated current source inverters, which provide comparatively poorer output side performance. The purpose of this thesis is to investigate both the conventional cycloconverter, which will be referred as standard cycloconverter in the thesis, and the new hybrid cycloconverter topologies, which are capable of improving the performance of the standard cycloconverter by adding an auxiliary forced commutated inverter with reduced installed power. It will be shown that the new topology is not only able to improve the quality of the output voltage, but also to enhance the control over the circulating current and therefore, for some of the standard cycloconverter arrangements, to improve the input power quality.

To realize the evaluation of the standard cycloconverter and validate the feasibility of the new hybrid cycloconverter in both circulating current and circulating current-free mode, SABER simulation models are developed in the first place to perform the initial analysis. A configurable three-phase input to three-phase output cycloconverter prototype which can be easily changed via a switch box to test four different cycloconverter topologies (standard and hybrid) is designed and implemented in the laboratory. Finally, the whole system is debugged and tested. All the relevant results obtained from both the simulation and experiment will be thoroughly analyzed in the thesis.

Acknowledgement

谨此感谢我的最亲爱的父母，家人和祖国⋯

Contents

7. Conclusions 224

References 229

Nomenclature 236

Appendix A: Papers Published 242

Appendix B: Derivation of Input Current General Equations 243

Appendix C: Switching States Analysis of the Auxiliary Inverters 245

Appendix D: Circuit Diagrams of the Simulated Standard and Hybrid Cycloconverter Saber Models 249

Appendix E: Theoretical FFT of the Output Voltage and Input Current in Standard Cycloconverter 254

List of Figures

List of Tables

Chapter 1

Introduction

Power electronic converters based exclusively on IGBTs deliver excellent load side performance especially in the low voltage (200 – 690V)/low power range and are steadily gaining performance in the medium voltage range as well. However, the medium (>3kV) and high voltage (>10kV)/high power range remains dominated by converters using naturally commutated thyristors (i.e. line-commutated cycloconverters, current source inverters, load commutated inverters). This is because, compared with IGBTs, MOSFETs or even GTOs, the thyristor device is available in a wide variety of high voltage and current ratings [pp.1, 1], as shown in Fig. 1.1. This figure is a summary of the different types of power semiconductor device capabilities in term of voltage, current and typical switching frequency.
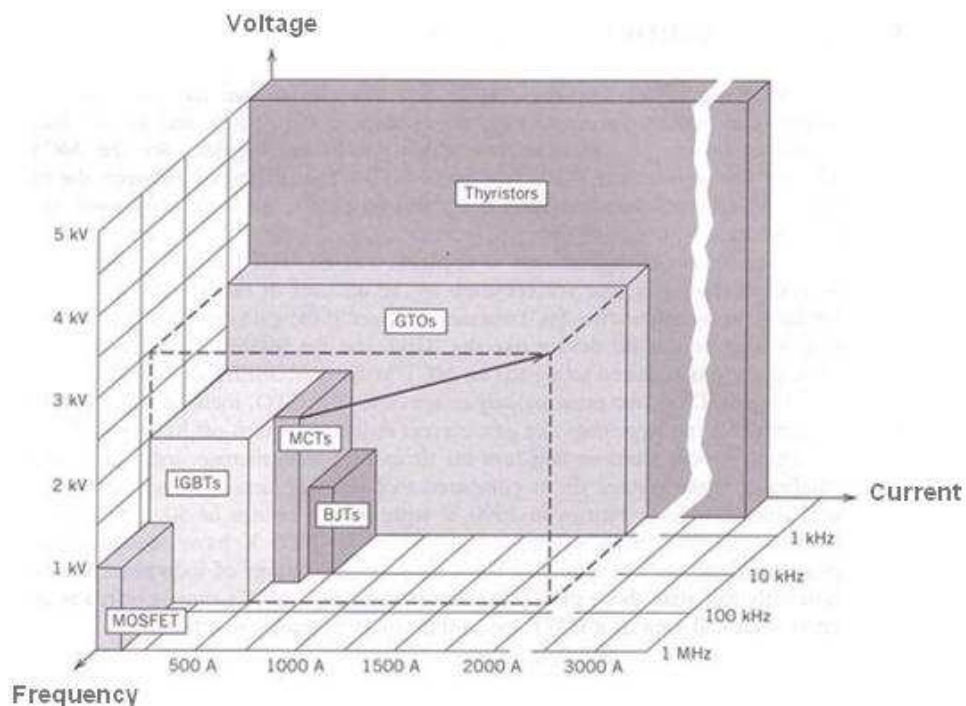
Fig. 1.1: The application range of different power devices ([pp.30, 2], the dashed box indicates the possible expansion of MCT)

At the time of writing this thesis, both the voltage and current rating of the state-of-the-art thyristors have increased to a great extent compared to the summary figure shown above. The blocking voltage is up to 8500V whilst the conducting current is up to 9600A rms. However, the thyristor can only be used in the low frequency switching range as also shown in Fig. 1.1 due to its switching characteristics.

A direct AC-AC power converter, such as a cycloconverter or a matrix converter, is able to generate an AC output voltage at the load frequency from an AC voltage at the supply frequency directly, without any intermediate DC-link [pp.199, 3]. The line-commutated cycloconverter [1, 3, 4-5], which is built using the thyristors mentioned above, is attractive for high power AC motor drives [6-22] and will be the target of this research work. Fig. 1.2 shows a typical topology of a three-phase/3-pulse output cycloconverter topology. Although the cycloconverter can be used at high powers due to the characteristics of the thyristors, it has relatively poor output side performance because of the natural commutation of the thyristors. This means that the frequency of the load side voltage can only be a fraction, typically 1/3, of the supply frequency depending on the number of the pulses in the output voltage waveform [pp.202, 3, 23]. A good synthesis of the output voltage waveform can also be achieved by employing a multiphase supply with a small phase displacement between the voltage phasors [pp.208-228, 1] but increasing the number of pulses and will result in an increased complexity. Moreover, special attention should be paid to the design of the circulating current reactors (CCR) [23] that are used to limit the circulating current between the positive and negative thyristor half bridges if the cycloconverter is operating in circulating current mode. These reactors tend to be bulky for this type of converter since the frequency of the ripple is rather low. However, although the circulating current can be limited by bulky reactors, poor control over the circulating current due to the slow reaction time of the firing angle control can cause additional distortion of the load current and will further degrade the power quality on the input side [24, 25]. Therefore, the circulating current mode is not often recommended although [26] has proposed to use a controlled circulating current together with input capacitors to improve the input power factor.
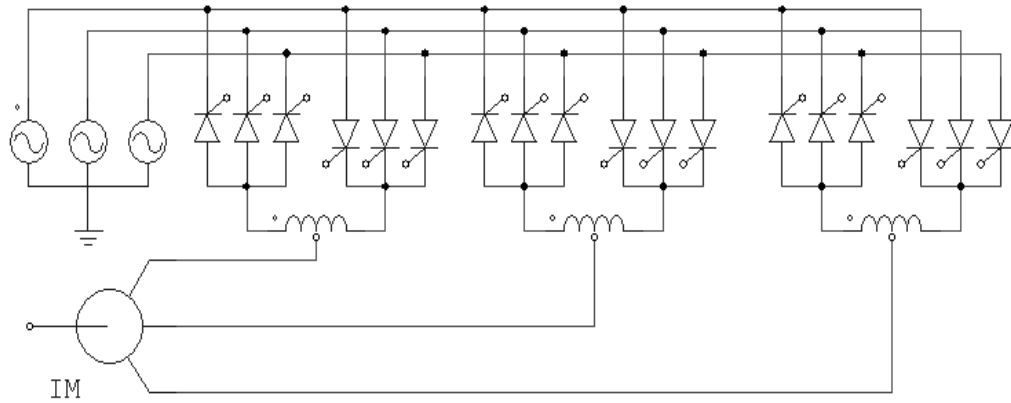
Fig. 1.2: Topology of a standard 3-pulse cycloconverter

1.1 Project Objectives

All of the existing solutions proposed in the past to mitigate the problems related to poor output and input performance of the cycloconverter are exclusively based on the use of passive components, such as phase shift transformers and circulating current reactors. However, they are both very bulky, not to mention the number of power semiconductors required that increases if the number of pulses are increased. However, the cycloconverter is still used in very high power range (>10MW) drives, where there is no other type of semiconductor switch available. Therefore, this project aims to investigate alternative methods based on auxiliary power electronics (hybrid) to improve the electrical performance of the cycloconverter whilst minimizing the size and the added cost of the converter. In this thesis, the category of conventional cycloconverters will be referred to as standard cycloconverters. The proposed new topologies will be referred to as hybrid cycloconverters. For these hybrid cycloconverters, the following objectives are addressed in this project.

First of all, the quality of the output voltage in hybrid cycloconverters has to be improved in comparison with the standard cycloconverter. The better the output voltage waveform is, the smaller the disturbance will be fed to the load. Secondly, the size of circulating current reactors has to be reduced by controlling the circulating current with good accuracy in hybrid cycloconverters. The input power quality can also be improved on the basis of improvement of the above two aspects. Finally, the power switches added in the hybrid cycloconverters should handle a fraction of the voltage rating of the thyristors for small added cost. The overall objective is to

demonstrate that the new hybrid topologies can be superior compared with previous method of increasing the number of pulses to improve the performance of the cycloconverter.

For the project as a whole, a number of evaluations and comparisons will be made between not only standard and hybrid topologies, but also considering the two operating modes, circulating current mode (CCM) and circulating current-free mode (CCFM), to give a comprehensive evaluation with regard to the performance and cost of all types of cycloconverters.

1.2   Thesis Structure Overview

This thesis is divided into 7 chapters.

Chapter 1 gives a brief introduction to the project and its objectives.

Chapter 2 reviews the conventional cycloconverter technology. The main application of the cycloconverter is reviewed at first. Then the basic principle of cycloconverter operation will be introduced and the two operating modes of the cycloconverter, circulating current mode [pp.151, 1, 23] and circulating current-free mode [pp.151, 1, 27], will be explained. The important issues related to the operation of cycloconverters will also be discussed, i.e. circuit types, firing pulse control methods, problems and existing approaches associate with standard cycloconverter, harmonic analysis of input and output side. The material presented in Chapter 2 serves as the basis upon which the hybrid cycloconverter has been developed and the baseline upon which the hybrid cycloconverter should improve.

Chapter 3 introduces the hybrid cycloconverter concept in detail. Similar to the standard cycloconverter, the hybrid topologies also have two operating modes, circulating current mode and circulating current-free mode. The hybrid cycloconverter concept is then demonstrated in three different aspects: topology variant, control, and the switching states for the auxiliary inverter for different situations. From the illustration and demonstration, a foundation is provided for realizing the hybrid

cycloconverter in simulation model and prototype implementation.

In Chapter 4, the implementation of simulation models of both standard cycloconverters and hybrid cycloconverters will be described. SABER is used to initially verify the expected benefits of the hybrid cycloconverter. Simulation studies of standard and hybrid cycloconverters in two operating modes are described. Both the three-phase input to single-phase output structure and the three-phase to three-phase structure are evaluated using simulations. Based on the simulation results, a comprehensive comparison of the different topologies, standard and hybrid operating in both modes and using different pulse numbers, are presented in terms of converter performance, cost and complexity. This allows both the advantages and disadvantages of the different circuits to be evaluated.

Following the simulation study, the hybrid cycloconverter was implemented as a laboratory prototype. Chapter 5 describes the process of designing and building of the prototype. A description of the design and assembly of the different power circuits is given followed by a discussion of the control strategy implemention using the standard PEMC (Power Electronics, Machines and Control Group) research group control platform.

In Chapter 6 full scale experimental results of the two standard and two hybrid topologies are presented. Consistency with the simulation results will be demonstrated through the practical verification of the proposed solution. Although it will be seen that slight differences between the practical results and simulation results exist due to the impact of some practical factors, the results presented in this chapter strongly demonstrate the clear improvement in quality achieved by the hybrid cycloconverter topologies.

The conclusions drawn from this project and the further work identified by the author with respect to this research area are presented in Chapter 7.

Chapter 2

Review of the Cycloconverter Technology

2.1   Introduction

A phase-controlled thyristor converter is able to provide continuously variable DC voltage of both positive and negative polarity at its output terminals. Due to the unidirectional current carrying capability of thyristors, the output current can flow in only one direction which means a single bridge can only operate in two-quadrants of the V-I plane.

The dual-converter is a topology which is able to operate within all quadrants of the V-I plane. This is realized by connecting two phase-controlled bridges in anti-parallel, providing a bidirectional path for the current at their DC terminals [pp.111, 1]. Thus the dual-converter is capable of operating with both polarities of output voltage and current

By controlling the phase of the firing pulses for the thyristors, with respect to the input AC supply voltage, the dual converter is able to produce different mean output voltages of desired polarity. A cycloconverter is realized by modulating the converter firing angles at a specific frequency to produce a continuously varying output voltage (AC). By controlling the frequency and depth of phase modulation of the firing angles, it is possible to control the frequency and amplitude of the main fundamental component of output voltage [pp.145, 1]. Thus the cycloconverter, which is illustrated in a simplified diagram in Fig. 2.1, is not only a "Four-Quadrant" converter but can also provide continuous AC output voltage with adjustable frequency.
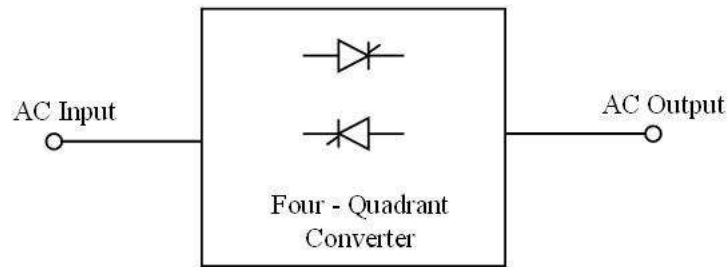
Fig. 2.1: A simplified diagram of a "Four-Quadrant" converter used as a cycloconverter

2.2   Applications of Thyristor Cycloconverters

Due to the power capability of the devices and the upper frequency limitation of the output, it is possible to use the thyristor line-commutated cycloconverters to control low speed but very large horsepower motors. There are presently two main applications for the cycloconverter [pp. 18, 1]. In first application area, the cycloconverter is used as a variable frequency variable speed drives for AC machines. The input of the cycloconverter is connected to a power supply with fixed frequency and the machine to be driven is connected to the output of the cycloconverter. In the second application area, in contrast, the cycloconverter is used to provide constant frequency power output from a variable frequency power source.

2.2.1 Variable Speed AC Machine Drives

The AC machines have found wide application in variable speed drives. Compared with DC machines, the AC machines does not require commutator and as a result it is generally less expensive and much less in need of maintenance. However, unlike the DC machine, where the speed is controlled by adjusting the voltage, the speed of the AC machines is a function of the applied frequency. Various means to control the speed of the AC motors by connecting to a constant frequency power supply has been devised. However, they are not generally applicable to a drive which is required to provide a high performance over a wide range of load and speed. Therefore, a power supply with the capability of accurately controlling both the frequency and the amplitude of the voltage is demanded in order to provide an efficient variable speed drive.

With a fixed frequency supply, the torque may become inevitably much less than the pullout torque (maximum torque the machine is able to provide). This is because under some specific situations, for example, when the rotor is standstill, the slip frequency (the absolute difference between the appied stator frequency and the output rator frequency) is much greater than the pullout slip frequency (the frequency where the maximum torque is produced by the machine). This could result in the induction machine operating at the negative slope of the torque/slip characteristic curve. Therefore, the applied frequency for the machine has to be controlled so as to always keep the slip frequency less than (or equal to) the pullout slip frequency. Furthermore, a constant flux is always required to control the AC machines in a manner which is similar to the control of a separately excited DC machines. In practice, it is necessary to adjust the applied voltage in order to offset the voltage drop across the impedance of the stator winding, especially when the operating frequeny is low. As has been mentioned, the cycloconverter is able to control both the output frequency and voltage, independently of one another. Moreover, the cycloconverter can be used to operate with load of any power factor, including regenerative loads, since it is a "Four-Quadrant" converter. Therefore, the cycloconverter is ideally suited to be an efficient variable speed control of AC machines. A cycloconverter-fed adjustable speed drive system now is well established and finds application with induction/synchronous motors of large power rating, such as steel rolling mills, gearless cement mills, pumps and compressors, mine winders and ship drives [28].

A basic diagram of a variable frequency speed control for an induction motor with the cycloconverter is shown in Fig. 2.2. As can be seen from the diagram, the cycloconverter is used to provide three-phase variable frequency output power from a fixed frequency three-phase input. Here, the cycloconverter can be regarded as an amplifier. Therefore, the output frequency and voltage of the cycloconverter is proportional to the frequency and the amplitude of the three-phase analog sine wave reference voltages, obtained from the reference voltage generator. The slip frequency measuring circuit is able to generate a DC analog signal proportional to the slip frequency. The threshold of the "excess slip" amplifier is set at a value which is less than or equal to the pullout slip frequency. During the steady state, the output of the "excess slip" amplifer is zero. However, if the slip frequency exceeds the preset threshold in the amplifier, for example, a sudden change of the load, the amplifier will

produce a corresponding sharply increasing or decreasing output signal. Since the absolute value of the signal generated by the amplifer is much higher than the frequency reference, the system can operate with a constant slip frequency which is always smaller than (or equal to) the pullout slip frequency. Therefore, the system shown in Fig. 2.2 can ensure that the machine operates on the most favorable positive slop portion of its torque-slip characteristics all the time [pp. 25, 1].
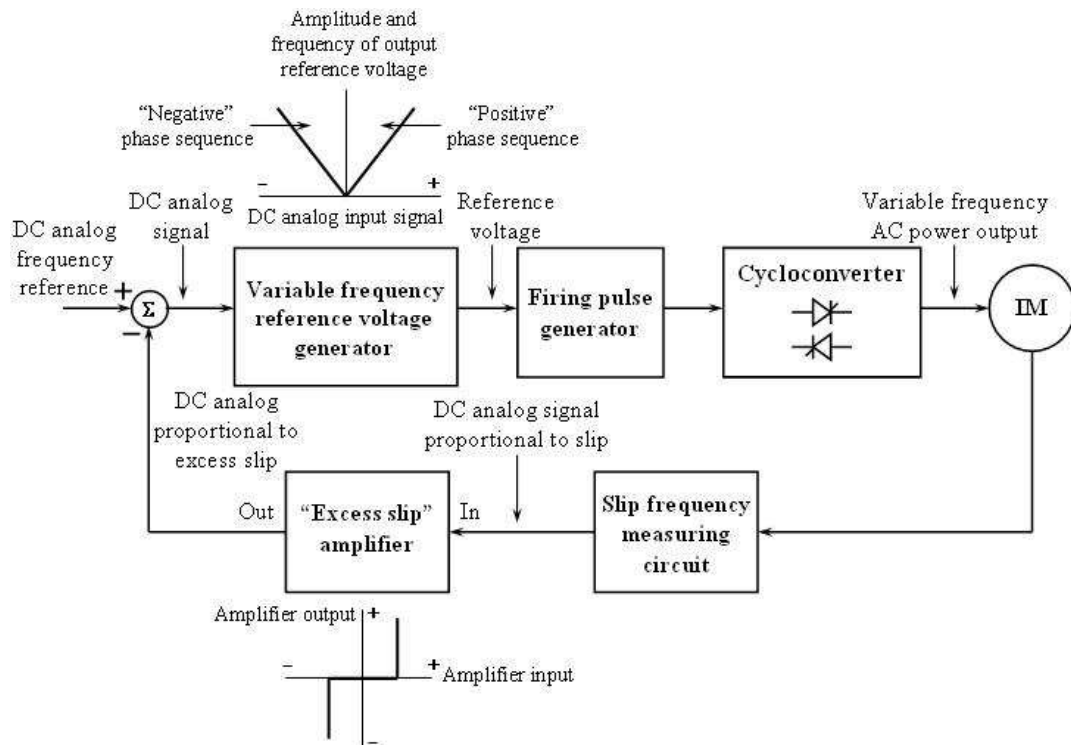
Fig. 2.2: The diagram of a variable frequency speed control with cycloconverter

2.2.2 Constant Frequency Power Supplies

There are several applications which require the production of an accurately regulated fixed frequency power output from a variable frequency power source. One typical application in this area is aircraft power conversion, where the source of electrical power is an alternator. As the machnanical power input for the alternator is the engine of the aircraft and the speed of the engine is not constant, the alternator is not able to produce a constant frequency power output. Although in practice a hydraulic constant speed coupling device [pp. 25, 1] can be inserted between the engine and the alternator to provide a constant speed to the alternator, such a system needs frequently and costly maintenance.

The ruggedness and low weight of the solid-state cycloconverter makes it attractive for aircraft electrical systems [3]. As can be seen from Fig. 2.3, the diagram of a variable speed constant frequency (VSCF) system, the alternator is connected directly to the aircraft engine and the cycloconverter is used to convert the variable frequency power to appropriately regulated constant frequency power output. The advantage of such a system over the hydraulic constant speed drive is that it requires much less maintenance and the electrical performance is generally superior [pp. 26, 1]. For example, the speed response of VSCF with cycloconverter is instantaneous and it is possible to provide a phase balance control between outputs.
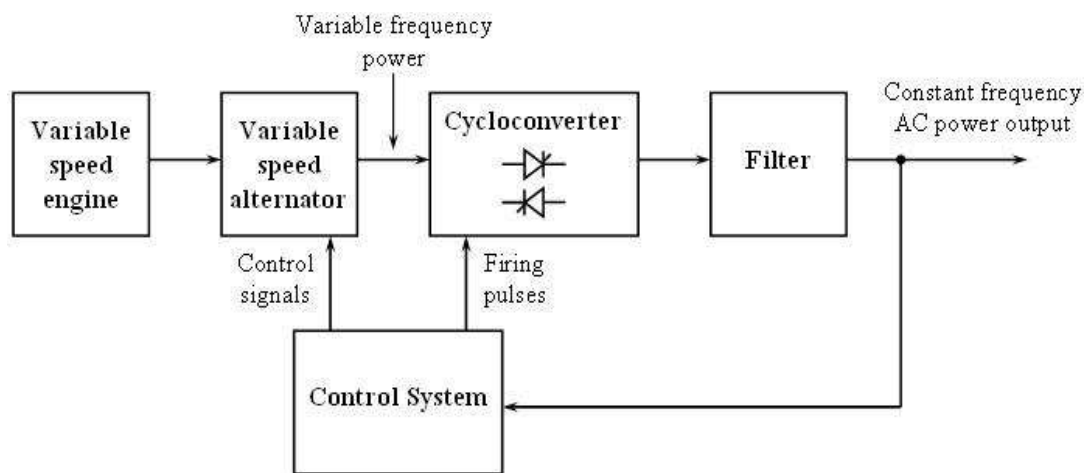
Fig. 2.3: The diagram of a variable speed constant frequency (VSCF) system using cycloconverter

2.3 The Operation of the Cycloconverter

In this section, the principle of the cycloconverter will be explained and then the two operating modes of the cycloconverter, namely circulating current mode (CCM) and circulating current-free mode (CCFM), will be illustrated.

2.3.1 The Basic Principle of the Cycloconverter

The line-commutated cycloconverter consists of a number of phase-controlled converter circuits connected to a poly-phase AC supply system that provides the voltages necessary for natural commutation. The individual circuits are controlled so

that a low-frequency output voltage waveform is fabricated from segments of the polyphase input voltages.

Consider a 3-pulse cycloconverter, supplying an inductive load which maintains continuous current flow, and, for simplicity, neglect thyristor on-state voltage and commutation overlap. With these simplifications, the output voltage V_{out} controlled by adjusting the firing angle (α) is [pp.147, 1]:

$$V_{out} = V_{max} \cdot \cos(\alpha) \qquad\qquad V_{max} = 3\sqrt{3}/2\pi \cdot V_{N\_pk} \qquad\qquad (2.1)$$

where α is the firing angle, or delay angle, and V_{max} is the average output voltage with zero firing delay, V_{N_pk} is the peak value of the input phase-to-supply neutral voltage. The ability to control the output voltage by delaying the turn on of the incoming device is the basis on which the naturally commutated, phase-controlled cycloconverter operates. If the firing angle is kept constant, the output is a DC voltage. Whereas if the angle is modulated according to Equation (2.2), the cyclcoconverter will generate a sinusoidal output voltage of adjustable frequency and amplitude:

$$\alpha = \cos^{-1}[V_{o\_ref\_pk}/V_{max} \cdot \sin(2\pi \cdot f_{out} \cdot t)] \qquad\qquad (2.2)$$

Where $V_{o\_ref\_pk}$ is the peak value of the output reference voltage and f_{out} is the output frequency.

Fig. 2.4 shows the block diagram of a three-phase input to single-phase output cycloconverter (L_{cir1} and L_{cir2} are bypassed if the cycloconverter operates in circulating current-free mode). The reference signal V_{o_ref} is a sinusoidal waveform of a lower frequency than that of the supply voltage. The frequency of the fundamental component in the output voltage will be the same as that of the reference signal. Moreover, the average output voltage over a switching period is also proportional to the instantaneous value of the reference signal. Hence, as shown in Equation (2.1) and (2.2), both the amplitude and frequency of the output voltage can be controlled by the firing angle by varying the amplitude and frequency of the reference signal.
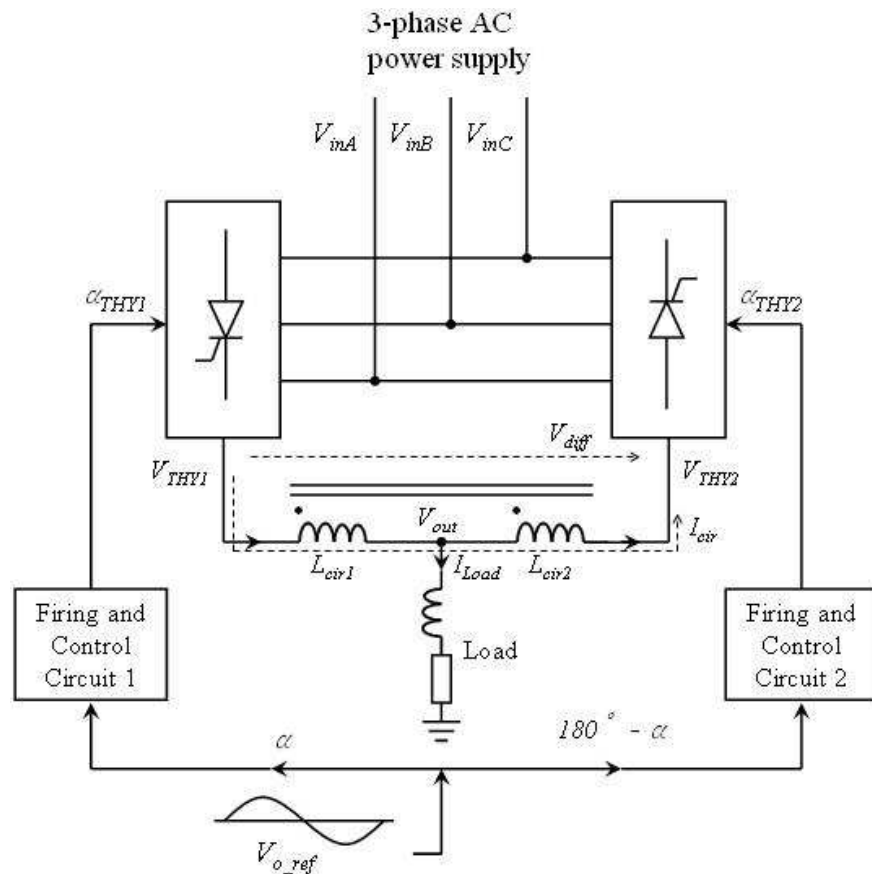
Fig. 2.4: Block diagram of controlling three/single phase cycloconverter

If the firing angle is varied from zero to 180 degrees and back again to zero, one complete cycle of the low-frequency variation can be superimposed on the average output voltage. The superimposed frequency is determined solely by the rate of variation of α and is independent of the supply frequency. Each thyristor opens and closes at suitable instants, so that a low-frequency output wave shape (V_{THYI}) is fabricated from segments of the input waveform as shown in Fig. 2.5(a). Fig. 2.5(b) shows a part of the enlarged output voltage waveform by indicating the firing delay angle for each commutation instant when the voltage is changing from positive to negative. It can be seen from the Fig. 2.5(c) which is the spectrum of V_{THYI}, the output voltage of a thyristor half bridge contains a large amount of low frequency harmonics, which is a result of the basic operation of the cycloconverter. Since the harmonic frequency is a function of both the input and output frequency [pp.306, 1], the output voltage may also contain subharmonics, the frequency of which is less than the wanted output frequency. The harmonic content of the output voltage waveform decreases as the ratio of output to input frequency is reduced and as the number of supply phases is increased.
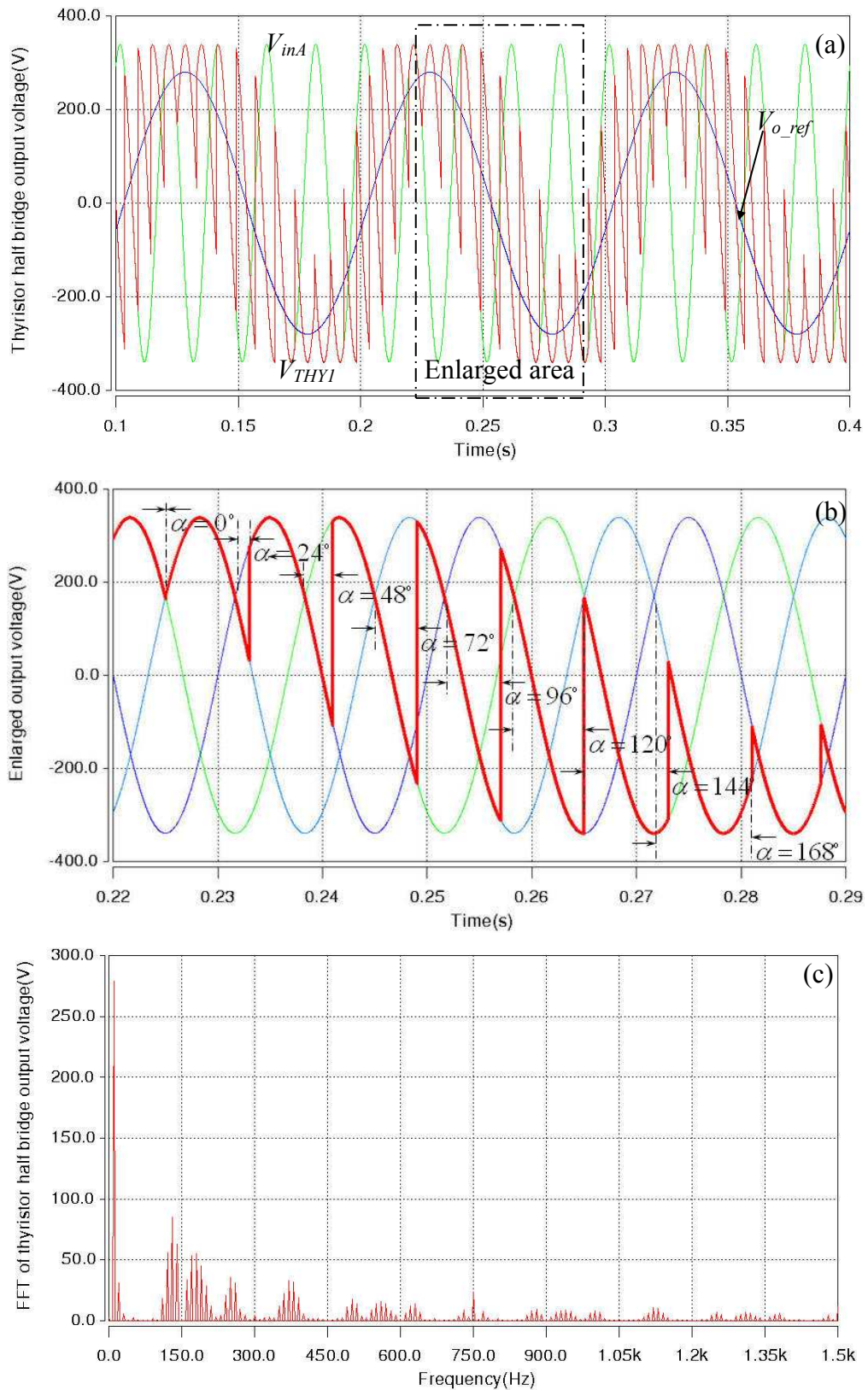
Fig. 2.5: a) The voltage waveform of thyristor half bridge for a 3-pulse cycloconverter

b) The enlarged voltage waveform indicating the firing delay angles

c) Spectrum of the voltage of thyristor half bridge for a 3-pulse cycloconverter

The harmonics or subharmonics present in the output voltage are detrimental to the load which is normally induction/synchronous motors. The equivalent circuit of an induction motor is shown in Fig. 2.6 (all the symbols are defined in Nomenclature), where the speed of rotor is assumed to be the same as the synchronous speed. With more harmonics present in the output voltage (V_s), more harmonic currents (I_h) will be injected into the load. If the magnetizing inductance (L_o) is neglected, the harmonic currents can be reduced by increasing the frequencies (s_h) of the harmonics as the leakage inductances (L_s and L_r) become dominative over the resistances (R_s and R_r). The flux produced by the harmonic components can rotate at a different speed or even different directions compared to that of rotor depending on the harmonic frequency. Therefore, the presense of the harmonics in the stator excitation may result in pulsating-torque components, which can cause troublesome speed fluctuations and shaft fatigue especially when they are at low frequencies [pp.417, 2]. Additionally, the harmonic current can lead to more copper loss of both the stator and rotor windings, which will consequently generate more heat in the motor.
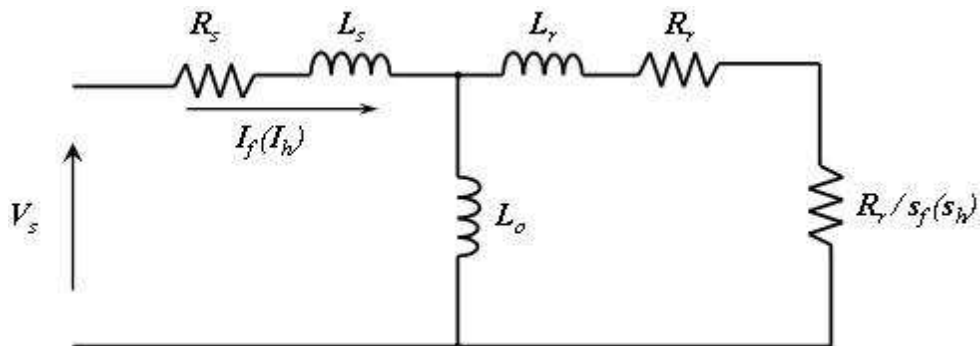
Fig. 2.6: The equivalent circuit of the induction machines

As the load current can only flow in one direction through one half bridge, and, in order to produce a complete cycle of low-frequency output current, two similar half bridges must be connected in inverse parallel so that the average out put voltages of the two half bridges is identical. Hence the output voltage of the cycloconverter can also be thought of as a common mode voltage as it is the common part between the potentials of two thyristor half bridges. The positive thyristor half bridge permits current flow during the positive half-cycle of the low-frequency output, while the negative half bridge allows current flow during the negative half-cycle. The simplest arrangement uses two three-phase half-wave circuits for a single-phase output. When

a three-phase output is required, three single-phase cycloconverters with a phase displacement of 120° between their outputs need to be used. However, although the average output voltages of two half bridges are the same, the instantaneous output voltages are different, which will result in large harmonic currents circulating between the two thyristor half bridges. The difference between the potentials of two thyristor half bridges is the differential mode voltage, as shown in Fig. 2.7(a), and its spectrum as shown in Fig. 2.7(b) shows that the differential mode voltage contains a significant amount of low frequency harmonics. The current circulating between the two half bridges is called the circulating current which is really detrimental to the input power factor of the cycloconverter [pp.208, 3]. In this situation, circulating current inductors can be employed between the two thyristor half bridges to limit the circulating current, but these inductors can be very bulky.
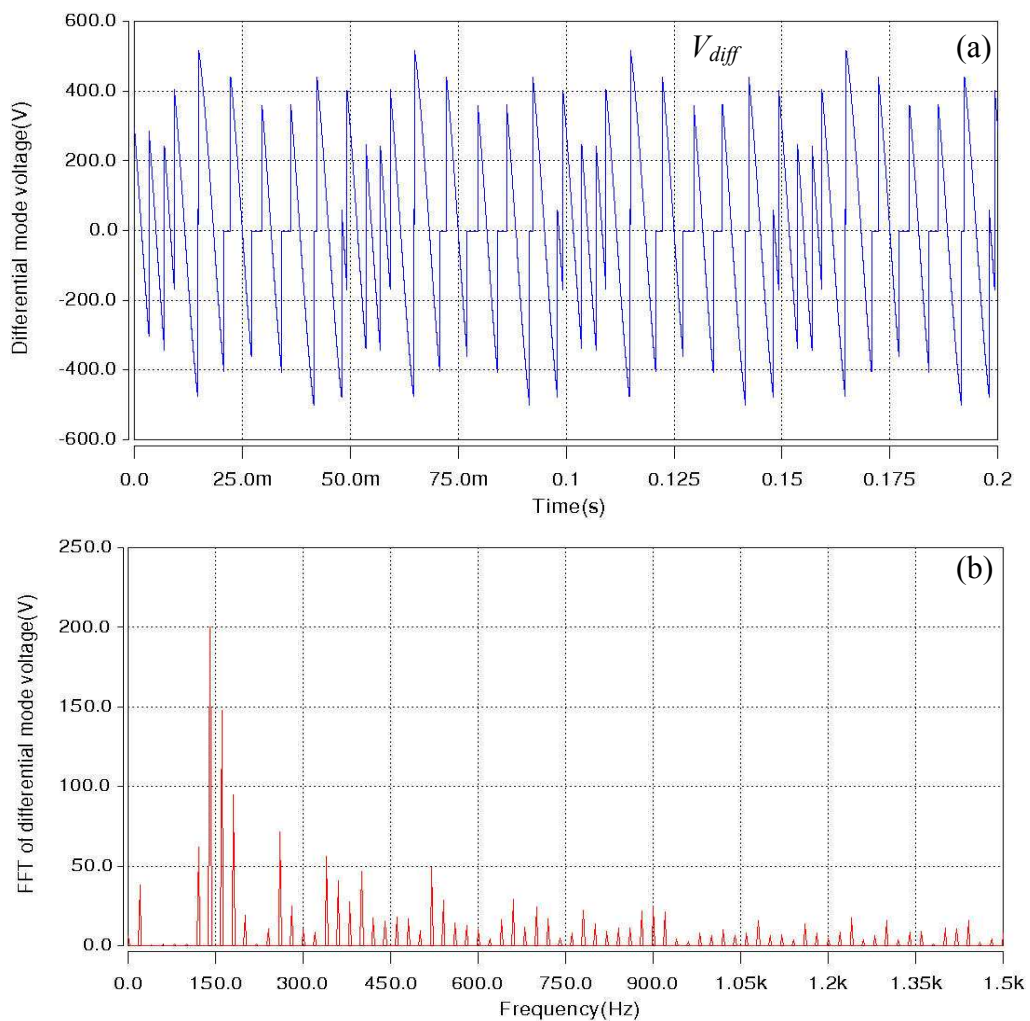
Fig. 2.7: a) Differential mode voltage waveform for a 3-pulse cycloconverter

b) Spectrum of the differential mode voltage for a 3-pulse cycloconverter

Therefore, there are some major disadvantages for the cycloconverter. Firstly, the maximum output frequency can only be a fraction (up to one-third) of the supply frequency to achieve a reasonable performance [pp.202, 3, 23]. Thus the cycloconverter is essentially a high to low-frequency AC-AC converter. Secondly, the large amount of harmonics or even subharmonics present in the output voltage are detrimental to the load as they can give rise to increased motor loss, noise and vibration [29-33]. Therefore, a large number of thyristors are always required to implement a high pulse number cycloconverter in order to achieve good waveforms [pp.306-313, 1]. This is obviously not economical for small installations but probably worthwhile in the high power region. The last disadvantage is that the input power factor of a cycloconverter is always low, especially at reduced output voltage or when circulating current operation is allowed [pp.208, 3, 24].

2.3.2 Operating Modes

There are two basic operating modes of the cycloconverter, which are decided by whether the cycloconverter operates with or without circulating current [pp.150-161, 1]. When the cycloconverter operates in circulating current mode the circulating current is allowed to flow all the time between the positive and negative thyristor half bridges. Conversely, there is no circulating current flow between the two half bridges at any time when the cycloconverter operates strictly in circulating current-free mode. However, within a certain specific interval of each output cycle some circulating current can be allowed even if the cycloconverter operates in circulating current-free mode to mitigate the "voltage distortion" and "bridge selection" problems [pp.187-198, 1].

2.3.2.1 The Circulating Current Mode

As explained in Subsection 2.3.1, although the average output voltage of the positive thyristor half bridge is maintained equal to the average output voltage of the negative thyristor half bridge, the instantaneous voltages of the positive and negative half bridge are not identical and this will cause large circulating currents unless they are limited or suppressed. These circulating currents are not desirable because they

increase circuit losses and impose a heavier current loading on the thyristors. They also reduce the input displacement factor of the system [pp.208, 3]. The flow of harmonic currents may be reduced by the introduction of a circulating current reactor, or may be completely suppressed by removing the gating pulses from the non-conducting bridge (circulating current-free mode) [23, 27].

When the circulating current is reduced by a circulating current reactor, the reactor is connected between the two thyristor half bridges in order to limit the flow of the current, and the load is connected at the mid-point of the reactor shown in Fig. 2.8. The circulating current of the cycloconverter is attenuated by the inductance, $2X$, due to the two circulating current reactors (assuming the resistance is zero as normally it is relatively small compared to the inductance). If the two reactors are tightly coupled together, the flow of the current between the bridges will be attenuated by an inductance $4X$, if it is assumed that the coupling coefficient is close to 1.0. No matter how large the circulating current reactor is, provided that it is not saturated, the output voltage of the cycloconverter is always the average of the two thyristor half bridge output voltages so long as the resistance in the reactor is small enough to be ignored. In Section 2.7 where the output voltage of the cycloconverter is analyzed we will see that the output voltage in circulating current mode has a better waveform quality than that of the cycloconverter operating in circulating current-free mode due to some harmonic cancellation at the middle point of the circulating current reactor. A suitable choice of inductance will restrict the flow of harmonic current without seriously affecting the fundamental output current.

The circulating current waveform is determined by the volt-second integral of the differential voltage between the positive and negative thyristor half bridges. Therefore, with a 6-pulse cycloconverter under consideration as shown in Fig. 2.8, the maximum circulating current occurs when the firing angle α_P is 60 degrees and α_N is 120 degrees or α_P is 120 degrees and α_N is 60 degrees. Moreover, if the pulses number of the cycloconverter is increased to 12, or 24, both the differential voltage and circulating current will be significantly reduced and the angle where the maximum circulating current occurs will be different [34, 35].
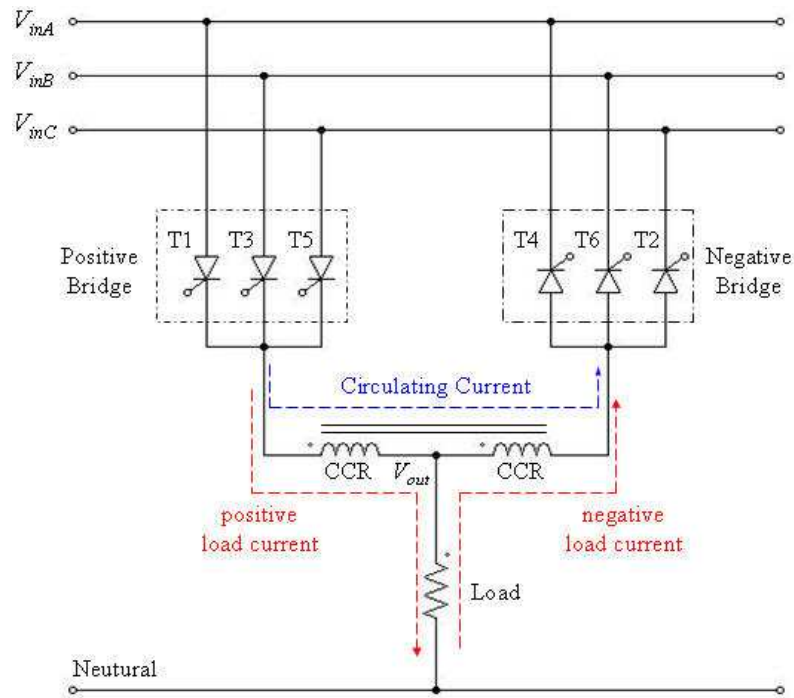
Fig. 2.8: Topology of a three-phase to single-phase cycloconverter with CCR

2.3.2.2 The Circulating Current-Free Mode

If the cycloconverter is in circulating current-free mode, the two thyristor half bridges only conduct during their associated half cycle of the load current to synthesize the desired output voltage waveform at the output terminal. Thus, only one thyristor half bridge is in conduction whilst another one is completely blocked at any one time. Through proper control of the firing pulses for each half bridge there is no possibility to build up a circulating current between the two bridges. Therefore, there is no need for a circulating current reactor connected between the two thyristor half bridges shown in Fig. 2.9.

Without circulating current the efficiency of the cycloconverter and the input displacement factor are better than with circulating current due to the lower loss in the circuit and less reactive power drawn from the input side [pp.208, 3]. However, the control in circulating current-free mode is more complicated due to the output voltage distortion in some conditions as well as bridge selection problems [pp.186-206, 1], which will be discussed in Section 2.6. Therefore, sometimes the cycloconverter is designed to operate in different modes in different intervals, instead of purely operating in just one mode, to improve the overall performance of the converter.
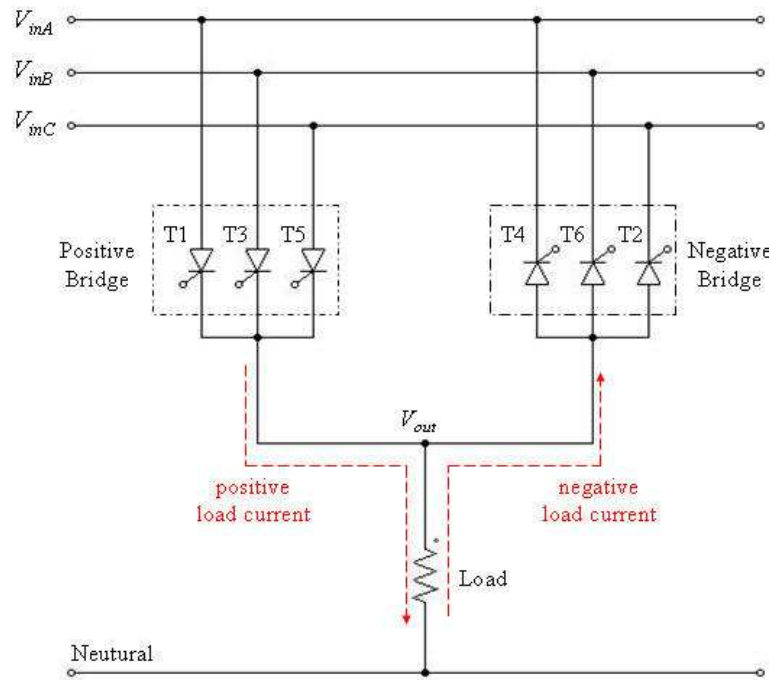
Fig. 2.9: Topology of a three-phase to single-phase cycloconverter without CCR

2.4 Cycloconverter Topology Types

Nowadays, there are many topologies of cycloconverter circuits in use depending on the number of pulses of the thyristor bridges, single or multiphase inputs and outputs and if their operation relies on circulating current or not. Since only the circulating current reactor is required to connect between the positive and negative thyristor half bridges if the cycloconverter operates with circulating current, the type of topology introduced in this section is not distinguished by the operating mode. The number of pulses defined for a cycloconverter is the number of controlled timing pulses generated for an individual thyristor half bridge in an input supply voltage period. Normally this number is the same as the number of thyristors in each thyristor half bridge. However, for the same cycloconverter topology the number of pulses when it has circulating current is double than without circulating current. This is because in circulating current mode, both positive and negative thyristor half bridges are conducting instead of just one of the thyristor half bridges in circulating current-free mode, and the circulating current reactor will combine the ripple (no. of pulses) existing in each of the thyristor half bridge outputs. As a large number of essentially similar circuits have been developed until now, only some of most representative cycloconverter arrangements are reviewed in the following subsections.

2.4.1 Single-Phase Input to Single-Phase Output Cycloconverter

The topology of a single-phase input to single-phase output cycloconverter is shown in Fig. 2.10, the simplest cycloconverter circuit [36]. The secondary transformer of the power supply for the cycloconverter consists of two separate windings, as shown in Fig. 2.10, which can provide 180° displaced input voltages to each of the two thyristor half bridges. As there are two controlled timing pulses for each thyristor half bridge, this topology is referred as a 2-pulse (or 4-pulse in circulating current mode) cycloconverter [36].
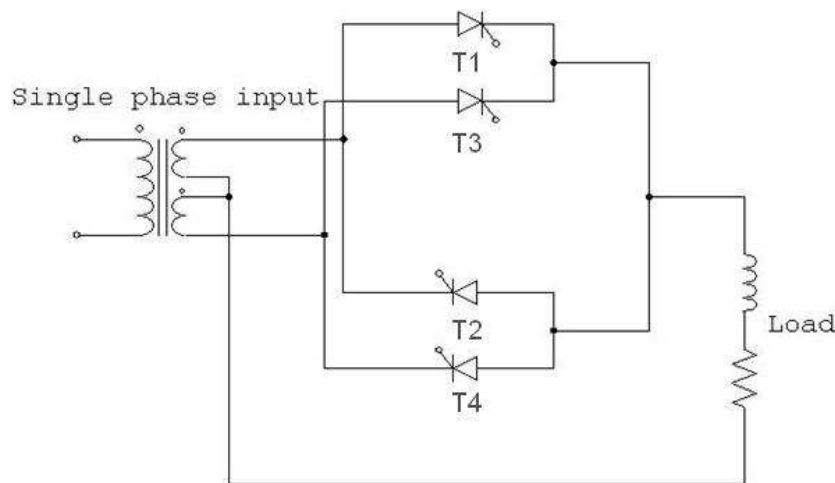
Fig. 2.10: Single-phase input cycloconverter without CCR

The operation of this single-phase input cycloconverter is the same as that described in Subsection 2.3.1. If the cycloconverter is connected as shown in Fig. 2.10, which is operating without circulating current, the non-conducting thyristors should always be kept off otherwise the input power supply could be shorted via the positive and negative thyristor half bridges. When the load current is positive, the output voltage is only controlled by phase control of thyristors T1 and T3 whilst the other two negative thyristors T2 and T4 are kept off and vice versa when the load current is negative. There is more discussion in Section 2.6 with regard to the control problems of the cycloconverter operating without circulating current and how to swap between the two thyristor half bridges in the shortest time possible to avoid output voltage distortion when the load current changes direction whilst ensuring that the two thyristor half

bridges do not conduct at the same time. Fig. 2.11 is the typical output voltage waveform and spectrum of a 2-pulse cycloconverter in circulating current-free mode.
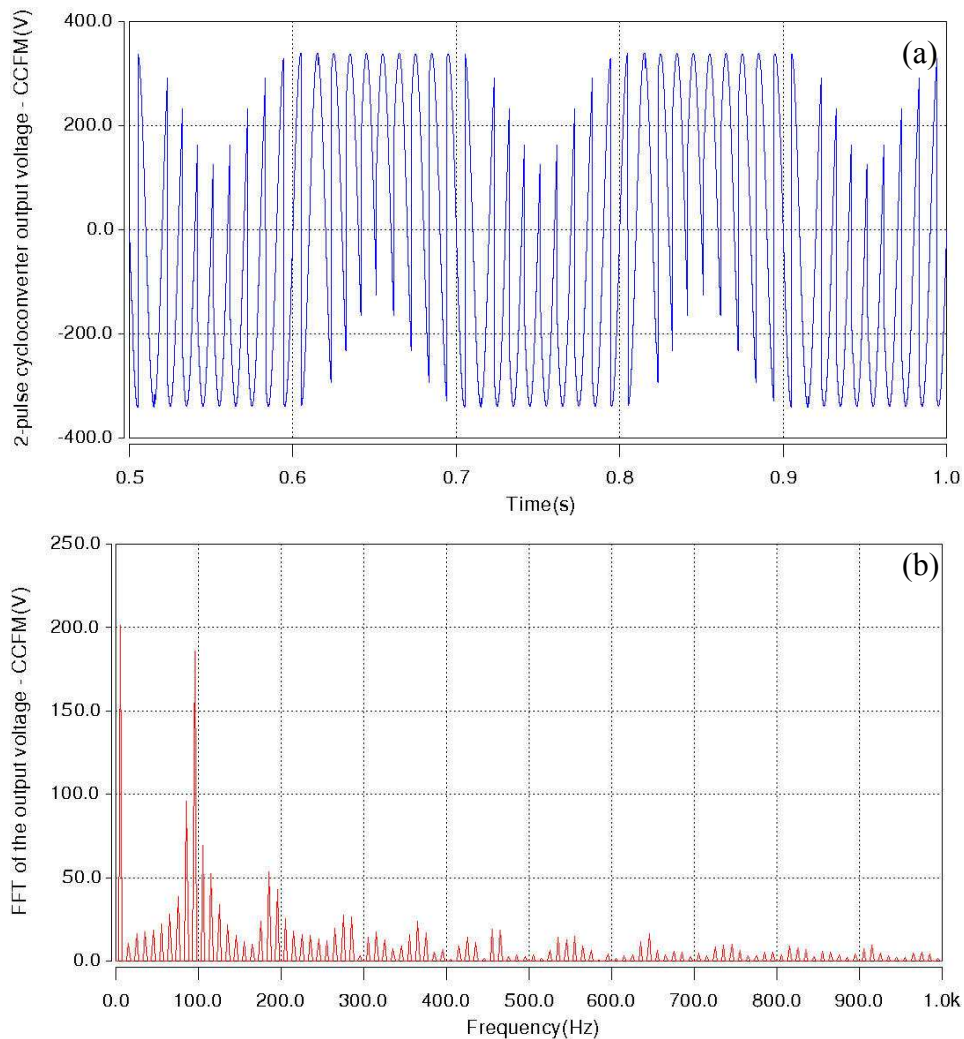
Fig. 2.11: a) The output voltage waveform of a 2-pulse cycloconverter in CCFM
b) Spectrum of the output voltage of a 2-pulse cycloconverter in CCFM

If the cycloconverter is operating in circulating current mode, both thyristor half bridges are continuously conducting, eliminating the output voltage distortion during load current zero crossing but additional coupled reactors are required between the two thyristor half bridges to limit the circulating current as shown in Fig. 2.12. Although the output voltage of the cycloconverter can be improved in circulating current mode [pp.156, 1], as mentioned in Subsection 2.3.1, the circulating current reactor tends to be bulky and more expensive and the presence of the circulating current will degrade the input power factor. Fig. 2.13 shows the typical output voltage waveform and spectrum of a 4-pulse cycloconverter in circulating current mode.
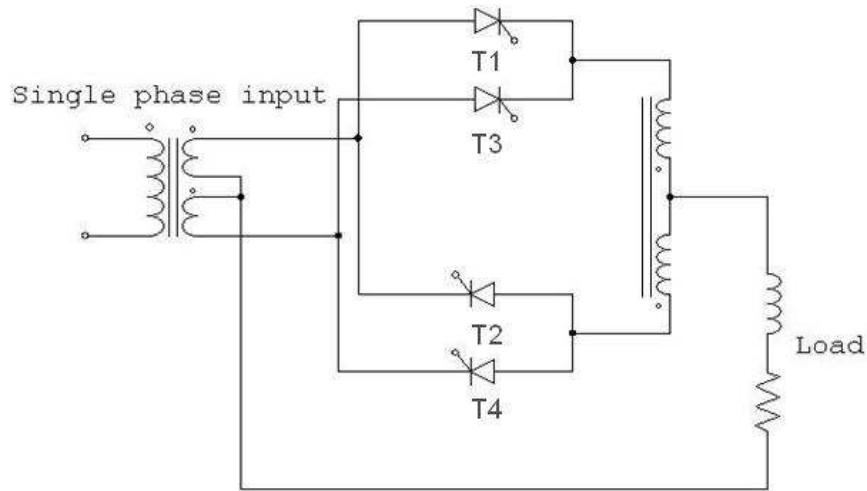
Fig. 2.12: Single-phase input cycloconverter with CCR
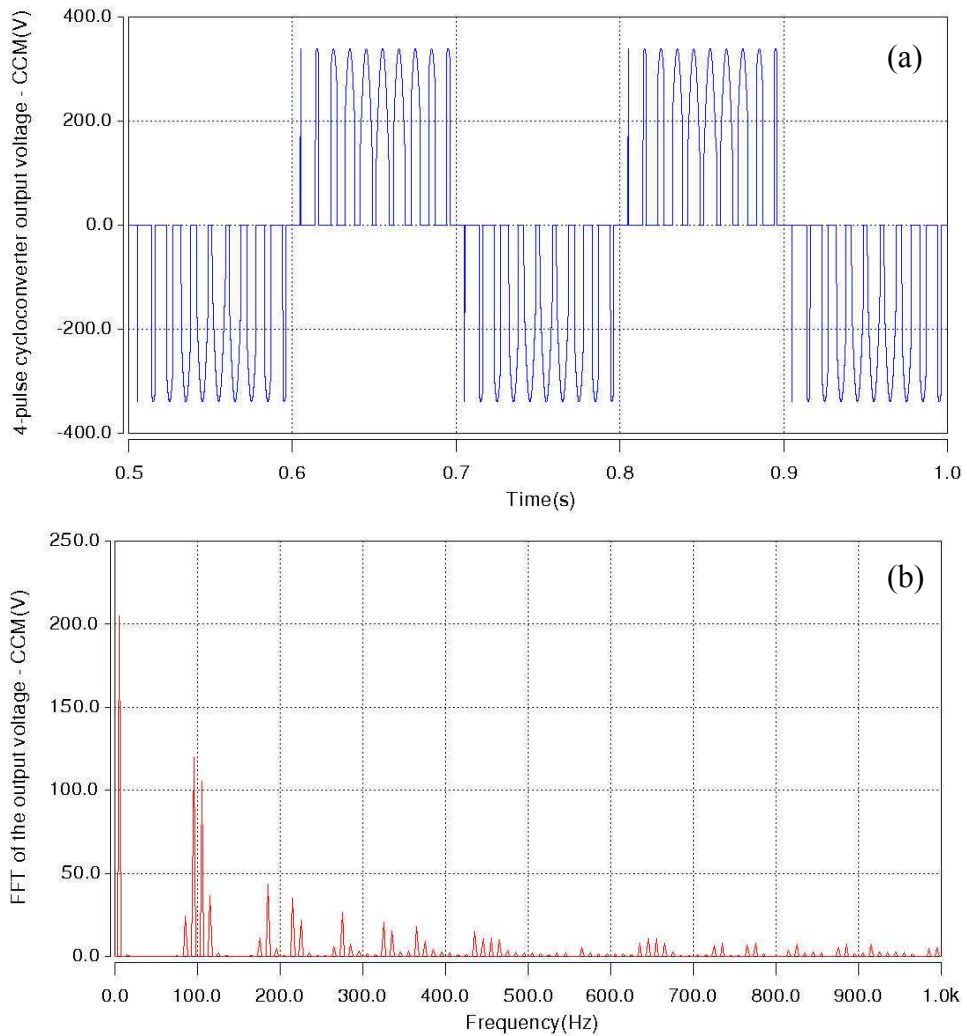
Fig. 2.13: a) The output voltage waveform of a 4-pulse cycloconverter in CCM

b) Spectrum of the output voltage of a 4-pulse cycloconverter in CCM

2.4.2 Three-Phase Input to Single-Phase Output Cycloconverter

The principle of the three-phase input cycloconverter is identical to that of the single-phase input cycloconverter except that there are three input voltages which have 120° shift between each other instead of 180°. Some arrangements of three-phase input to single-phase output will be presented in this section. From the point of view of reducing the output voltage and current harmonics to a minimum level, the number of pulses of the cycloconverter should be as large as possible [pp.306-323, pp.359-368, 1]. But this is also achieved by increasing the complexity of the circuit, which requires a relatively large number of thyristors in the circuit.

2.4.2.1 The 3-Pulse Cycloconverter

The topology of a three-phase input, 3-pulse (or 6-pulse in circulating current mode) cycloconverter is shown in Fig. 2.14 [pp.209, 1]. This basic circuit can be modified to accommodate a 6-pulse, 12-pulse or even 24-pulse cycloconverter to reduce the harmonics at the output as much as possible.
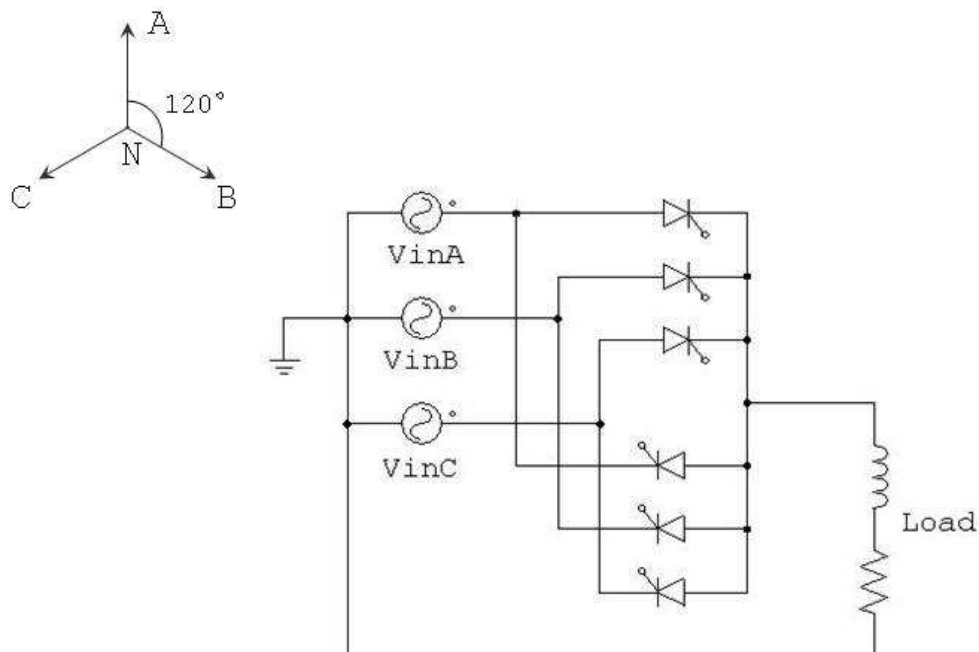
Fig. 2.14: Three-phase input, 3-pulse cycloconverter

2.4.2.2 The 6-Pulse Cycloconverter

The topology of a three-phase input, 6-pulse (or 12-pulse in circulating current mode) cycloconverter is shown in Fig. 2.15 [pp.211, 1]. Normally, the input of the cycloconverter is generated from a three-phase power supply via a phase shift transformer which is able to provide the 60° between each phase on its secondary side. As mentioned above, both the quality of the output voltage and input current waveform is better than that of the 3-pulse cycloconverter at the expense of doubling the number of thyristors and a more complex control circuit. This improvement will also be explained in Section 2.7.
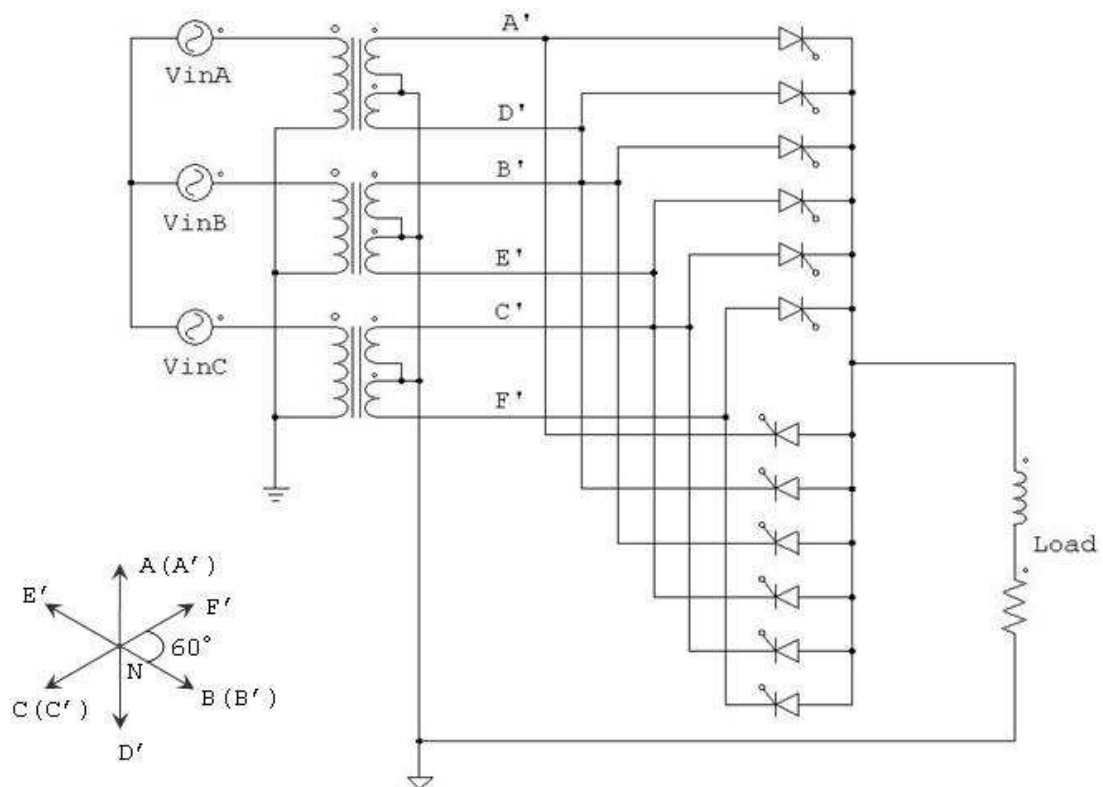
Fig. 2.15: Three-phase input, 6-pulse cycloconverter

2.4.2.3 The 6-Pulse Bridge Cycloconverter

The topology of a three-phase input, 6-pulse (or 12-pulse in circulating current mode) bridge cycloconverter is shown in Fig. 2.16 [pp.213, 1]. In practice, it is necessary to provide electrical isolation either between the inputs to the individual thyristor half bridges, or between the output load circuits, if the cycloconverter is connected with a

three-phase output arrangement [pp.210, 1]. This is because there is no point of common connection between the input and output sides of circuit. If the input is isolated, the total volt-amps handled by the secondary windings are higher than those handled by the primary side. This is because each secondary transformer copes with a separate cycloconverter supplying a single-phase load and therefore it carries the harmonics currents due to the pulsating power of the associated single-phase output [pp.213-216, 1].
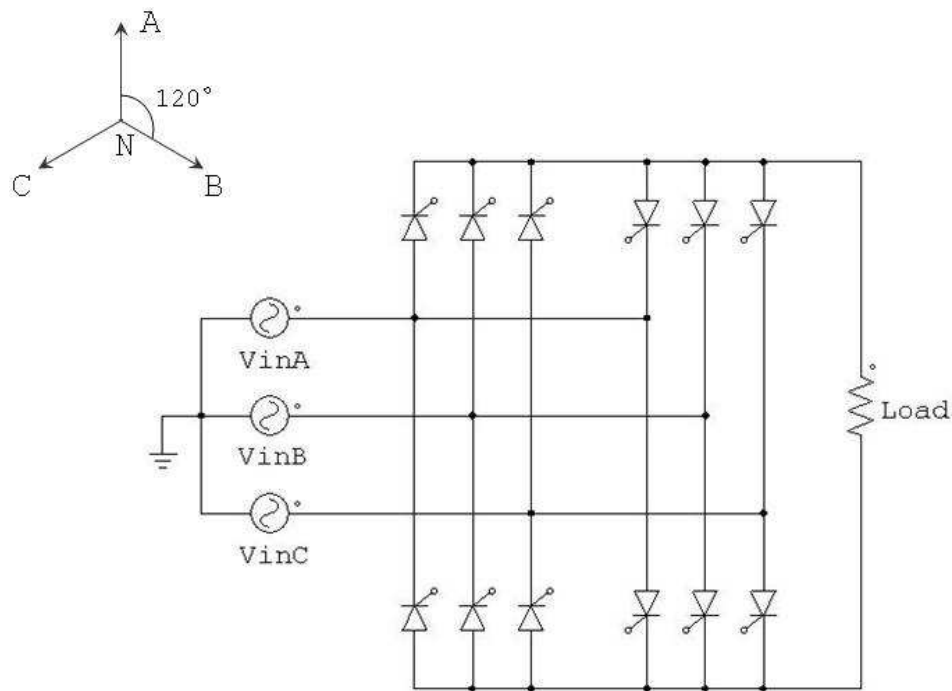
Fig. 2.16: Three-phase input, 6-pulse bridge cycloconverter

2.4.3 Three-Phase Input to Three-Phase Output Cycloconverter

Fig. 2.17 shows three identical three-phase input to single-phase output, 3-pulse (or 6-pulse in circulating current mode) cycloconverters connected together to supply a three-phase load. As will be seen in Section 2.7, for a balanced three-phase output, theoretically, there is no need to connect the load neutral to the supply neutral and therefore it is not possible to have zero-sequence current components in the input lines. Another advantage of three-phase output circuits with a floating neutral point or even without a neutral point such as the delta connection is that it provides a better harmonic content in the output line-to-line voltage due to the cancellation of the common mode voltage harmonics between the outputs.
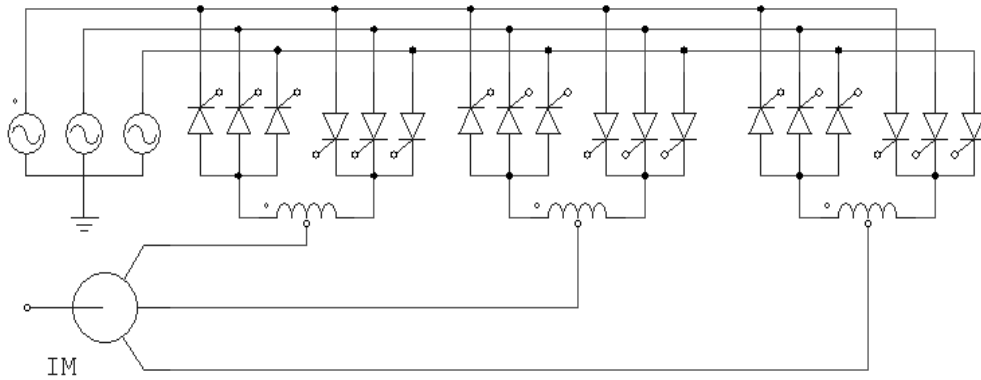
Fig. 2.17: Three-phase input, three-phase output, 3-pulse cycloconverter

2.5 Cosine Wave Crossing Pulse Timing Method

The purpose of the firing pulse generator is to generate correctly timed and sequenced firing pulses for the gates of thyristors in the cycloconverter. Although a wide range of control schemes have been proposed [pp.229-247, 1, 36, 39-43], only the cosine wave crossing control method which is described below is widely used, as it has the unique property that produces the minimum possible total distortion of the output voltage waveform [pp.234-238, 1, 36]. Some other control methods, such as integral control, pre-integral control, or double integral control, which are irrelevant for this PhD thesis, will not be described in this section.

Generally, only the rising edge of each firing pulse is useful in firing the thyristor and the remainder is redundant. Nevertheless, the firing pulses are always generated for longer than needed to ensure that the thyristor is completely latched, which is important for the correct operation of power converter under all operating conditions.

2.5.1 The Principle of Operation

In the cosine wave crossing control method, the analog output reference voltage is compared with a series of cosine timing waves which have a 360°/(no. of pulses) phase shift between each other and the same frequency as the cycloconverter input voltage. The triggering pulses for each thyristor are generated when the reference voltage intersects with the corresponding cosine wave. Fig. 2.18 shows the principle of operation assuming that the analog reference voltage is constant. In such a way, the

amplitude of the fundamental component of the output voltage is proportional to the reference voltage providing the output current is continuous or the cycloconverter is operating with circulating current [pp.229, 1]. Based on this linear relationship between the output voltage and the reference, the cycloconverter behaves like a linear amplifier with linear control characteristic versus output voltage [pp.229, 1].
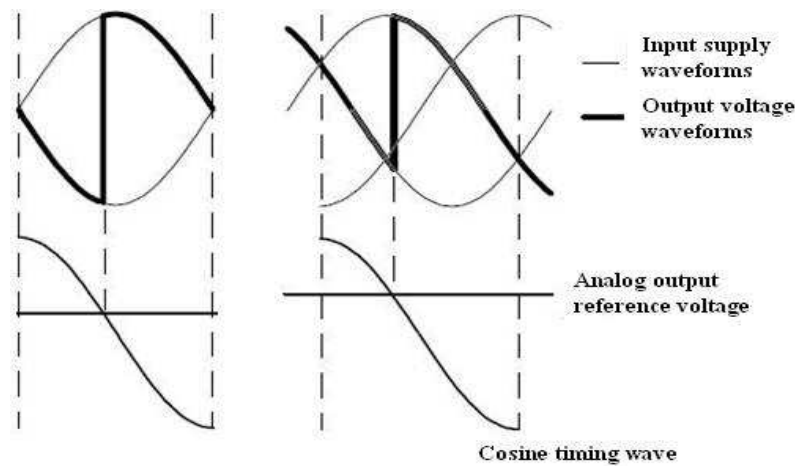
Fig. 2.18: Waveforms illustrating the principle of cosine wave crossing control [36]

2.5.2   The Limitation of the Method

Although the cosine wave crossing control has found widespread use [36], the method still has some limitations. This is because the cosine wave crossing control is a very inflexible procedure, which is in correspondence with the pre-determined cosine reference voltage and has only an open-loop relationship with the output voltage.

The first limitation is the unwanted distortions of the output voltage in the event that the load current becomes discontinuous, when the cycloconverter is operating in circulating current-free mode [pp.239, 1]. For example, when the cycloconverter is operating at light load, the fundamental current is low compared to the switching ripple. This will be discussed further in the Section 2.6.

Apart from the situation of discontinuous current, an open-loop pulse control itself may produce certain highly objectionable distortion components at the output even if the load current is continuous or the cycloconverter operates in circulating current mode [pp.239, 1, 29-33]. One source of the objectionable distortion is that the output

voltage may contain subharmonics or even zero frequency component except at certain discrete output-to-input frequency ratios [pp.239, 1]. Although the amplitudes of these harmonics are relatively small compared to the fundamental waveform, the adverse effect cannot be neglected if the load has low impedance at those subharmonic frequencies which is the case with an inductive load. This means an excessive amount of subharmonic current may flow through the output load.

According to [pp.239-240, 1], another objectionable distortion comes from the imperfections of the pulse timing circuits, which give rise to errors in the timing of the firing pulses. These timing errors are directly reflected on the output voltage waveform of the cycloconverter, as additional distortion. Normally, these timing errors do not matter very much but under some conditions they are very important, for example when the output voltage ratio is low [pp.239, 1].

2.5.3 Corrective Methods for Cosine Wave Crossing Control

Various techniques which are able to overcome the deficiencies of the cosine wave crossing control method for the cycloconverter have been investigated [pp.240-247, 1, 37-39], the most relevant ones are described below.

A. Regular Sampling

The regular sampling method developed in [37] is specifically applied to circulating current mode cycloconverters. The principle of this method is to modify the cosine reference voltage waveform through a sample and hold action at the start of each cosine wave. The benefit of this method is to reduce the subharmonics in the output voltage [37]. Moreover, some further improvement can be obtained by pre-distorting the cosine reference voltage wave [39].

B. The Use of Feedback

The objectionable components present at the output of cycloconvertr, which are obviously not good for the whole system operation, have relative low amplitude

compared to the maximum wanted output voltage. Therefore, by adding a negative feedback, a closed loop control of the cycloconverter is achieved in order to reduce these distortion terms and remove some unwanted components [pp.240, 1]. However, apart from the objectionable components, the major distortion of the output voltage cannot be removed by using the feedback control due to the basic mechanism of the cycloconverter. The use of feedback for all the distortions present in the output voltage may lead to an unstable operation of the cycloconverter and therefore a consequent deterioration of the output waveform.

The control system can use load voltage or current as the feedback depending upon the application. A block diagram using a voltage feedback control scheme to suppress the harmonics on the output voltage is shown in Fig. 2.19 [38]. The limitation of this method is that the maximum stable loop gain is rather low and further reduces if the maximum output frequency is increased [36]. Sometimes, current feedback is preferred as the voltage distortion terms are more readily measurable in the current waveform [pp.241, 1]. A block diagram of a current feedback control scheme is shown in Fig. 2.20.
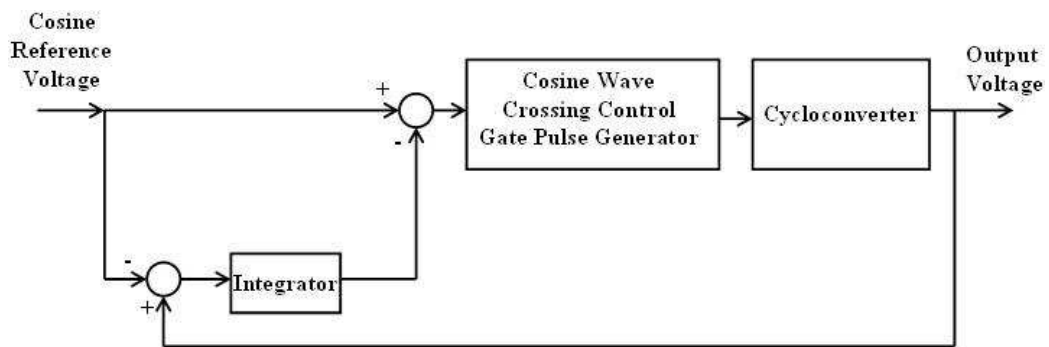
Fig. 2.19: Block diagram of voltage feedback control scheme
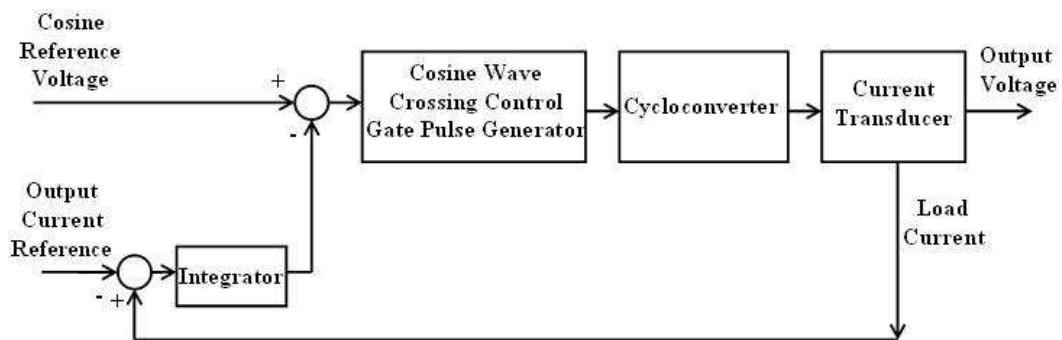
Fig. 2.20: Block diagram of current feedback control scheme

2.6 Problems and Solutions Associated with Standard Cycloconverters

There are some problems associated with the standard cycloconverter with or without circulating current. These problems, as well as some of their corresponding solutions, will be presented in below.

2.6.1 Issues Related to Circulating Current-Free Mode and Potential Solutions

Since the circulating current-free standard cycloconverter operates under the assumption that the output current is pure sinusoid, the control is relatively straightforward. For example, the selection of which of the two thyristor half bridges to be fired, can be implemented simply by switching the firing pulses from one half bridge to the other when the load current crosses zero.

In practice, the output current can become discontinuous which creates more difficulties for the control of the cycloconverter. There are two main difficulties that arise with discontinuous load current. Firstly, the output voltage will have additional distortions under open-loop firing pulse timing control. Secondly, it is not easy to decide when it is the correct time to commutate from one thyristor half bridge to the other as the load current may cross zero more than one time.

2.6.1.1 Output Voltage Distortion Problem and Possible Solutions

Normally the induction/synchronous motors connected to the cycloconverter can be approximated as an L-R inductive load, so whether the load current is continuous or not depends on both the nature and the state of the load and also on the desired quality of the output voltage waveform. For example, when the resistive part of the load overrides the inductive part, the load can be approximated as a pure resistor. With this load, the output current has the same wave shape as the output voltage, and this means discontinuous conduction inevitably occurs since sometimes the firing pulses are

applied on the positive thyristor half bridge when the negative output voltage needs to be generated or vice versa. The mean output voltage under this discontinuous condition is greater than what it would be under continuous current due to fact that the corresponding thyristor half bridge cannot carry on the reverse current.

One solution to solve the voltage distortion problem is to implement a negative feedback loop which naturally compensates for the distorted output voltage and forces the output voltage to follow the reference waveform [pp.186, 1]. With this solution, most of the distortion in the output voltage can be eliminated. However, it is difficult to achieve any improvement in the distortion of the output voltage during zero crossing of the load current.

Clearly, if the cycloconverter operates in circulating current mode instead of circulating current-free mode, the voltage distortion problem will be easily avoided. Because of the circulating current, both of the thyristor half bridges are conducting all the time (ignoring instants when the circulating current momentarily reaches zero) and this will allow the load current to reverse direction at any moment. The output voltage then is only the result of the open loop firing pulse timing control and it will follow the sinusoidal reference waveform if the pulse timing control works properly. Moreover, as will be seen in Section 2.7, the output voltage of the cycloconverter operating with circulating current has lower harmonic content than that of the cycloconverter without circulating current due to the harmonic cancellation between the two thyristor half bridges. However, the presence of circulating current requires bulky circulating current reactor and also worsen the input power quality. Therefore, some schemes are proposed which operate the cycloconverter with circulating current only when there is a tendency for the load current to become discontinuous and which operate without circulating current when the load current is continuous. However, these schemes require more complex control of the circuit and still need some small circulating current reactors to limit the circulating current [pp.187-198, 1].

2.6.1.2 Bridge Selection Problem and Possible Solutions

When the cycloconverter is operating without circulating current, there is always a

practical problem that needs to be considered. That is how to automatically and reliably switch the current from one thyristor half bridge to the other at the proper instants especially when the load current has several zero crossings during direction change [pp.199, 1]. Some alternative solutions to this problem have been proposed.

A simple solution, named "First Current-Zero" bridge selection, was proposed to take the first current-zero point as the condition to switch the firing pulses from one thyristor half bridge to the other [pp.199, 1, 44, 45]. The advantage of this method is that it provides a reliable bridge selection scheme with minimum complexity. However, this method also results in an incorrect output voltage waveform and hence added load current distortion because it forces the cycloconverter switch from one bridge to another at a point which may not correspond to requirements of the reference waveform.

Another, more complicated method, named "Fundamental Current-Zero" bridge selection is able to provide a commutation which does not cause any additional voltage distortion by switching between the thyristor half bridges when the fundamental component of the load current reaches zero [pp.202, 1]. Although this method is much more accurate than the "First Current-Zero" method with some certain types of load, it is not easy to be implemented since the both control and the circuit are more complicated to ensure no flow of the circulating current as well as no phase shift occurs in the filtered component of the output current waveform.

A completely different solution to solve the bridge selection problem is to employ a closed-loop control of the output voltage. This is similar to the methods described in Subsection 2.6.1.1 and is not expanded on further here.

Clearly, the allowance of circulating current is another way to eliminate the bridge selection problem as both of the bridges are conducting during the commutation instant and bridge selection is not required. Thus, allowing for circulating current mode provides the solution for both the "voltage distortion" and "bridge selection" problems without taking into consideration any additional control functions to handle the load current zero crossing and bridge commutation.

2.6.2 Issues Related to Circulating Current Mode and Potential Solutions

From the discussion above, the circulating current mode is one of the best options to overcome all the problems that are caused by the circulating current-free mode. As has been mentioned already, the circulating current needs to be minimized by bulky reactors and also has a bad impact on the input power factor. As can be seen from equation (2.3) the value of the circulating current reactor depends on the amplitude and the frequency of the differential mode voltage as well as the value of the ripple of the circulating current. Therefore, the reactor becomes bulky when the circulating current ripple is required to be small under the influence of a low frequency, high amplitude differential mode voltage.

$$L_{cir} = V_{diff\_pk} / \omega_{diff} \cdot \Delta I_{cir} \qquad (2.3)$$

Where L_{CCR} is the circulating current reactor inductance, V_{diff_pk} is the amplitude of the differential mode voltage between two thyristor half bridges, ω_{diff} is the frequency of the differential mode voltage, ΔI_{cir} is the circulating current ripple.

Fig. 2.21(a) and (b) show the circulating current waveform and its spectrum for a 6-pulse cycloconverter with a given circulating current reactor. From the figures it can be seen that the circulating current waveform contains not only low frequency harmonics around 150Hz, but also relatively larger amplitude DC and 20Hz component. These low frequency harmonics will seriously impact the input power quality of the cycloconverter especially when the power rating of the converter is small, or the value of the circulating current reactor is even smaller. Therefore, the circulating current-free mode and circulating current mode can be used together in a standard cycloconverter in order to make use of both their advantages. But having circulating current without proper control can still causes some problems to the converter operation, for example, when the circulating current reaches zero, as shown in Fig. 2.21(a).
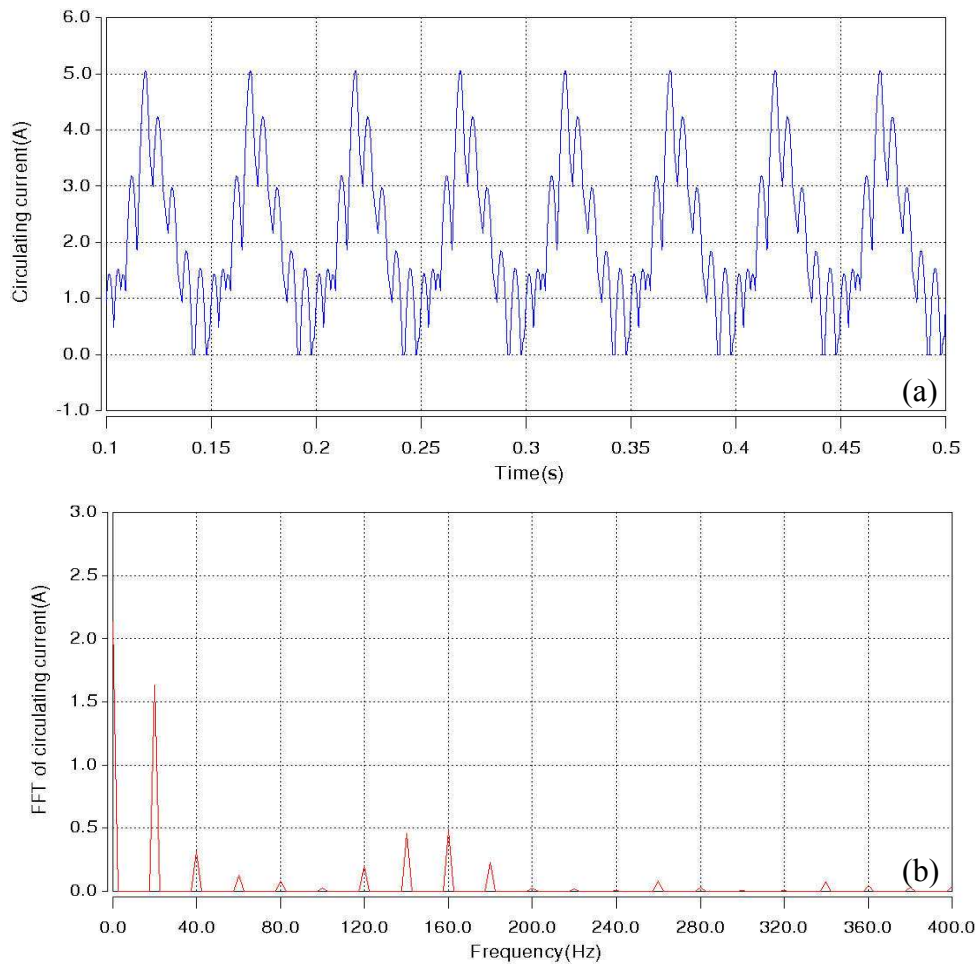
Fig. 2.21: a) Circulating current waveform for a 6-pulse cycloconverter

b) Spectrum of the circulating current for a 6-pulse cycloconverter

The solution to the problems mentioned for circulating current mode will be discussed in the next chapter. A hybrid cycloconverter, which has the capability to accurately control the circulating current around a small DC reference, will be presented. This new topology is proposed to not only minimize the required circulating current reactance but also improve the input power quality.

2.7   Harmonic Analysis of the Output Voltage and Input Current

In this section a theoretical harmonic analysis is carried out under the assumption of continuous load current, smooth bridge switching at zero output current whilst using an open loop cosine wave crossing control method applied.

2.7.1 Output Voltage Harmonic Analysis

The analysis for output voltage for both the circulating current-free mode and circulating current mode will be presented in this subsection.

2.7.1.1 General Equation for the 3-Pulse Voltage Waveform

In this subsection the output voltage harmonic analysis is derived for a 3-pulse thyristor bridge (or 6-pulse in CCM) as it is the basic building block of a three-phase input cycloconverter and also of circuits investigated in later chapters.

According to the [pp.285, 1], the output of the positive and negative thyristor half bridges can be expressed as:

$$V_{THY1} = \frac{3\sqrt{3}V_{N\_pk}}{2\pi}\{\sin f(\theta_o) + \frac{1}{2}[\sin 3\theta_i \cos 2f(\theta_o) + \cos 3\theta_i \sin 2f(\theta_o)]$$

$$+ \frac{1}{4}[\sin 3\theta_i \cos 4f(\theta_o) + \cos 3\theta_i \sin 4f(\theta_o)] + \frac{1}{5}[\sin 6\theta_i \cos 5f(\theta_o) + \cos 6\theta_i \sin 5f(\theta_o)]$$

$$+ \frac{1}{7}[\sin 6\theta_i \cos 7f(\theta_o) + \cos 6\theta_i \sin 7f(\theta_o)] + \cdots\}$$

$$(2.4)$$

$$V_{THY2} = \frac{3\sqrt{3}V_{N\_pk}}{2\pi}\{\sin f(\theta_0) + \frac{1}{2}[\sin 3\theta_i \cos 2f(\theta_o) - \cos 3\theta_i \sin 2f(\theta_o)]$$

$$+ \frac{1}{4}[\sin 3\theta_i \cos 4f(\theta_o) - \cos 3\theta_i \sin 4f(\theta_o)] + \frac{1}{5}[-\sin 6\theta_i \cos 5f(\theta_o) + \cos 6\theta_i \sin 5f(\theta_o)]$$

$$+ \frac{1}{7}[-\sin 6\theta_i \cos 7f(\theta_o) + \cos 6\theta_i \sin 7f(\theta_o)] + \cdots\}$$

$$(2.5)$$

Where V_{THY1} and V_{THY2} are the output voltage of the positive and negative thyristor half bridge respectively; V_{N_pk} is the peak value of the input supply voltage; θ_i is the degree ($2\pi f_{in}t$) of the input voltage at any instant; θ_o is the degree ($2\pi f_{out}t$) of the output reference voltage at any instant, $f(\theta_o)$ is the expression for the phase shift with respect to the quiescent position $\pi/2$. The value of $f(\theta_o)$ oscillates symmetrically to and fro

about zero at a repetition frequency equal to the wanted output frequency. The maximum possible absolute value for $f(\theta_o)$ is $\pi/2$.

As mentioned in Section 2.3, if the cycloconverter is operating in circulating current-free mode, each thyristor half bridge conducts alternatively for half of the output period, and the start of each conduction period of the corresponding half bridge is determined by the displacement angle of the load. If we assume the displacement angle is Φ_o, then the output voltage will be [pp.289, 1]:

$$
\begin{aligned}
V_{out} = \frac{3\sqrt{3}V_{N\_pk}}{2\pi} & \{ \sin f(\theta_o) + \frac{1}{2}\sin 3\theta_i \cos 2f(\theta_o) + \frac{1}{4}\sin 3\theta_i \cos 4f(\theta_o) + \frac{1}{5}\cos 6\theta_i \sin 5f(\theta_o) \\
& + \frac{1}{7}\cos 6\theta_i \sin 7f(\theta_o) + \cdots \} + \frac{3\sqrt{3}V_{N\_pk}}{2\pi} \{ [\frac{1}{2}\cos 3\theta_i \sin 2f(\theta_o) + \frac{1}{4}\cos 3\theta_i \sin 4f(\theta_o) \\
& + \frac{1}{5}\sin 6\theta_i \cos 5f(\theta_o) + \frac{1}{7}\sin 6\theta_i \cos 7f(\theta_o) + \cdots] \times \frac{4}{\pi} [\sin(\theta_o + \phi_o) + \frac{1}{3}\sin 3(\theta_o + \phi_o) \\
& + \frac{1}{5}\sin 5(\theta_o + \phi_o) + \frac{1}{7}\sin 7(\theta_o + \phi_o) + \cdots] \}
\end{aligned}
$$

(2.6)

If the cycloconverter is operating in circulating current mode, the output voltage will be the half of the sum of two thyristor output voltage:

$$
V_{out} = \frac{V_{THY1} + V_{THY2}}{2}
$$

(2.7)

Therefore, by substituting V_{THY1} and V_{THY2} from (2.4) and (2.5), the output voltage of cycloconverter is [pp.285, 1]:

$$
\begin{aligned}
V_{out} = \frac{3\sqrt{3}V_{N\_pk}}{2\pi} & [\sin f(\theta_o) + \frac{1}{2}\sin 3\theta_i \cos 2f(\theta_o) + \frac{1}{4}\sin 3\theta_i \cos 4f(\theta_o) + \frac{1}{5}\cos 6\theta_i \sin 5f(\theta_o) \\
& + \frac{1}{7}\cos 6\theta_i \sin 7f(\theta_o) + \cdots]
\end{aligned}
$$

(2.8)

The reference voltage waveform used by the cosine wave crossing control method is

given by:

$$V_{o\_ref} = r\sin\theta_o \tag{2.9}$$

Where *r* is the modulation index of output voltage.

Thus the firing angle phase modulating function is defined by

$$f(\theta_o) = \sin^{-1} r\sin\theta_o \tag{2.10}$$

If Equation (2.10) is substituted into Equation (2.6) and (2.8) the equation for both the circulating current-free mode and circulating current mode is derived.

Circulating current-free mode:

As the equation for the circulating current-free mode after the substitution of *f(θ_o)* is extremely complicated, the equation presented here is the one which assumes *r* = 1.0 and *Φ_o* = 90°, the full equation can be found in [pp.301, 1].

$$V_{out} = \frac{3\sqrt{3}V_{N\_pk}}{2\pi}[\sin\theta_o + \frac{1}{2}\sin(3\theta_i + 2\theta_o) + \frac{1}{4}\sin(3\theta_i + 4\theta_o) + \frac{1}{5}\sin(6\theta_i + 5\theta_o) + \frac{1}{7}\sin(6\theta_i + 7\theta_o)\cdots]$$

$$\tag{2.11}$$

Circulating current mode:

$$V_{out} = \frac{3\sqrt{3}V_{N\_pk}}{2\pi}\{r\sin\theta_o +$$

$$\frac{1}{2}\sum_{p=1}^{p=\infty}\{\sum_{n=0}^{2n=3[2p-1]+1}[\frac{\alpha_{(3[2p-1]-1)_{2n}}}{3[2p-1]-1} + \frac{\alpha_{(3[2p-1]+1)_{2n}}}{3[2p-1]+1}]\times[\sin(3[2p-1]\theta_i + 2n\theta_o) + \sin(3[2p-1]\theta_i - 2n\theta_o)]$$

$$+ \sum_{n=0}^{2n+1=6p+1}[\frac{\alpha_{(6p-1)_{(2n+1)}}}{6p-1} + \frac{\alpha_{(6p+1)_{(2n+1)}}}{6p+1}]\times[\sin(6p\theta_i + [2n+1]\theta_o) - \sin(6p\theta_i - [2n+1]\theta_o)]\}\}$$

$$\tag{2.12}$$

If we assume $r = 1.0$, then the above equation will be reduced to:

$$V_{out} = \frac{3\sqrt{3}\hat{V}_N}{2\pi}\{\sin\theta_o + \frac{1}{2}(\frac{1}{2}[\sin(3\theta_i + 2\theta_o) + \sin(3\theta_i - 2\theta_o)] + \frac{1}{4}[\sin(3\theta_i + 4\theta_o) + \sin(3\theta_i - 4\theta_o)]$$
$$+ \frac{1}{5}[\sin(6\theta_i + 5\theta_o) - \sin(6\theta_i - 5\theta_o)] + \frac{1}{7}[\sin(6\theta_i + 7\theta_o) - \sin(6\theta_i - 7\theta_o)]\cdots)\}$$

(2.13)

2.7.1.2 The Frequencies and Amplitudes of Harmonics

From the above equation it can be seen that the harmonic or sub-harmonic distortion are the frequencies which are sums or differences between multiples of the input and output frequencies.

For the 3-pulse cycloconverter operating in circulating current-free mode, the frequencies of the harmonic components contained in output voltage are expressed by the following equation [pp.307, 1]:

$$f_{H1} = |3(2p-1)f_{in} \pm 2nf_{out}|$$

(2.14)

And

$$f_{H2} = |6pf_{in} \pm (2n+1)f_{out}|$$

(2.15)

Where p is any integer from 1 to infinity, n is any integer from 0 to infinity.

With increasing the number of pulses, the number of harmonic components will be reduced compared to a 3-pulse cycloconverter. For example, the harmonic components associated with the output voltage of a 6-pulse cycloconverter are expressed as Equation (2.16) [pp.310, 1] which is the same as part of the harmonics present in the 3-pulse cycloconverter output voltage shown in Equation (2.15).

$$f_H = \left| 6pf_{in} \pm (2n+1)f_{out} \right| \tag{2.16}$$

The harmonic components associated with the output voltage of a 12-pulse cycloconverter are expressed as [pp.311, 1]:

$$f_H = \left| 12pf_{in} \pm (2n+1)f_{out} \right| \tag{2.17}$$

For a 3-pulse cycloconverter operating in circulating current mode [pp.311, 1],

$$f_{H1} = \left| 3(2p-1)f_{in} \pm 2nf_{out} \right| \tag{2.18}$$

Where $n \leq 3(2p\text{-}1)$ and

$$f_{H2} = \left| 6pf_{in} \pm (2n+1)f_{out} \right| \tag{2.19}$$

Where $(2n+1) \leq (6p+1)$

From the above equation it can be seen that at a given value of p the number of harmonics is limited instead of infinite harmonic components in the circulating current mode.

For 6- and 12-pulse cycloconverters, the harmonic components are expressed as the following [pp.312-313, 1]:

$$f_H = \left| 6pf_{in} \pm (2n+1)f_{out} \right| \tag{2.20}$$

Where $(2n+1) \leq (6p+1)$

$$f_H = \left| 12pf_i \pm (2n+1)f_o \right| \tag{2.21}$$

Where $(2n+1) \leq (12p+1)$

From the previous general expressions the amplitude of each harmonic component present in the output voltage is dependent on output voltage ratio as well as the load displacement angle if the cycloconverter is operating in circulating current-free mode or only on the output voltage ratio if the cycloconverter is operating in circulating current mode. For comprehensive quantitative data with regard to the amplitude of harmonics please refer to Tables 11.3 to 11.6 in [pp.318-320, 1].

2.7.2 Input Current Harmonic Analysis

The analysis for the input current for the circulating current-free mode will be presented in this subsection.

2.7.1.1 General Equation for the 3-Pulse Current Waveform

As the derivation principle for the input current harmonic components is similar to the output voltage harmonic equation derivation, the final equation will be given directly and for the detailed derivation refer to Appendix B. As the circulating current is to be kept as small as possible, the harmonics of the input current are only analyzed under the circulating current-free mode which would naturally result in zero circulating current. An extensive input current harmonic comparison for both operating modes will be presented in Chapter 4, based on the simulation results of the cycloconverter.

For simplicity, only the result for the condition of $r = 1.0$ and $\Phi_o = 90°$ is provided for a single-phase output cycloconverter in circulating current-free mode [p.336, 1].

$$i_A = \frac{-\sqrt{3}I_{o\_pk}}{2\pi}\cos\theta_i + \frac{1}{3}I_{o\_pk}\cos\theta_o + \frac{\sqrt{3}I_{o\_pk}}{2\pi}\{-\cos(\theta_i + 2\theta_o) + \frac{1}{2}[\cos(2\theta_i + \theta_o) + \cos(2\theta_i + 3\theta_o)]$$

$$-\frac{1}{4}[\cos(4\theta_i + 3\theta_o) + \cos(4\theta_i + 5\theta_o)] + \frac{1}{5}[\cos(5\theta_i + 4\theta_o) + \cos(5\theta_i + 6\theta_o)]$$

$$-\frac{1}{7}[\cos(7\theta_i + 6\theta_o) + \cos(7\theta_i + 8\theta_o)]\cdots\}$$

$$(2.22)$$

Where i_A is the input current; I_{o_pk} is the peak value of the load current;

If the cycloconverter is connected to a three-phase output, the equation of the input current can be derived by adding all the three input currents produced by each of the single-phase cycloconverters together, by making the substitution (θ_i - $2\pi/3$) and (θ_i + $2\pi/3$) for θ_i.

The differences between the input current harmonics for single-phase output and three-phase output are: i) the amplitudes of all terms with no θ_o times 3; ii) the amplitudes of all terms containing integer multiples of $3\theta_i$ times 3; iii) all remaining harmonic terms disappear. Thus, the input phase current for a cycloconverter with three-phase output will have higher amplitude at the input frequency but reduced amplitude at the output frequency compared to the single-phase output cycloconverter, with some harmonics fully canceling each other. Therefore, the input power factor of a three-phase output cycloconverter is better than that of a single-phase output.

The input current of a cycloconverter will also be improved with an increase of the number of pulses [pp.360-375, 1].

2.7.2.2 The Frequencies and Amplitudes of the Harmonics

There are some harmonics of input current, which defined as "characteristic cycloconverter harmonics", which are independent of the circuit configuration or the number of pulses. The frequencies of these components are given by the equations shown below [pp.361, 1].

For a single-phase output cycloconverter:

$$f_{ch} = f_{in} \pm 2nf_{out} \tag{2.23}$$

For a three-phase output cycloconverter:

$$f_{ch} = f_{in} \pm 6nf_{out} \tag{2.24}$$

Where *n* is any integer from 1 to infinity.

Other harmonics are dependent on the circuit configuration. For example, if it is a 3-pulse cycloconverter, expressions are given below [pp.362, 1]:

For a single-phase output:

$$f_{H1} = f_{out} \tag{2.25}$$

$$f_{H2} = \left| [3(2p-1) \pm 1] f_{in} \pm (2n+1) f_{out} \right| \tag{2.26}$$

And

$$f_{H3} = \left| [6p \pm 1] f_{in} \pm 2n f_{out} \right| \tag{2.27}$$

For a three-phase output:

$$f_{H2} = \left| [3(2p-1) \pm 1] f_{in} \pm 3(2n+1) f_{out} \right| \tag{2.28}$$

And

$$f_{H} = \left| [6p \pm 1] f_{in} \pm 6n f_{out} \right| \tag{2.29}$$

Where *p* is any integer from 1 to infinity and *n* is any integer from zero to infinity.

Some given harmonic frequencies are absent when the number of pulses increases to 6, 12 or even 24. For more equations please refer to [pp.362-363, 1].

Similar to the output voltage harmonics, the amplitude of the input current harmonics is also a function of the output voltage ratio and the load displacement angle and is independent of the frequency of the component. For further quantitative data please refer to [pp.369-373, 1] from Table 12.1 to 12.4.

2.8   Summary

- 43 -

In this chapter, the application of the cycloconverter and the basic topologies in both circulating current and circulating current-free mode have been introduced. Cosine wave crossing control and the corrective methods that address the shortcomings of cosine wave crossing have been described. Some issues present in cycloconverters operating in circulating current-free mode have been presented. The circulating current mode is considered as one of the best ways to overcome these problems although it also has some shortcomings for which solutions will be discussed in detail in the next chapter. This chapter concludes with a brief analysis of the harmonics present in both the output voltage and the input current of the standard cycloconverter, which will be one of the main focus points in this thesis.

Chapter 3

Hybrid Cycloconverter

3.1 Introduction

As mentioned in Chapter 2, there are a series of disadvantages for the standard cycloconverter technology. One disadvantage is that a high content of harmonics is present in the output voltage, depending on the number of pulses; the greater the number of pulses, the better the waveform, but the downside is that this will result in an increased number of devices and complexity. Another disadvantage is that if the cycloconverter operates with circulating current. Having a poor control over the circulating current causes poorer power quality on the input side. All existing solutions to mitigate these problems are exclusively based on passive components (phase shift transformers and circulating current reactors) and, as a result, they are bulky, as the size of magnetics is dependent on the frequency of the ripple (number of pulses multiplied by the input frequency).

Some methods have already been proposed to reduce the output voltage or input current harmonics [28, 46-51], although most of them are focused on developing the control method of the cycloconverter and the improvemet are very limited. A method called frequency selective feedback was developed to achieve suppression of significant subharmonics and low frequency interharmonics present in the output of cycloconverter [28]. Although this method is an extension of the ripple voltage integral feedback as mentioned in Chapter 2, the major distortion of the output voltage still cannot be removed by feedback control due to the basic mechanism of the cycloconverter. Another output voltage harmonic reduction technique was proposed for cycloconverter by allowing the firing angle delay of each thyristor in the bridge circuit to be advanced or retarded, which is named jitter harmonic control [46]. Since

this method was developed to reduce those harmonics considered to be particularly troublesome in a typical marine electrical propulsion system, it can only be used to attenuate specific harmonic components. This is also at the expense of increasing the total output distortion. Some other methods [47-51] are proposed to improve the input power quality of the cycloconverter. For example, a selective active filter control system with tracking of interharmonics was proposed to compensate the target harmonics and interharmonics [47-49]. With this method, the rating of the active filter can be much reduced as only the most troublesome components are selected to be compensated. However, the method relies heavily on the estimation of the input current spectrum which requires complicated control system. Apart from all the methods mentioned above, hardly a method can be found to reducing or controlling the circulating current and minimizing the size of the circulating current reactors if the cycloconverter operates in circulating current mode.

In this chapter a new topology, the hybrid cycloconverter, is proposed to improve the performance of the standard cycloconverter [52-54]. With an added auxiliary inverter operating in a similar way to an active filter, the hybrid solution is not only aim to improve the output voltage, but also accurately control the circulating current at reduced installed power. The input power quality can be also improved with the hybrid topologies especially in circulating current mode. The principle of the hybrid cycloconverter as well as its two operating modes, circulating current mode and circulating current-free mode, will be explained. Then all the proposed hybrid cycloconverter topologies and control strategies for different parts of the circuit will be presented. Finally, the switching states for each topology in circulating current and circulating current-free mode will be illustrated. Together with Chapter 2, this chapter will be the basis for the implementation of simulation models as well as a prototype power converter.

3.2 Operation of the Hybrid Cycloconverter

In this section the principle of the hybrid cycloconverter will be explained. Moreover, in correspondence to the standard cycloconverter, the two operating modes, circulating current and circulating current-free mode will be illustrated.

3.2.1 The Hybrid Cycloconverter Concept

The key to reduce the size the of magnetic components is to increase the frequency of the ripple (thereby reducing the volt-time-area of the ripple) by employing an auxiliary forced commutated power converter operating in a similar way to a series active filter [55]. This converter will cancel the low frequency ripple in the output voltage and facilitate accurate control over the circulating current by switching faster whilst being rated at only a fraction of the supply voltage.

Fig. 3.1 shows a three-phase input thyristor rectifier operating as a cycloconverter with an additional H-bridge inverter inserted in series with the positive thyristor half bridge. In Fig. 3.2(a), the waveforms of one of the input phase voltages, the cycloconverter reference voltage, and the output voltage of one of the thyristor half bridges (V_{THY1}) are presented. The reference voltage of the cycloconverter in this situation was imposed to follow a sinusoid of a lower frequency than the supply to resemble the operation of a standard cycloconverter. The H-bridge inverter uses as its reference the difference between the reference voltage of the cycloconverter and the voltage that the cycloconverter is actually producing V_{THY}, which has a high 300Hz harmonic content (Fig. 3.3(a)), typical for the operation of a 6-pulse thyristor bridge. If the H-bridge inverter switches at a high frequency, such as five times faster (1.5kHz) than the thyristor bridge, it is able to compensate the 300 Hz ripple, as shown in Fig. 3.2(b) (waveform) and Fig. 3.3(b) (its spectrum) [52].
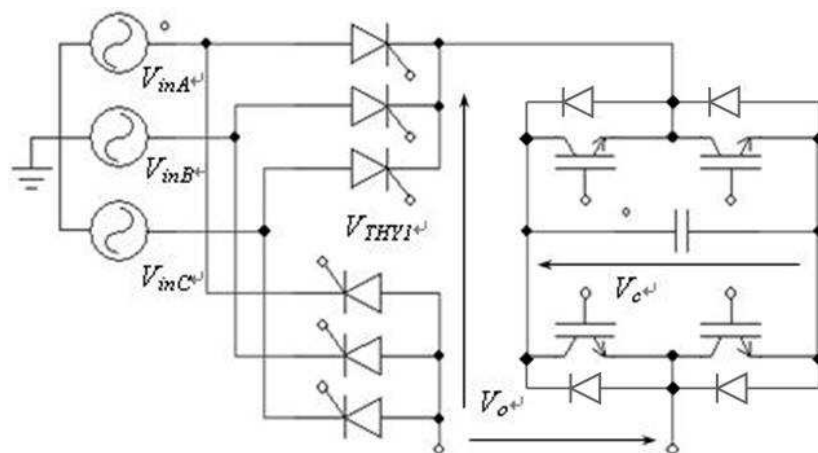
Fig. 3.1: Three-phase input to single-phase output hybrid cycloconverter
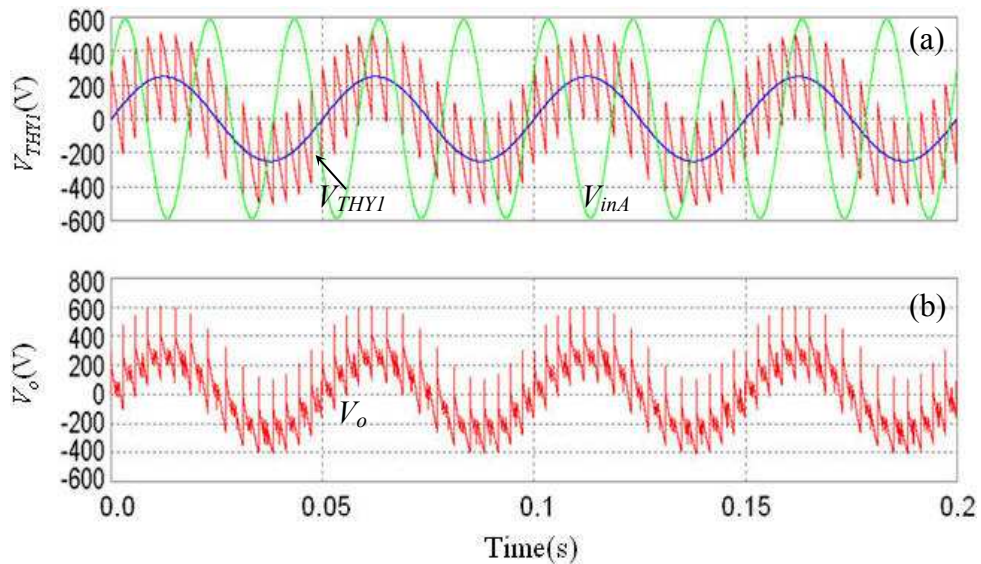
Fig. 3.2: The output voltage waveform of: a) the standard b) the hybrid cycloconverter
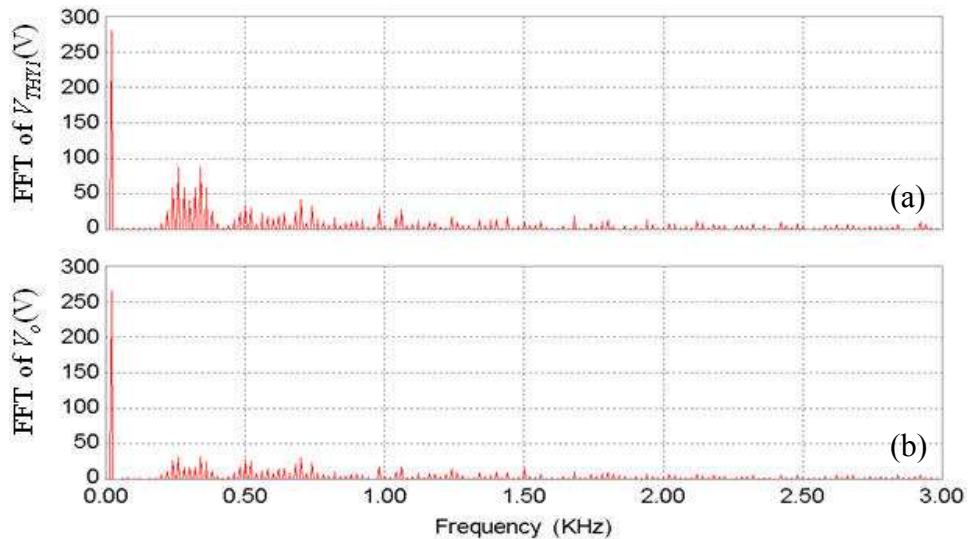
Fig. 3.3: The spectrum of: a) the standard b) the hybrid cycloconverter output voltage

The voltage waveform is clearly improved from a THD of approx. 81 % down to 47% with most of the harmonics appearing now at a higher frequency, which could be filtered much more effectively by an inductive type of load. More advanced control based on a closed loop or that can actually calculate the real average voltage that needs to be compensated would provide much better performance. The feasibility of the idea can be better evaluated by looking at the reduction of the highest in magnitude low order frequency harmonics (260Hz and 340 Hz) from about 85 V to 30 V. Also the 60V side bands (240 Hz, 280 Hz, 320 Hz and 360 Hz) are reduced to approx 25 V. The degree of the reduction is dependent on the amplitude of both the

H-bridge inverter reference and the DC-link capacitor voltage (V_c). More detailed analysis with respect to to this relationship will be presented in Chapter 4.

However, having identified the potential benefits of the hybrid concept, it is necessary to implement it into a realistic simulation model that will take into account realistic thyristor models and the necessity of having circulating current in the cycloconverter.

3.2.2 The Operating Modes

Similar to a standard cycloconverter, the hybrid cycloconverter has two alternative modes of operation, circulating current mode and circulating current-free mode. In both operating modes, an H-bridge inverter is connected with the standard cycloconverter structure to improve its performance.

3.2.2.1 The Circulating Current Mode Hybrid Cycloconverter

If the cycloconverter operates with circulating current, a poor control over the circulating current will cause the converter to draw more input current and result in a poor power factor on the input side. Therefore a bulky inductance (circulating current reactor) needs to be introduced into the circuit between the positive and negative thyristor half bridges to limit the flow of harmonic current. In order to minimize the size of the circulating current reactor, an additional feature should be added to the H-bridge inverter. The reduction/cancellation of the differential mode voltage components between the outputs of the two thyristor half bridge halves. In order to do that, a modified hybrid topology, consisting of four IGBTs with anti-parallel diodes embedded in a single full H-bridge inverter with split DC-link capacitors, as shown in Fig. 3.4, derived from the topology shown in Fig. 3.1, should be employed. The H-bridge inverter is connected between the positive and negative thyristor half bridges via two coupled circulating current reactors. Similar to the topology shown in Fig. 3.1, the H-bridge inverter in this topology still generates a high frequency PWM voltage. However, in this case, the differential voltage between positive and negative thyristor half bridges is directly used as a reference for H-bridge inverter. This means the H-bridge inverter is able to cancel the low frequency harmonics of differential voltage

by operating at high frequency. As a result, the size of the circulating current reactors, which is dependent not only on the inductance value but also the square of the peak current, can be reduced significantly as only high frequency voltage ripple is seen across this inductance after the cancellation.
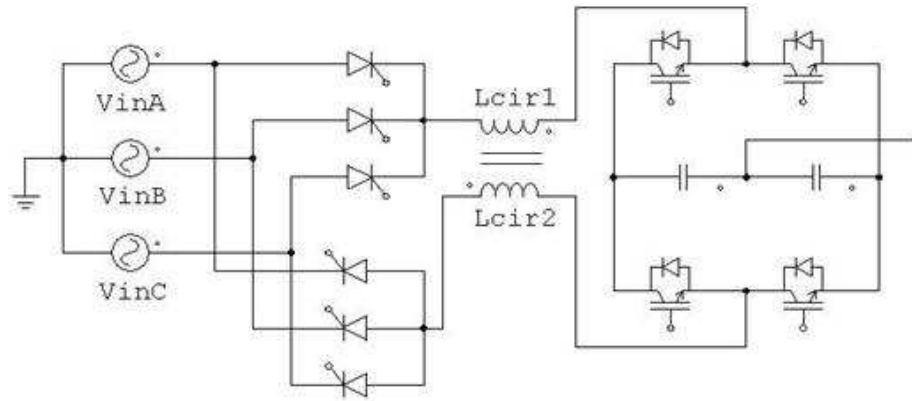
Fig. 3.4: Single-phase output hybrid cycloconverter in CCM

In order to improve the quality of the output voltage, which in this arrangement represents the common mode voltage component generated by the cycloconverter, the DC-link capacitor in Fig. 3.1 is split into two similar capacitors connected in series and the load is connected to the middle point of these two capacitors. This means that the cycloconverter is able to make use of the voltage across these two capacitors to compensate the difference between the actual output voltage delivered by the standard cycloconverter and the required reference output voltage.

In addition, as the circulating current can only flow from the positive thyristor half bridge to the negative thyristor half bridge due to the unidirectional conducting characteristics of the thyristors, the switches in H-bridge inverter do not need to have bidirectional capability. This means that the H-bridge through connecting one IGBT (without anti-parallel diode) and one diode in series for each leg is enough to handle both directions of the load current and the circulating current. Therefore, an asymmetrical inverter leg structure is a perfect fit to each thyristor half bridge, as both are designed to handle unidirectional (only positive or only negative) current.

An alternative topology to the two-leg H-bridge inverter shown in Fig. 3.4 uses a three-leg bridge inverter with two asymmetric legs and a full inverter leg added and

works on the same operational principle but has some advantages compared to the two-leg topology. This three-leg topology will be discussed in Section 3.3.

3.2.2.2 The Circulating Current-Free Mode Hybrid Cycloconverter

If the hybrid cycloconverter is operating in circulating current-free mode, no circulating current reactor is needed and thus the output of the positive thyristor half bridge is shorted with the output of negative thyristor half bridge, as shown in Fig. 3.5. The output voltage of the thyristor bridge is controlled by phase control of three positive bridge thyristors whilst the negative bridge thyristors are kept off when the positive current is supplied to the load; when load current is negative, the output voltage is controlled by phase control of the three negative bridge thyristors whilst the positive bridge thyristors are kept off. Similar to the topology shown in Fig. 3.4, the load is still connected to the middle point of the split DC-link capacitors. However, only one full inverter leg is connected with the output of both positive and negative thyristor half bridges as it is able to handle both the positive and negative load current. In this situation, according to the reference which is the difference between the actual output of the standard cycloconverter (shorted thyristor half bridges) and the required output voltage, the auxiliary inverter is able to improve the output voltage significantly without having to take any actions (handle any stresses) in regard to the differential mode voltage.
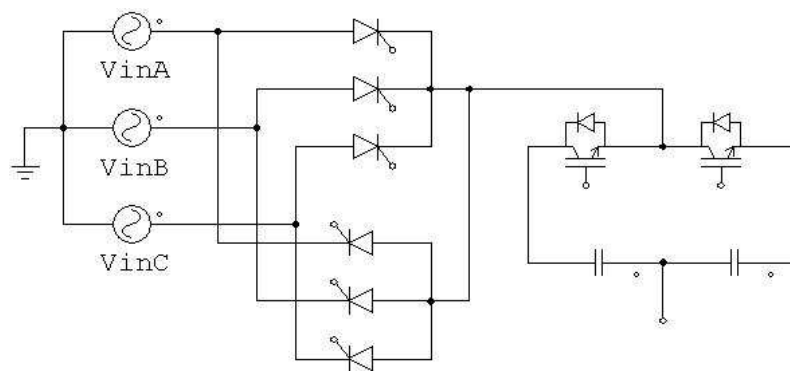
Fig. 3.5: Single-phase output hybrid cycloconverter in CCFM

In the following sections, to avoid any confusion between the topologies of circulating current mode and circulating current-free mode, the single full inverter leg shown in Fig. 3.5 will be split to two asymmetric legs to make the auxiliary inverter an

H-bridge inverter which is similar to the topology of the circulating current mode. A three-leg bridge inverter implementation in circulating current-free mode will also be presented in Section 3.3.

3.3   Hybrid Cycloconverter Topologies

Based on the previous explanation, the possible topologies for three-phase to single-phase and the resulting three-phase to three-phase arrangements will be presented in this section. Since the thyristor half bridges remain the same regardless of the operating mode, the main characteristics which are used to distinguish the different topologies of hybrid cycloconverter are: i) if the circulating current reactor is employed ii) the structure of the added bridge.

3.3.1 Three-Phase to Single-Phase Hybrid Cycloconverters

Two possible topologies of hybrid cycloconverter, the two-asymmetric-leg H-bridge inverter with split DC-link capacitors and the three-leg bridge inverter single DC-link capacitor, have been proposed. The latter is used as the topology of this work as it has some advantages compared with the former.

3.3.1.1 The Asymmetric H-bridge Inverter with Split DC-link Capacitors

In circulating current mode, as shown in Fig. 3.6, two IGBTs and two diodes embedded in a two-asymmetrical-leg H-bridge inverter with split DC-link capacitors. As mentioned in Section 3.2, the asymmetrical inverter leg structure is a perfect fit for each thyristor half bridge in handling unidirectional (positive/negative) current, as only two IGBTs without anti-parallel diode and two diodes are needed in the H-bridge inverter. As the left leg is used to handle the positive load current whilst the right leg is used to handle negative load current, *C1/C2* will be charged/discharged by load current when the current is positive and discharged/charged by load current when the current negative. Although *C1* and *C2* will also both be charged or discharged by circulating current, the frequency of load current is much lower and the amplitude is relatively high. Therefore, the ripple across the two DC-link capacitors is mainly

decided by the load current. However, the total DC-link capacitor voltage may not be affected by the load current seriously as whenever *C1* is charged by the load current *C2* is discharged by the load current and vice versa.
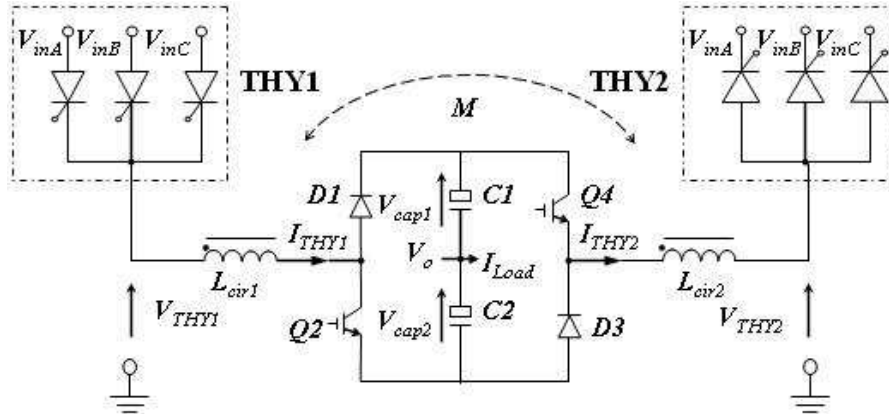
Fig. 3.6: The diagram of a three-phase to single-phase hybrid cycloconverter with split DC-link capacitors operating in CCM

As the circulating current reactor is only needed when the cycloconverter operates in circulating current mode, the output of each thyristor half bridge can be connected together when the cycloconverter is operating in circulating current-free mode as shown in Fig. 3.7, the two asymmetric legs of the H-bridge inverter become a single full leg (half bridge inverter). However, as mentioned Subsection 3.2.2.2, to avoid any confusion with circulating current mode, the two-asymmetric-leg H-bridge is still used for circulating current-free mode.
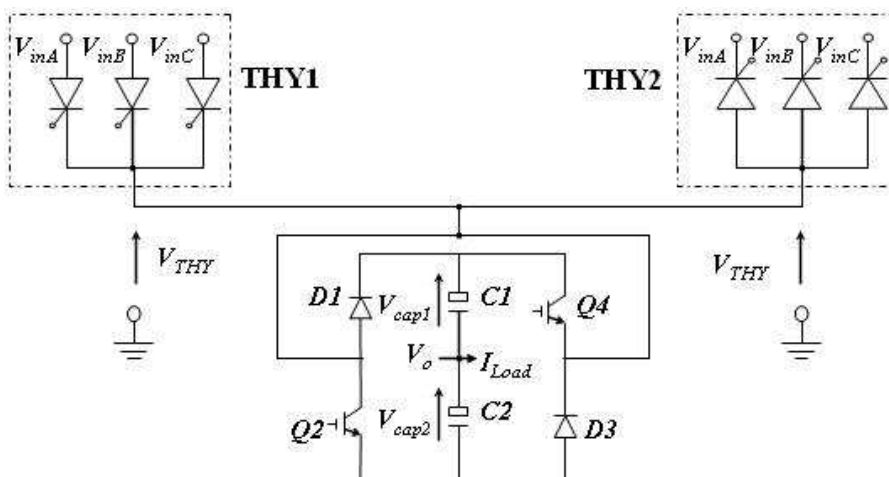
Fig. 3.7: The diagram of a three-phase to single-phase hybrid cycloconverter with split DC-link capacitors operating in CCFM

3.3.1.2 The Three-leg Bridge Inverter with a Single DC-link Capacitor

Another alternative hybrid cycloconverter operating in circulating current mode, as shown in Fig. 3.8, is the one in which an additional full inverter leg is added to the bridge and the load is connected to the middle point of the added leg. Therefore, the split DC-link capacitors in two-leg H-bridge can be merged into one capacitor. The advantage of this topology is that the DC-link capacitor voltage is half of the voltage in two-leg H-bridge. This characteristic will help to reduce the voltage rating of power devices in the bridge inverter by 50%. Furthermore, unlike the two-leg H-bridge, the charging or discharging of the DC-link capacitor by the load current not only depends on the direction of the load current, but also depends on the common mode voltage control. A detailed explanation will be presented in Section 3.5. Therefore, the DC-link capacitor in the three-leg bridge inverter handles only a fraction of the load current amplitude at much higher frequency which means the load current is less influential on the DC-link capacitor. This makes the control of the DC-link capacitor voltage easier than the two-leg H-bridge. Hence, the three-leg bridge inverter is preferred in this work to be used for the hybrid cycloconverter although two extra IGBTs with anti-parallel diodes are needed to constitute the third symmetric leg.
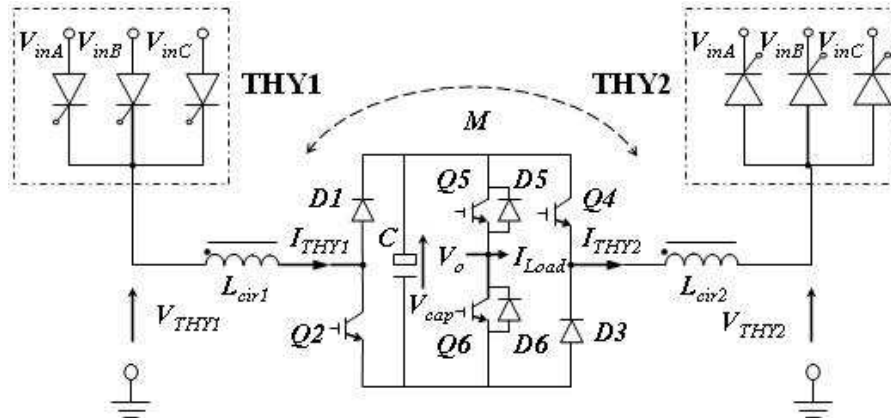
Fig. 3.8: The diagram of a three-phase to single-phase hybrid cycloconverter with a single DC-link capacitor operating in CCM

In addition, as the two-leg H-bridge inverter, the three-leg bridge inverter does not need any circulating current reactors if the auxiliary inverter operates under circulating current-free mode as shown in Fig. 3.9.
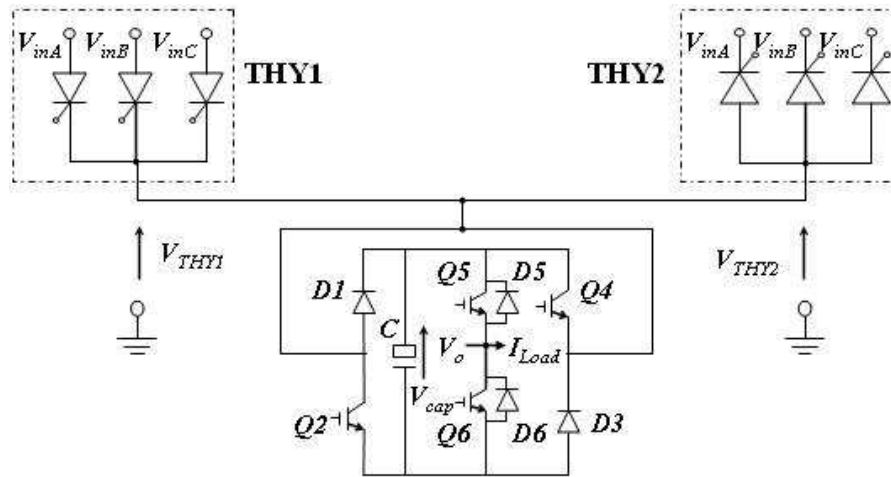
Fig. 3.9: The diagram of a three-phase to single-phase hybrid cycloconverter with a single DC-link capacitor operating in CCFM

3.3.2 Three-Phase to Three-Phase Hybrid Cycloconverter Arrangements

Fig. 3.10 shows topology for three-phase input to three-phase output hybrid cycloconverter in circulating current mode.
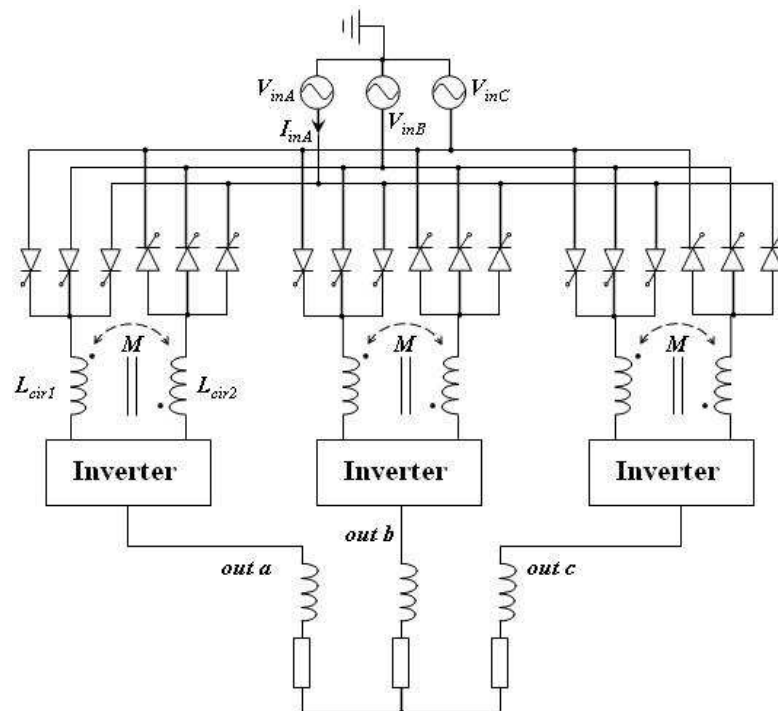
Fig. 3.10: The diagram of a three-phase to three-phase hybrid cycloconverter operating in CCM (for the "Inverter" topology, see Fig. 3.6 and 3.8)

Fig. 3.11 shows topology for three-phase input to three-phase output hybrid cycloconverter in circulating current-free mode. As most of the loads have a floating neutral, it means that the line-to-line voltage waveform is most relevant for evaluating the harmonic load side performance of the converter. Zero sequence voltages that appear in all outputs will not be able to produce current harmonics and therefore it is possible to have an improvement in quality for a three-phase output connection. More explanation in regard to this improvement will be presented in Chapter 4.
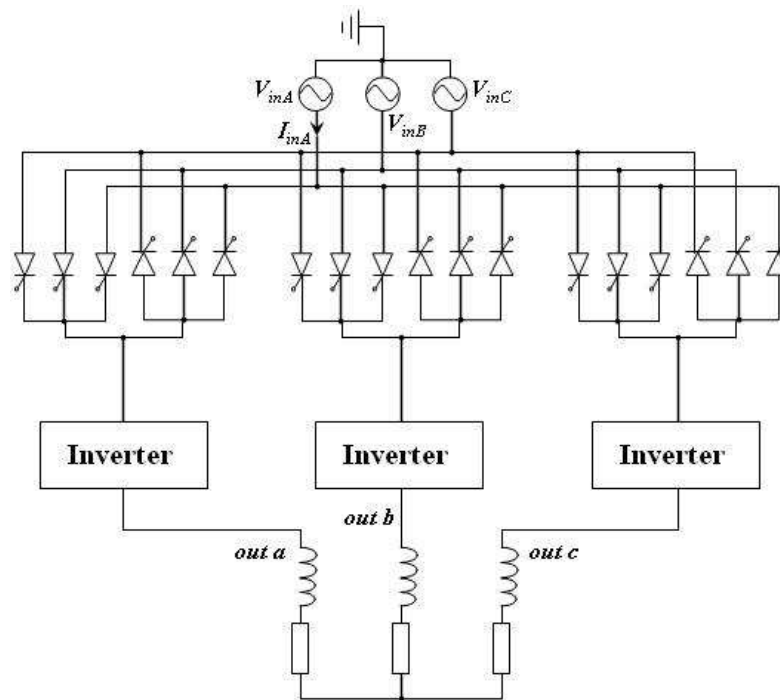
Fig. 3.11: The diagram of a three-phase to three-phase hybrid cycloconverter operating in CCFM (for the "Inverter" topology, see Fig. 3.7 and 3.9)

3.4   Control of the Hybrid Cycloconverter

In the hybrid cycloconverter, as shown in Fig. 3.12, the control circuit mainly comprises four parts: i) the differential mode voltage control; ii) the common mode voltage control; iii) the DC-link capacitor voltage control; iv) the PWM generation for the auxiliary inverter. Fig. 3.13 is a control diagram for the hybrid cycloconverter containing the detailed control loops for all the significant parts.

Fig. 3.12: Overall control diagram of the hybrid cycloconverter

Fig. 3.13: Detailed control loop of the hybrid cycloconverter

Differential mode voltage control is only needed when the hybrid cycloconverter operates in circulating current mode. Although there are some slight differences between the control methods when the cycloconverter operates in different modes, the principles are the same. As mentioned above, each inverter leg is able to generate a high frequency PWM voltage waveform which is used to cancel the low frequency harmonics present in both the differential mode voltage and the common mode

voltage produced by the thyristor bridges. In this section, the control principle for the circulating current mode and circulating current-free mode hybrid arrangements will be explained, and unless the corresponding figures are mentioned, all the explanation below is applied to the topologies from Fig. 3.6 – 3.9. For the detailed switching states explanation please refer to Section 3.5.

3.4.1 Differential Mode Voltage Control

Differential mode voltage (V_{diff}) control, as shown in Fig. 3.14, is needed if the hybrid cycloconverter operates with circulating current. As illustrated in Section 3.2, the auxiliary inverter is able to operate at high frequency in order to cancel the low frequency harmonics contained in the differential mode voltage, resulting in only high frequency ripple added on the circulating current.
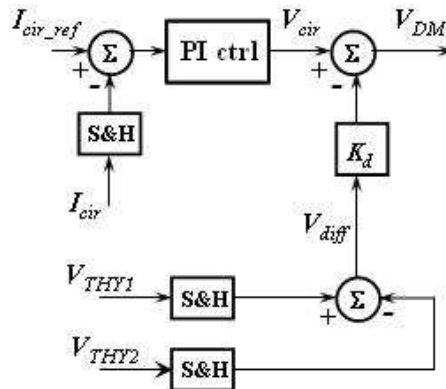
Fig. 3.14: Differential mode voltage control loop

In order to accurately control the circulating current around a DC reference, a fast PI controller should be employed which will produce a reference voltage (V_{cir}) estimating the amount of voltage drop that will appear across the two circulating current reactors in order to make the circulating current follow its reference. However, in order to ease the task of the PI controller and ensure the circulating current through the reactors is as smooth as possible without any low frequency components present, the method of feedforward compensation is used in the differential mode voltage control. By knowing that the disturbance for the PI controller is the variable differential mode voltage produced by the two thyristor half bridges, feedforward is applied by adding this voltage to the output of the PI controller to generate the actual differential mode

voltage reference (V_{DM}) that needs to be synthesized by the auxiliary inverter. With this reference voltage, the auxiliary inverter is able to produce a high frequency PWM voltage (Fig. 3.6 and 3.8: *Q2* and *Q4* = ON inserts $+V_{cap}$ *or* $+(V_{cap1} + V_{cap2})$ and *Q2* and *Q4* = OFF inserts $-V_{cap}$ *or* $-(V_{cap1} + V_{cap2})$)) which contains components that have the same frequency but anti-phase as the differential mode voltage harmonics in its low frequency spectrum. With the low frequency harmonic cancellation between the differential mode voltage produced by the thyristor half bridges and the PWM voltage produced by the auxiliary inverter, the low frequency harmonic voltage across the circulating current reactors is much reduced and only the small high switching frequency components are left across the reactors. Therefore, according to Equation (2.3), the circulating current reactor can be minimized and the circulating current can also be controlled as a DC current with some small ripple on it, since the $V_{diff\text{-}pk}$ across the circulating current reactor is much reduced and the ω is equal to the high switching frequency. The switching states which will be referred to in the following subsections are defined as: D_{active} when *Q2* and *Q4* are both ON or OFF to insert a positive or negative DC-link capacitor voltage between the two thyristor half bridges and D_{zero} when one of *Q2* and *Q4* is ON and another one is OFF resulting in zero voltage insertion between the two thyristor half bridges.

3.4.2 Common Mode Voltage Control

The common mode voltage produced by the two thyristor half bridges is normally the output voltage in a standard cycloconverter (($V_{THY1} + V_{THY2}$)/2 or V_{THY}). This common mode voltage contains, besides the desired output frequency component, the low order harmonics caused by the way the thyristor devices are commutated. These harmonics need to be minimized using the forced commutated auxiliary inverter in both circulating current mode and circulating current-free mode.

In circulating current mode, as shown in Fig. 3.15, the reference of the common mode voltage V_{CM} to be injected by the forced commutated auxiliary inverter is generated by using the standard cycloconverter output voltage and subtracting it from the reference of the output voltage when the inverter is a two-leg H-bridge structure. However, when the auxiliary inverter is connected as a three-leg bridge structure, the reference

of the common mode voltage V_{CM} generated in the H-bridge structure can only be applied to the inverter after the effect of the active duty cycle on the generated output voltage is taken into consideration. This means that V_{CM} for the three-leg auxiliary inverter is derived from adding or subtracting D_{active} times the half of the DC-link capacitor voltage from the reference of the output voltage depending on both the direction of the differential mode voltage and the load current. A proportional gain controller K_c is also needed to adapt the common mode voltage reference to the same scaling as the output voltage of the standard cycloconverter.

In circulating current-free mode, the output voltage of the active thyristor half bridge ($V_{THY} = V_{THY1} = V_{THY2}$) is subtracted from the ripple-free reference waveform (V_{out_ref}) to produce the common-mode voltage reference that needs to be injected by the auxiliary inverter in order to remove the unwanted low frequency voltage distortions.
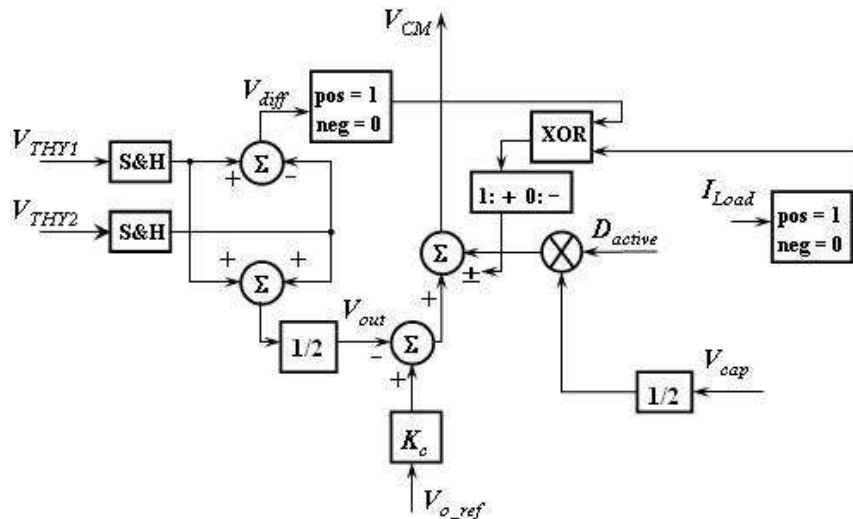
Fig. 3.15: Common mode voltage control loop

3.4.3 DC-link Capacitor Voltage Control

The voltage across the auxiliary inverter DC-link capacitor(s) is used as the voltage source to perform the desired actions on the differential mode voltage and the common mode voltage generated by the thyristor half bridges. Therefore, the DC-link capacitor voltage control loop is needed to maintain the average voltage across the capacitor(s) constant and equal to the DC-link capacitor voltage reference. The DC-link capacitor voltage control loop is shown in Fig. 3.16.
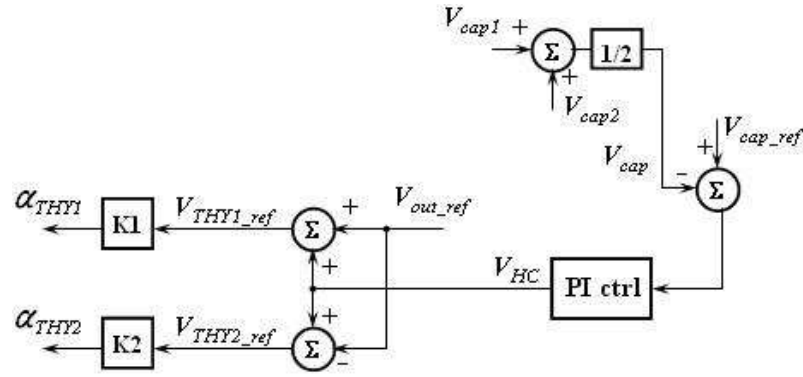
Fig. 3.16: DC-link capacitor voltage control loop of the auxiliary inverter

First of all, there is a minimum voltage level that the DC-link capacitor voltage has to meet in order to avoid over-modulation which limits the action of the auxiliary inverter. The DC-link capacitor voltage has also to be higher than the peak value of the differential mode voltage if the auxiliary inverter is operating in circulating current mode to ensure the circulating current is under control all the time. Moreover, due to the differential mode and common mode voltage control, the differential current and the load current will inevitably flow through the auxiliary inverter DC-link capacitor(s), charging or discharging it, and will inevitably cause a voltage ripple across it. If there is any disturbance or any small DC component in the current, the capacitor voltage may drift away from the pre-set voltage level. Therefore, in order to ensure proper operation of the auxiliary inverter, the DC-link capacitor voltage has to be under control as well. To implement this, the average of the capacitor voltages V_{cap1} and V_{cap2} (Fig. 3.6 and 3.7, or only one capacitor voltage V_{cap} for the three-leg bridge inverter in Fig. 3.8 and 3.9) are monitored by a PI controller, which generates a smooth offset signal that is added/subtracted to/from the reference of the output voltage that produces the firing angles for the two thyristor half bridges. If the imbalance between the two capacitor voltages in the H-bridge inverter topology is taken into consideration, the difference between these two voltages may have to be monitored and controlled as well. This feature has not been presented in the control loop as only the three-leg bridge inverter will be implemented in this work. The speed of the PI controller for the DC-link capacitor voltage does not have to be very fast as only the average, not the instantaneous capacitor voltage, has to be controlled.

When the cycloconverter operates in the circulating current mode, in the active state the DC-link capacitor(s) is charged by the circulating current when the differential

mode voltage is positive and discharged by the circulating current when the instantaneous differential mode voltage is negative. Hence, increase in the DC-link capacitor voltage can be achieved by generating a positive offset between the voltage of the positive thyristor half bridge and the voltage of the negative thyristor half bridge because during an active state, the time of charging the DC-link capacitor by the circulating current will be longer than discharging it. As the positive/negative reference will generate negative/positive voltage in the negative half bridge, the DC-link capacitor voltage can be increased by increasing both the reference voltage for the positive and the negative thyristor half bridges, and vice versa if the DC-capacitor voltage needs to be decreased. But there is one more issue that needs to be considered: when the differential mode voltage is positive in the active state, if the auxiliary inverter is a two-leg H-bridge topology (Fig. 3.6 and 3.7), the upper capacitor (*C1*) will be charged by the load current when the load current is positive whilst the lower capacitor (*C2*) will also be charged by the load current when the load current is negative. Similarily, one of the split capacitors will be discharged by the load current in the active state depending on the direction of the current when the differential mode voltage is negative. Therefore, for a two-leg H-bridge inverter, the total DC-link capacitor voltage will raise for a positive differential mode voltage and reduce for a negative differential mode voltage due to both the circulating current and the load current in the active state. However, for a three-leg bridge inverter (Fig. 3.8 and 3.9), the variation of the DC-link capacitor voltage is decided only by the circulating current in the active state since only the circulating current is flowing through the DC-link capacitor during this state.

During the zero state, the DC-link capacitor voltage can only be controlled by the load current because the circulating current loop has been bypassed by excluding the DC-link capacitor(s) in all circumstances. When the load current is positive, the time for charging the capacitor is longer than discharging if the common mode voltage of the two thyristor half bridges increases (increasing the positive thyristor half bridge reference voltage and decreasing the negative thyristor half bridge reference voltage) and vice versa when the common mode voltage of two thyristor half bridges decreases. Similarly, when the load current is negative, the time for charging the capacitor is longer than discharging if the common mode voltage of two thyristor half bridges decreases (decreasing the positive thyristor half bridge reference and increasing the

negative thyristor half bridge reference voltage) and vice versa when the common mode voltage of two thyristor half bridges increases.

Therefore, based on the above analysis, there are two ways to control the DC-link capacitor voltage: i) control the differential mode voltage of the standard cycloconverter; ii) control the common mode voltage of the standard cycloconverter. However, as mentioned above, the first method causes the two thyristor half bridge reference voltages to change in opposite directions (injecting differential mode voltage whilst keeping the common mode voltage unchanged), which is completely different from the second method where the positive and negative reference voltages always change in the same direction (injecting common mode voltage whilst keeping the differential mode voltage unchanged). Therefore, these two methods cannot be fully used at the same time as they will undermine the ability of each other's outcome. In another words, the DC-link capacitor voltage can be controlled solely by either the differential mode voltage or the common mode voltage, or can be controlled partially by the differential mode voltage and the common mode voltage at the same time. In this work, the differential mode voltage in the active state is selected to control the DC-link capacitor voltage in circulating current mode. This is because the circulating current used to charge or discharge the capacitor will be controlled to be a DC current which is much easier when using a PI controller with a limited bandwidth than to achieve a variable reference (i.e. the load current as mentioned above) and, as mentioned above, the load current control may introduce some very low frequency harmonics to the output of cycloconverter, which should be avoided.

When the auxiliary inverter operates in circulating current-free mode, the DC-link capacitor voltage can only be controlled by the common mode voltage as there is no differential mode voltage between the two thyristor half bridges. When the load current is positive, the time of charging by load current for the capacitor is longer than discharging when the common mode voltage of the thyristor half bridges increases. In contrast, when the load current is negative decreasing the common mode voltage of thyristor bridges will provide more time for charging the capacitor than discharging. As the inverter is operating without circulating current, only the positive thyristor half bridge will be conducting if the load current is positive whilst the negative thyristor half bridge will be conducting if the load current is negative. Therefore, to increase the

DC-link capacitor voltage, when the current is positive the reference voltage for the positive thyristor half bridge has to be increased; when the current is negative the reference voltage for the negative thyristor half bridge has to be increased when the current is negative. All the description for increasing the DC-link capacitor voltage above is reversed if the DC-link capacitor voltage needs to be reduced.

3.4.4 PWM Generation for the Auxiliary Inverter

The differential mode voltage control loop produces the differential mode voltage reference, V_{DM}, and the common mode voltage control loop circuit generates the common mode voltage reference, V_{CM}. These two voltage references can be used to generate the references for the voltage between each leg of the auxiliary inverter and the output of the load side, V_{HB1_ref} and V_{HB2_ref}, as shown in Fig. 3.17. Therefore, the duty-cycles for the two transistors *Q2* and *Q4* can be determined by dividing the reference voltage of each inverter leg by the DC-link capacitor voltage. The gate pulses are then produced by the PWM generator block by multiplying the two duty-cycles with the switching period and arranging the switching states of the auxiliary inverter accordingly. The zero switching state will generate the desired common mode voltage according to the reference V_{CM}, whilst the ratio between the two active switching states (Fig. 3.6 and 3.8: *Q1* and *Q2* = ON or *Q1* and *Q2* = OFF which means that the auxiliary inverter inserts V_{cap1} and V_{cap2} (or just V_{cap}) with opposite polarities in the circuit, ideally canceling each other) generates the desired differential mode voltage according to the reference V_{DM}. When the hybrid cycloconverter is connected with a three-leg bridge inverter (Fig. 3.8 and 3.9), the duty cycles of *Q5* and *Q6* can be decided by the states of *Q2* and *Q4* as well as the direction of the load current and the common mode voltage reference for the auxiliary inverter (V_{CM}).

However, the loop as shown in Fig. 3.17 is an alternative approach to generate the gate pulses for the auxiliary inverter, which will be used in this work. In circulating current mode, the active duty cycle (D_{active}) is the result of summing the output of the circulating current PI controller to the feedforward compensation of the differential mode voltage. Therefore, only the states within the zero duty cycle for the auxiliary

inverter need to be calculated through the duty cycle calculator block shown in Fig. 3.17. All the relevant equations in this block used for calculation can be derived as shown below. In circulating current-free mode, as the differential mode voltage control is no longer required, only the zero state is generated by the PWM generation which means the entire switching period can be used for compensating the common mode voltage without considering the differential mode voltage. Therefore, the duty cycles of all the possible states within the zero state in this mode can be obtained by just substituting 0 for D_{active} and 1.0 for D_{zero} in the following equations.
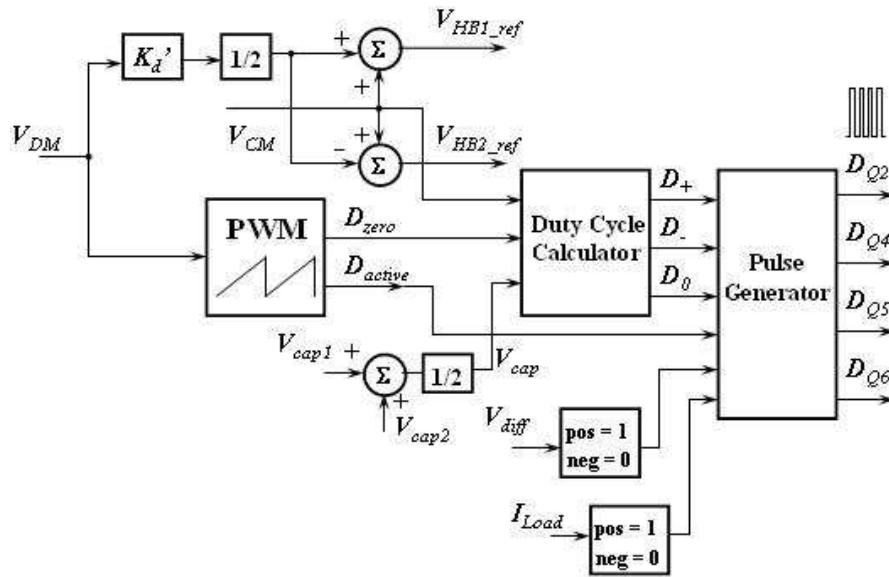
Fig. 3.17: PWM generation loop of the auxiliary inverter

Before giving the equations of all the duty cycles in the zero state in the different topologies, the equations of the differential mode voltage and the common mode voltage of the thyristor half bridges are given for reference:

$$V_{diff} = V_{THY1} - V_{THY2} \tag{3.1}$$

$$V_{out} = \frac{V_{THY1} + V_{THY2}}{2} \text{ (CCM)} \quad \text{or} \quad V_{out} = V_{THY} \text{ (CCFM)} \tag{3.2}$$

When the auxiliary inverter is a two-leg H-bridge topology, it is assumed that the total DC-link capacitor voltage is $2V_c$ with the upper capacitor voltage V_{cap1} having the same level as the lower capacitor voltage V_{cap2}. Hence, the common mode voltage will

be controlled using two-level PWM voltages ($+V_c$ and $-V_c$). This means that during the zero state the output voltage of the hybrid cycloconverter is obtained from the standard cycloconverter output voltage ((V_{THY1}+ V_{THY2})/2) plus or minus V_c. Therefore, the zero state (D_{zero}) in the two-leg H-bridge topology comprises two duty cycles: D_+ when the positive V_c is injected by the auxiliary inverter; D_- when the negative V_c is injected by the auxiliary inverter. A switching sequence comprising all the possible states within a switching period for the H-bridge inverter is shown as Fig.3.18.
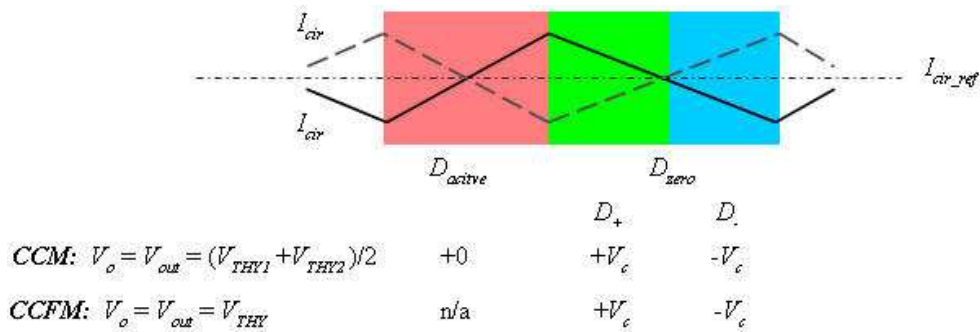
Fig. 3.18: The switching sequence for the two-leg H-bridge inverter

For the two-leg H-bridge inverter, all the duty cycles can be expressed:

$$D_{zero} = 1 - D_{active} \tag{3.3}$$

$$D_- = \frac{V_{CM} - D_{zero} \times V_c}{-2 \cdot V_c} = \frac{(K_c \cdot V_{o\_ref} - V_{out}) - D_{zero} \times V_c}{-2 \cdot V_c} \tag{3.4}$$

$$D_+ = D_{zero} - D_- \tag{3.5}$$

The output voltage of the hybrid cycloconverter can be calculated accordingly:

$$V_o = V_{out} \times D_{active} + (V_{out} - V_c) \times D_- + (V_{out} + V_c) \times D_+ \tag{3.6}$$

When the auxiliary inverter is a three-leg bridge topology, assuming that the DC-link capacitor voltage is V_c, all the three level PWM voltages available ($+V_c$, $-V_c$ and 0) can be used to control the common mode voltage. This means that during the zero state the output voltage of the hybrid cycloconverter is generated by adding or subtracting V_c to

or from the standard cycloconverter output voltage ((V_{THY1}+ V_{THY2})/2). Therefore, in addition to the duty cycles (D_+, D_-) mentioned in the case of the H-bridge topology, there is a duty cycle (D_0), existing within the zero state, during which the DC-link capacitor of the auxiliary inverter is bypassed between the output of the hybrid and the standard cycloconverter. All the relevant duty cycles are calculated according to the following equations. Similar to the two-leg H-bridge inverter, a switching sequence which includes all the possible states within a switching period for the three-leg bridge inverter is shown as Fig. 3.19.

		D_+	D_0
CCM: $V_o = V_{out} = (V_{THY1} + V_{THY2})/2$	$+V_c/2$ or $-V_c/2$	$+V_c$	$+0$
CCFM: $V_o = V_{out} = V_{THY}$	n/a	$+V_c$	n/a
		D_-	D_0
CCM: $V_o = V_{out} = (V_{THY1} + V_{THY2})/2$	$+V_c/2$ or $-V_c/2$	$-V_c$	$+0$
CCFM: $V_o = V_{out} = V_{THY}$	n/a	$+V_c$	n/a
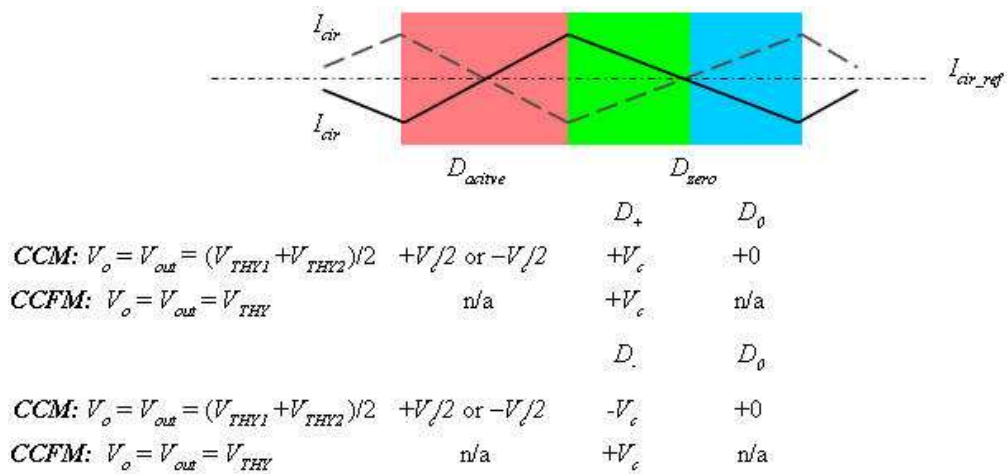
Fig. 3.19: The switching sequence for the three-leg bridge inverter

For the three-leg bridge inverter, all the duty cycles stated here can be expressed:

$$D_{zero} = 1 - D_{active} \tag{3.7}$$

There are two situations. When $V_{diff} > 0$ and $I_{Load} > 0$ or $V_{diff} < 0$ and $I_{Load} < 0$:

If $V_{CM} = ((V_{o\_ref} - V_{out}) - D_{active} \times \dfrac{V_c}{2}) < 0$

$$D_- = \frac{V_{CM}}{-V_c} = \frac{(V_{o\_ref} - V_{out}) - D_{active} \times \dfrac{V_c}{2}}{-V_c} \tag{3.8}$$

$$D_0 = D_{zero} - D_- \tag{3.9}$$

$$D_+ = 0 \tag{3.10}$$

$$V_o = (V_{out} + \frac{V_c}{2}) \times D_{active} + (V_{out} - V_c) \times D_- + V_{out} \times D_0 \tag{3.11}$$

If $V_{CM} = ((V_{o\_ref} - V_{out}) - D_{active} \times \frac{V_c}{2}) > 0$

$$D_+ = \frac{V_{CM}}{V_c} = \frac{(V_{o\_ref} - V_{out}) - D_{active} \times \frac{V_c}{2}}{V_c} \tag{3.12}$$

$$D_0 = D_{zero} - D_+ \tag{3.13}$$

$$D_- = 0 \tag{3.14}$$

$$V_o = (V_{out} + \frac{V_c}{2}) \times D_{active} + (V_{out} + V_c) \times D_+ + V_{out} \times D_0 \tag{3.15}$$

When $V_{diff} > 0$ and $I_{Load} < 0$ or $V_{diff} < 0$ and $I_{Load} > 0$

If $V_{CM} = ((V_{o\_ref} - V_{out}) + D_{active} \times \frac{V_c}{2}) < 0$

$$D_- = \frac{V_{CM}}{-V_c} = \frac{(V_{o\_ref} - V_{out}) + D_{active} \times \frac{V_c}{2}}{-V_c} \tag{3.16}$$

$$D_0 = D_{zero} - D_- \tag{3.17}$$

$$D_+ = 0 \tag{3.18}$$

$$V_o = (V_{out} - \frac{V_c}{2}) \times D_{active} + (V_{out} - V_c) \times D_- + V_{out} \times D_0 \tag{3.19}$$

If $V_{CM} = ((V_{o\_ref} - V_{out}) + D_{active} \times \dfrac{V_c}{2}) > 0$

$$D_+ = \frac{V_{CM}}{V_c} = \frac{(V_{o\_ref} - V_{out}) + D_{active} \times \dfrac{V_c}{2}}{V_c} \tag{3.20}$$

$$D_0 = D_{zero} - D_+ \tag{3.21}$$

$$D_- = 0 \tag{3.22}$$

$$V_o = (V_{out} - \frac{V_c}{2}) \times D_{active} + (V_{out} + V_c) \times D_+ + V_{out} \times D_0 \tag{3.23}$$

After D_{active} and D_{zero} (D_+ , D_- and D_0) have been obtained and by knowing the direction of both the differential mode voltage and the load current, the gate pulses for IGBTs in the auxiliary inverter can be generated. The detailed switching states will be explained in the next section and the truth tables are listed in Appendix C.

3.5   Switching States Analysis

As mentioned above, the auxiliary inverter is able to produce two voltage or three voltage levels for both the differential mode voltage control and the common mode voltage control depending on the number of legs in the bridge. The interconnection is also different when the cycloconverter is operating with or without circulating current; this is because for the circulating current-free mode, there is no differential voltage generated by the thyristor half bridges for the auxiliary inverter to cancel.

In general, in order to implement the differential mode voltage and common mode voltage control, an appropriate switching sequence to gate the power devices of the auxiliary inverter should be employed. However, the switching states in this sequence may be different from each other for different hybrid topologies or operating modes. In this section, the detailed analysis for all the possible switching states in the different

topologies will be presented. The analysis below is based on an assumption that the parameters of the whole circuit are symmetrical, for example the values of the two circulating current reactors are identical, the voltages across the two DC-link capacitors are identical, the voltages drop in all the diodes are identical. The truth tables for the semiconductors in the auxiliary inverter and all the relevant values or directions of voltages and currents have also been exhibited as tables in Appendix C.

3.5.1 The Asymmetric H-bridge Inverter with Split DC-link Capacitors

In the following subsections, the detailed switching states of two-leg H-bridge inverter in both circulating current mode and circulating current-free mode will be presented.

3.5.1.1 Circulating Current Mode Switching States

Even though the H-bridge inverter has only two legs, the inverter is still able to produce three-level PWM voltages for the cancelation of the differential mode voltage but can produce only two-level voltages to control the common mode voltage ripple. In every switching period, the active switch state (D_{active}) is the duty cycle when the H-bridge inverter inserts $-2V_c$ (*Q2* and *Q4* off) or $+2V_c$ (*Q2* and *Q4* on) between the outputs of the thyristor half bridges whilst the zero switch state (D_{zero}) is the duty cycle when the H-bridge inverter generates zero voltage (*Q4* on and *Q2* off or *Q4* off and *Q2* on) between the outputs of the thyristor half bridges. In circulating current mode the DC-link capacitor voltage will be controlled only by the differential mode voltage although both the differential mode voltage and the common mode voltage can be used no matter if the auxiliary inverter is a two-leg H-bridge or a three-leg bridge topology. In the active states, both of the DC-link capacitors in the H-bridge are charged by the circulating current when the differential mode voltage is positive and are discharged by the circulating current when the differential mode voltage is negative. This indicates that it is possible to control the DC-link capacitor voltage by means of injecting a positive or negative offset in the differential mode voltage.

When the differential mode voltage is positive, *D1* and *D3* are conducting in the active state (D_{active}) to insert an opposite voltage ($-2V_c$) between the positive and negative

thyristor half bridges in order to force the reduction of the circulating current as shown in Fig. 3.20 and Fig. 3.21. Due to the unipolar characteristics of the thyristor half bridges, both of the DC-link capacitors are charged by the circulating current during the active state. Moreover, due to the same reason, if the load current is positive, the load current will flow through *D1* and charge *C1* and charge *C2* and flow back through *D3* if the load current is negative. As the output of the hybrid cycloconverter is connected to the mid point of the circuit defined by the circulating current path during the active state, it means that the common mode voltage contribution of the auxiliary inverter will cancel and that the output voltage will be equal to half the sum of the two thyristor output voltages ((V_{THY1} + V_{THY2})/2) under the assumption that the parameters of the whole circuit are symmetrical.

Fig. 3.22 and Fig. 3.23 shows the conduction path through the auxiliary inverter when the thyristor half bridges differential mode voltage is negative. *Q2* and *Q4* are the devices to conduct during the active state to insert a positive voltage (+$2V_c$) between the thyristor half bridges in order to force the circulating current to rise; both of the DC-link capacitors are then discharged by the circulating current. In this situation, the load current discharges *C2* if its direction is positive and discharges *C1* if its direction is negative. Similar to the situation when the differential mode voltage is positive, the output voltage is still half the sum of the positive and the negative thyristor half bridge output voltages ((V_{THY1} + V_{THY2})/2) during the active state.

$C1$ & $C2$ are charged by I_{cir}, $C1$ is charged by I_{Load}
$$V_o = (V_{THY1} + V_{THY2})/2$$

Fig. 3.20: Conduction path through the auxiliary inverter during the active switching state when *Q2* and *Q4* are off and the load current is positive - two-leg H-bridge in CCM

C1 & C2 are charged by I_{cir}, C2 is charged by I_{Load}
$V_o = (V_{THY1} + V_{THY2})/2$

Fig. 3.21: Conduction path through the auxiliary inverter during the active switching state when *Q2* and *Q4* are off and the load current is negative - two-leg H-bridge in CCM

C1 & C2 are discharged by I_{cir}, C2 is discharged by I_{Load}
$V_o = (V_{THY1} + V_{THY2})/2$

Fig. 3.22: Conduction path through the auxiliary inverter during the active switching state when *Q2* and *Q4* are on and the load current is positive - two-leg H-bridge in CCM

C1 & C2 are discharged by I_{cir}, C1 is discharged by I_{Load}
$V_o = (V_{THY1} + V_{THY2})/2$
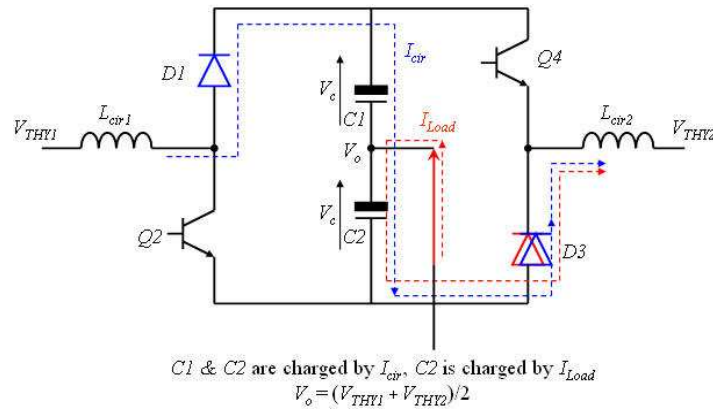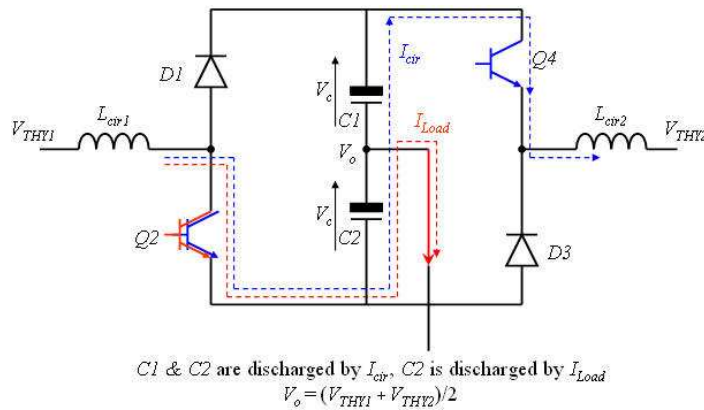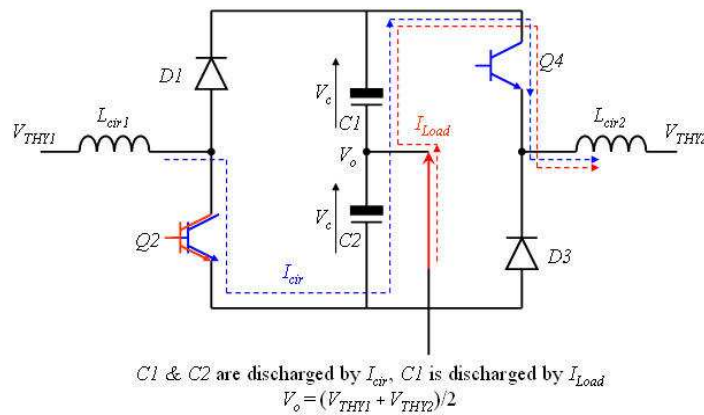
Fig. 3.23: Conduction path through the auxiliary inverter during the active switching state when *Q2* and *Q4* are on and the load current is negative - two-leg H-bridge in CCM

Whenever the differential voltage is positive or negative, during the zero state the H-bridge inverter inserts zero voltage between the outputs of the positive and negative thyristor half bridges, which means *D1* and *Q4* or *Q2* and *D3* will be in conduction. The circulating current will then follow the differential mode voltage: it will increase if the differential mode voltage is positive and will decrease if the differential mode voltage is negative. Since the DC-link capacitors are bypassed, both of the capacitors will maintain their state of charge. As referred to in Subsection 3.4.2, the common mode voltage of the two thyristor half bridges can only be controlled with the two available voltage levels that correspond to the zero state of the inverter: the output voltage is generated by adding or subtracting V_c to or from the standard cycloconverter output voltage (Equation (3.6)).

When *D1* and *Q4* are conducting, as shown in Fig. 3.24 and Fig. 3.25, the output voltage is half the sum of two thyristor half bridge voltages minus V_c ((V_{THY1}+ V_{THY2})/2 - V_c). *C1* is charged or discharged by the load current determined by its direction whilst the voltage across *C2* remains constant.

When *Q2* and *D3* are conducting, as shown in Fig. 3.26 and Fig. 3.27, half the DC-link voltage $+V_c$ is inserted between the output voltages of the hybrid cycloconverter ((V_{THY1}+ V_{THY2})/2 + V_c) and the standard cycloconverter. Under this circumstance, the voltage across *C1* remains constant and *C2* is charged or discharged by the load current depending on its direction.

$C1$ is charged by I_{Load}, $V_o = (V_{THY1} + V_{THY2})/2 - V_c$

Fig. 3.24: Conduction path through the auxiliary inverter during the zero switching state when *Q2* is off and *Q4* is on and the load current is positive - two-leg H-bridge in CCM

$C1$ is discharged by I_{Load}, $V_o = (V_{THY1} + V_{THY2})/2 - V_c$

Fig. 3.25: Conduction path through the auxiliary inverter during the zero switching state when *Q2* is off and *Q4* is on and the load current is negative - two-leg H-bridge in CCM

$C2$ is discharged by I_{Load}, $V_o = (V_{THY1} + V_{THY2})/2 + V_c$

Fig. 3.26: Conduction path through the auxiliary inverter during the zero switching state when *Q2* is on and *Q4* is off and the load current is positive - two-leg H-bridge in CCM

$C2$ is charged by I_{Load}, $V_o = (V_{THY1} + V_{THY2})/2 + V_c$
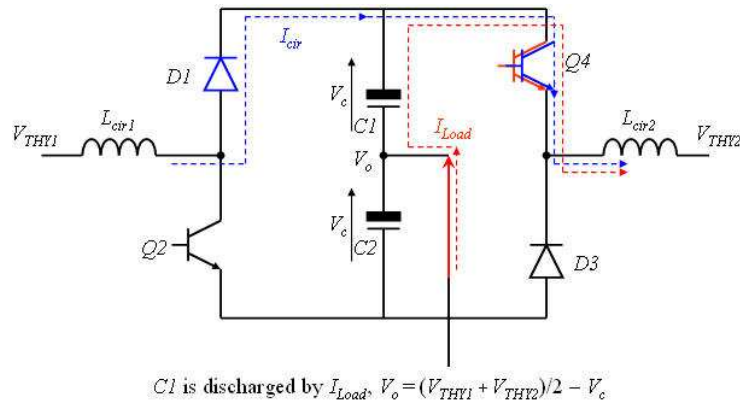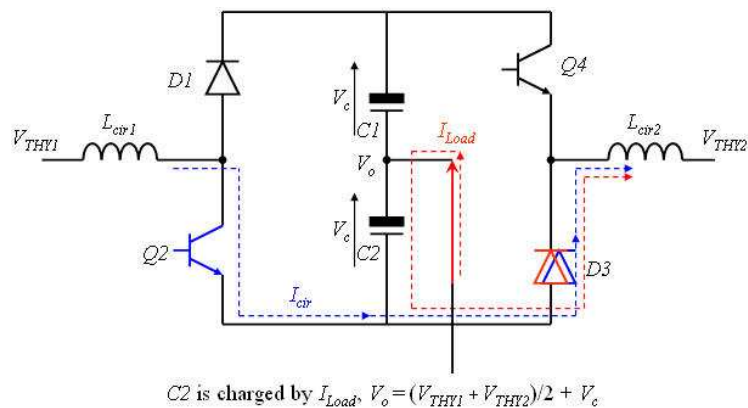
Fig. 3.27: Conduction path through the auxiliary inverter during the zero switching state when *Q2* is on and *Q4* is off and the load current is negative - two-leg H-bridge in CCM

3.5.1.2 Circulating Current-Free Mode Switching States

When the hybrid cycloconverter is operating in circulating current-free mode, the positive thyristor half bridge is directly connected to the negative thyristor half bridge, which means that there are no active states but only zero states. Therefore, in circulating current-free mode, unlike the circulating current mode, only the output voltage of the standard cycloconverter needs to be corrected by the auxiliary inverter, although it is still controlled by two-level PWM voltages due to the two-leg H-bridge inverter structure. This means that the output voltage of the hybrid cycloconverter is the output voltage of the standard cycloconverter plus or minus V_c. Similar to the previous circuit, *C1* is charged by the positive half wave of the load current and discharged by the negative load current whilst in opposition, *C2* is discharged by the positive half wave of the load current and charged by the negative load current.

If the output voltage of the standard cycloconverter is lower than the ripple-free reference voltage, $+V_c$ should be added to it for a given time to generate the correct hybrid cycloconverter output voltage ($V_{THY} + V_c$). As shown in Fig. 3.28 and Fig. 3.29, *Q2* needs to be switched on when the load current is positive and only *D3* is in conduction when the load current is negative to achieve the desired effect of inserting $+V_c$ between the output of the hybrid cycloconverter and the standard cycloconverter. C2 is charged or discharged by the load current based on its direction.

If the output voltage of the standard cycloconverter is higher than the output reference voltage, $-V_c$ has to be inserted between the output of the hybrid cycloconverter ($V_{THY} - V_c$) and the standard cycloconverter. When the load current is positive, Q4 has to be switched on but *D1* will provide the conduction path when the load current is negative as shown in Fig. 3.30 and Fig. 3.31. The DC-link capacitor is still charged or discharged by the load current depending on its direction.

C2 is discharged by I_{Load}, $V_o = V_{THY} + V_c$

Fig. 3.28: Conduction path through the auxiliary inverter when *Q2* is on and the load current is positive - two-leg H-bridge in CCFM

C2 is charged by I_{Load}, $V_o = V_{THY} + V_c$

Fig. 3.29: Conduction path through the auxiliary inverter when *Q4* is off and the load current is negative - two-leg H-bridge in CCFM

C1 is charged by I_{Load}, $V_o = V_{THY} - V_c$

Fig. 3.30: Conduction path through the auxiliary inverter when *Q2* is off and the load current is positive - two-leg H-bridge in CCFM

C1 is discharged by I_{Load}, $V_o = V_{THY} - V_c$
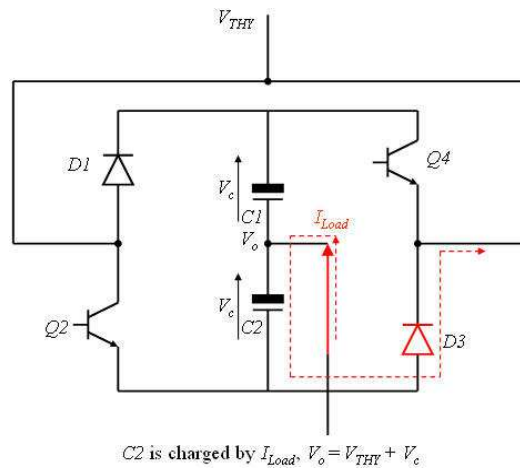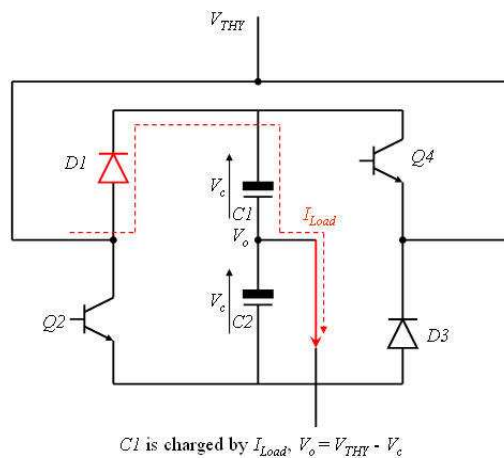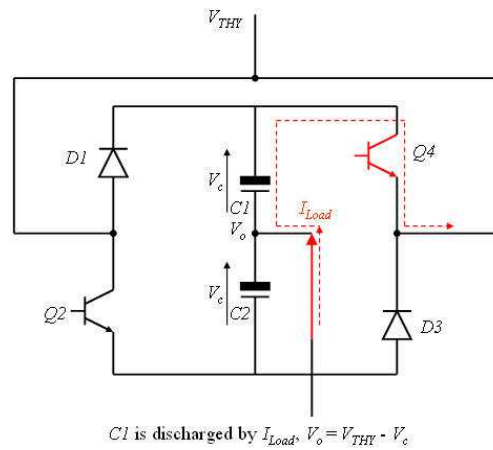
Fig. 3.31: Conduction path through the auxiliary inverter when *Q4* is on and the load current is negative - two-leg H-bridge in CCFM

3.5.2 The Three-leg Bridge Inverter with a Single DC-link Capacitor

Similar to the two-leg H-bridge inverter, the three-leg bridge inverter needs a proper switching sequence. The comprehensive analysis of the switching states in both circulating current mode and circulating current-free mode will be presented in the following two subsections.

3.5.2.1 Circulating Current Mode Switching States

In order to cancel the low frequency harmonics present in the differential mode voltage of the standard cycloconverter, the auxiliary inverter has to operate with a high switching frequency to generate an adjustable output voltage that is able to cancel the distortion present in the differential mode voltage. Furthermore, to ensure the circulating current can be kept under control, the DC-link capacitor voltage (V_c) should always be equal or higher than the peak of the differential mode voltage.

As the auxiliary inverter contains three legs, it is obvious that it is able to produce three-level PWM voltages to control both the differential mode voltage and the common mode voltage. As mentioned in Subsection 3.4.1, in every switching period, the active switching state (D_{active}) is defined as the duty cycle when the auxiliary

inverter inserts $-V_c$ (*D1* and *D3* ON) or $+V_c$ (*Q2* and *Q4* ON) between the thyristor half bridges whilst the zero switch state (D_{zero}) is defined as the duty cycle when the auxiliary inverter generates zero voltage (*D1* and *Q4* ON or *Q2* and *D3* ON) between the thyristor half bridges. When the hybrid cyclconverter is operating with circulating current, the DC-link capacitor voltage will be controlled by the differential mode voltage.

When the existing differential mode voltage of the two thyristor half bridges is positive, as shown in Fig. 3.32 and Fig. 3.33, *D1* and *D3* are conducting during the active state, inserting an opposite voltage ($-V_c$) between the positive and negative thyristor half bridge in order to reduce the circulating current. In this case, due to the unipolar characteristic of the circulating current, the DC-link capacitor is charged by the circulating current during the active state. Because the DC-link capacitor voltage is only controlled by the differential mode voltage and also to ensure the ripple across the capacitor is as small as possible, *Q5* is switched ON when the load current is positive and *Q6* is switched ON when the load current is negative, so as to avoid load current flowing through the capacitor. If it is assumed that the DC-link capacitor consists of two series capacitors, each having an equal $V_c/2$ across it, then the potential of the imaginary middle point of the two capacitors is half the sum of the positive and negative thyristor half bridge output voltages $((V_{THY1} + V_{THY2})/2)$. Therefore, the output voltage of the hybrid cycloconverter is $((V_{THY1} + V_{THY2})/2 + V_c/2)$ when *Q5* is ON and $((V_{THY1} + V_{THY2})/2 - V_c/2)$ when *Q6* is ON.

When the differential mode voltage is negative, *Q2* and *Q4* are conducting during the active state to insert a positive voltage ($+V_c$) between the positive and negative thyristor half bridges, as shown in Fig. 3.34 and Fig. 3.35, in order to raise the circulating current In this situation the DC-link capacitor is discharged by the circulating current. Furthermore, to avoid the load current flowing through the capacitor, both *Q5* and *Q6* are switched OFF during the whole active state whilst their anti-parallel diodes *D5* or *D6* are in conduction depending on the direction of the load current. This means that the output voltage is $((V_{THY1} + V_{THY2})/2 - V_c/2)$ when the load current is positive and $((V_{THY1} + V_{THY2})/2 + V_c/2)$ when the load current is negative.

C is charged by I_{cir}, $V_o = (V_{THY1} + V_{THY2})/2 + V_c/2$

Fig. 3.32: Conduction path through the auxiliary inverter during the active switching state when *Q2* and *Q4* are off and the load current is positive - three-leg bridge inverter in CCM

C is charged by I_{cir}, $V_o = (V_{THY1} + V_{THY2})/2 - V_c/2$

Fig. 3.33: Conduction path through the auxiliary inverter during the active switching state when *Q2* and *Q4* are off and the load current is negative - three-leg bridge inverter in CCM

C is discharged by I_{cir}, $V_o = (V_{THY1} + V_{THY2})/2 - V_c/2$

Fig. 3.34: Conduction path through the auxiliary inverter during the active switching state when *Q2* and *Q4* are on and the load current is positive - three-leg bridge inverter in CCM

C is discharged by I_{cir}, $V_o = (V_{THY1} + V_{THY2})/2 + V_c/2$
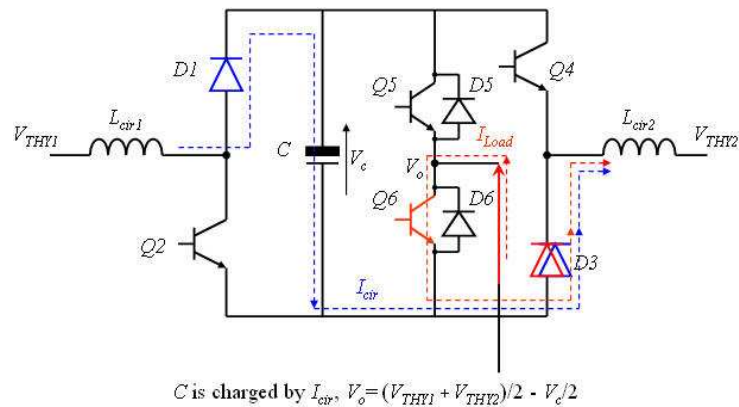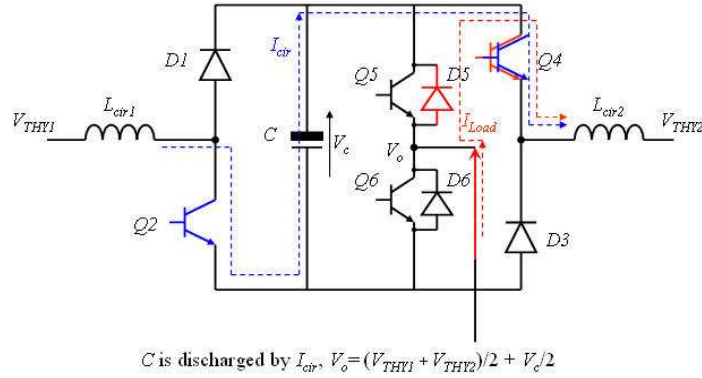
Fig. 3.35: Conduction path through the auxiliary inverter during the active switching state when *Q2* and *Q4* are on and the load current is negative - three-leg bridge inverter in CCM

Whenever the differential voltage is positive or negative, during the zero state the DC-link capacitor is bypassed by connecting the terminals of the circulating current reactor leading to the positive and negative thyristor half bridges, and this means *D1* and *Q4* or *Q2* and *D3* will be conducting. When the auxiliary inverter is a three-leg bridge topology, the common mode voltage of two thyristor half bridges is controlled during the zero state by a three-level PWM voltage; the output voltage is generated by adding/subtracting V_c to/from or remaining the same as the standard cycloconverter output voltage (($V_{THY1} + V_{THY2}$)/2).

When *D1* and *Q4* are conducting, as shown in Fig. 3.36 and Fig. 3.37, both *Q5* and *Q6* are switched off and only *D6* is in conduction when the load current is positive; when the load current is negative, only *Q6* is switched on, to generate $-V_c$ between the output voltage of the hybrid cycloconverter and the standard cycloconverter (($V_{THY1} + V_{THY2}$)/2 $- V_c$) (Equation (3.11), (3.19)). The DC-link capacitor is exclusively charged or discharged by the load current depending on the direction of the current itself.

When *Q2* and *D3* are conducting, *Q5* is switched on when the load current is positive; when the load current is negative, both *Q5* and *Q6* are switched off and only *D5* is in conduction, as shown in Fig. 3.38 and Fig. 3.39. The result is that a positive voltage $+V_c$ is inserted between the output of the hybrid cycloconverter (($V_{THY1} + V_{THY2}$)/2 $+ V_c$) and the standard cycloconverter (Equation (3.15), (3.23)). Again, the direction of the load current decides whether the DC-link capacitor voltage is charged or discharged by the load current.

C is charged by I_{Load}, $V_o = (V_{THY1} + V_{THY2})/2 - V_c$

Fig. 3.36: Conduction path through the auxiliary inverter during the zero switching state when *Q2* is off and *Q4* is on and the load current is positive - three-leg bridge inverter in CCM

C is discharged by I_{Load}, $V_o = (V_{THY1} + V_{THY2})/2 - V_c$

Fig. 3.37: Conduction path through the auxiliary inverter during the zero switching state when *Q2* is off and *Q4* is on and the load current is negative - three-leg bridge inverter in CCM

C is discharged by I_{Load}, $V_o = (V_{THY1} + V_{THY2})/2 + V_c$

Fig. 3.38: Conduction path through the auxiliary inverter during the zero switching state when *Q2* is on and *Q4* is off and the load current is positive - three-leg bridge inverter in CCM

V_C charged by I_{Load}, $V_o = (V_{THY1} + V_{THY2})/2 + V_c$
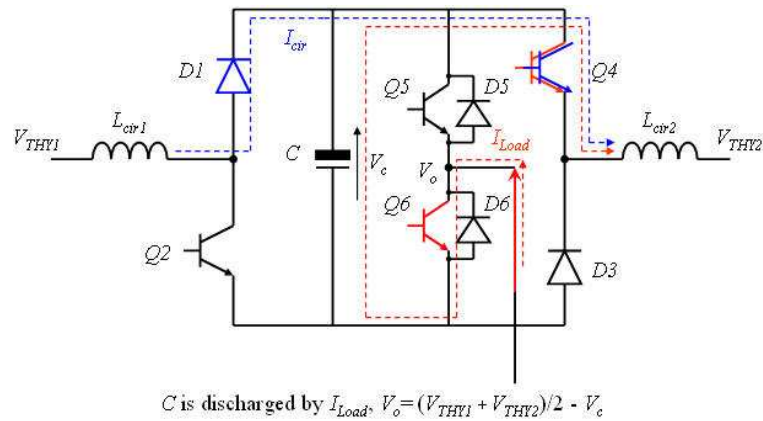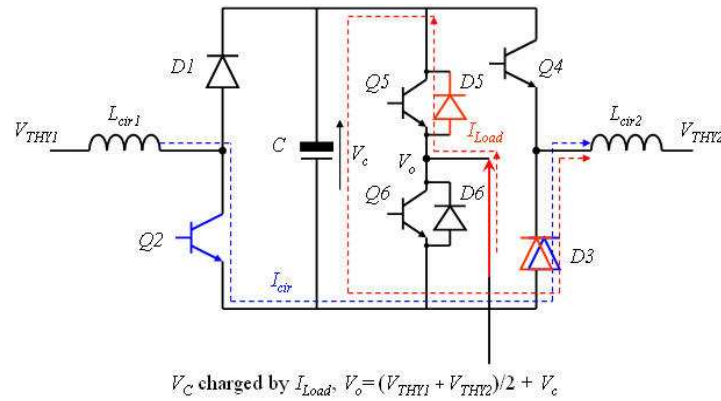
Fig. 3.39: Conduction path through the auxiliary inverter during the zero switching state when *Q2* is on and *Q4* is off and the load current is negative - three-leg bridge inverter in CCM

As the common mode voltage is under three-level PWM voltage control, in every zero state, there is a given time (D_0) in which the DC-link capacitor of the auxiliary inverter is bypassed. If during the D_0 state the load current is positive, *Q2* and *D3* are switched ON and *Q5* and *Q6* are switched OFF (or alternatively *D1* and *Q4* ON and *Q5* ON) to avoid the load current flowing through the DC-link capacitor and to ensure that the output voltage is equal to the standard cycloconverter output voltage. As there is a possibility of shoot-through between *Q5* and *Q6*, a dead time is needed between their gating signals during the commutation between these two switches. Therefore, it is better to minimize the number of switchings of *Q5* or *Q6*. This is why Fig. 3.40 shown below is the switching state without *Q5* or *Q6* conducting during the zero state.

V_c keeps constant, $V_o = (V_{THY1} + V_{THY2})/2$
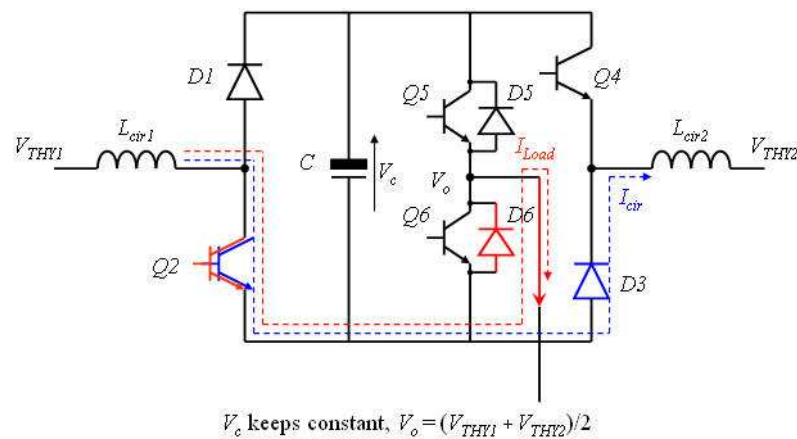
Fig. 3.40: Conduction path through the auxiliary inverter during the zero switching state when *Q2* is on and *Q4* is off, V_c remains constant and the load current is positive - three-leg bridge inverter in CCM

Similarly, if the load current is negative, *D1* and *Q4* have to be switched ON and *Q5* and *Q6* have to be kept OFF again (or alternatively *Q2* and *D3* ON and *Q6* ON) to achieve the same effect. For the same reason mentioned for the case of positive current, the *Q5* and *Q6* are choosen to be always kept off during D_0 state, as shown in Fig. 3.41.

V_c keeps constant, $V_o = (V_{THY1} + V_{THY2})/2$
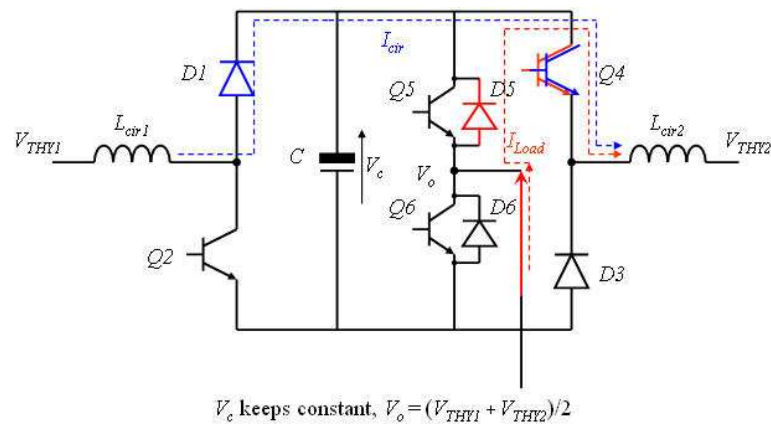
Fig. 3.41: Conduction path through the auxiliary inverter during the zero switching state when *Q2* is off and *Q4* is on, V_c remains constant and the load current is negative – three-leg bridge inverter in CCM

3.5.2.2 Circulating Current-Free Mode Switching States

When the hybrid cycloconverter is operating in circulating current-free mode, there are no active states but only zero states, as the positive thyristor half bridge output is directly connected with the negative thyristor half bridge output. Therefore, only the common mode voltage of the thyristor half bridges is needed to be improved by the auxiliary inverter. Similar to the circulating current mode situation, the three-leg bridge inverter is still able to control the common mode voltage by synthesizing a three-level PWM voltage, due to its structure. Whenever the load current is positive or negative, the output voltage of the hybrid cycloconverter is equal to the output voltage of the standard cycloconverter plus or minus V_c during D_+ or D_- or just the standard cycloconverter output voltage during in D_0.

If the output voltage of the standard cycloconverter is lower than the output ripple-free reference voltage, a positive voltage $+V_c$ should be added to it. When the load current is positive *Q2* and *Q5* are switched on whilst when the load current is negative, *D3*

and *D5* are in conduction to insert the wanted positive voltage $+V_c$ between the output of the hybrid cycloconverter and the standard cycloconverter ($V_{THY} + V_c$), as shown in Fig. 3.42 and Fig. 3.43 respectively. The DC-link capacitor is charged or discharged by the load current depending on its direction.
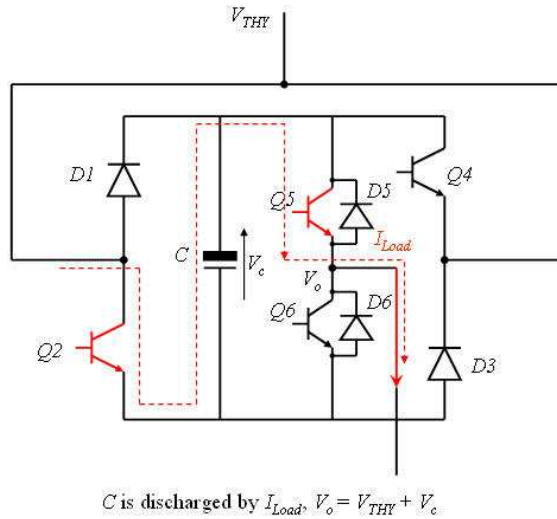
C is discharged by I_{Load}, $V_o = V_{THY} + V_c$

Fig. 3.42: Conduction path through the auxiliary inverter when *Q2* is on and the load current is positive - three-leg bridge inverter in CCFM

C is charged by I_{Load}, $V_o = V_{THY} + V_c$
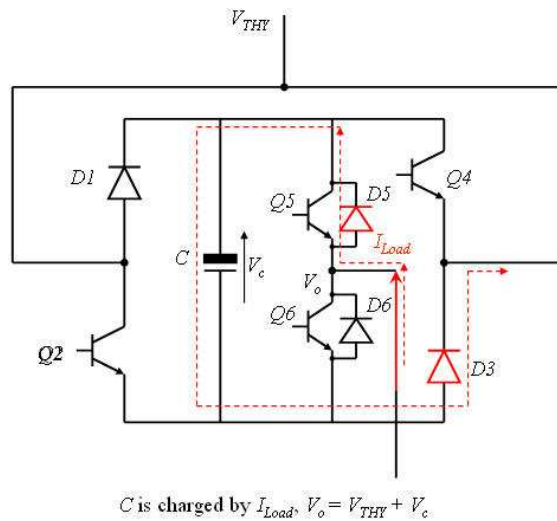
Fig. 3.43: Conduction path through the auxiliary inverter when *Q4* is off and the load current is negative - three-leg bridge inverter in CCFM

If the output voltage of the standard cycloconverter is higher than the reference of the hybrid cycloconverter output voltage, a negative voltage $-V_c$ is necessary to be inserted between the output voltage of the hybrid cycloconverter and the standard

cycloconverter ($V_{THY} - V_c$). This can be achieved by having *D1* and *D6* conducting when the load current is positive or when the load current is negative, switching ON *Q4* and *Q6* as shown in Fig. 3.44 and Fig. 3.45 respectively. The DC-link capacitor is still charged or discharged by the load current depending on its direction.
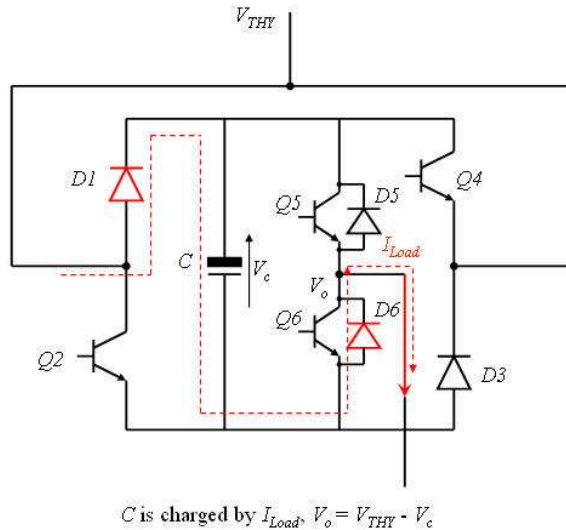
Fig. 3.44: Conduction path through the auxiliary inverter when *Q2* is off and the load current is positive - three-leg bridge inverter in CCFM
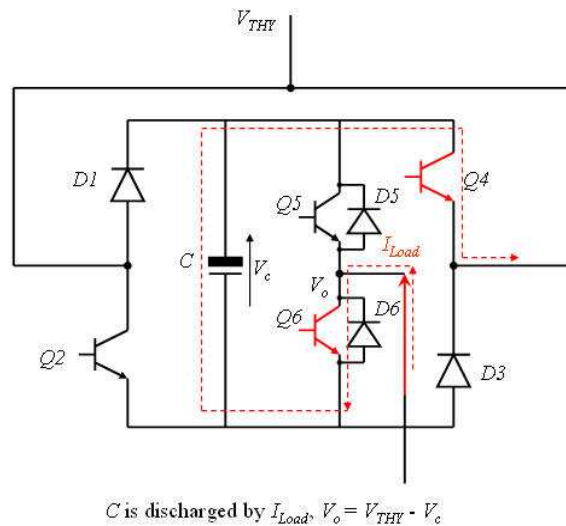
Fig. 3.45: Conduction path through the auxiliary inverter when *Q2* is on and the load current is negative - three-leg bridge inverter in CCFM

Similar to the circulating current mode, during the zero state there is a duty cycle (D_0) in which the output of the auxiliary inverter is completely bypassed to the output of the standard cycloconverter and the length of the duty cycle depends on the difference

between the output voltage of the standard cycloconverter and the output voltage reference. *Q5* and *Q6* have to remain switched off during this duty cycle to ensure that there is less chance of a shoot-through in the middle leg. When the load current is positive *Q2* and *D6* are in conduction whilst when the load current is negative *Q4* and *D5* are in conduction to connect the output of the hybrid cycloconverter directly to the output of the standard cycloconverter without any alteration caused by the DC-link capacitor voltage as shown in Fig. 3.46 and Fig. 3.47.

.
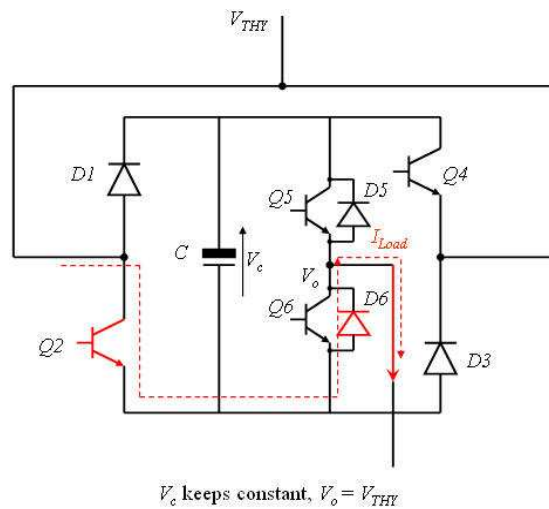
Fig. 3.46: Conduction path through the auxiliary inverter when *Q2* is on, V_c remains constant and the load current is positive - three-leg bridge inverter in CCFM
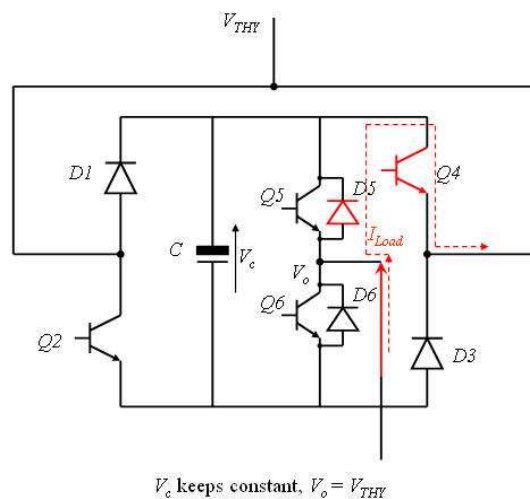
Fig. 3.47: Conduction path through the auxiliary inverter when *Q4* is on, V_c remains constant and the load current is negative - three-leg bridge inverter in CCFM

3.6 Summary

- 86 -

In this chapter a new power converter concept, the hybrid cycloconverter, has been presented as an alternative to the conventional cycloconverter in order to improve its performance. The hybrid concept is shown to have various implementation topologies depending on the operating mode and the structure of the auxiliary inverter. After the discussion the hybrid cycloconverter with a three-leg bridge inverter is selected as the topology for this work. An extensive analysis of the control structure for different parts of the circuit, such as differential mode voltage, common mode voltage, DC-link capacitor voltage, is presented. Then the illustration for all the possible switching states in different topologies is presented followed with the corresponding schematics of the conduction paths in the inverter. The analysis in this chapter reveals that this new concept is able to reduce low order distortion in the output voltage and to provide means to control the circulating current.

Chapter 4

Evaluation of Standard and Hybrid Cycloconverter with Saber Simulation

4.1 Introduction

In the previous two chapters, the principles of operation for both of the standard and hybrid cycloconverters have been illustrated theoretically. In this chapter, using the SABER software package, simulation models are implemented for both the standard and the hybrid cycloconverter (with three-leg bridge inverter) in circulating current mode and circulating current-free mode respectively. The SABER software is a powerful simulation engine particularly suited to power electronics; simulation models for a wide range of components and subsystems can be implemented in this software to emulate very accurately (depending on the complexity of the model) their real behaviour.

The detailed structures of the different topologies and their control strategies have been already presented in Chapter 2 and Chapter 3. Both the standard and the hybrid cycloconverters are 3-pulse (circulating current-free mode) and 6-pulse (circulating current mode) topologies, with a three-leg bridge inverter used for the hybrid topology. This chapter starts with an illustration of the design for each subsystem implemented in the simulation model. Thereafter, the simulation results for both the standard and the the hybrid cycloconverter operating in the two modes, with and without circulating current, are presented. Finally, the chapter concludes with a comparison between the standard and the hybrid cycloconverters, including those with higher number of pulses.

4.2   Simulation Model Design

Before the complete simulation can be created, some significant subsystems need to be implemented for the four different topologies. Most of the subsystems are comprised of electrical components obtained from the SABER standard library, selecting the required parameters for each of them. However, there are some blocks, such as the firing pulse generator, need to be written in the MAST modelling language, one of the most important features in the SABER. Since the hybrid topology is derived from the standard cycloconverter by adding an auxiliary inverter, a brief explanation of each subsystem implemented in the standard cycloconverter and the auxiliary inverter is outlined in this section.

4.2.1   The Standard Cycloconverter Design

In this subsection, the design for both the power converter and the control circuits of the standard cycloconverter is presented.

Three-Phase Power Supply

The mains power supply used in the simulation model is implemented by connecting three sine wave voltage sources obtained from the standard library of SABER, as shown in Fig. 4.1. The rated input voltage and frequency of the supply are set at 415V (rms, line-to-line voltage) and 50Hz respectively.
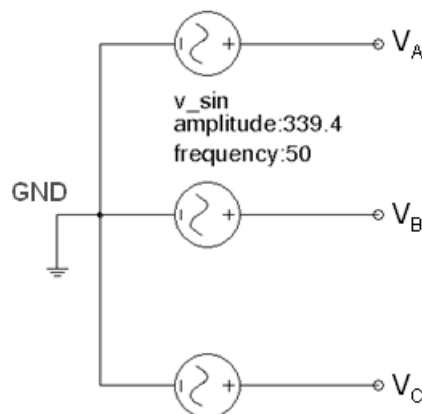
Fig. 4.1: Three-phase power supply in the simulation model

Thyristor Bridge

The thyristors, which are the SCR (silicon controlled rectifier) choosen from the category of semiconductor devices in standard library, are connected as positive and negative half bridges, as shown in Fig. 4.2. In order to make the simulation results as close as possible to the experimental results, the parameters of the thyristors are therefore configured with practical values. For example, the on-state resistance is set at 2mΩ, the direct forward voltage is set at 1.55V and the circuit commutated turn-off time is set at 100μs (all the values are close to those of the thyristors choosen for the prototype in order to make the comparison between the simulation results and experimental results).
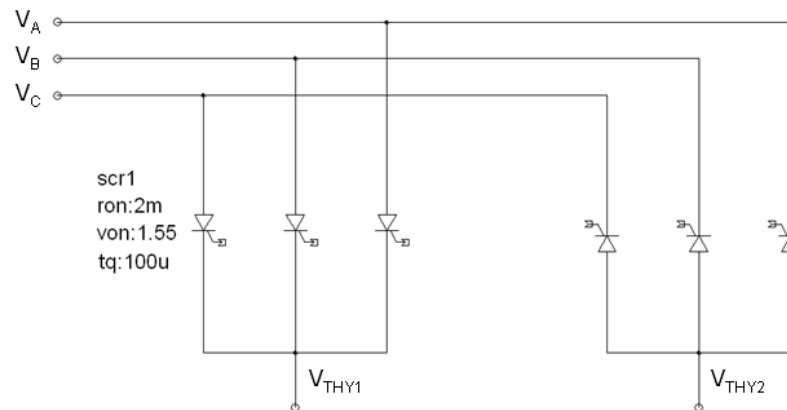
Fig. 4.2: The positive and negative thyristor half bridges in the simulation model

Thyristor Firing Pulse Generator

As the standard topology is able to achieve better performance with lower output frequency and higher output voltage ratio [pp.161, 1, pp.202, 3, 23], the 5Hz output frequency with 0.8 output modulation index (in order to allow sufficient reverse bias time for the thyristor to safely turn off) is selected as the benchmark operating point for all the topologies, with the simulation results being presented in Section 4.3 – 4.5. Therefore, as shown in Fig. 4.3, the amplitude and the frequency of the sine wave voltage source which is used as the reference of the output voltage are set at 0.8V and 5Hz. A 180º phase shift needs to be set between the references for the positive and negative thyristor half bridges to ensure the fundamental voltages generated by two half bridges are always in phase. In order to generalize some of the findings, two

additional operating points will be explored in Section 4.6: one at higher frequency (13Hz output frequency and 0.8 output modulation index) and another one at lower output modulation index (5Hz output frequency and 0.3 output modulation index).
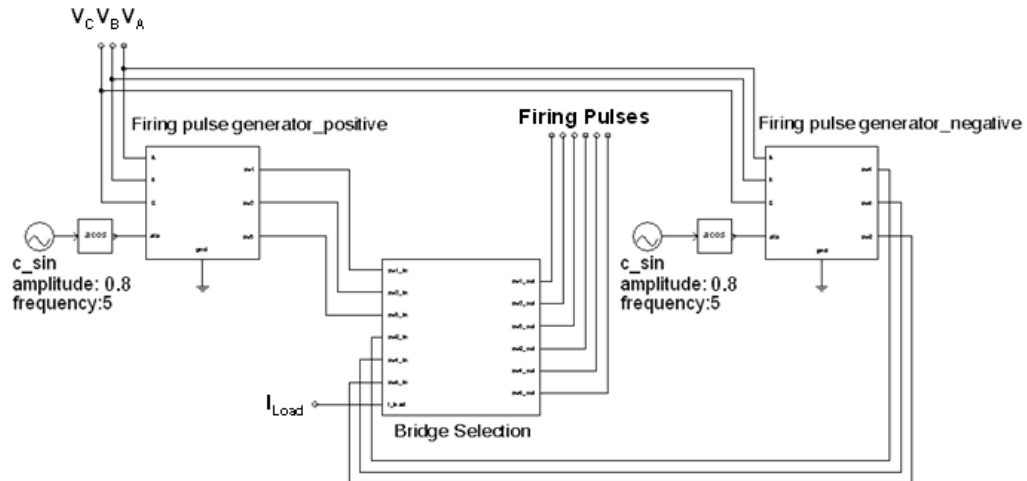
Fig. 4.3: Thyristor firing pulse generators and the bridge selection block in the simulation model

The firing pulse generators and the bridge selection block, as shown in Fig. 4.3, are all implemented by using the MAST modelling language. The sampling frequency of all the blocks is set at 5kHz. According to the provided sine wave references, the pulse generators can work out the time of the corresponding firing delay at each sampling point. Meanwhile, as can be seen from Fig. 4.3, the input phase-to-supply neutral voltages are all monitored by the pulse generators in order to detect the every intersection of the two input voltages which is the start of a firing delay. Therefore, with the obtained informations, the pulse generators are able to generate demanded firing pulses for both the positive and negative thyristor half bridges. The duration of each pulse is set at 2ms. If the standard cycloconverter operates in circulating current mode, the outputs of the pulse generators can be connected directly to the gate of the thyristors. However, the bridge selection block is required in circulating current-free mode to ensure safely commutation between two thyristor half bridges everytime when the load current changes polarity. As shown in Fig. 4.3, all the firing pulses generated by both pulses generators are connected to the selection block and the load current needs to be monitored by the block as well. The firing pulses for one thyristor half bridge from the output of the selection block are always blinded while the pulses are provided for the other one during the steady state. Nevertheless, every time when

the load current is detected to be near zero crossing, a trigger pulse is given to the thyristor in the complementary half bridge which is connected to the same input phase as the thyristor in conduction in order to enable bidirectional conduction path. After the current crosses zero and the outgoing thyristor has completely switched off, the firing pulses will be applied to the incoming thyristor half bridge. In this way, the bridge selection block is not only able to avoid any short circuit from happening but also prevent any over-voltage caused by disconnection of the load current from occurring, as the load current keeps flowing during the commutation.

Load

In this work, instead of using an inductive or synchronous motor (filter may also be required sometimes), a 400mH inductor and a 20Ω resistor are used to comprise a highly inductive load for the standard cycloconverters, as shown in Fig. 4.4. This load is also used in the hybrid cycloconverter models.
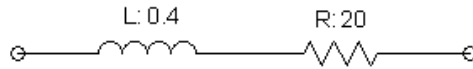
Fig. 4.4: The load used in the cycloconverter simulation models

Circulating Current Rectors and Measurement Circuit

The circulating current reactors are needed when the standard cycloconverter operates in circulating current mode. As can be seen from Fig. 4.5, two 100mH inductors are coupled together with 0.95 coupling coefficient. Two 0.5Ω resistors are connected in series with the inductors by taking the winding resistance into consideration.

The circulating current measurement circuit is implemented to obtain the circulating current waveform. If the two reactor currents (I_{THY1}, I_{THY2}) and the load current (I_{Load}) are obtained, it is not difficult to generate the circulating current (I_{cir}) based on Equation (4.1) by employing the summer and subtractor blocks, as shown in Fig. 4.5.

$$I_{cir} = \frac{(I_{THY1} + I_{THY2}) - |I_{Load}|}{2}$$

(4.1)

Both the circulating current reactors and the circulating current measurement circuit are also used in the hybrid topologies with the same parameters.
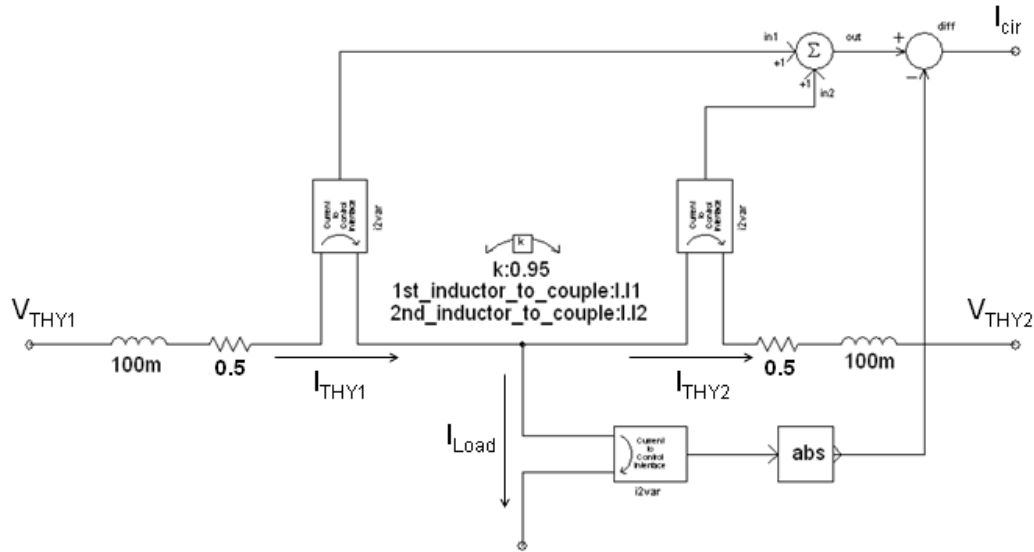
Fig. 4.5: The circulating current reactors and measurement circuit in the simulation model

4.2.2 The Auxiliary Inverter Design

In this subsection, the design for the three-leg bridge auxiliary inverter and the relevant control circuit in the hybrid cycloconverter is presented.

Three-leg Bridge Inverter

The three-leg bridge auxiliary inverter is built as shown in Fig. 4.6 with the parameters configured for the corresponding semiconductors (the values are similar to those of the devices choosen for prototype). These parameters incude: the on-state resistance of the diodes, the collector-to-emitter saturation voltage and the turn-on, turn-off time of the IGBTs. In order to achieve better control of the differential and common mode voltage, an 8200μF capacitor is selected as the DC-link capacitor to reduce the voltage ripple as smaller as possible. The value of the DC-link capacitor voltage is decided by taking both the installed power of the auxiliary inverter and the electrical performance of the hybrid cycloconverter into consideration, which will be explained in Section 4.3.
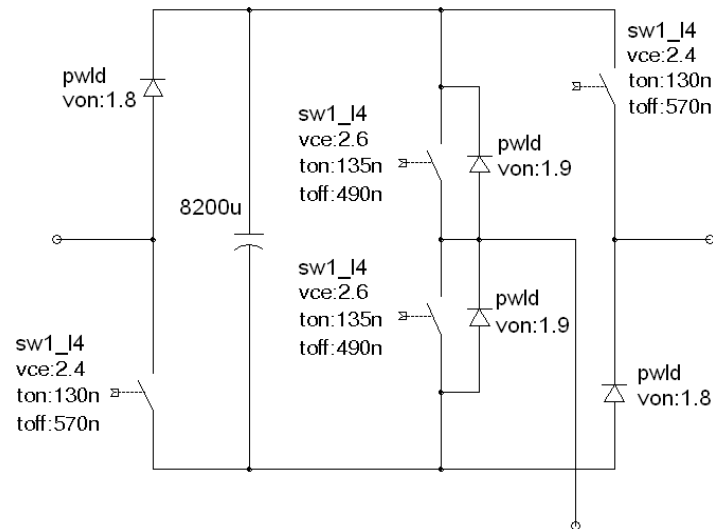
Fig. 4.6: The three-leg bridge inverter in the simulation model

Circulating Current PI controller

In the hybrid cycloconverter the circulating current needs to be monitored and controlled, which is realized by using PI controller. The circulating current PI controller is designed according to the Unitrode Application Note [56]. Fig. 4.7 shows a typical structure of a PWM controlled boost converter that uses a PI current controller, where the input voltage should be considered as the 150Hz low frequency differential mode voltage and the output voltage is equal the DC-link capacitor voltage for the case of this work.
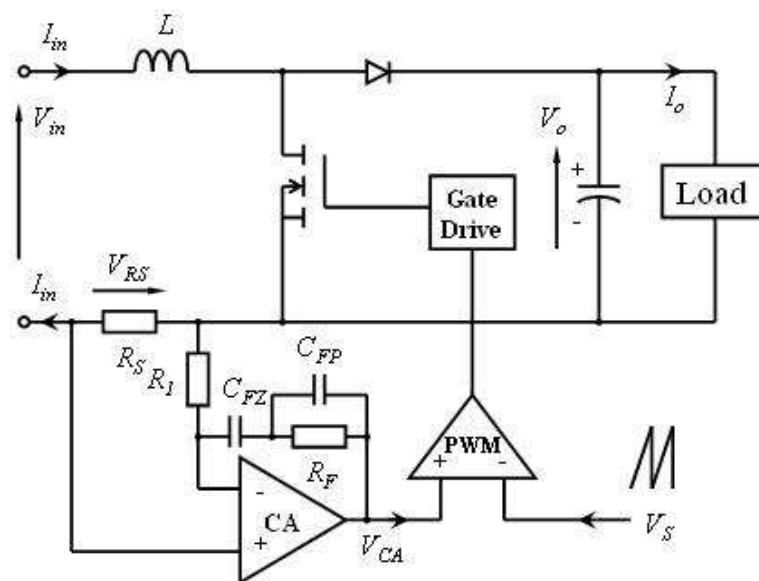
Fig. 4.7: Schematic of a boost converter that uses a PI current controller

The parameters which are relevant for designning the PI current controller are defined in Table. 4.1. The sense resistance is supposed to be 1Ω as the value of the circulating current is directly applied to the input of the PI controller without any current-to-voltage transformation procedure.

Symbols	Description	Value
V_s	Osillator peak to peak voltage	1V
f_s	Switching frequency of the auxiliary inverter	5kHz
R_s	The sense resistance	1Ω
V_o	Output voltage of boost converter	V_c

Table. 4.1: The value of the parameters used for designning a PI current controller

Therefore, the maximum Current Amplifier gain is:

$$G_{CA\_max} = \frac{V_{CA}}{V_{RS}} = \frac{V_S \times f_S \times (4 \times L_{cir})}{V_O \times R_S} = \frac{1 \times 5000 \times 0.4}{V_C \times 1} = \frac{2000}{V_C} = \frac{R_F}{R_1} \tag{4.2}$$

If suppose R_F is 1kΩ, the R_1 will be a variable depending on the value of the DC-link capacitor voltage:

$$R_1 = \frac{V_C}{2} \tag{4.3}$$

According to [56], the crossover frequency f_C is fixed at $f_S/6$ and the zero $R_F\, C_{FZ}$ of the circuiting current PI controller is set at 1/2 of the minimum crossover frequency:

$$C_{FZ} = \frac{12}{1000 \times 2\pi \times 5000} = 0.4\mu F \quad \text{for} \quad \frac{1}{R_F \times C_{FZ}} = 2\pi \times \frac{f_S}{12} \tag{4.4}$$

The pole of the controller is set at 6 times the zero frequency to eliminate noise spikes:

$$C_{FP} = \frac{C_{FZ}}{5} = 0.08\mu F \quad \text{for} \quad \frac{C_{FZ} + C_{FP}}{2\pi \times R_F \times C_{FZ} \times C_{FP}} = 6 \times \frac{1}{2\pi \times R_F \times C_{FZ}} \tag{4.5}$$

Therefore, the proportional gain, $K_{P\text{-}CCPI}$, and the integral gain, $K_{I\text{-}CCPI}$, of the circulating current PI controller can be obtained by Equation (4.6). If both the proportional gain and the integral gain are reduced, the speed of the controller will become slower.

$$K_{P-CCPI} = \frac{R_F}{R_1} \quad \text{and} \quad K_{I-CCPI} = \frac{1}{C_{FZ} \times R_1} \tag{4.6}$$

The circulating current PI controller implemented in the simulation model is shown in Fig. 4.8. The value of all the resistors and capacitors can be configured by using t he Equation (4.3) – (4.5) depending on the speed of the PI controller. As can be seen from the schematic, two extra DC voltage sources (0.5V and 2.5V) in conjunction with two diodes are used to ensure that the output of the PI controller remains within ±1V. In this way, the over-modulation can be avoided during PWM generation.
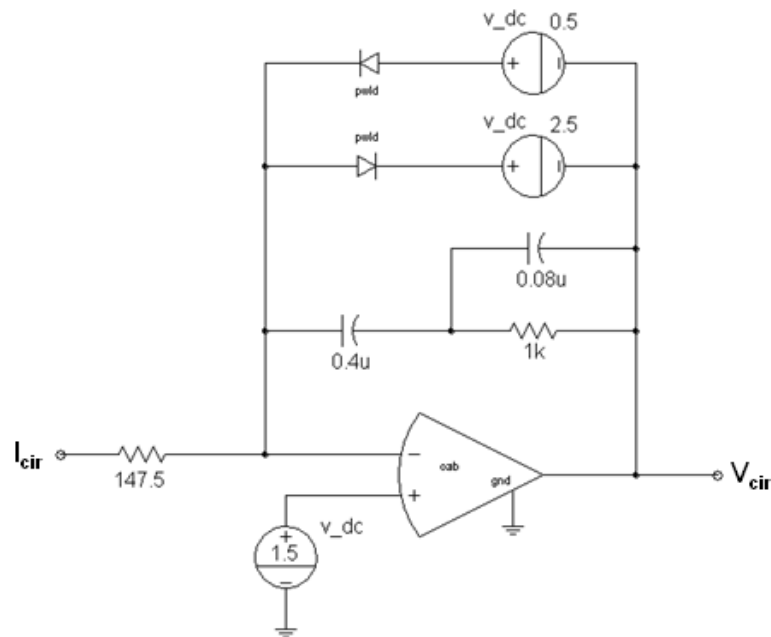
Fig. 4.8: The circulating current PI controller in the simulation model

DC-link Capacitor Voltage controller

Fig. 4.9 shows the schematic of the DC-link capacitor voltage controller in the simulation model. As can be seen from this figure, a transformer is used to reduce the DC-link capacitor voltage to a small value which can be used for control. The speed of

the controller for the DC-link capacitor voltage can be slower compared to the circulating current PI controller since only the average of the DC-link capacitor voltage needs to be controlled. Therefore, only an integral circuit is used as the controller to generate the offset for the output voltage reference in order to control the voltage across the DC-link capacitor to be maintained around the reference. If assuming R_D is 1kΩ and C_D is 1mF, according to Equation (5.29) the integral gain K_{I-DCPI} is 1.0, which is enough for ensuring the stability of the DC-link capacitor voltage.

$$K_{I-DCPI} = \frac{1}{R_D \times C_D} = \frac{1}{1000 \times 1 \times 10^{-3}} = 1 \qquad (4.7)$$

Since the output modulation index is 0.8, the absolute value of the output generated by the DC-link capacitor voltage controller should be smaller than 0.2V. Therefore, similar to the circulating current PI controller, two extra DC voltage sources with two diodes are utilized ensure that the output of the controller will not exceed ±0.1V.
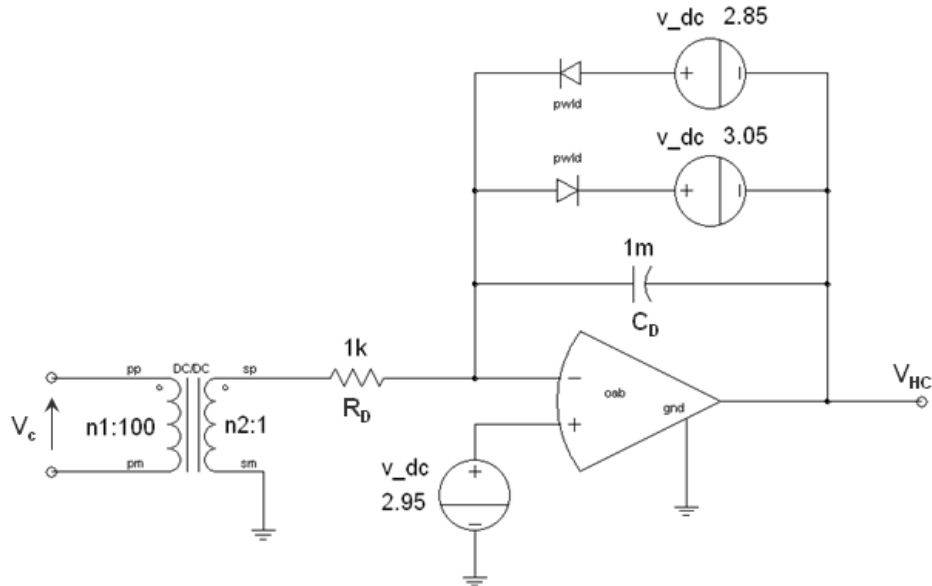
Fig. 4.9: The DC-link capacitor voltage controller in the simulation model

IGBT Gating Pulse Generator

As described in Chapter 3, the differential mode voltage reference, V_{DM}, is generated by adding the differential mode voltage (V_{diff}) to the output of the circulating current

PI controller (V_{cir}), as shown in Fig. 4.10. The active duty cycle (D_{active}) is derived from comparing the V_{DM} with 5kHz, ±1V triangle carrier waveforms. The common mode voltage reference, V_{CM}, is generated by subtracting the output voltage reference from the common mode voltage of the two thyristor half bridges (the effect of the active duty cycle on the output voltage will be considered in the IGBT gate pulse generator block). Therefore, with the acquired active duty cycle, common mode voltage reference and DC-link capacitor voltage (V_c), the zero duty cycle (D_{zero}) and the duty cycles of all the possible states within the zero state can be calculated according to the analysis in Chapter 3 (Equation (3.7) – (3.23)). These algorithms are realized in IGBT gate pulse generator block which is written in MAST modeling language. Furthermore, this pulse generator block is able to produce the gating pulses for all the IGBTs in the auxiliary inverter based on the previous calculations in conjuction with the direction of the load current and the differential mode voltage reference (Appendix C, Table C.3 and C.4). When the hybrid cyclocoverter operates in circulating current-free mode, the circuit used to generate the differential mode voltage reference is blinded and the active duty cycle connected to the pulse generator block is zero.
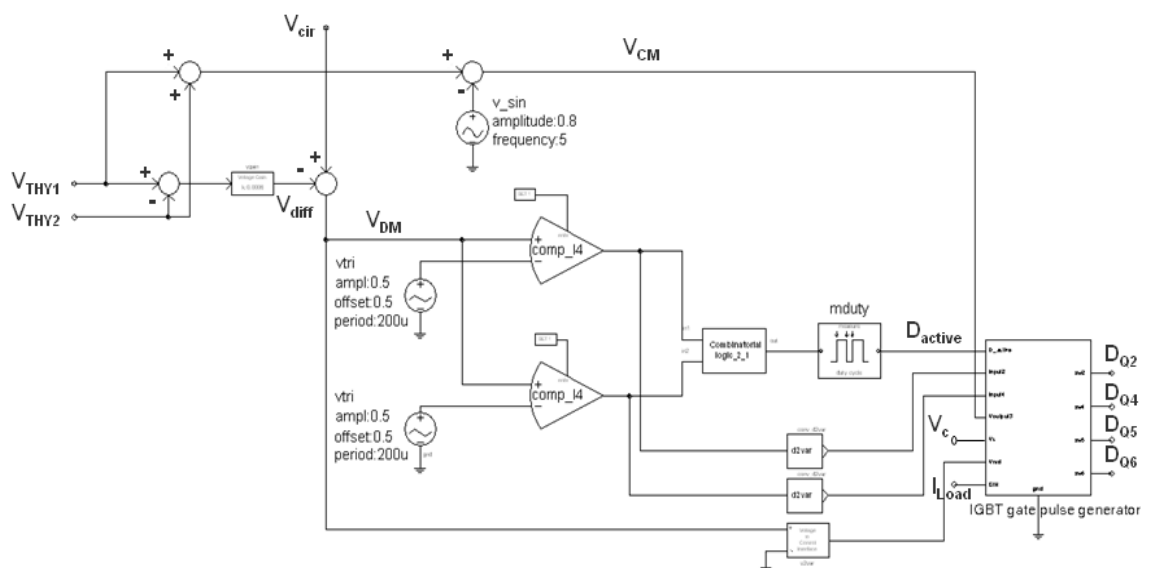
Fig. 4.10: The IGBT gating pulse generator in the simulation model

Based on the previous analysis, all the circuit parameters are shown in Table. 4.2 and the schematics of all the topologies implemented in SABER are shown in the Appendix D (Fig. D.1 - Fig. D.4).

Symbols	Value	Remarks
$V_{in\text{-}line}$	415 V	RMS
r	0.8	
f_{in}/f_{out}	50Hz / 5Hz	
L_{Load}/R_{Load}	0.4H /20Ω	
L_{cir1}, L_{cir2}	2×100mH	Coupled
M	0.95	Coupling coefficient
R_{CCR}	2*0.5Ω	
f_S	5kHz	
V_c	550V/295V	Full/Half DC-link capacitor voltage
I_{cir_ref}	1.5A	
C	8200μF	
$K_{P\text{-}CCPI}$	3.63	Fast CCPI, full DC-link capacitor voltage
	6.78	Fast CCPI, reduced DC-link capacitor voltage
	0.3	Slow CCPI, reduced DC-link capacitor voltage
$K_{I\text{-}CCPI}$	9090	Fast CCPI, full DC-link capacitor voltage
	16950	Fast CCPI, reduced DC-link capacitor voltage
	16	Slow CCPI, reduced DC-link capacitor voltage
$K_{I\text{-}DCPI}$	1.0	
K_d	0.002	Fast CCPI, full DC-link capacitor voltage
	0.0012	Slow CCPI, reduced DC-link capacitor voltage
K_c	280	

Table. 4.2: Standard and hybrid cycloconverter parameters in simulation

4.3 The Three-Phase Input to Single-Phase Output Standard Cycloconverter

The simulation results of the standard cycloconverter in both the circulating current and the circulating current-free mode are presented in this section. The corresponding variables measured with simulation are shown on Fig. 4.11, which is the diagram of a three-phase to single-phase standard cycloconverter in circulating current mode. For simplicity, only one diagram is presented below and the two coupled circulating

current reactors can be just bypassed if the standard cyclocoverter operates in circulating current-free mode.
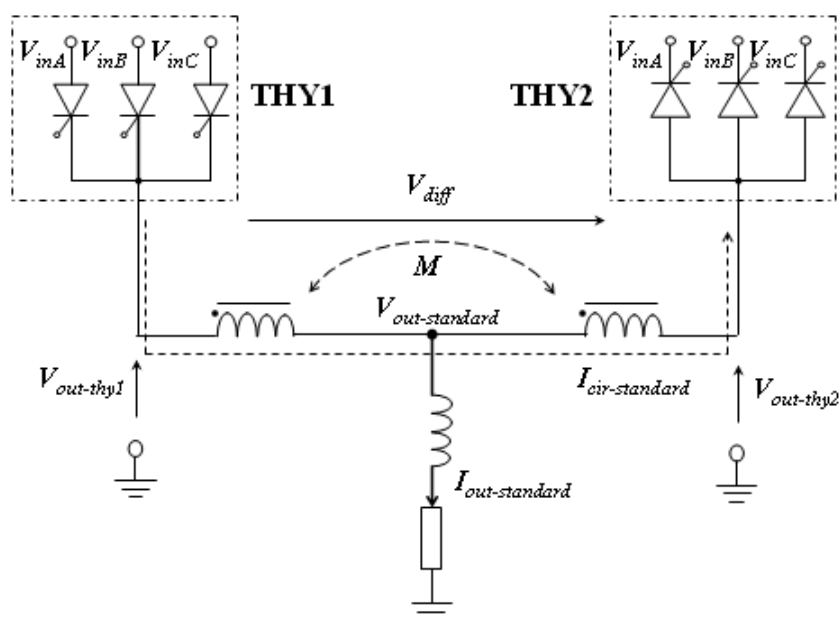
Fig. 4.11: The diagram of a three-phase to single-phase standard cycloconverter with variables for measurement

4.3.1 The Standard Cycloconverter in Circulating Current Mode

Fig. 4.12(a) and 4.12(b) show respectively the output voltage waveforms generated by the positive and negative thyristor half bridge of the standard cycloconverter. As can be seen from these two figures in conjunction with their spectrum shown in Fig. 4.13, the low-pass filtered components are equal both in amplitude and frequency (5Hz) as the firing angle for the two thyristor half bridges are complementary. However, it is obvious that the instantaneous output voltages of the two thyristor half bridges are quite different, which is the reason why a large circulating current between the two half bridges can build up, especially if the current limiting reactor is small. Fig. 4.13(a) and 4.13(b) show the spectra of the output voltages generated by the two thyristor half bridges, revealing a 225V_{pk} at 5Hz fundamental voltage component for both half bridges. Furthermore, there are some major harmonic components around multiples of 150Hz, such as 150Hz, 300Hz, 450Hz, which is typical for a 3-pulse thyristor half bridge with an input frequency supply of 50Hz.
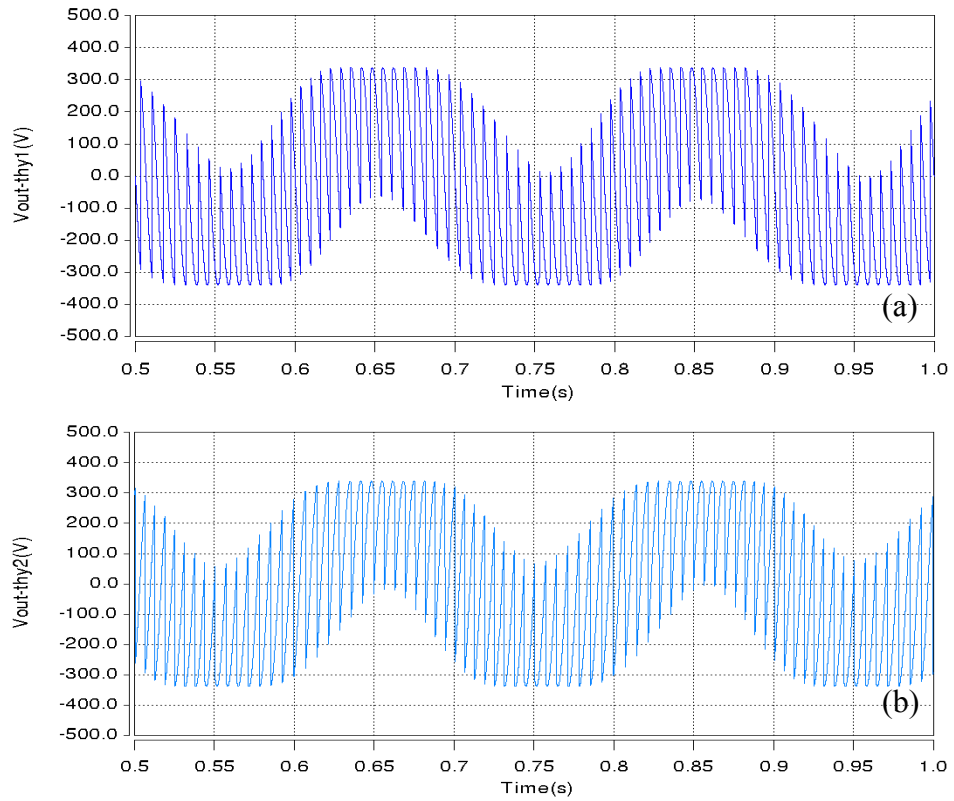
Fig. 4.12: Output voltage waveforms generated by a) the positive and b) the negative
thyristor half bridge in CCM
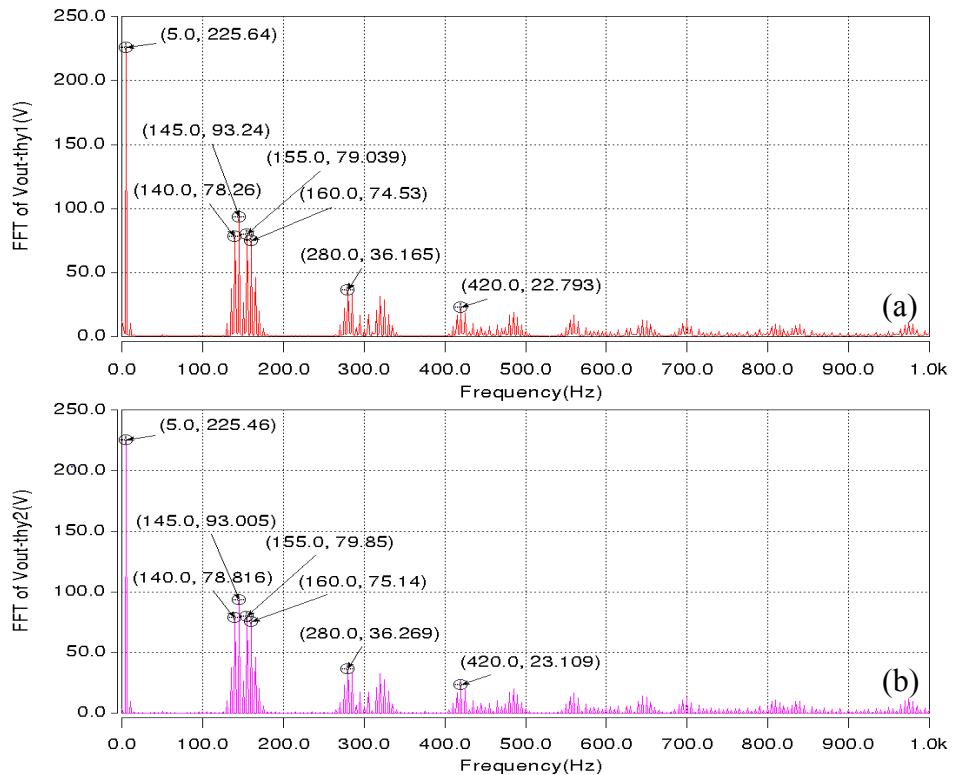
Fig. 4.13: Spectra of the output voltages generated by a) the positive and b) the
negative thyristor half bridge in CCM

As mentioned above, due to the difference between the instantaneous output voltages of the two thyristor half bridges, a large differential mode voltage shown in Fig. 4.14 is generated. The peak value of the differential mode voltage is around 506V which, as mentioned in Chapter 3, is the minimum voltage level that the auxiliary inverter has to inject in order to ensure that the circulating current caused by the differential mode voltage, is under control all the time. Fig. 4.15 shows the spectrum of the differential mode voltage indicating that the largest harmonic components ($187V_{pk}$ at 145Hz and $161V_{pk}$ at 155Hz) appear around 150Hz; some other major harmonics are still visible around multiples of 150Hz, for example, 300Hz, 450Hz. In addition, one important aspect that needs to be mentioned is that quite a large 10Hz low frequency harmonic is present and it is the largest harmonic below 100Hz. This harmonic is caused by the way the cycloconverter operates and cannot be removed by altering the cycloconverter control. Therefore, due to its low frequency, this harmonic in the differential mode voltage may result in a large harmonic circulating current, even when a large differential mode inductor is connected between the two thyristor half bridge outputs.

The circulating current waveform and its spectrum are shown in Fig. 4.16 and 4.17 for the situation in which the circulating current reactor consists of two 100mH coupled inductors with a coupling coefficient of 0.95 that gives a 380mH mutual inductance (differential mode). From the Fig. 4.17 it can be seen that the spectrum of the circulating current does not only contain harmonics around 150Hz ($0.41A_{pk}$ at 145Hz, $0.5A_{pk}$ at 155Hz), but also a DC component of 2.19A (limited only by the circuit resistance and the device voltage drop) and a 10Hz component of $1.64A_{pk}$. Although there is no obvious DC component in the differential mode voltage, the DC component cannot be avoided in the circulating current since the circulating current is only allowed to flow from the positive to the negative thyristor half bridge due to the unipolar characteristics of thyristor bridge. Thus, the presence of this large DC component and the 10Hz low frequency current ripple which is double the output frequency (typically low for a cycloconverter) are the downsides of limiting the circulating current by using a circulating current reactor.
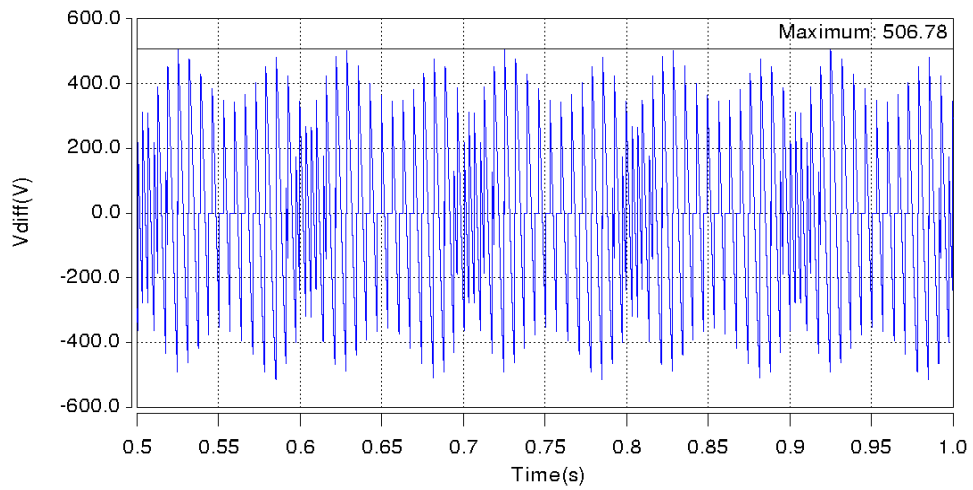
Fig. 4.14: Differential mode voltage waveform seen between the two thyristor half bridge outputs in CCM
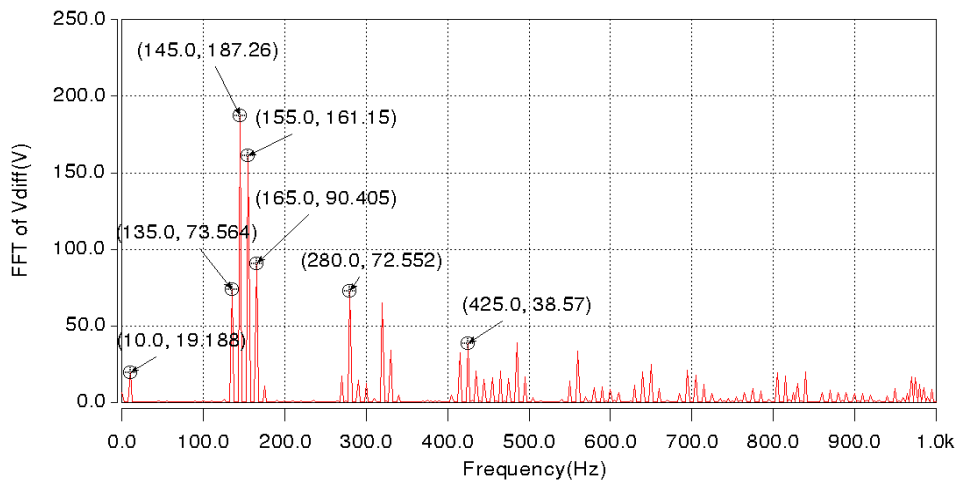
Fig. 4.15: Spectrum of the differential mode voltage seen between the two thyristor half bridge outputs in CCM
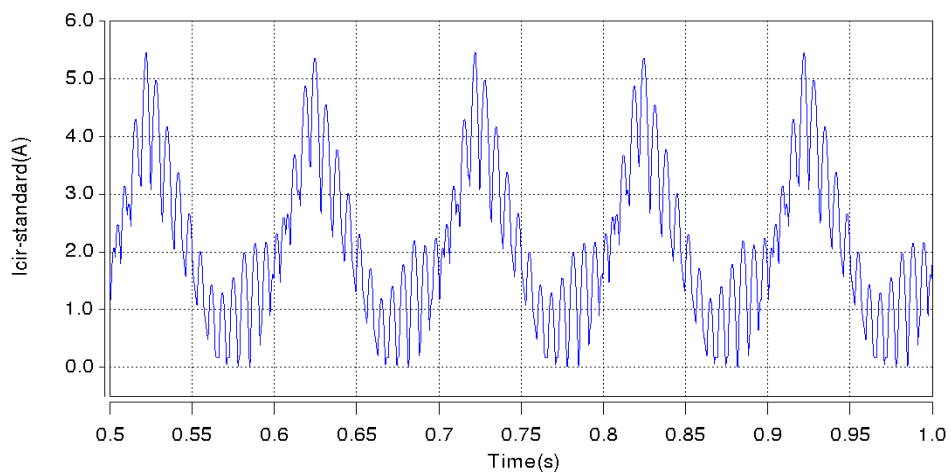
Fig. 4.16: Circulating current waveform of the standard cycloconverter in CCM
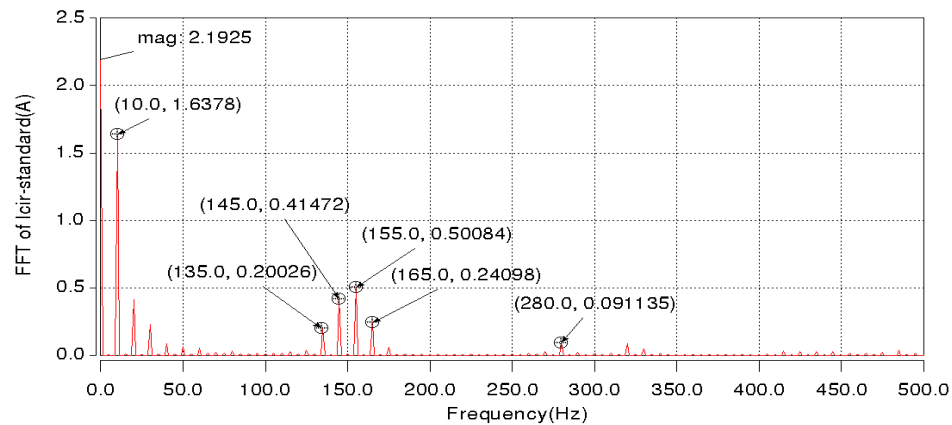
Fig. 4.17: Spectrum of the circulating current of the standard cycloconverter in CCM

Since the two outputs of the thyristor half bridges are connected together via the circulating current reactor, as shown in Fig. 4.18, the common mode voltage which is the average of the two thyristor half bridge output voltages is actually the phase-to-supply neutral output voltage of the standard cycloconverter. Fig. 4.19 shows the spectrum of the output voltage of the cycloconverter. It can be seen that the fundamental component remains the same (224V$_{pk}$ at 5Hz) as the thyristor half bridge output voltage since it is very little attenuated by the circulating current reactor (voltage drop across its resistance). However, as some of the switching voltage ripples of two thyristor half bridges are 180° displaced they will cancel each other completely at the centre tap of the reactor (For example the 145Hz and 155Hz harmonic components). In contrast, for some other harmonic components which are in-phase, such as the 140Hz and 160Hz, the amplitude of these components remains the same at the centre tap of the circulating current reactor as those generated by the thyristor half bridges. Hence, the output voltage of the standard cycloconverter operating in circulating current mode has better harmonic performance than that of each thyristor half bridge, although the performance is still far from good. Furthermore, from the spectrum of the output voltage shown in Fig. 4.19, it can be seen that the frequencies and their corresponding amplitudes are very similar to those in Fig. E.1 (Appendix D), which is the theoretical spectrum of the standard cycloconverter output voltage operating in circulating current mode based on the analysis presented in [pp.322, 1].

Fig. 4.20 shows the load current waveform of the standard cycloconverter. As the load in the simulation is highly inductive, the large low frequency harmonics present in the output voltage are not particularly apparent in the quality of the load current.
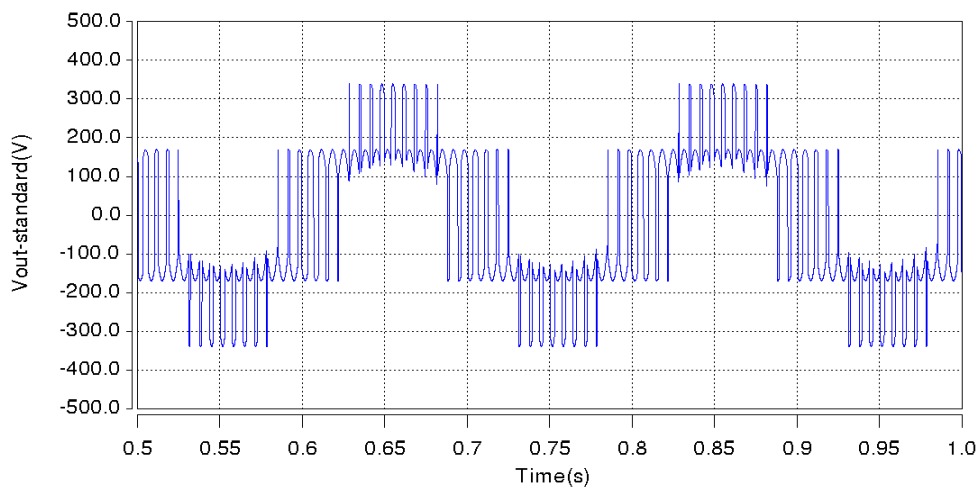
Fig. 4.18: Phase-to-supply neutral output voltage waveform of the standard cycloconverter in CCM
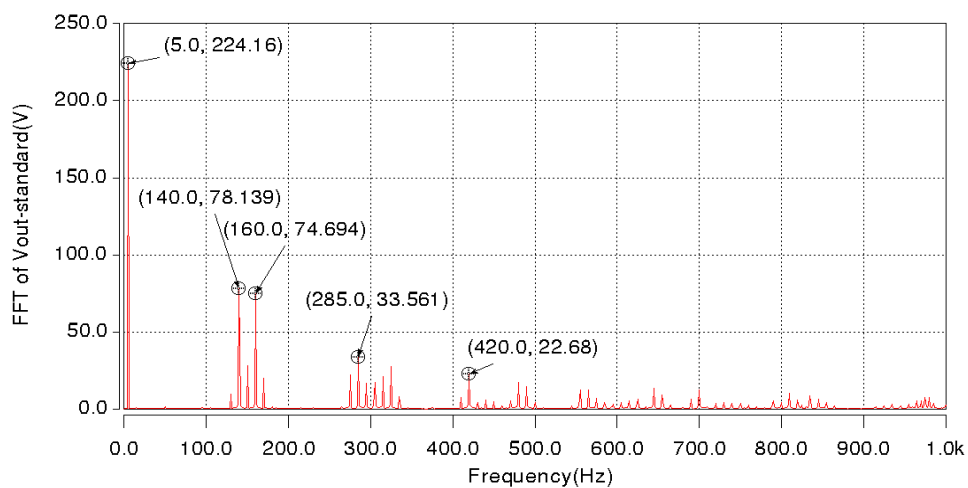
Fig. 4.19: Spectrum of the phase-to-supply neutral output voltage of the standard cycloconverter in CCM
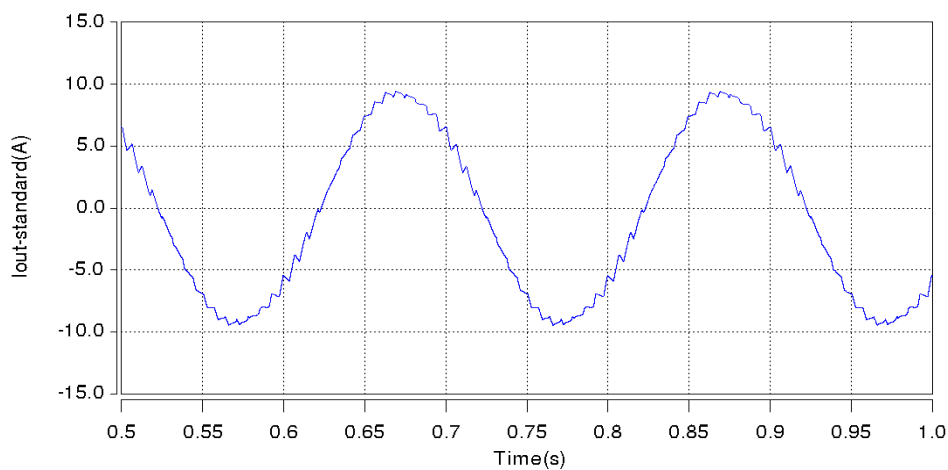
Fig. 4.20: Load current waveform of the standard cycloconverter in CCM

4.3.2 The Standard Cycloconverter in Circulating Current-Free Mode

When the standard cycloconverter operates in circulating current-free mode, the positive and negative thyristor half bridges are directly connected together and the circulating current reactor is omitted as no circulating current is allowed to flow between the two half bridges. A control method as described in Section 4.2 is applied to ensure the safely commutation between the two thyristor half bridges.

Fig. 4.21 shows the phase-to-supply neutral output voltage waveform of the standard cycloconverter in this operating mode. It is obvious that the output voltage is fabricated from the input power supply via positive thyristor half bridge when load current is positive and vice versa when the load current is negative. There is an obvious deviation from the normal pattern that appears twice in a period due to the commutation between two thyristor half bridges. From the spectrum of the phase-to-supply neutral output voltage shown in Fig. 4.22, the waveform looks worse than the standard cycloconverter with circulating current ($101V_{pk}$ compared to $78V_{pk}$ at 140Hz) although the fundamental component still remains almost the same ($219V_{pk}$ at 5Hz). Since the output voltage harmonics are results of the interaction of both the input and output frequency [pp.162, 1], the harmonic components in circulating current-free mode are infinite for a given multiple of the input frequency as mentioned in Chapter 2. Therefore, unlike the spectrum of the output voltage in circulating current mode shown in Fig. 4.19, there are some very low frequency components, such as 10Hz, 15Hz, 20Hz, in the spectrum shown in Fig. 4.22. These low frequency components are very detrimental to the load side and therefore need to be removed by the hybrid solution. The spectrum of the output voltage is very similar to that in Fig. E.2 (Appendix E), which is the theoretical spectrum of the standard cycloconverter output voltage in circulating current-free mode according to the analysis in [pp.318-320, 1].

Fig. 4.23 shows the waveform of load current of the standard cycloconverter. As in the circulating current mode, the load current is reasonably sinusoidal due to the highly inductive nature of the load.
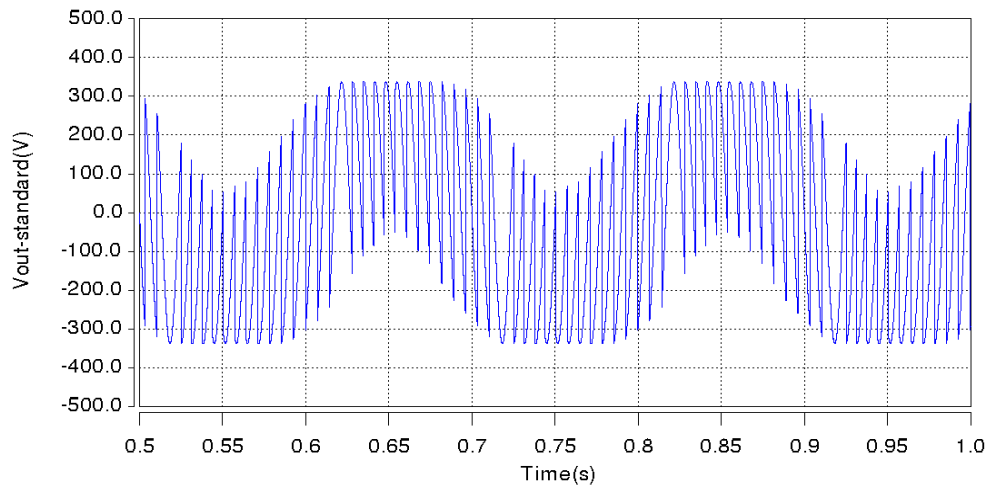
Fig. 4.21: Phase-to-supply neutral output voltage waveform of the standard cycloconverter in CCFM
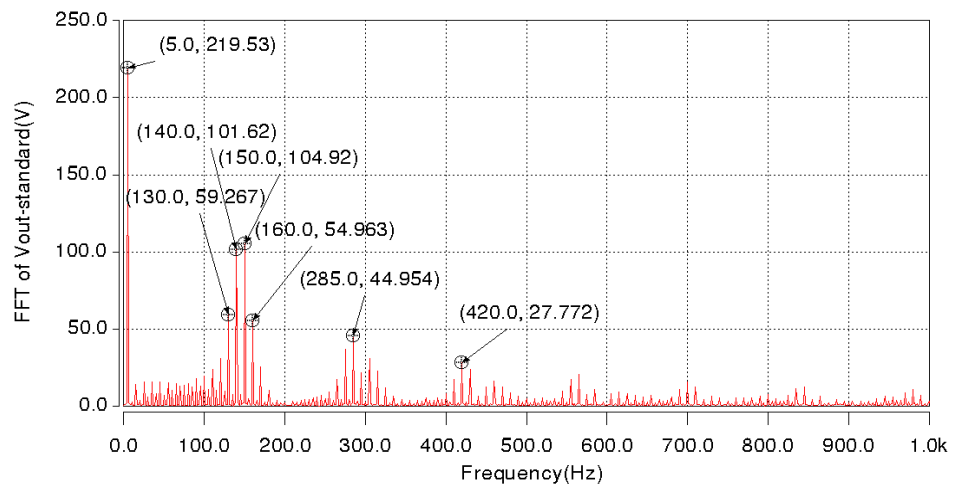
Fig. 4.22: Spectrum of the phase-to-supply neutral output voltage of the standard cycloconverter in CCFM
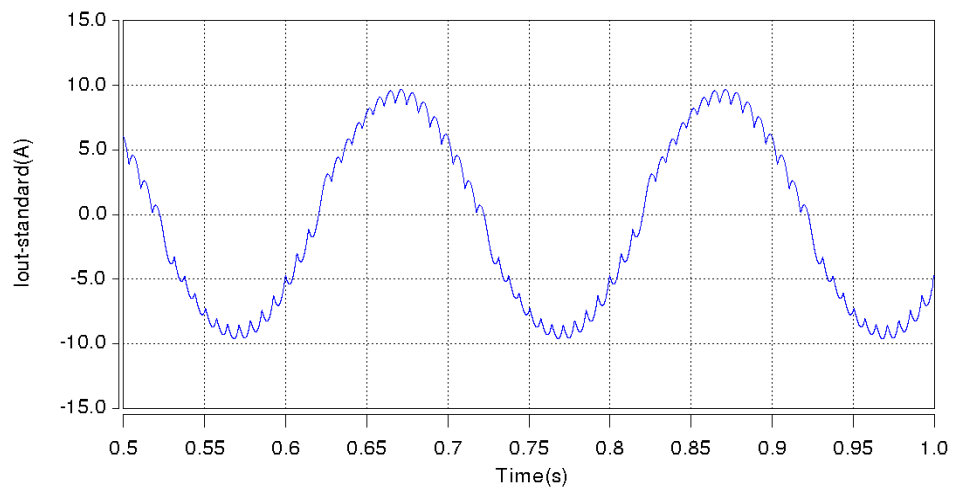
Fig. 4.23: Load current waveform of the standard cycloconverter in CCFM

4.4 The Three-Phase Input to Single-Phase Output Hybrid Cycloconverter

In this section, the simulation results from the SABER models of the hybrid cycloconverter operating in circulating current mode and circulating current-free mode are presented and analyzed. A three-phase to single-phase hybrid cycloconverter is shown in Fig. 4.24, with all the measured variables on it. Similar to Section 4.3, only the topology in circulating current mode is presented as the coupled inductors can be just shorted in circulating current-free mode.
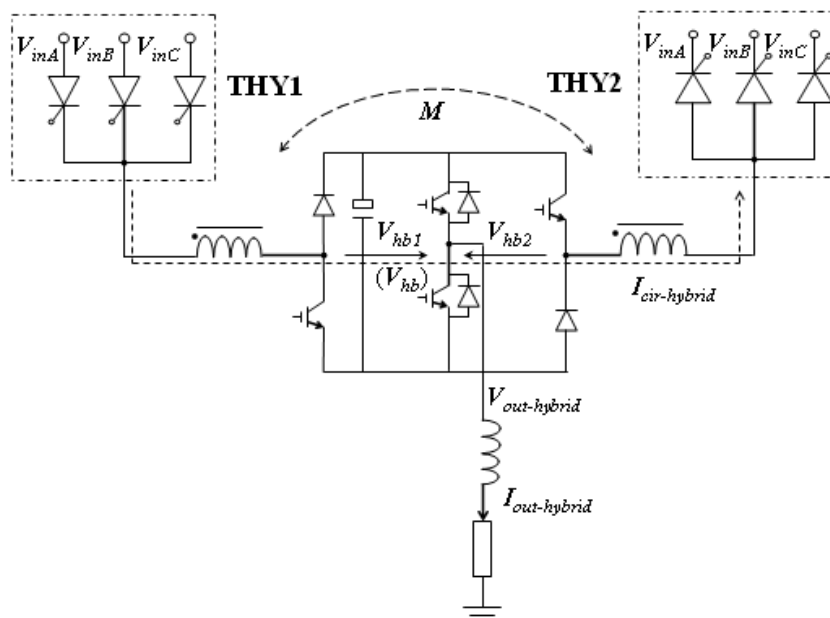
Fig. 4.24: The diagram of a three-phase to single-phase hybrid cycloconverter with variables for measurement

4.4.1 The Hybrid Cycloconverter in Circulating Current Mode

The simulation results of the standard cycloconverter reveal that even if a large circulating current reactor is connected between the outputs of the two thyristor half bridges, the circulating current still reaches an unacceptable level. In contrast, the hybrid cycloconverter operating in circulating current mode, as shown in Chapter 3, is able to provide the control of the circulating current around a given DC reference that just exceeds the thyristor holding (or latching) current, with only a minimal switching

ripple. Moreover, as mentioned in Chapter 3, the hybrid cyloconverter also has the ability to improve the output voltage of the converter by injecting a common mode voltage by using the auxiliary inverter to cancel the differences between the output voltage of the standard cycloconverter and the output voltage reference.

4.4.1.1 Operation with Full DC-link Capacitor Voltage in the Auxiliary Inverter

As mentioned in Chapter 3, the DC-link capacitor voltage in the auxiliary inverter should always be kept charged at a higher voltage level than the peak value of the differential mode voltage generated between the two thyristor half bridges to ensure that the circulating current is always under control. For a 415 rms supply, the peak value of the differential mode voltage is around 505V, as shown in Fig. 4.14, so the reference of the DC-link capacitor voltage for the full capacitor voltage mode is set at 550V.

Fig. 4.25 shows that if sufficient DC-link capacitor voltage is available in the auxiliary inverter, the circulating current of the hybrid cycloconverter model can be accurately controlled, in this chosen situation at 1.5A, with a very small ripple around it. Thus, by varying the value of DC current reference, the circulating current can be reduced and maintained to a minimum level dictated by the thyristor's holding (or latching) current given in the datasheet to ensure that the thyristor remains always ON when a corresponding firing pulse is applied. Moreover, the amount of stored energy in the circulating current reactor is minimized since not only the required inductance value can be smaller due to the actively controlled circulating current, but also both the DC component (1.5A or even smaller compared to 2.2A) and the peak value (1.5A_{pk} compared to 5.5A_{pk}) of the circulating current that the inductance needs to handle is much smaller. Therefore, by controlling the circulating current in this way, it would lead to a more accurate and cost effective design of the circulating current reactor. Fig. 4.26 shows the spectrum of the circulating current, which further indicates the improvement in performance of the hybrid cycloconverter, having only a DC component of 1.5A whilst other harmonics are small enough to be considered irrelevant.
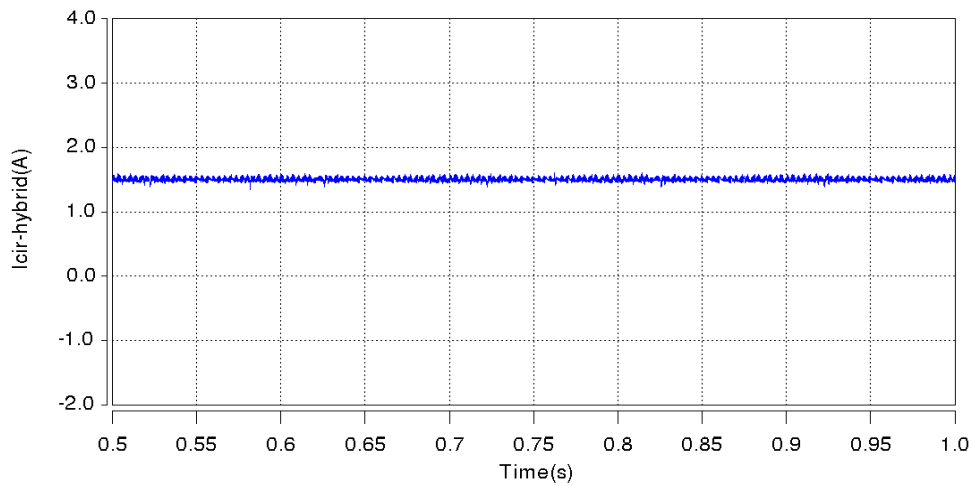
Fig. 4.25: Circulating current waveform of the hybrid cycloconverter when using a fast PI controller and full DC-link capacitor voltage in CCM
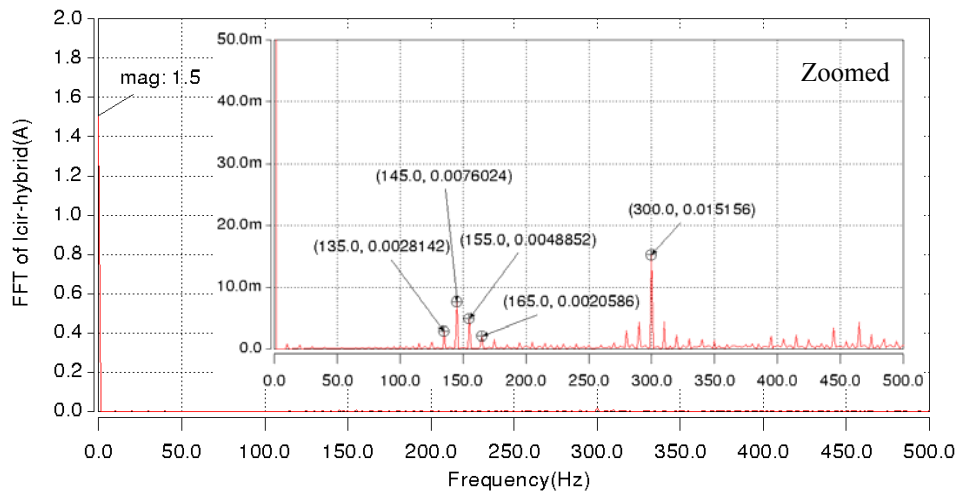
Fig. 4.26: Spectrum of the circulating current of the hybrid cycloconverter when using a fast PI controller and full DC-link capacitor voltage in CCM

As referred to in Chapter 3, another important improvement provided by the hybrid cycloconverter is a better output voltage waveform at the load side. Fig. 4.27 shows the phase-to-supply neutral output voltage waveform of the hybrid cycloconverter. The output voltage shape is improved by the auxiliary inverter by injecting a common mode voltage to minimize the differences between the output voltage of the standard cycloconverter and the output voltage reference. Although by using a large enough circulating current reactor, an obvious improvement in the output voltage waveform of the standard cycloconverter can also be obtained, the hybrid cycloconverter has the ability to further reduce the low order output voltage harmonics from $78V_{pk}$ at 140Hz and $75V_{pk}$ at 160Hz to $31V_{pk}$ at 140Hz and $30V_{pk}$ at 160Hz, as shown in Fig. 4.28.

- 109 -
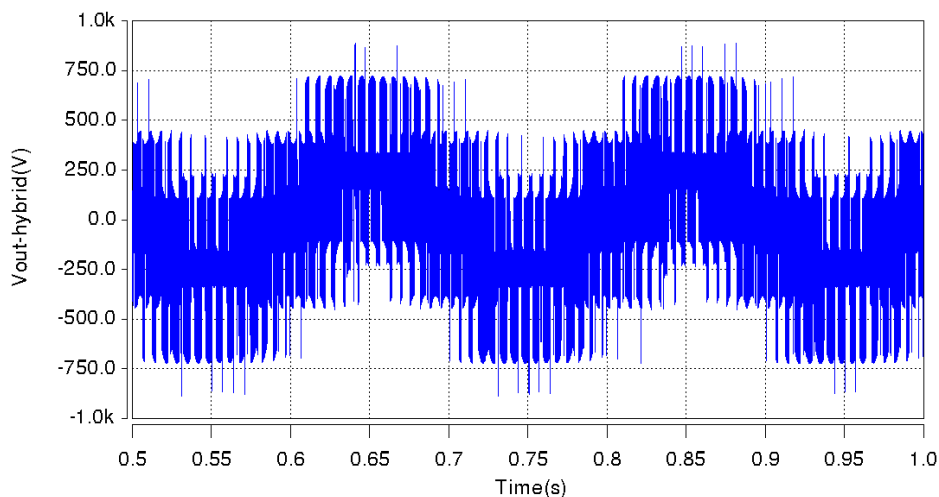
Fig. 4.27: Phase-to-supply neutral output voltage waveform of the hybrid
cycloconverter when using a fast PI controller and full DC-link
capacitor voltage in CCM
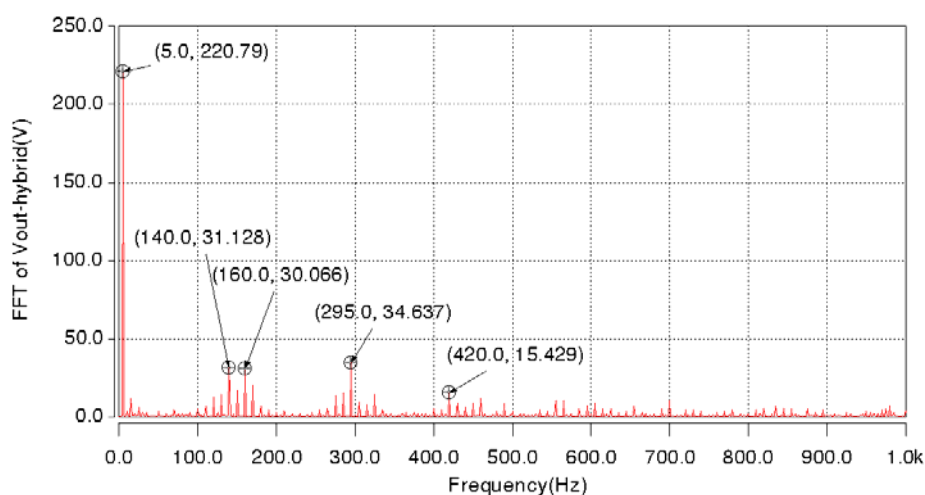
Fig. 4.28: Spectrum of the phase-to-supply neutral output voltage of the hybrid
cycloconverter when using a fast PI controller and full DC-link
capacitor voltage in CCM

Although the hybrid cycloconverter with 550V DC-link capacitor voltage is able to realize both accurate control of the circulating current as well as improving the output voltage waveform, the high voltage rating of the power devices in the auxiliary inverter which means higher added cost, due to the necessity to maintain the DC-link capacitor voltage at a high level, is not desirable. Therefore, investigations in reducing the DC-link capacitor voltage level are carried out in order to identify if it will be possible to reach a cost vs performance compromise.

4.4.1.2 Operation with Reduced DC-link Capacitor Voltage in the Auxiliary Inverter

Another hybrid cycloconverter simulation model with a modified control was implemented using only 295V DC-link capacitor voltage, which is almost half of the voltage level used in the previous situation, in the auxiliary inverter. The 295V is also half of the peak voltage seen across the thyristor, which for 415V rms supply, is around 590V (equal to the peak value of the line-to-line supply voltage if the on state forward voltage of the thyristor is ignored).

Fig. 4.29 shows the circulating current waveform of the same hybrid cycloconverter model as tested in the previous section but using only 295V DC-link capacitor voltage. It is obvious that in this situation the circulating current waveform, with a 0.5A peak-to-peak maximum ripple on it, is not as good as the waveform shown in Fig. 4.25, although the DC component is still accurately controlled at around 1.5A. This is because every time when the differential mode voltage between the outputs of the two thyristor half bridges exceeds the DC-link capacitor voltage, the auxiliary inverter will not be able to ensure that the circulating current can still be accurately controlled around the reference. Although the PI controller has already responded fast enough, the modulation index of PWM gating pattern for the auxiliary inverter is limited. However, from the spectrum of the circulating current waveform shown in Fig. 4.30, it can be concluded that after reducing the auxiliary inverter voltage rating and therefore the installed power by 50%, the quality of the circulating current in this situation is still much better than that in the standard cycloconverter. This achievement can be seen from the reduction of not only the DC component but also the low order harmonics, such as the 10Hz, 20Hz, 145Hz, 155Hz.

It can be seen from Fig. 4.31, which shows the phase-to-supply neutral output voltage waveform of the hybrid cycloconverter, that the action of the high frequency common mode voltage injected by the auxiliary inverter to improve the output voltage of the hybrid cycloconverter is frequently under limitation. This is because every time when the differential mode voltage is higher than the DC-link capacitor voltage, the PI controller will respond very fast to ensure that the whole switching period of the

auxiliary inverter is used to control the circulating current and therefore there will be no time left (duty cycle of the zero switching state) for compensating the disturbance in the common mode voltage. Hence, the improvement of the output voltage in this situation will be much more limited than when using the full DC-link capacitor voltage. This is further illustrated by the spectrum of the phase-to-supply neutral output voltage which is shown in Fig. 4.32, with relevant low frequency harmonics of $48V_{pk}$ at 140Hz and $72V_{pk}$ at 150Hz.
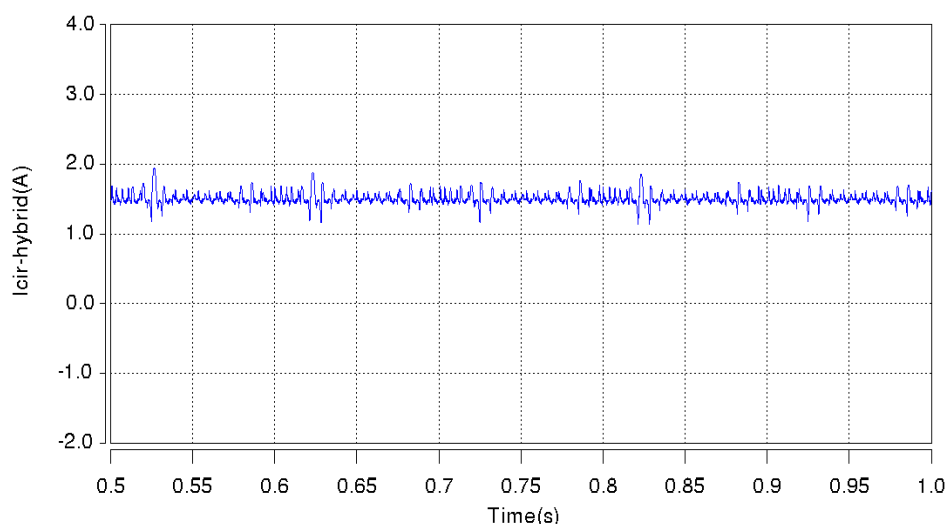
Fig. 4.29: Circulating current waveform of the hybrid cycloconverter when using a fast PI controller and reduced DC-link capacitor voltage in CCM
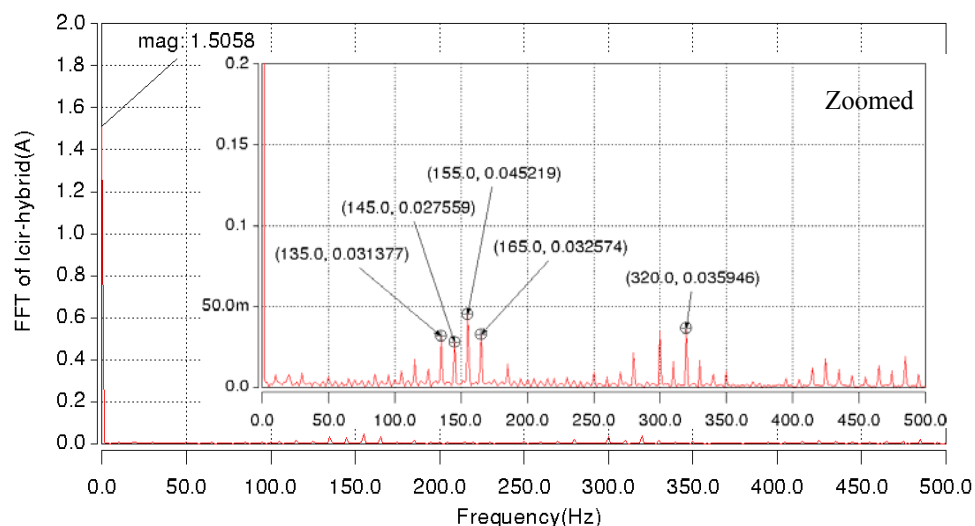
Fig. 4.30: Spectrum of the circulating current of the hybrid cycloconverter when using a fast PI controller and reduced DC-link capacitor voltage in CCM
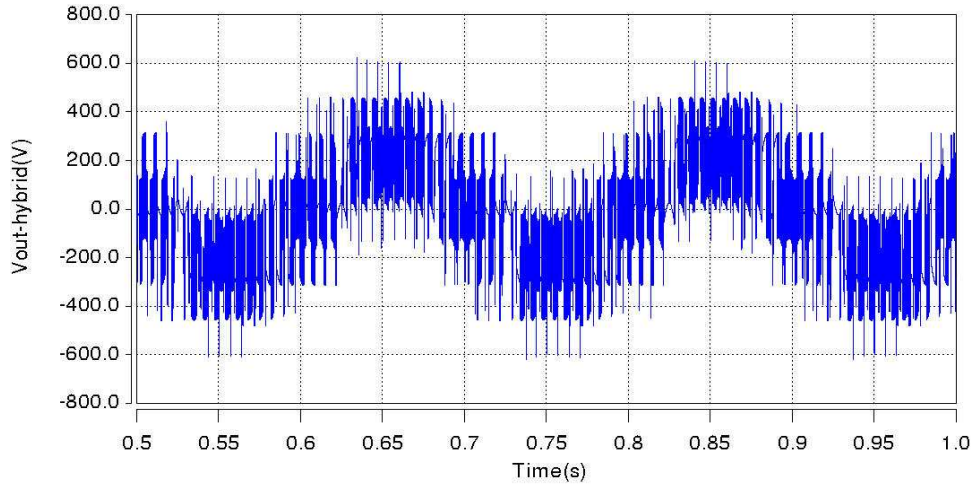
Fig. 4.31: Phase-to-supply neutral output voltage waveform of the hybrid cycloconverter when using a fast PI controller and half DC-link capacitor voltage in CCM
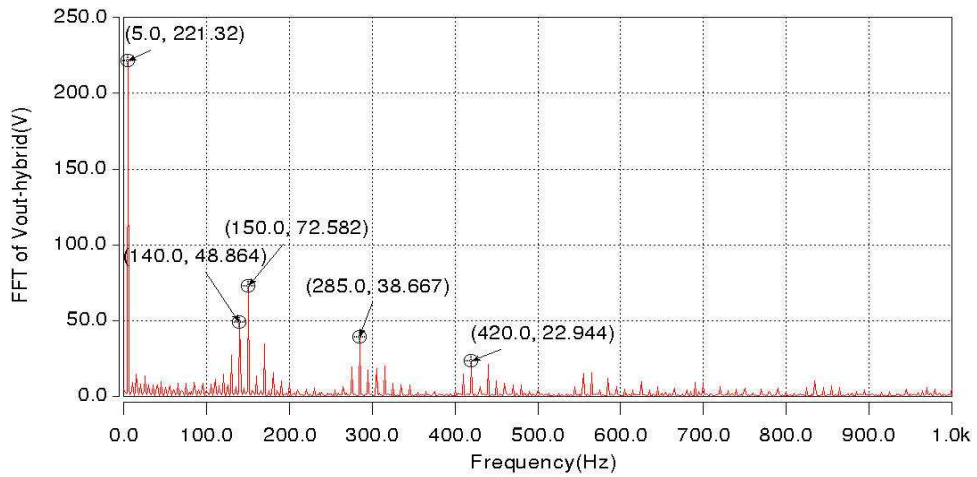
Fig. 4.32: Spectrum of the phase-to-supply neutral output voltage of the hybrid cycloconverter when using a fast PI controller and reduced DC-link capacitor voltage in CCM

In this case, the improvement of the output voltage of the hybrid cycloconverter is too small to be considered acceptable compared to the output voltage of the standard cycloconverter. Therefore, in order to ensure a compromise between the common mode and differential mode voltage injection, the whole switching period can allocated to the active state and the zero state in proportion to the value of the corresponding differential mode voltage reference and the common mode voltage reference. The control method is realized in the following way: if $(V_{DM} + V_{CM}) \leq 1$, D_{active} remains the same; if $(V_{DM} + V_{CM}) > 1$,

$$D_{active} = \frac{V_{DM}}{V_{DM} + V_{CM}} \tag{4.8}$$

In both situations, D_{zero} is generated according to Equation (4.9) and the duty cycles of all the possible states within the zero state can be obtained through the corresponding equations (Equation (3.8) – (3.23)) mentioned in Chapter 3.

$$D_{zero} = 1 - D_{active} \tag{4.9}$$

However, as mentioned in Chapter 3, for the three-leg bridge inverter, the reference of the common mode voltage is composed by two parts: V_{CM}' by subtracting the output voltage of the standard cycloconverter from the reference of the output voltage; D_{active} times the half of the DC-link capacitor voltage and the polarity is depending on both the direction of the differential mode voltage and the load current. Therefore, the new common mode voltage reference can be express as Equation (4.10). By substituting this equation for the V_{CM} in Equation (4.8), the D_{active} for the three-leg bridge inverter can be derived from Equation (4.11).

$$V_{CM} = V_{CM}' \pm D_{active} \cdot V_c / 2 \tag{4.10}$$

$$D_{active} = \frac{V_{DM}}{V_{DM} + V_{CM}' \pm D_{active} \cdot V_c / 2} \tag{4.11}$$

Compared with the Equation (4.8), it would be much more complicated to implement the Equation (4.11) with MAST modeling language in the SABER to obtain the value of D_{active}. Therefore, another method is chosen by reducing the bandwidth (speed) of the circulating current PI controller below 150Hz in order to make sure that the duty cycle of the zero switching state in each switching period is always above zero to be able to inject the common mode voltage when the differential mode voltage is typically higher than the DC-link capacitor voltage. Therefore, the PI controller of the circulating current in the simulation is set to be able to handle only the DC and the 10Hz low frequency components present in the differential mode voltage, which cannot be limited by the circulating current reactor. Meanwhile, the reduction of the

150Hz or above harmonics relies mainly on the feedforward compensation of the differential mode voltage. Fig. 4.33 shows the circulating current waveform obtained when using a slow PI controller. The 10Hz and 150Hz harmonics, as revealed by the spectrum of the current waveform in Fig. 4.34, have been partially reduced compared to the circulating current of the standard cycloconverter shown in Fig. 4.16 and 4.17. Although the improvement over the circulating current is quite limited compared to a fast PI controller, additional benefits (consuming less reactive power from the supply) are achievable, as will be seen later.
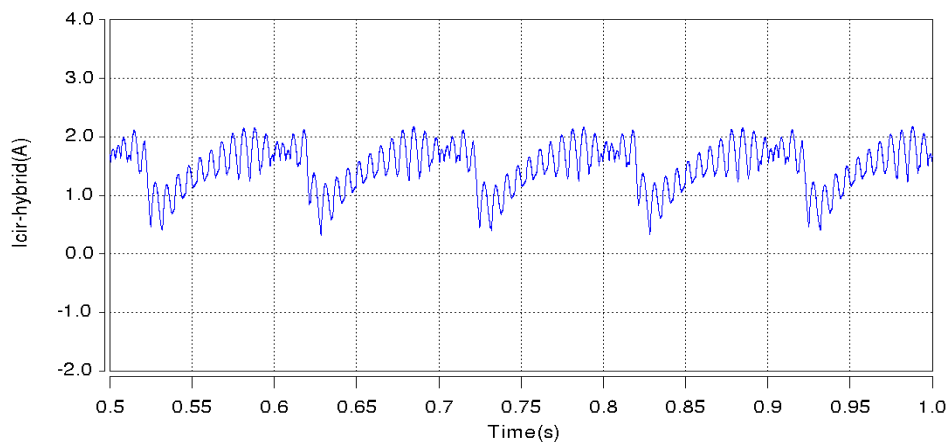
Fig. 4.33: Circulating current waveform of the hybrid cycloconverter when using a slow PI controller and reduced DC-link capacitor voltage in CCM
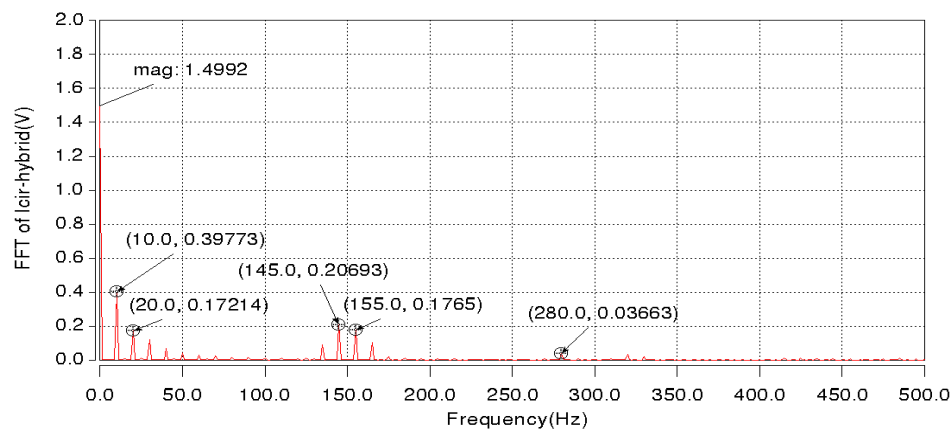
Fig. 4.34: Spectrum of the circulating current of the hybrid cycloconverter when using a slow PI controller and reduced DC-link capacitor voltage in CCM

Fig. 4.35 shows the phase-to-supply neutral output voltage waveform of the hybrid cycloconverter using a slow circulating current PI controller and reduced DC-link capacitor voltage. Fig. 4.36(a) shows the spectrum of the output voltage in the 0 to

25kHz frequency range. From this figure it can be seen that the harmonics above 1kHz are placed in clusters around multiples of the switching frequenciy (5kHz) due to the way the high frequency pulse width modulation of the auxiliary inverter works. The output voltage of the hybrid cycloconverter, as revealed by its spectrum shown in Fig. 4.36(b), is able to achieve the best performance compared to the previous two situations, with the low order voltage harmonics being reduced significantly, for example $15V_{pk}$ at 150Hz and $9V_{pk}$ at 160Hz compared to $31V_{pk}$ at 140Hz and $30V_{pk}$ at 160Hz shown in Fig. 4.28.

When taking both the performance and the cost of the hybrid cycloconverter into consideration, the hybrid cycloconverter topology that uses a reduced DC-link capacitor voltage and slow circulating current PI controller will be the baseline for circulating current mode operation. Therefore, the rest of the simulation waveforms from this point forward apply only to the latter case.

Fig. 4.37 shows the waveform of the load current of the hybrid cycloconverter with a slow PI controller and reduced DC-link voltage. Due to the highly inductive behaviour of the load which tends to filter more the higher voltage distortions, it is not realistic to use the load current to reflect the improvement of performance in the output voltage. However, compared to the load current of the standard cycloconverter, the elimination of the ripple superimposed on the fundamental component can still be detected.
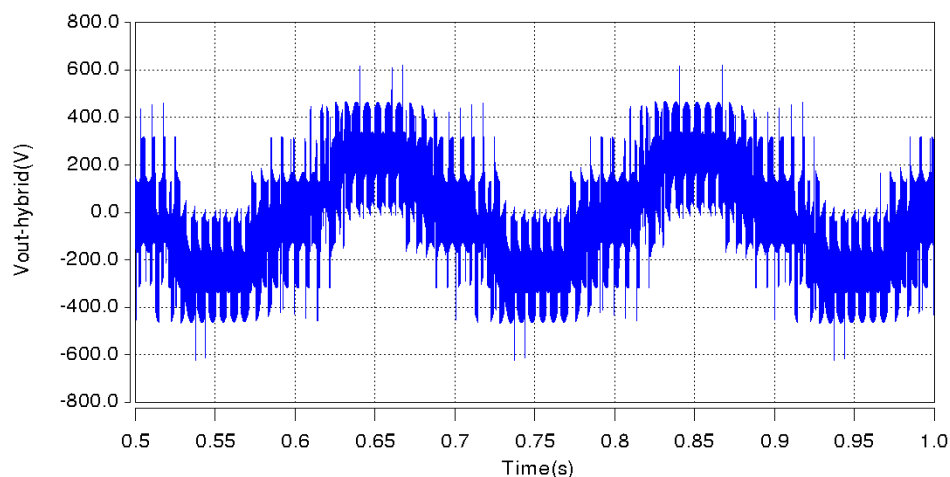
Fig. 4.35: Phase-to-supply neutral output voltage waveform of the hybrid cycloconverter when using a slow PI controller and reduced DC-link capacitor voltage in CCM
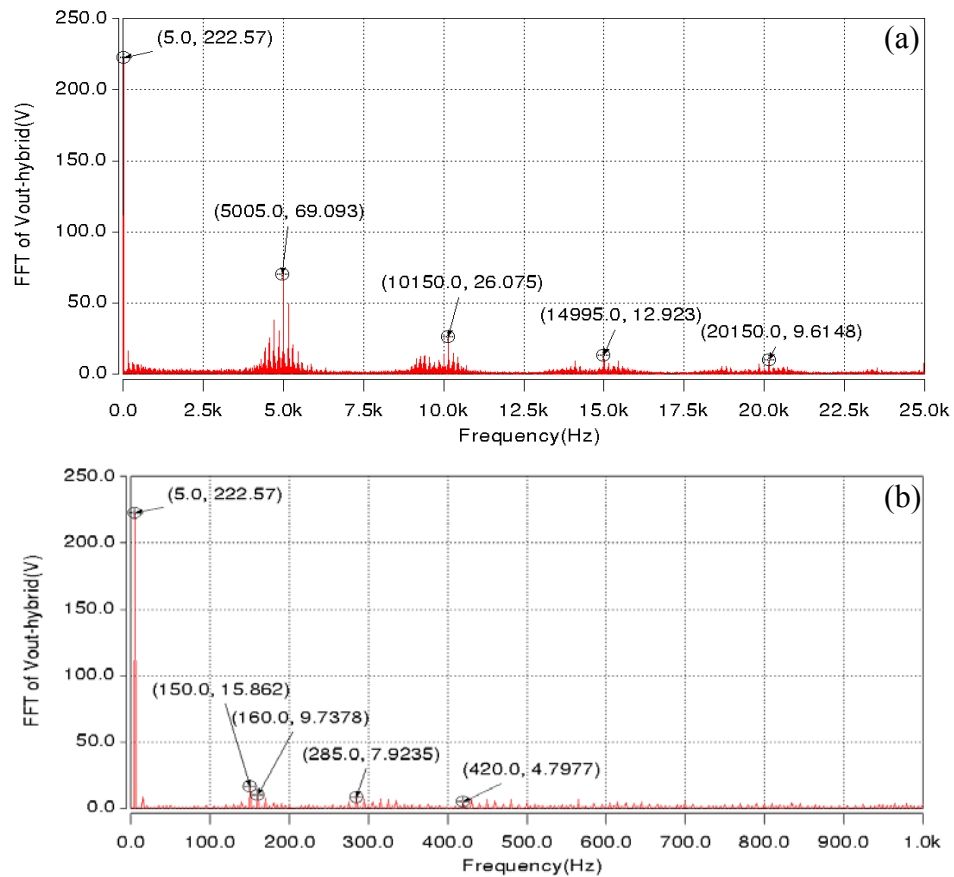
Fig. 4.36: Spectrum of the phase-to-supply neutral output voltage of the hybrid cycloconverter when using a fast PI controller and reduced DC-link capacitor voltage in CCM: a) 0-25kHz spectrum b) 0-1kHz spectrum
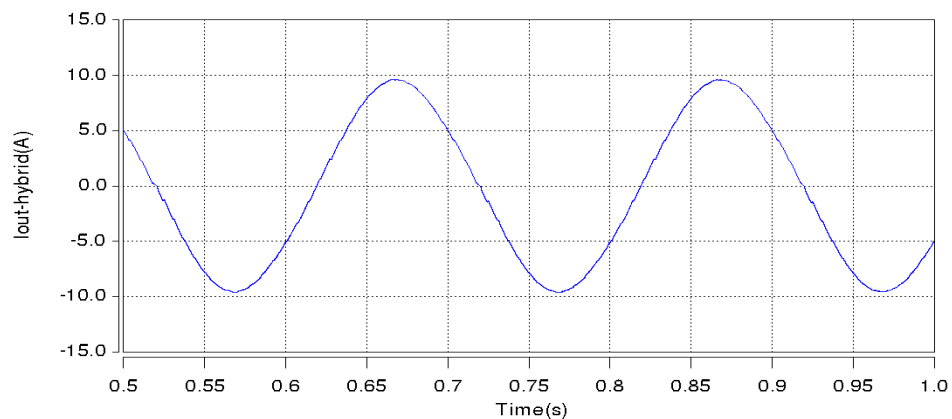
Fig. 4.37: Load current waveform of the hybrid cycloconverter when using a slow PI controller and reduced DC-link capacitor voltage in CCM

Fig. 4.38(a) and (b) show the voltages injected by the auxiliary inverter when the hybrid cycloconverter in circulating current mode; the plots show the voltage between the mid-point of one of the asymmetric legs and the output of the symmetric leg.
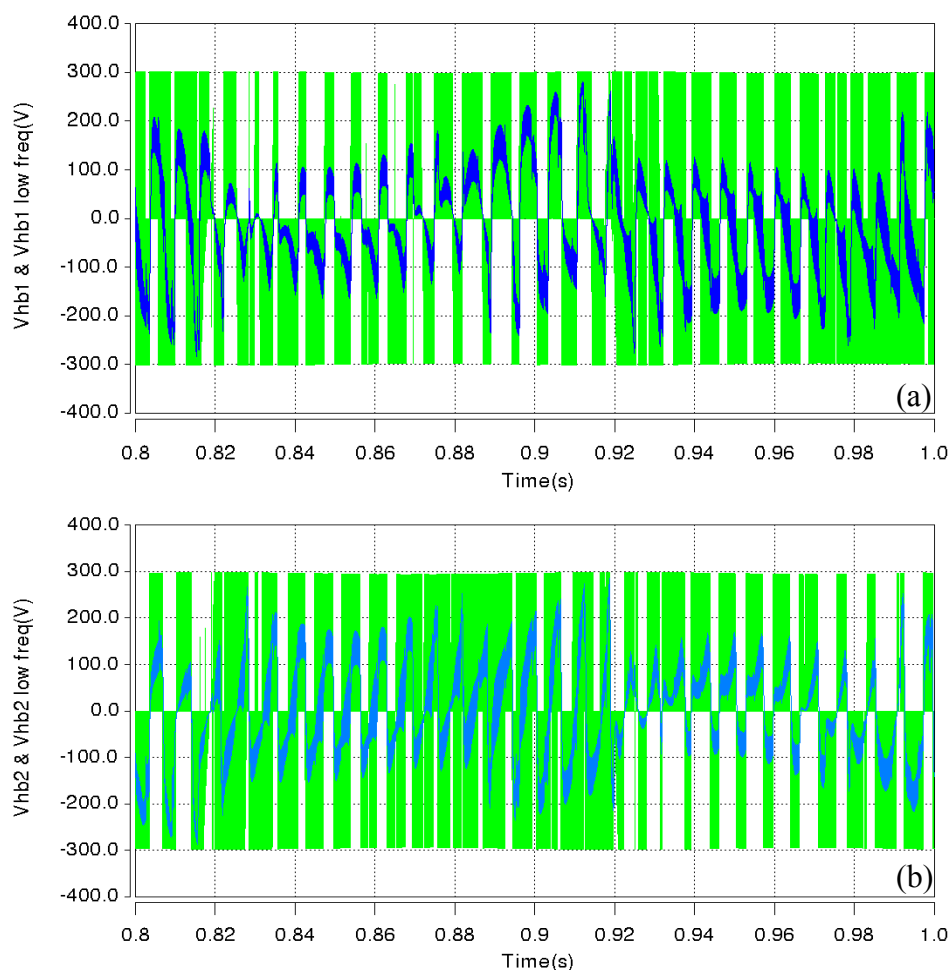
Fig. 4.38: PWM voltage and the corresponding low-pass filtered component injected by the auxiliary inverter in CCM: the voltage between the a) left b) right asymmetric leg and the full leg

As mentioned in Chapter 3, the auxiliary inverter has to generate both the differential mode voltage and the common mode voltage when operating in circulating current mode. The auxiliary inverter operates with 5kHz switching frequency to generate a PWM voltage between the two asymmetric leg midpoints to cancel the low order harmonics (around 150Hz) of the differential mode voltage in the active switching state. In the zero switching state, the auxiliary inverter also has to generate a PWM voltage which is used to cancel the difference between the output voltage of the standard cycloconverter and the output voltage reference. Thus, in order to illustrate explicitly the low frequency components of the auxiliary inverter which are the real effect in improving the performance of cycloconverter, Fig. 4.38 includes also the low-pass filtered component (blue) of the injected PWM voltage (green). As the maximum injected voltage cannot exceed the DC-link capacitor voltage, it can be seen

indirectly from Fig. 4.38 that the DC-link voltage used in the simulation is around 295V, which is around half of the peak of the differential mode voltage (Fig. 4.14). Although by increasing the capacitor voltage, it will be possible to further improve the circulating current, as well as the quality of the output voltage waveform, the rating of the power devices in the auxiliary inverter will also be increased. Therefore, a balance always needs to be found between the performance of the circulating current and the cost of the converter in order to achieve both of the quality and economic targets.

Fig. 4.39 shows the spectrum of the PWM voltages in Fig. 4.38 injected by the auxiliary inverter, where the harmonic components injected by the auxiliary inverter concentrate around multiples of 150Hz, such as 150Hz, 300Hz, 450Hz. As expected, these are also the harmonics that need to be cancelled in both of the differential mode voltage and the common mode voltage as generated by the standard cycloconverter.
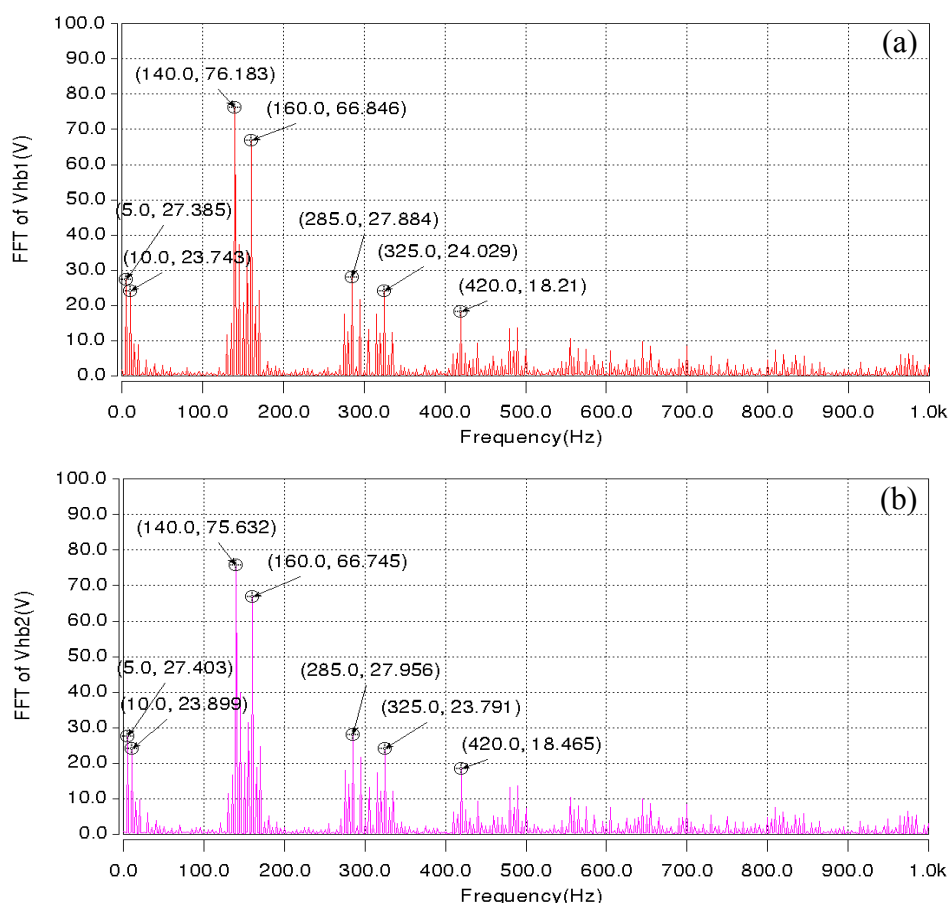
Fig. 4.39: Spectrum of the PWM voltage injected by the auxiliary inverter in CCM: the voltage between the a) left b) right asymmetric leg and the full leg

4.4.2 The Hybrid Cycloconverter in Circulating Current-Free Mode

In circulating current-free mode, the hybrid cycloconverter topology considered is the one with an auxiliary inverter having 295V DC-link capacitor voltage, which is the same as the last topology that was discussed in the circulating current mode. Since there is no circulating current to be analyzed, the analysis in this subsection starts with the load side performance. Fig. 4.40 shows the phase-to-supply neutral output voltage waveform of the hybrid cycloconverter in circulating current-free operating mode. The output voltage is improved through injecting a common mode voltage with the auxiliary inverter to minimize the difference between the output voltage of the standard cycloconverter and the output voltage reference. Compared to the circulating current mode, the auxiliary inverter in circulating current-free mode is only used to improve the common mode voltage, therefore the switching period does not have to be divided into two functional parts (active state + zero state). Fig. 4.41 shows the spectrum of the hybrid cycloconverter phase-to-supply neutral output voltage, revealing that the auxiliary inverter is able to improve the spectrum by reducing the unwanted harmonics to a negligible level (1.47V_{pk} at 130Hz and 1.43V_{pk} at 140Hz), which is a better achievement compared to the hybrid cycloconverter in circulating current mode. This improvement is also clearly reflected in the shape of the load current, shown in Fig. 4.42.
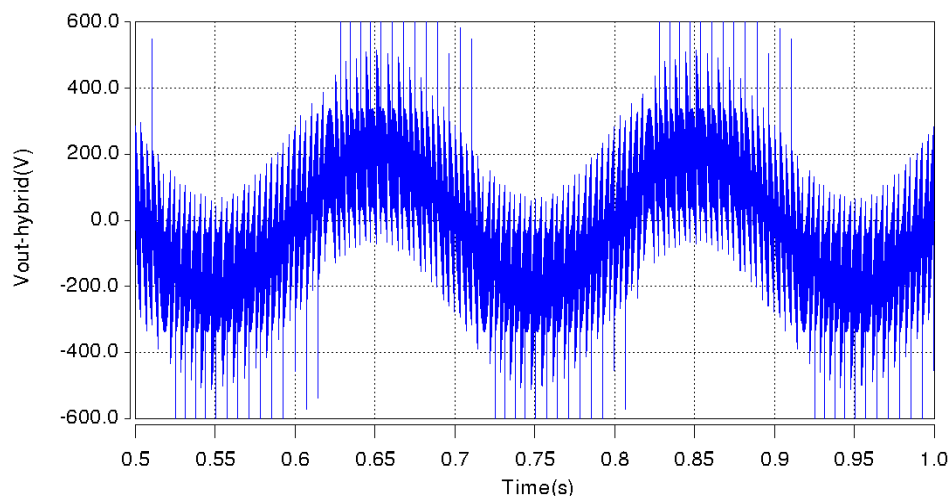
Fig. 4.40: Phase-to-supply neutral output voltage waveform of the hybrid cycloconverter in CCFM
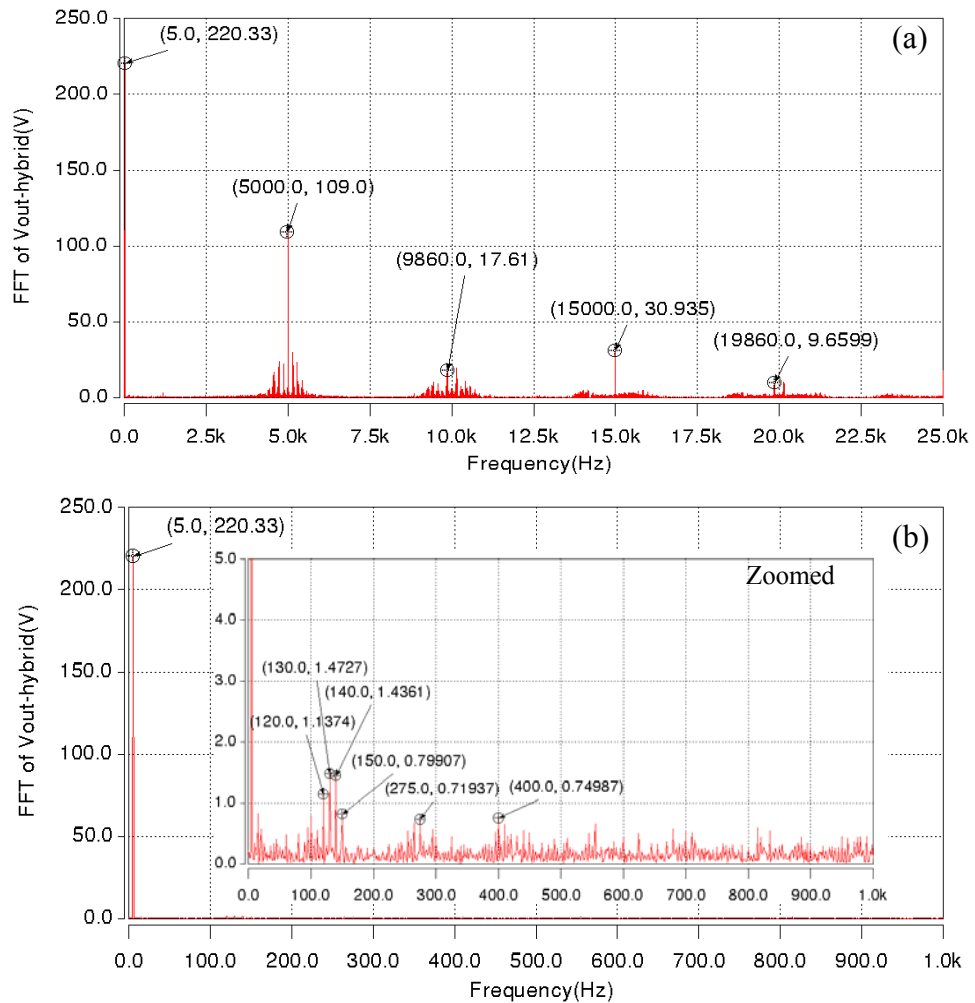
Fig. 4.41: Spectrum of the phase-to-supply neutral output voltage of the hybrid cycloconverter in CCFM: a) 0-25kHz range b) 0-1kHz range
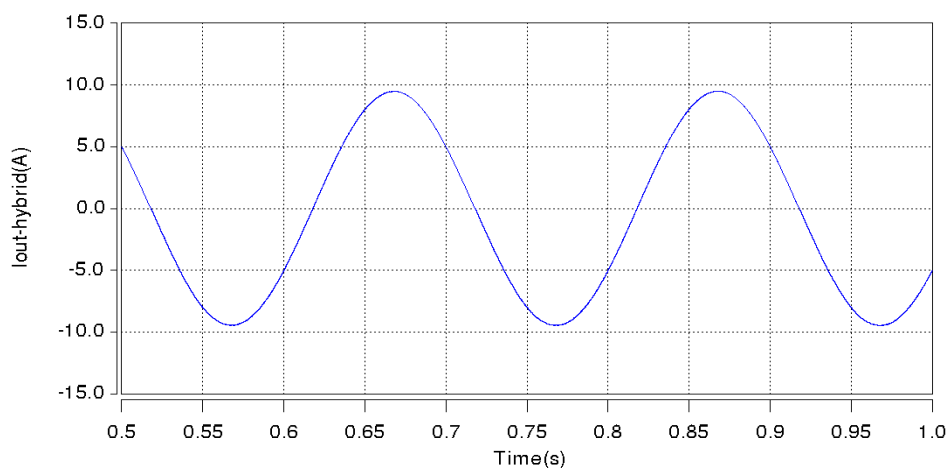
Fig. 4.42: Load current waveform of the hybrid cycloconverter in CCFM

In the circulating current-free mode, the injected voltage between the mid-point of either asymmetric leg and the mid-point of full leg of the auxiliary inverter is

exclusively applied to cancel the common mode voltage harmonics shown in Fig. 4.43, where both the PWM voltage and its low-pass filtered component are displayed together, to reveal the modulating signal. The DC-link capacitor voltage in the auxiliary inverter is equal to the amplitude of the injected PWM voltage as shown in Fig. 4.43, which for the situation considered, is around 295V. Fig. 4.44 shows the spectrum of the injected voltage, which looks very similar to the spectrum of the standard cycloconverter output voltage in circulating current-free mode (Fig. 4.22), except for the 5Hz fundamental component. Therefore, this proves that the voltage injected by the auxiliary inverter is only used to cancel the existing distortion in the output voltage of the standard cycloconverter.
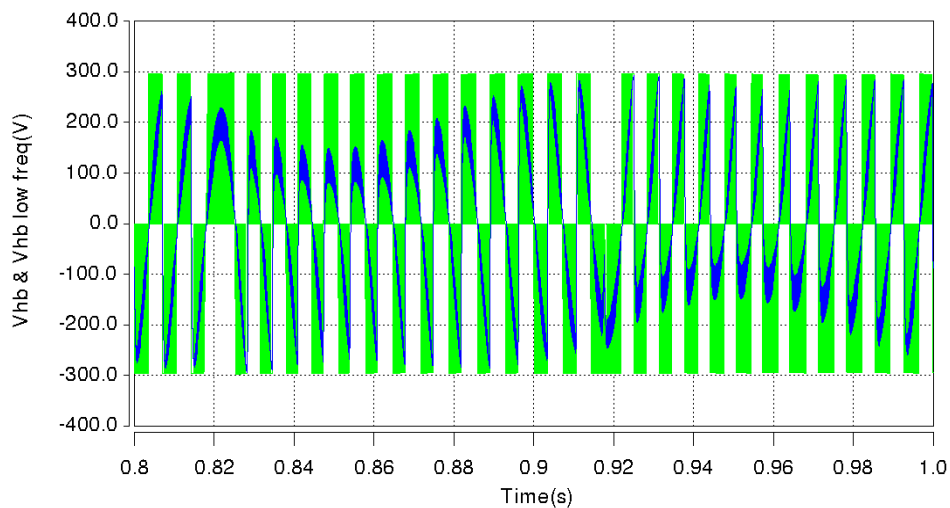
Fig. 4.43: PWM voltage waveform and the corresponding low-pass filtered component injected by the auxiliary inverter in CCFM
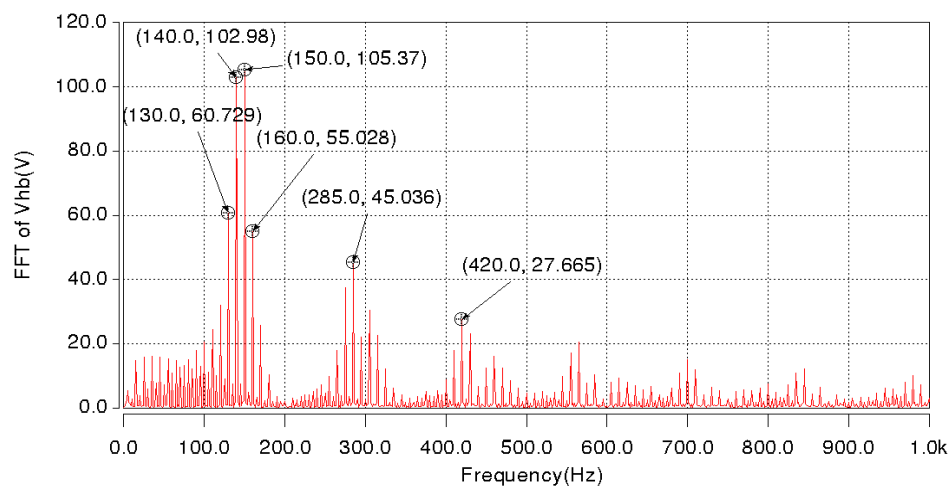
Fig. 4.44: Spectrum of the PWM voltage injected by the auxiliary inverter in CCFM

4.5   The Three-Phase Input to Three-Phase Output Cycloconverter

In this section, the line-to-line output voltage, the load current and the input current of the three-phase input to three-phase output standard and hybrid cycloconverters, in both circulating current and circulating current-free modes, will be analyzed. Fig. 4.45 shows the diagram of a three-phase to three-phase hybrid cycloconverter and the corresponding variables measured with simulation are shown on it. Since the circulating current reactors or the auxiliary inverter can be removed depending on the topology of the simulation model or the operating mode, only the hybrid cycloconverter in circulating current mode is shown below.
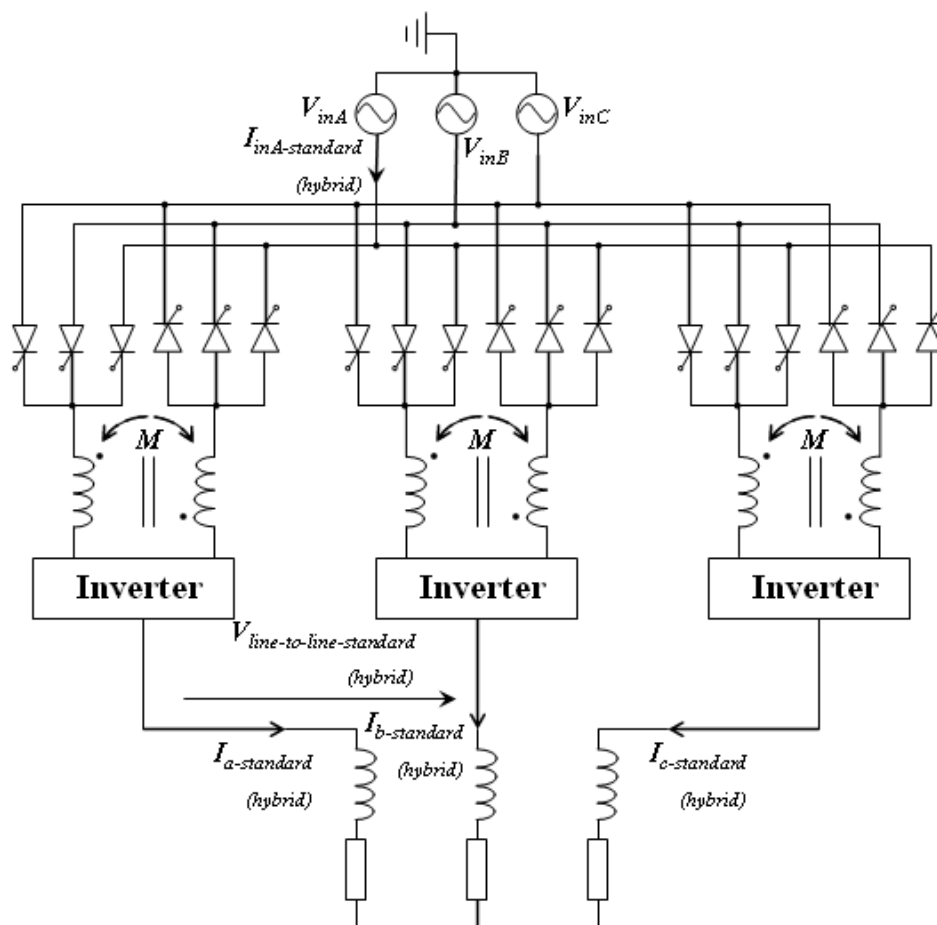
Fig. 4.45: The diagram of a three-phase to three-phase cycloconverter with variables for measurement

4.5.1 The Line-to-Line Output Voltage Evaluation

If the output of the cycloconverter is connected to a balanced three-phase load, the line-to-line output voltage is relevant for evaluating the load side performance of any converter. Moreover, the line-to-line voltage may achieve some degree of harmonic cancelation/reduction compared to the phase-to-supply neutral output voltage.

Fig. 4.46 and Fig. 4.47 show the line-to-line output voltage waveform and spectrum of the standard cycloconverter in circulating current mode respectively. Unlike the phase-to-supply neutral output voltage which is a 4-level voltage waveform shown in Fig. 4.18, the line-to-line voltage shown in Fig. 4.46 is a 5-level voltage waveform. Compared with the spectrum of the phase-to-supply neutral output voltage shown in Fig. 4.19, the spectrum of the line-to-line voltage still contains harmonics around multiples of 150Hz, such as 150Hz, 300Hz, and the ratio between the amplitude of these harmonics to the fundamental component (5Hz) remains more or less the same. However, some frequency harmonics present in the phase-to-supply neutral voltage spectrum such as the 150Hz, 285Hz, 420Hz, have been significantly reduced or even completely eliminated in the line-to-line spectrum. Thus, it can be concluded that some degree of improvement is naturally achieved in the quality of the line-to-line output voltage waveform compared to the phase-to-supply neutral output voltage.
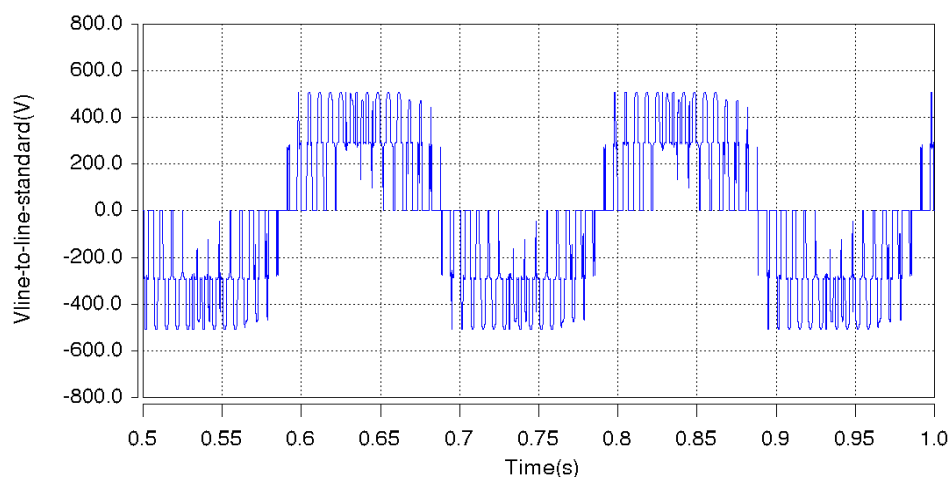
Fig. 4.46: Line-to-line output voltage waveform of the three-phase to three-phase standard cycloconverter in CCM
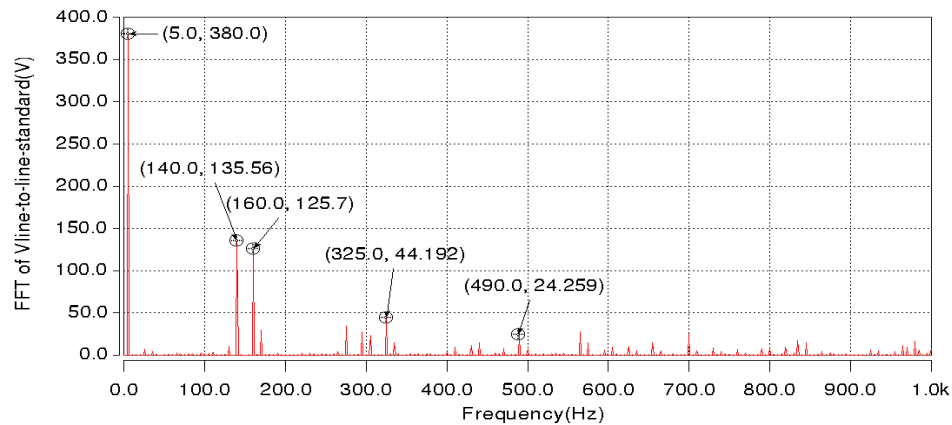
Fig. 4.47: Spectrum of the line-to-line output voltage of the three-phase to three-phase standard cycloconverter in CCM

Fig. 4.48 and Fig. 4.49 show the line-to-line output voltage waveform and spectrum of the hybrid cycloconverter in circulating current mode respectively. The wide frequency spectrum shown in Fig. 4.49(a) reveals that the significant high frequency components in the line-to-line output voltage still present are around multiples of the switching frequency (5kHz). Compared with the spectrum of the line-to-line output voltage generated by the standard cycloconverter shown in Fig. 4.47, the significant low frequency harmonics have all been much reduced by the hybrid cycloconverter, such as from $135V_{pk}$ to $14V_{pk}$ at 140Hz, from $125V_{pk}$ to $26V_{pk}$ at 160Hz, as shown in Fig. 4.49(b). Similar to what happens in the standard cycloconverter, some given harmonics such as the 150Hz, 285Hz, 420Hz in Fig. 4.49(b) have been almost eliminated compared to that present in the corresponding phase-to-supply neutral output voltage, as shown in Fig. 4.36.
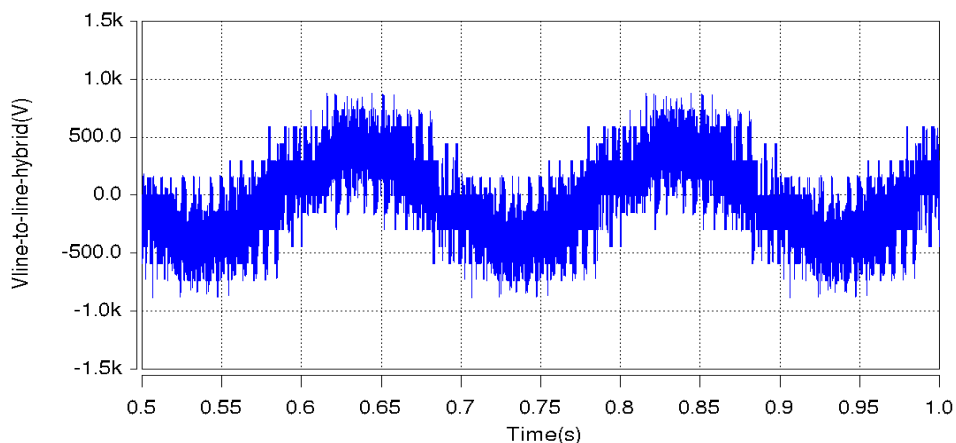
Fig. 4.48: Line-to-line output voltage waveform of the three-phase to three-phase hybrid cycloconverter in CCM

- 125 -
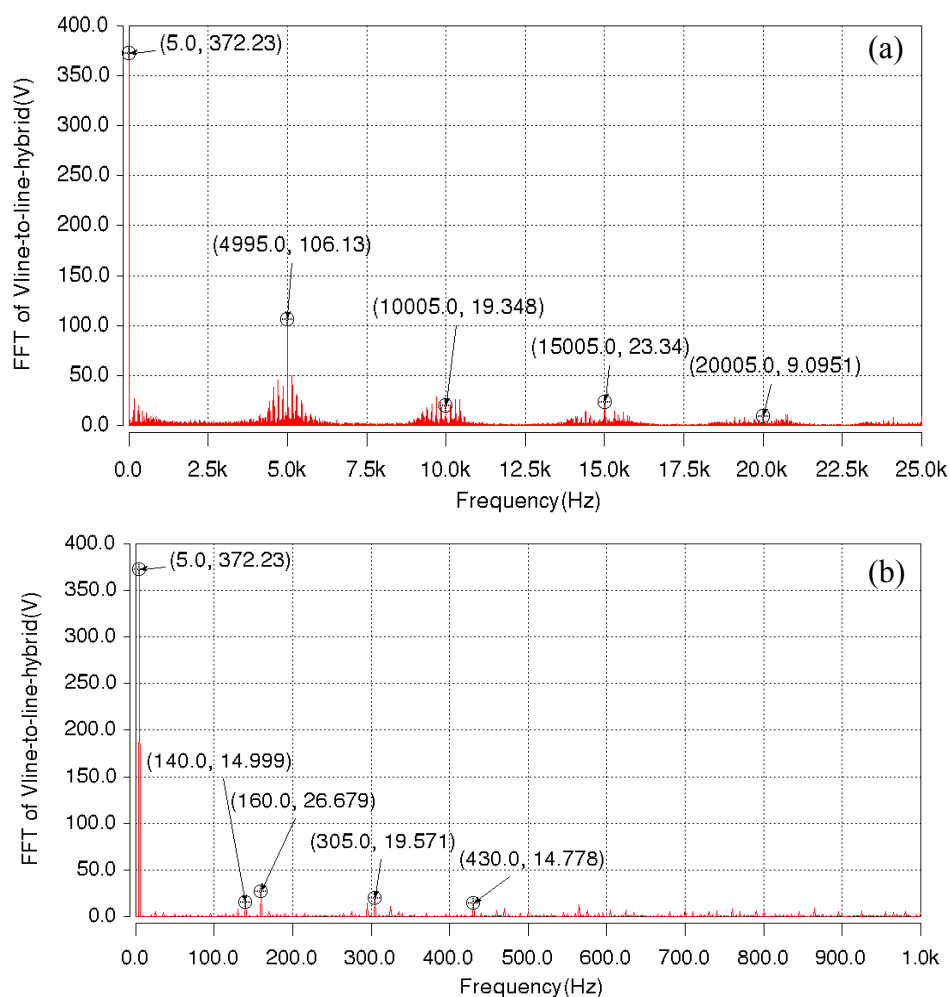
Fig. 4.49: Spectrum of the line-to-line output voltage of the three-phase to three-phase hybrid cycloconverter in CCM: a) 0-25kHz range b) 0-1kHz range

Fig. 4.50 and Fig. 4.51 show the waveform and the corresponding spectrum of the line-to-line output voltage of the standard cycloconverter in circulating current-free mode. Compared to Fig. 4.22, which shows the spectrum of the phase-to-supply neutral output voltage, some given frequency components such as 150Hz, 285Hz, 420Hz in the spectrum of the line-to-line voltage are eliminated because these components are all in phase (common mode) in the different phase-to-supply neutral output voltages, whilst the amplitude of the other harmonics maintain the same ratio to the fundamental component. Moreover, for the same reason mentioned for the phase-to-supply neutral output voltage, the spectrum of the line-to-line output voltage in circulating current-free mode also contains some extremely low frequency components which are just above the output frequency (5Hz).
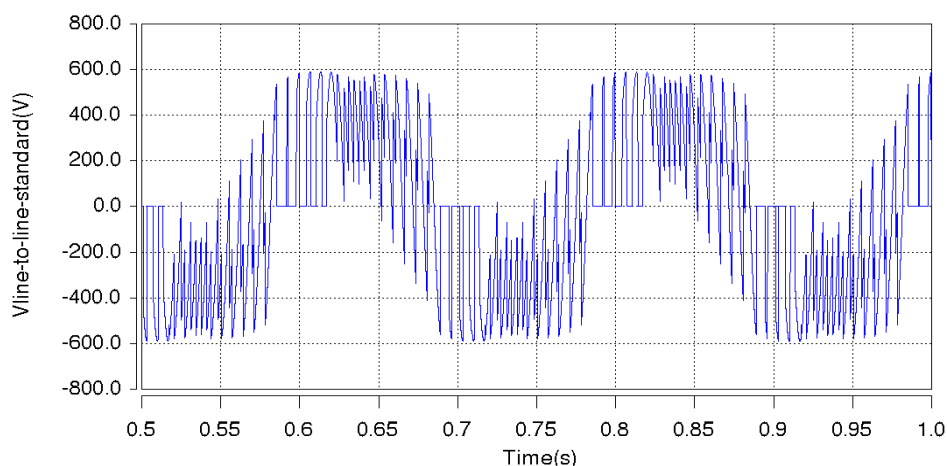
Fig. 4.50: Line-to-line output voltage waveform of the three-phase to three-phase standard cycloconverter in CCFM
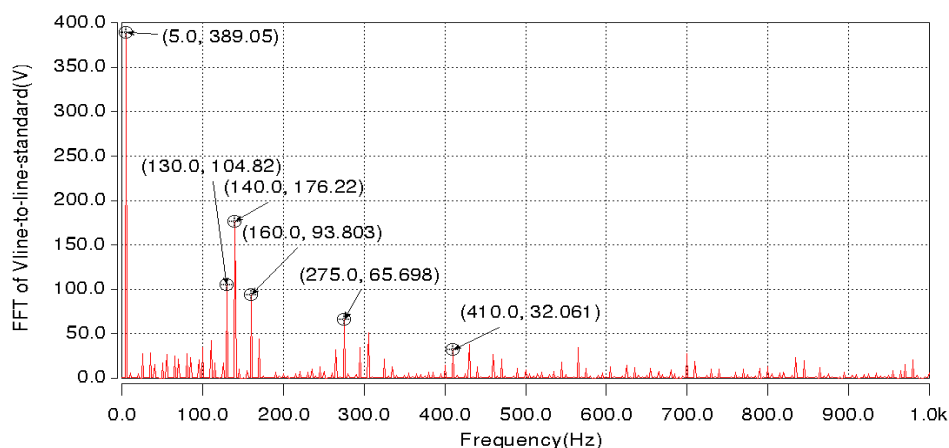
Fig. 4.51: Spectrum of the line-to-line output voltage of the three-phase to three-phase standard cycloconverter in CCFM

Fig. 4.52 and Fig. 4.53 show the line-to-line output voltage waveform and the corresponding spectrum of the hybrid cycloconverter in circulating current-free mode. Compared to the spectrum of the line-to-line output voltage generated by the standard cyclocoverter as shown in Fig. 4.51, all the low frequency harmonics are reduced to a negligible level by the hybrid cycloconverter, such as $2.16V_{pk}$ at 130Hz, $1.89V_{pk}$ at 140Hz, as shown in Fig. 4.53(b). Furthermore, similar to all the situations mentioned before in this subsection, the harmonics of 150Hz, 285Hz, 420Hz should still be significantly reduced or eliminated compared to the corresponding harmonics present in the phase-to-supply neutral voltage shown in Fig. 4.41. However, since all the low order harmonics present in the output voltage in circulating current-free mode have almost been completely eliminated by the hybrid cycloconverter, there may exist some

- 127 -

errors on the very small amplitude of the harmonics shown in the enlarged figure of Fig. 4.53. Therefore, it is not easy to make the comparison between the line-to-line output voltage and the phase-to-supply output voltage according to the figures.
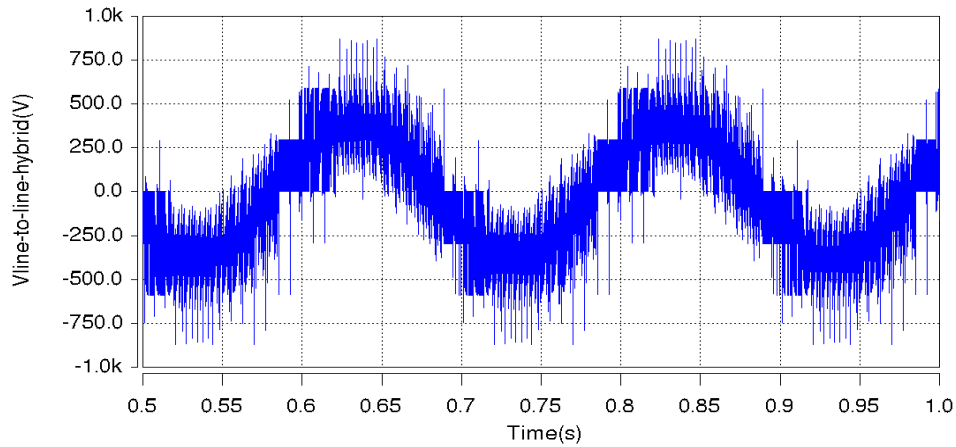
Fig. 4.52: Line-to-line output voltage waveform of the three-phase to three-phase hybrid cycloconverter in CCFM
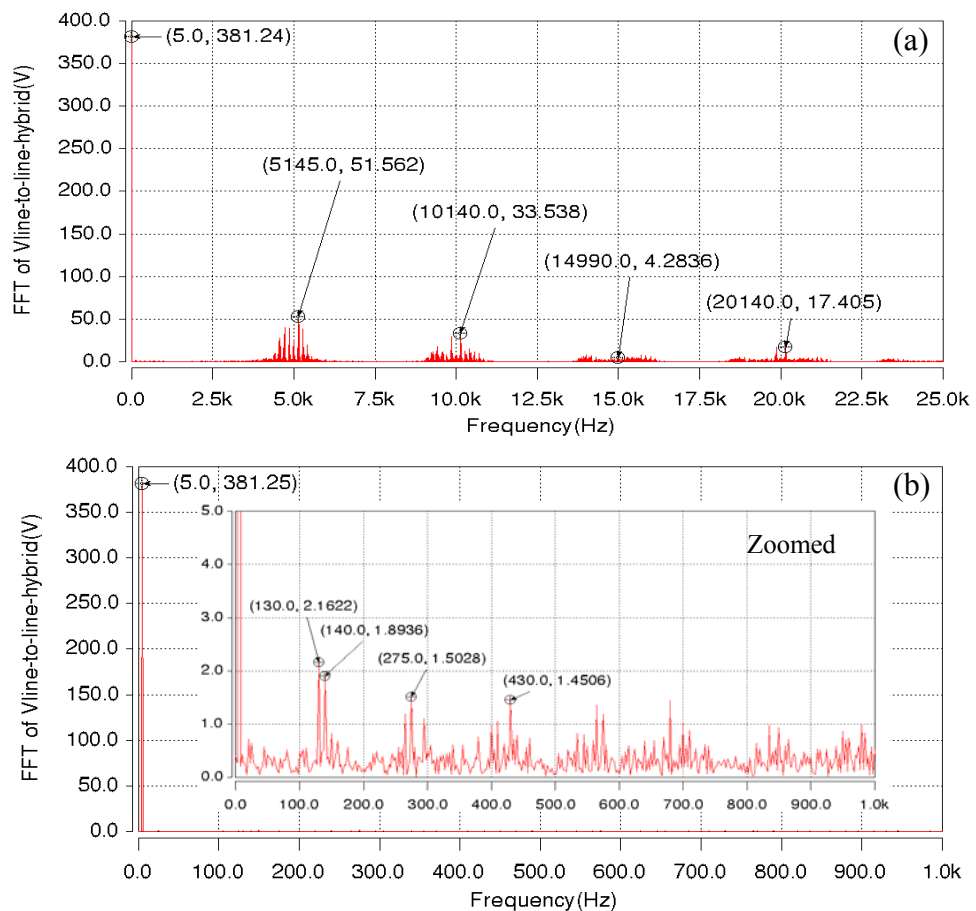
Fig. 4.53: Spectrum of the line-to-line output voltage of the three-phase to three-phase hybrid cycloconverter in CCFM: a) 0-25kHz range b) 0-1kHz range

Therefore, from all four cases analyzed above, it can be concluded that some harmonics at given frequencies present in the phase-to-supply neutral output voltage, such as the 150Hz, 285Hz, 420Hz, for 5Hz output frequency and 50Hz supply frequency, are eliminated in the line-to-line output voltage. This naturally harmonic cancellation between each phase is independent of cycloconverter type as well as its operating mode. This is an important fact in applications where the load operates with an isolated neutral since the line-to-line voltage of the converter is always the real output voltage which applied to the load side, causes corresponding currents (and its corresponding harmonics) and defines the converter performance. Therefore, to achieve the same improvement on the line-to-line output voltage waveform, the DC-link capacitor voltage may be further reduced (and therefore the smaller semiconductor's rated voltage) if the auxiliary inverter does not have to handle the harmonics present in all the phase-to-supply neutral output voltages mentioned above.

4.5.2 Three-Phase Load Current Evaluation

In order to illustrate the balance of the three-phase load, Fig.4. 54 to 4.57 show the three-phase load current waveforms for the standard and the hybrid cycloconverter, operating in circulating current and circulating-free mode. The improvement at the load side provided by the hybrid cycloconverter when compared with the standard cycloconverter is clearly visible in the lack of ripple in the load current waveform. Furthermore, from the amplitude of the load current in each phase it can be concluded that in all four situations, the three-phase system is properly balanced at the load side.
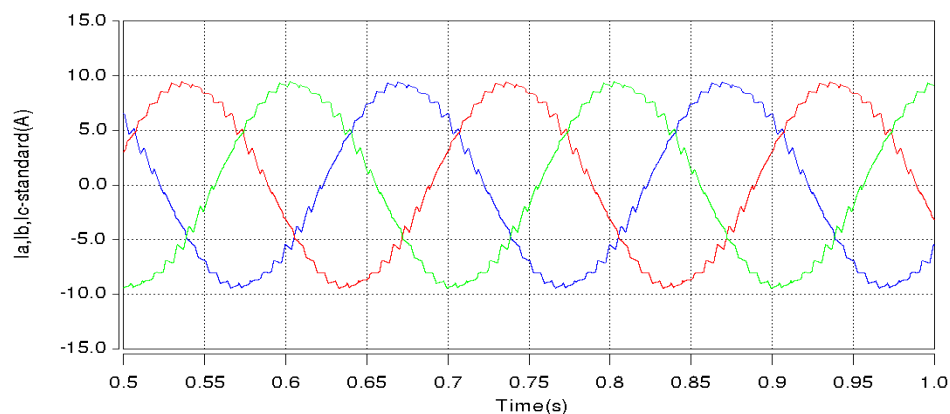
Fig. 4.54: Load currents waveform of the three-phase to three-phase standard cycloconverter in CCM
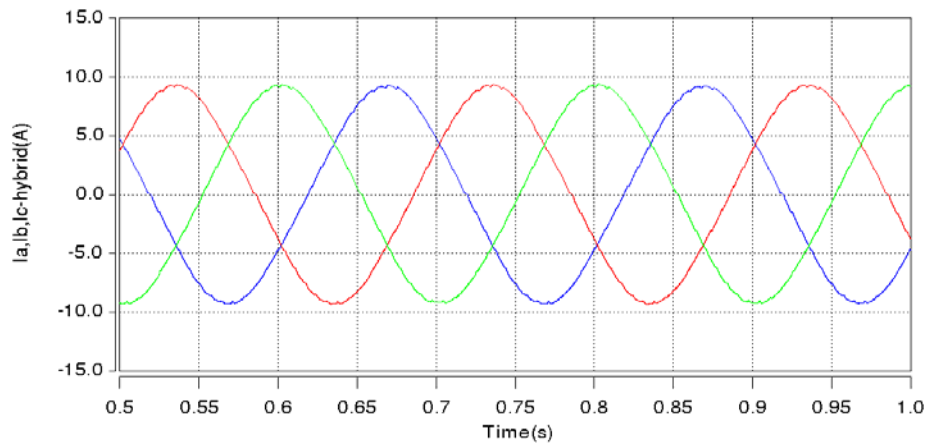
Fig. 4.55: Load currents waveform of the three-phase to three-phase hybrid cycloconverter in CCM
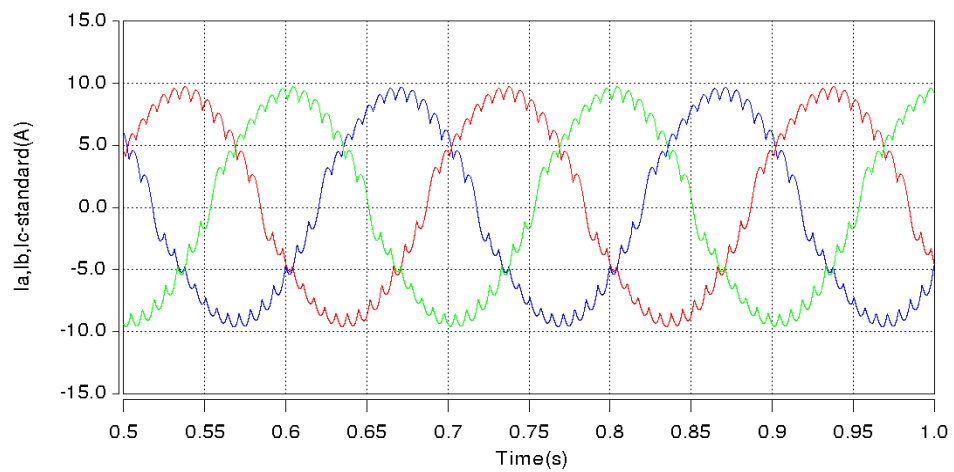
Fig. 4.56: Load currents waveform of the three-phase to three-phase standard cycloconverter in CCFM
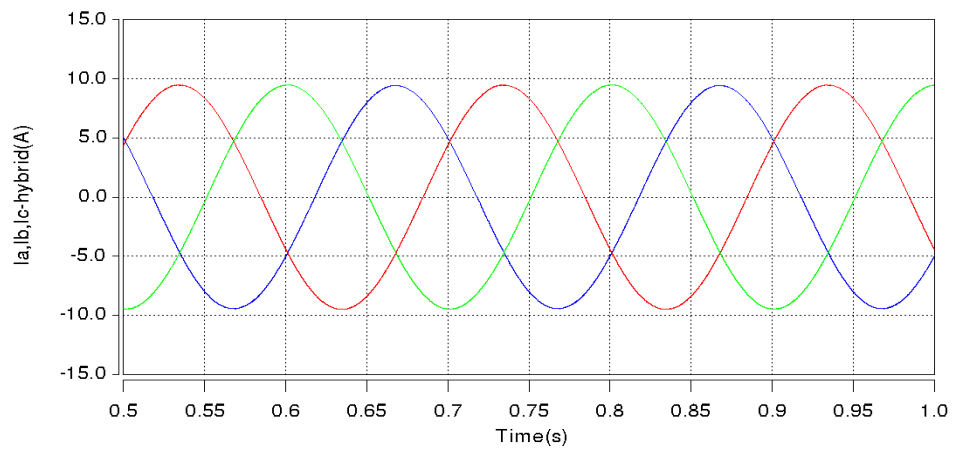
Fig. 4.57: Load currents waveform of the three-phase to three-phase hybrid cycloconverter in CCFM

4.5.3 The Input Current Evaluation

In this subsection, the input side performance, which is only relevant for a three-phase to three-phase system, is evaluated by using the waveforms and the spectrum of the input current in all four situations: the operation of the standard vs. hybrid cycloconverter with and without circulating current. It is known that the quality of the input current is a result of the number of pulses, the load side performance, and the circulating current [pp.365-366, 1]. Therefore in order to make a fair comparison, the input currents are extracted from simulations performed in similar conditions: same number of pulses and the same supply and connected load. The relevant data which are used to evaluate the input side performance, such as power displacement factor (DPF), power distortion factor (DF), are defined from Equation (4.12) to (4.15) and their value for each situation are summarized in Table. 4.5, at the end of this subsection.

Fig. 4.58 and Fig. 4.59 show the waveform and the spectrum of the input current of the standard cycloconverter in circulating current mode. As can be seen from the spectrum of the input current, the amplitude of the fundamental component (50Hz) drawn from the cycloconverter is around $15.3A_{pk}$. There are some other harmonics or inter-harmonics, which are sums or differences between multiples of the input and outoput frquencies [pp.369-371, 1], such as the 85Hz, 115Hz, 185Hz, 250Hz, present in the input current as well.
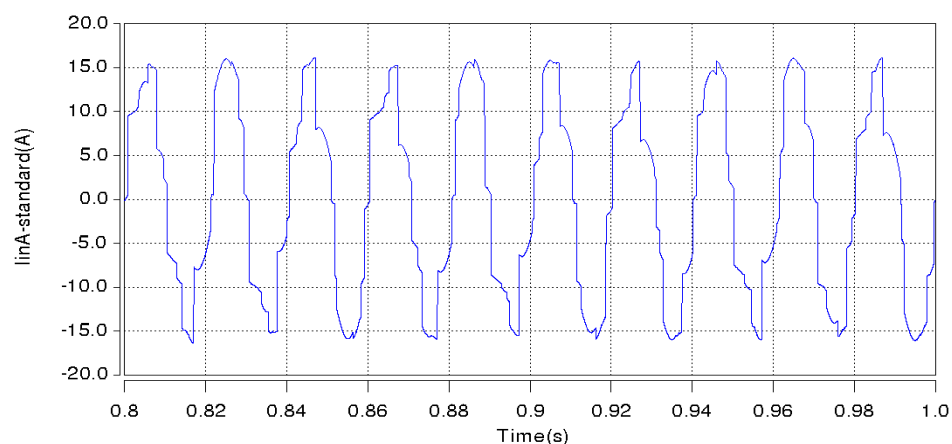
Fig. 4.58: Input current waveform of the three-phase to three-phase standard cycloconverter in CCM
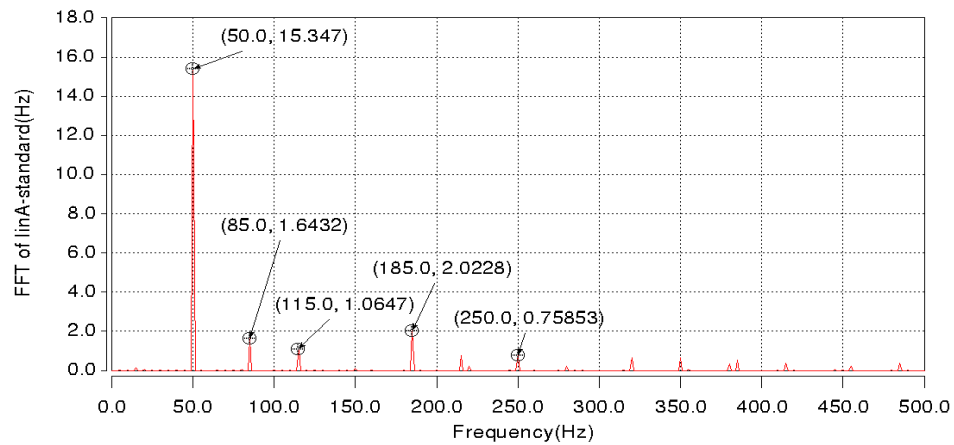
Fig. 4.59: Spectrum of the input current of the three-phase to three-phase standard cycloconverter in CCM

Fig. 4.60 and Fig. 4.61 show the waveform and its corresponding spectrum of the input current of the hybrid cycloconverter operating in circulating current mode. As can been seen from the spectrum of the input current, for the same amount of active power delivered to the load, the 50Hz fundamental component has been reduced from $15.3A_{pk}$ in the case of the standard cycloconverter with circulating current to $11.8A_{pk}$ or the hybrid one. Hence, the displacement power factor of the hybrid cycloconverter is significantly improved compared to the standard cycloconverter as shown in Table. 4.5. This is because the input current is not influenced much by the circulating current in the hybrid cycloconverter compared to the standard cycloconverter since the circulating current in the hybrid topology is under control around a given small DC component (see Fig. 4.33).
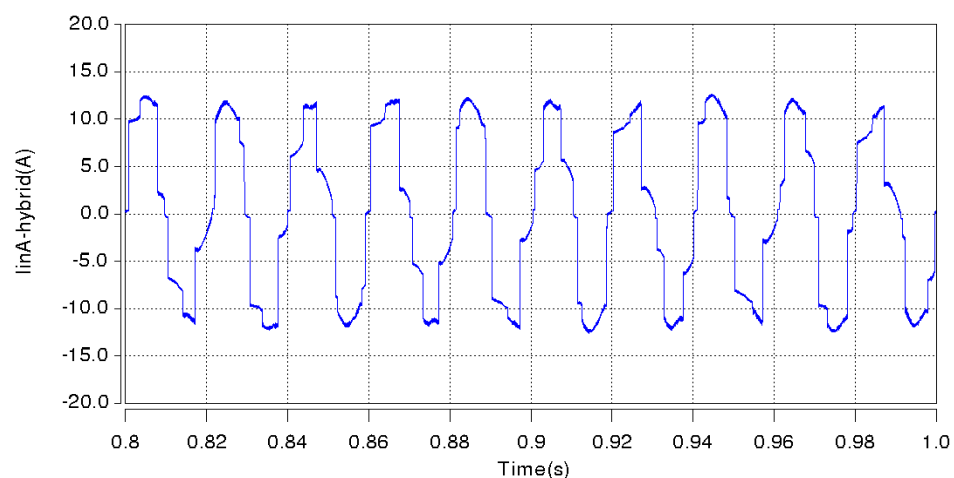
Fig. 4.60: Input current waveform of the three-phase to three-phase hybrid cycloconverter in CCM
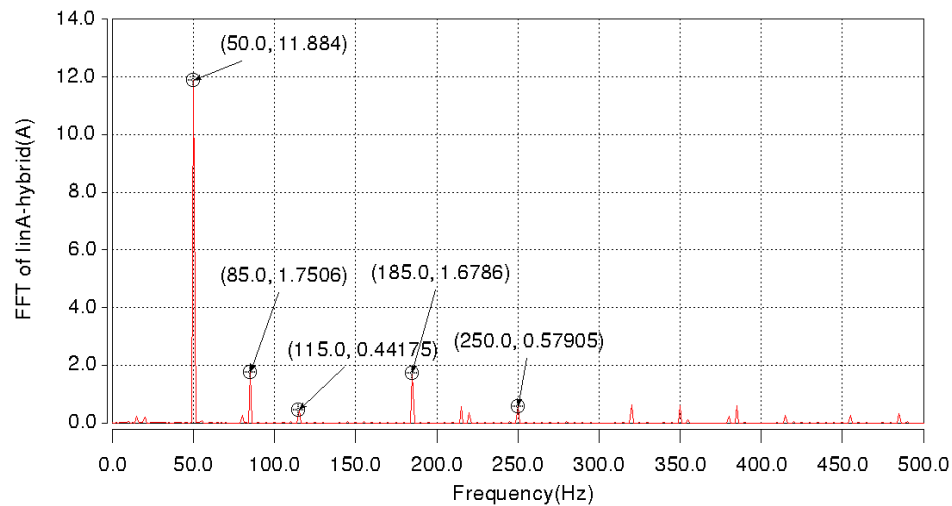
Fig. 4.61: Spectrum of the input current of the three-phase to three-phase hybrid cycloconverter in CCM

The harmonics present in the input current is dependent on the power harmonics drawn from the supply if the input voltage waveform is assumed to be a pure sinusoidal wave. Since the output power of the thyristor bridge in a cycle is the same as the input power (the standard cycloconverter is a direct frequency changer with no energy storage), the input current harmonics will depend on the output power ripple of the thyristor bridge. Due to the highly inductive load, the load current harmonics are much smaller compared to the output voltage harmonics of the thyristor half bridge, no matter in a standard or a hybrid cycloconverter. Hence, the input current harmonics is mainly dependent on the output voltage harmonics of the thyristor half bridge. As in the hybrid approach the operation of the thyristor half bridge remains the same, the amplitude of the input current harmonics drawn by the hybrid cycloconverter should be similar to those in the standard cycloconverter. This is verified by comparing the significant input current harmonics of both topologies, as presented in Table. 4.3. From this table it can be seen that the amplitudes of some frequency components are increased whilst the others are decreased in the hybrid cycloconverter compared to those drawn by the standard cycloconverter. This may be caused by the behavior of accurately controlling the circulating current in the hybrid solution. However, no obvious reduction of the harmonics takes place between the hybrid and the standard cycloconverter. Furthermore, the distortion power factors or the total harmonic distortion factors displayed in Table. 4.5 show that the values corresponding to the standard and the hybrid cycloconverters are very similar.

Therefore, the hybrid cycloconverter in circulating current mode is able to obtain a better input power factor than the standard cycloconverter although only the displacement power factor is clearly improved.

	85Hz	115Hz	185Hz	250Hz
Standard	1.64A$_{pk}$	1.06A$_{pk}$	2.02A$_{pk}$	0.75A$_{pk}$
Hybrid	1.75A$_{pk}$	0.44A$_{pk}$	1.68A$_{pk}$	0.57A$_{pk}$

Table. 4.3: Comparison of the amplitudes of significant harmonics present in the input current for both the standard and the hybrid cycloconverter in CCM

Fig. 4.62 and Fig. 4.63 show the waveform and its corresponding spectrum of the input current of the standard cycloconverter operating in circulating current-free mode. This situation can be considered as an extreme situation where the circulating current is decreased to its minimum (zero), therefore it can be seen that only 10.3A$_{pk}$ fundamental input current is drawn by the cycloconverter and the displacement power factor is better than that in the circulating current mode as shown in Table. 4.5. Similar to the circulating current mode, there are also some harmonics, inter-harmonics and even sub-harmonics present in the input current. Additionally, the spectrum of the input shown in Fig. 4.63 is very similar to that in Fig. E.3 (Appendix E), which represents the theoretical input current spectrum of the standard cycloconverter in circulating current-free mode according to the analysis in [pp.369-373, 1].
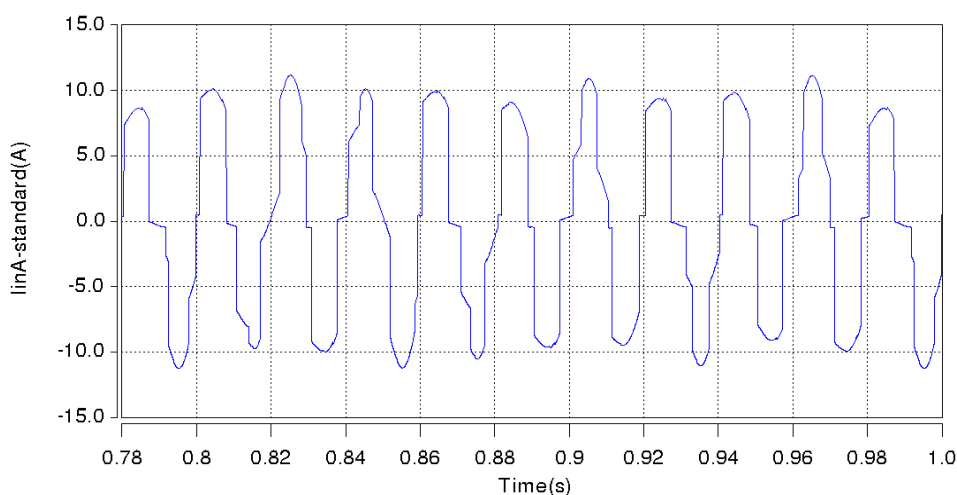
Fig. 4.62: Input current waveform of the three-phase to three-phase standard cycloconverter in CCFM
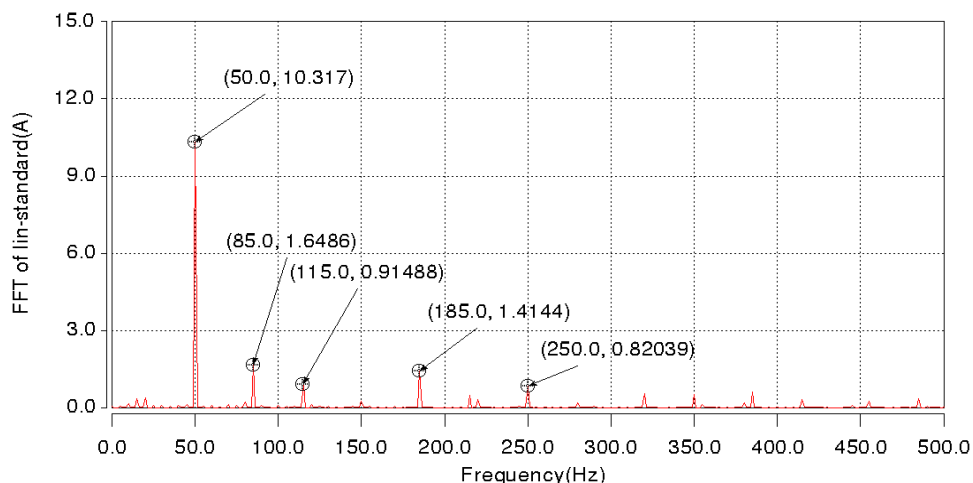
Fig. 4.63: Spectrum of the input current of the three-phase to three-phase standard cycloconverter in CCFM

Fig. 4.64 and Fig. 4.65 show the waveform and its corresponding spectrum of the hybrid cycloconverter input current operating in circulating current-free mode. The spectrum of the input current of the hybrid cycloconverter is very similar to that of the standard cycloconverter since there is no effect of the circulating current as well as almost the same effect of the output power harmonics due to the reason described for the circulating current mode. Therefore, the amplitude of all the significant harmonics compared to that of the standard cycloconverter remains more or less the same, as shown in Table. 4.4. Moreover, as shown in Table. 4.5, both the displacement power factor and the distortion power factor (or THD) produced by the hybrid cycloconverter are very similar to that of the standard cycloconverter.
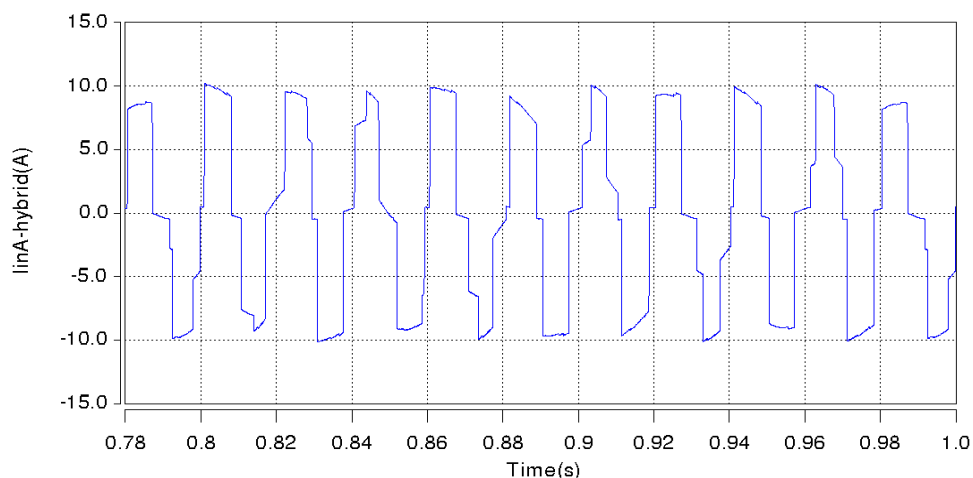
Fig. 4.64: Input current waveform of the three-phase to three-phase hybrid cycloconverter in CCFM
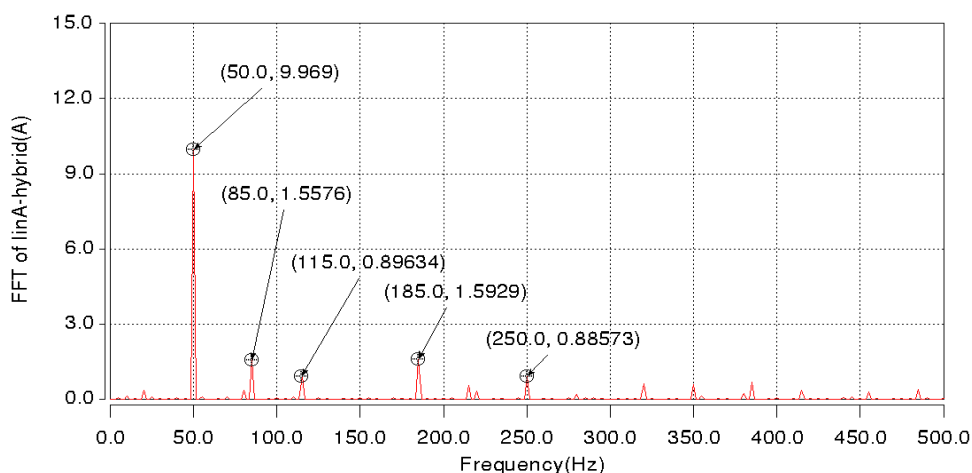
Fig. 4.65: Spectrum of the input current of the three-phase to three-phase hybrid cycloconverter in CCFM

	85Hz	115Hz	185Hz	250Hz
Standard	1.64A$_{pk}$	0.91A$_{pk}$	1.41A$_{pk}$	0.82A$_{pk}$
Hybrid	1.55A$_{pk}$	0.89A$_{pk}$	1.59A$_{pk}$	0.88A$_{pk}$

Table. 4.4: Comparison of the amplitudes of significant harmonics present in the input current for both the standard and the hybrid cycloconverter in CCFM

By summarizing the performance of all four cycloconverter arrangements, it can be concluded that whilst delivering the same amount of output power to the load, the standard cycloconverter in circulating current mode draws the largest fundamental input current compared to the other three situations since the circulating current, although limited by the coupled reactors, is poorly controlled. However, the fundamental component of the input current can be reduced by minimizing and accurately controlling the circulating current in the hybrid cycloconverter and this is also helpful in improving the input displacement power factor. Furthermore, the highly inductive load which improves by default the harmonic content of the load current compared to the output voltage, the power harmonics are much more sensitive to the output voltage harmonics than current. Therefore, the improvement on the load side performance due to the hybrid approach will not reflected on the input side and the distortion power factors for all the situations are similar to each other. But by considering the impact of the reactive current, it can be concluded that the cycloconverters without circulating current are able to achieve the best input power factor.

$$DPF = \frac{I_{out1,RMS}{}^2 \times R_{Load} \times 3}{\sqrt{3} \times V_{in-line,RMS} \times I_{inA1,RMS}}$$ (4.12)

$$DF = \frac{I_{inA\,1,RMS}}{I_{inA\,,RMS}}$$ (4.13)

$$THD = \frac{\sqrt{\sum_{h=2,3,\ldots}^{\infty} I_{inAh\,,RMS}{}^2}}{I_{inA\,1.RMS}}$$ (4.14)

$$PF = DPF \times DF$$ (4.15)

	CCM		CCFM	
	Standard	Hybrid	Standard	Hybrid
Displacement power factor (DPF)	0.334	0.427	0.521	0.519
Distortion power factor (DF)	0.971	0.964	0.955	0.947
Total harmonic distortion factor (THD)	0.246	0.275	0.311	0.339
Power factor (PF)	0.324	0.412	0.498	0.491

Table. 4.5: A summary of input side evaluation for both the standard and hybrid cycloconverters in CCM and CCFM

4.6 Simulation Results at a Different Output Frequency and a Different Output Modulation Index

In this section, two additional sets of simulation results are presented: one at a different output frequency (13Hz)/same output modulation index (0.8) and another one at a different output modulation index (0.3) but same output frequency (5Hz) to validate the idea that the hybrid solution is able to improve the performance of the cycloconverter in general operating conditions. All the variables measured with the simulation models in this section can be found in the diagrams (Fig. 4.11, Fig. 4.24, Fig. 4.45) shown in the previous sections.

4.6.1 Simulation Results at a Different Output Frequency

In this subsection, the simulation results of the differential mode voltage and the circulating current in circulating current mode and the results of the phase-to-supply neutral output voltage for both the circulating current mode and circulating current-free mode at 13Hz output frequency are presented. Since the harmonics present in the output votlage are results of the interaction of both the input and output frequency [pp.162, 1] and to ensure a complete different situation is presented for the purpose of comparison, the 13Hz is selected as it is not the multiple of 5Hz. All the other circuit parameters are kept the same as that shown in Table 4.2.

4.6.1.1 The Standard Cycloconverter with an Output Frequency of 13Hz

Fig. 4.66 to 4.73 show the waveforms of the differential mode voltage (only for CCM), the circulating current (only for CCM), the phase-to-supply neutral output voltage and their corresponding spectrum of the standard cycloconverter operating in circulating current mode and circulating current-free mode when the output frequency is 13Hz. The frequency of the harmonics present in these waveforms are different from those in the corresponding spectrum at 5Hz output frequency as the harmonic frequenies are sums or differences of multiples of both the input and output frequency [pp.162, 1]. However, all the significant harmonics are still grouped in clusters around multiples of 150Hz since the topologies are still the 3-pulse (CCFM) or 6-pulse (CCM) thyristor bridge and the input frequency is 50Hz.

The peak value of the differential mode voltage shown in Fig. 4.66 is 525V, which is similar to the 5Hz output frequency situation (506V). Compared with the circulating current waveform at 5Hz output frequency shown in Fig. 4.16, the peak value of the circulating current shown in Fig. 4.68 is not much reduced. This is because the amplitude of the 26Hz low frequency harmonic present in the differential mode voltage is around 2.5 times larger than that of the 10Hz harmonic present in the differential mode voltage at 5Hz output frequency as shown in Fig. 4.15, although the frequency has been increased from 10Hz to 26Hz.

Although the quality of the output voltage should be worse at higher output frequency than that at lower frequency [3, 23], no matter if the cycloconverter operates in circulating current or circulating current-free mode, it is not easy to distinguish this characteristic only from the comparison between the spectra of the 13Hz output voltages shown in Fig. 4.71 and 4.73 and the spectra of the 5Hz output voltages, which was shown in Fig. 4.19 and 4.22. However, the fundamental component of output voltages for both two operating modes remains at $220V_{pk}$ since the output modulation index is fixed at 0.8.
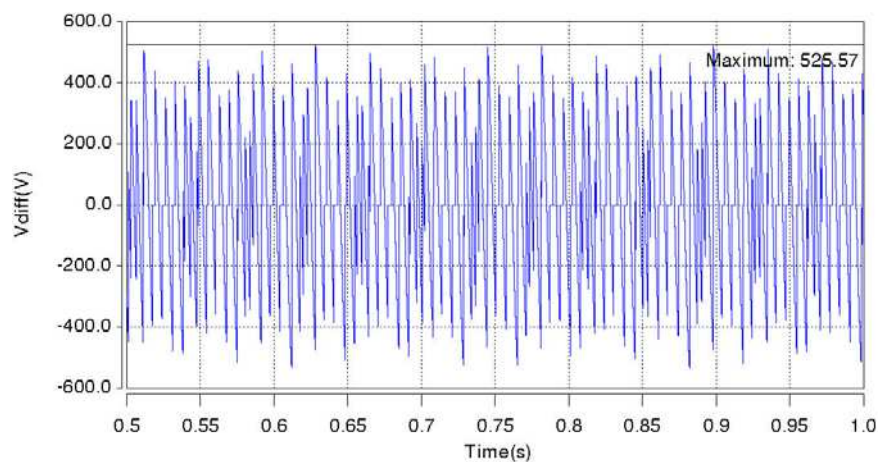
Fig. 4.66: Differential mode voltage waveform seen between the two thyristor half bridge outputs in CCM with an output frequency of 13Hz
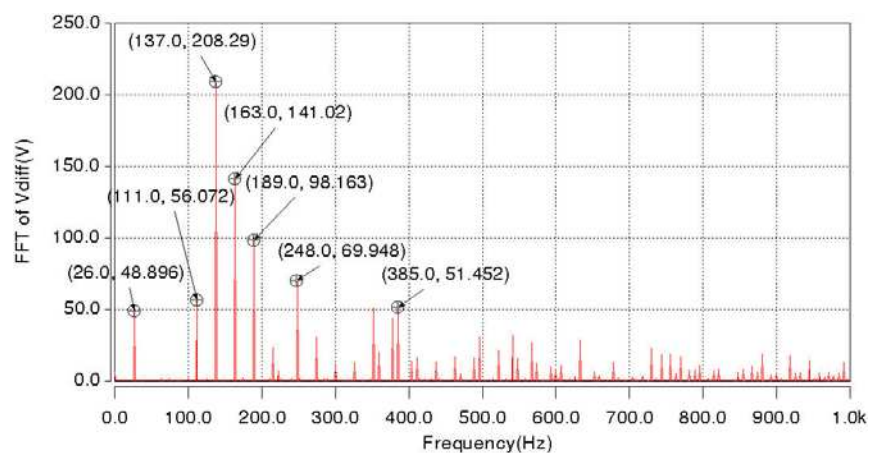
Fig. 4.67: Spectrum of the differential mode voltage seen between the two thyristor half bridge outputs in CCM with an output frequency of 13Hz
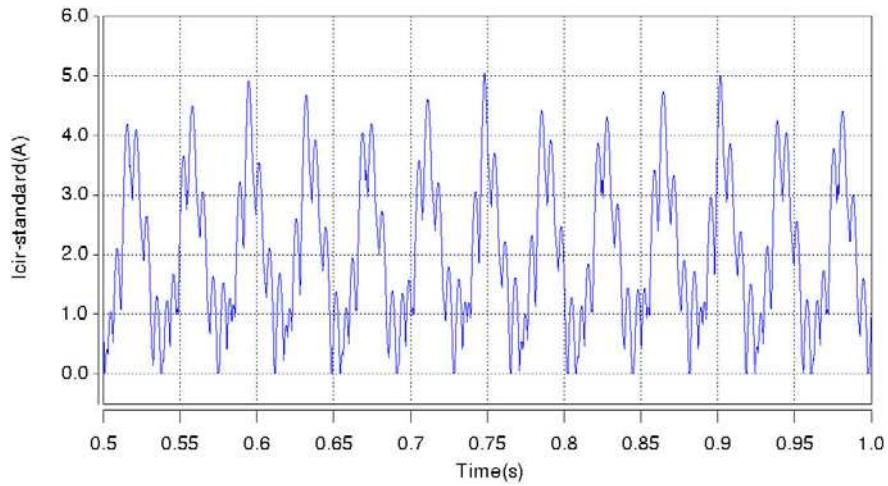
Fig. 4.68: Circulating current waveform of the standard cycloconverter in CCM with an output frequency of 13Hz
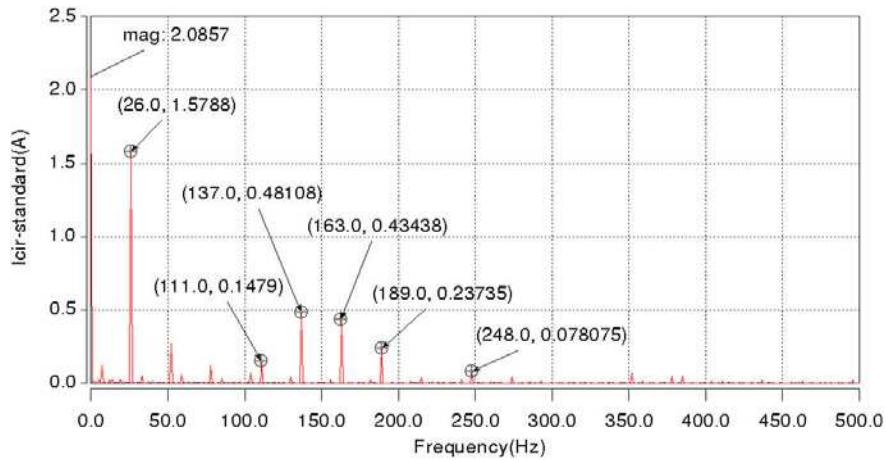
Fig. 4.69: Spectrum of the circulating current of the standard cycloconverter in CCM with an output frequency of 13Hz
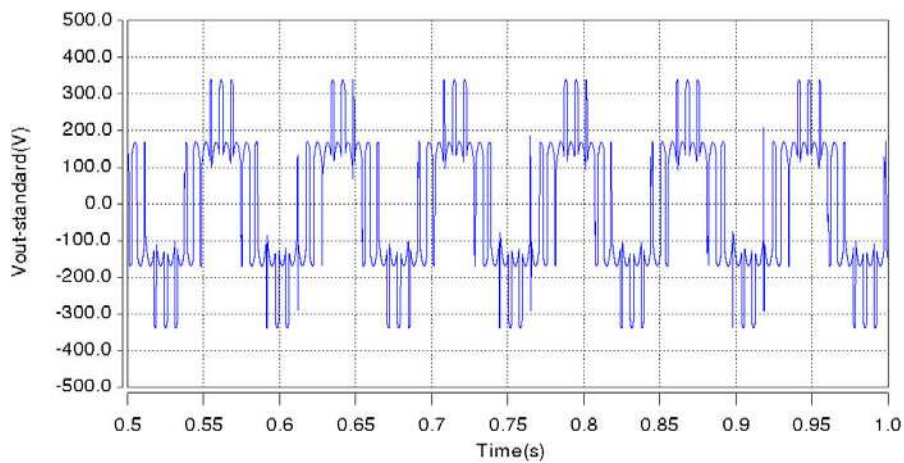
Fig. 4.70: Phase-to-supply neutral output voltage waveform of the standard cycloconverter in CCM with an output frequency of 13Hz
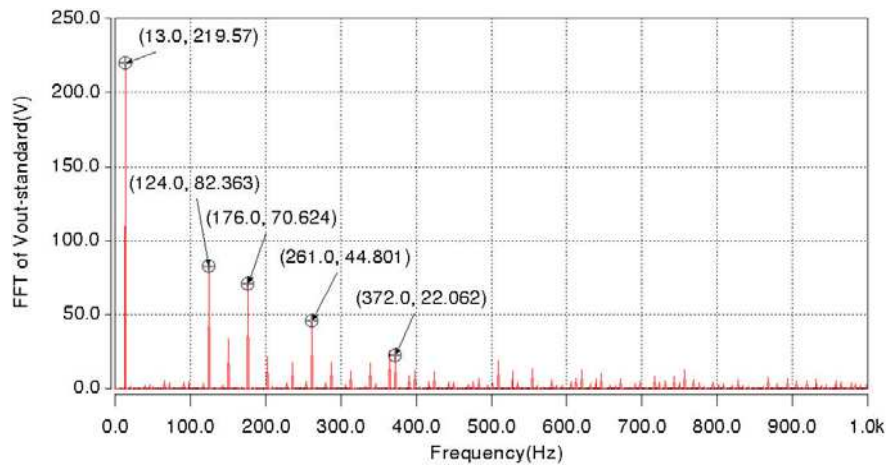
Fig. 4.71: Spectrum of the phase-to-supply neutral output voltage of the standard cycloconverter in CCM with an output frequency of 13Hz
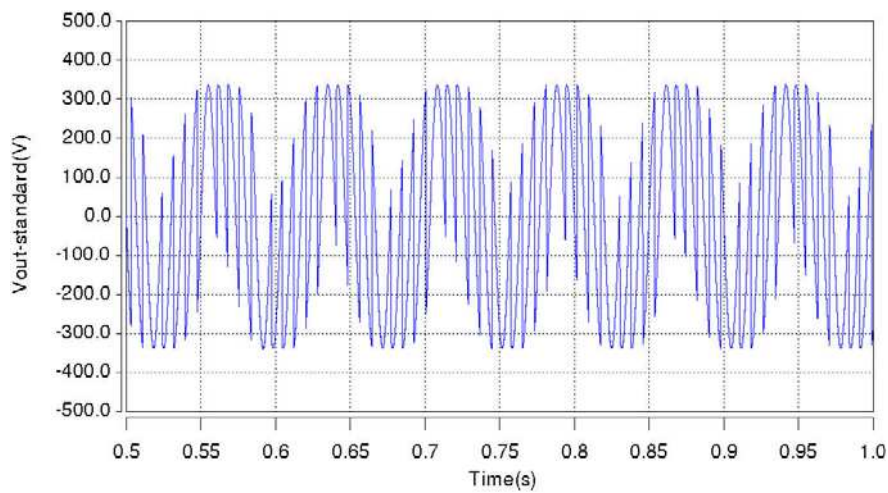
Fig. 4.72: Phase-to-supply neutral output voltage waveform of the standard cycloconverter in CCFM with an output frequency of 13Hz
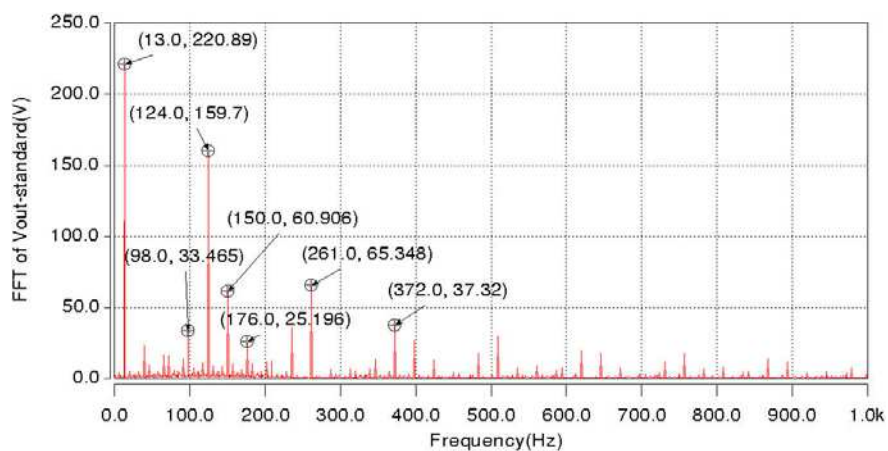
Fig. 4.73: Spectrum of the phase-to-supply neutral output voltage of the standard cycloconverter in CCFM with an output frequency of 13Hz

- 141 -

4.6.1.2 The Hybrid Cycloconverter with an Output Frequency of 13Hz

Fig. 4.74 to 4.79 show the waveform of the circulating current (only for CCM), the phase-to-supply neutral output voltage and their corresponding spectrum of the hybrid cycloconverter operating in circulating current mode and circulating current-free mode when the output frequency is 13Hz.

Similar to the 5Hz output frequency situation, the PI controller for the circulating current in the hybrid topology is used to handle the 26Hz low frequency harmonic present in the differential mode voltage whilst the other significant voltage harmonics are mainly canceled by using the feedforward compensation method. Moreover, since the peak value of the differential mode voltage remains around 500V, in order to achieve a similar effect to the 5Hz output frequency situation, the DC-link capacitor voltage of the auxiliary inverter is maintained at 295V to cancel the harmonics present in the differential mode voltage. This is also validated by the spectrum of the circulating current shown in Fig. 4.74, where the DC component of the circulating current is controlled at around 1.5A whilst the other harmonics have also been partially reduced compared to the standard cycloconverter.

According to the spectra of the output voltages for both operating modes as shown in Fig. 4.77 and 4.79, the hybrid cycloconverter can significantly reduce the low frequency harmonics present in the output voltage compared to that of the standard cycloconverter, such as $17V_{pk}$ compared to $82V_{pk}$ at 124Hz in circulating current mode or $13V_{pk}$ compared to $159V_{pk}$ at 124Hz in circulating current-free mode, which is similar to the achievement in 5Hz output frequency situation, as shown in Fig. 4.36 and Fig. 4.41. The high frequency components of the output voltages are still placed in clusters around multiples of the switching frequency (5kHz).
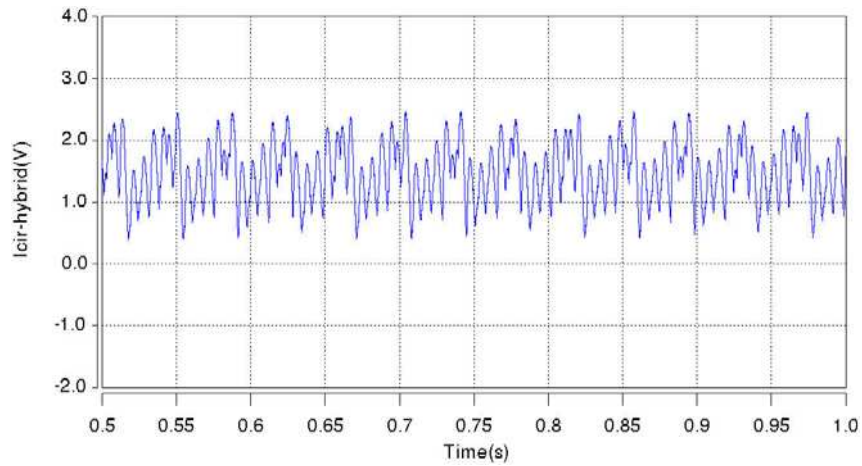
Fig. 4.74: Circulating current waveform of the hybrid cycloconverter in CCM with an output frequency of 13Hz
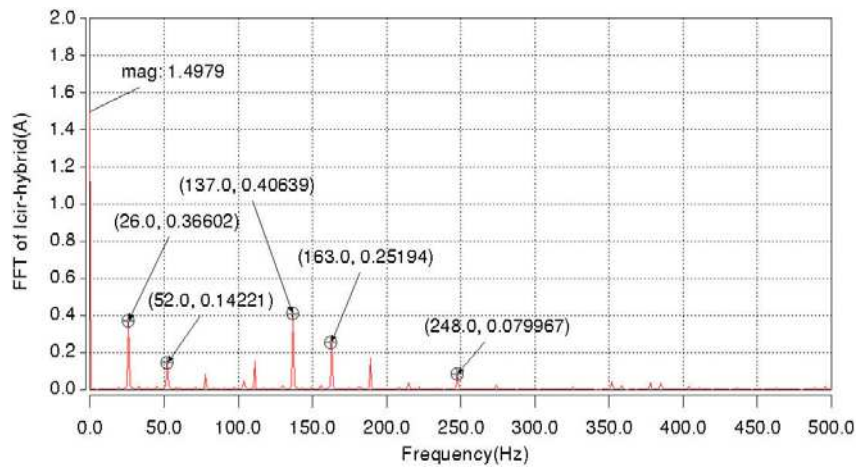
Fig. 4.75: Spectrum of the circulating current of the hybrid cycloconverter in CCM with an output frequency of 13Hz
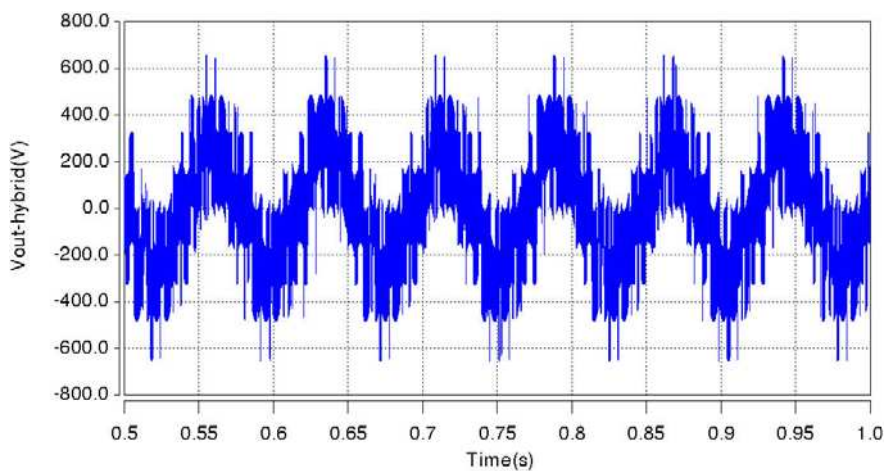
Fig. 4.76: Phase-to-supply neutral output voltage waveform of the hybrid cycloconverter in CCM with an output frequency of 13Hz
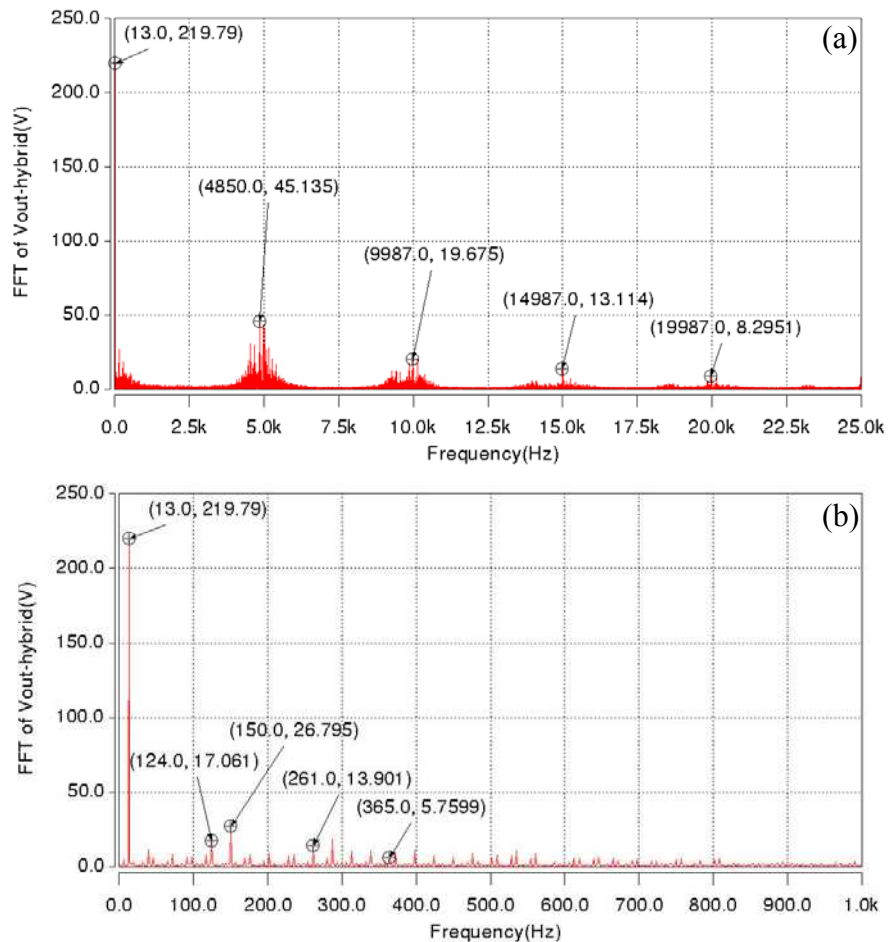
Fig. 4.77: Spectrum of the phase-to-supply neutral output voltage of the hybrid cycloconverter in CCM with an output frequency of 13Hz: a) 0-25kHz spectrum b) 0-1kHz spectrum
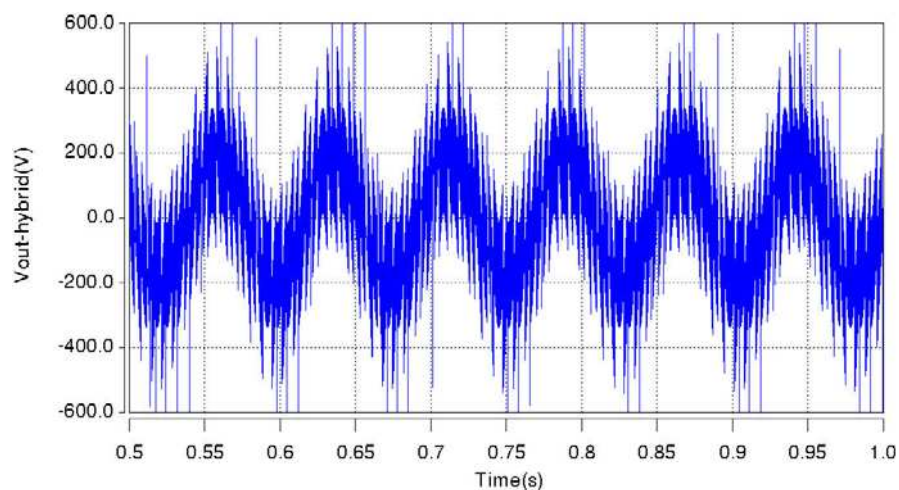
Fig. 4.78: Phase-to-supply neutral output voltage waveform of the hybrid cycloconverter in CCFM with an output frequency of 13Hz
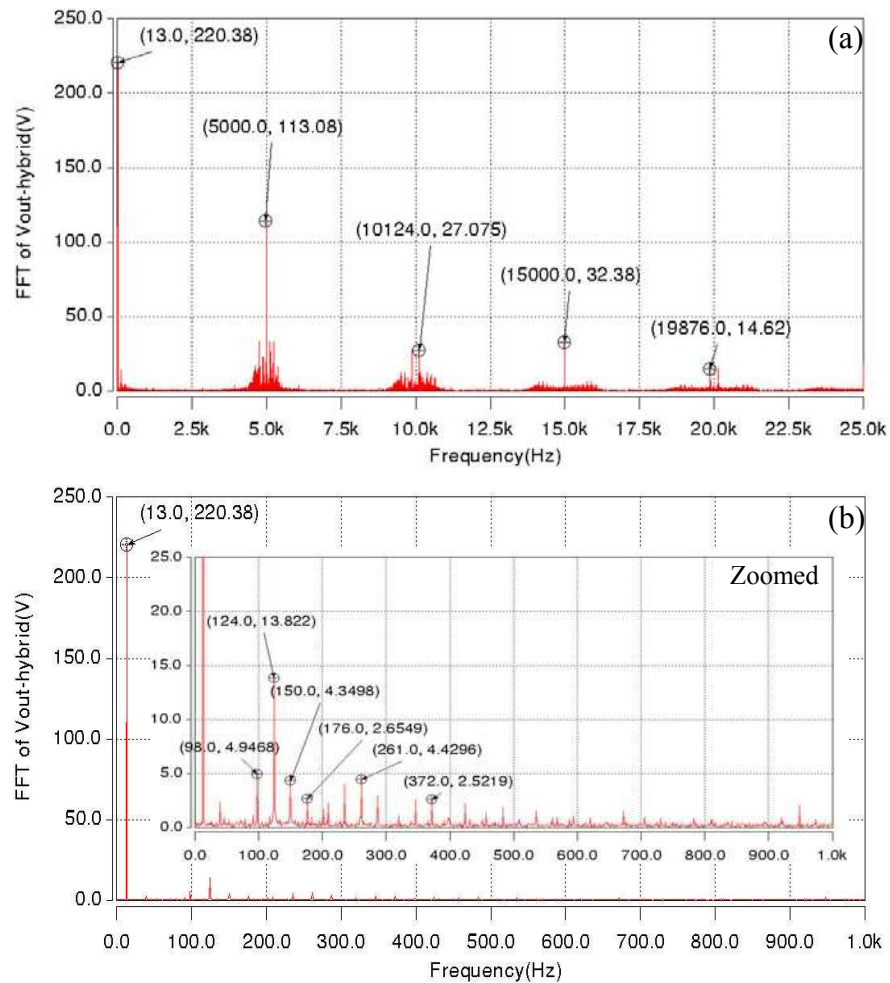
Fig. 4.79: Spectrum of the phase-to-supply neutral output voltage of the hybrid
cycloconverter in CCFM with an output frequency of 13Hz: a)
0-25kHz spectrum b) 0-1kHz spectrum

4.6.2 Simulation Results at a Different Output Modulation Index

In this subsection, the simulation results are presented at 0.3 output modulation index
for both the circulating current and circulating current-free mode. All the parameters
except the output modulation index keep the same as what has been shown in
Table 4.2.

4.6.2.1 The Standard Cycloconverter with an Output Modulation Index of 0.3

Fig. 4.80 to 4.87 show the waveform of the differential mode voltage (only for CCM), the circulating current (only for CCM), the phase-to-supply neutral output voltage and their corresponding spectrum of the standard cycloconverter operating in circulating current mode and circulating current-free mode when the output modulation index is 0.3. The frequency of the harmonics present in these waveforms are identical as those present in Section 4.3 since the input and output frequency of the cycloconverter are the same. Furthermore, all the significant harmonics remain grouped in clusters around multiples of 150Hz because of the unaltered 3-pulse (CCFM) or 6-pulse (CCM) thyristor bridge and the 50Hz input frequency.

The peak value of the differential mode voltage shown in Fig. 4.80 is a bit smaller than that with 0.8 modulation index. The peak value of the circulating current shown in Fig. 4.82 is around 2A which is smaller than that with 0.8 modulation index (Fig. 4.16) because the amplitude of the 10Hz low frequency harmonic present in the differential mode voltage is significantly reduced.

Compare with the spectra of the phase-to-supply neutral output voltages with 0.8 output modulation index shown in Fig. 4.19 and 4.22, the fundamental component of the output voltages in both operating modes is reduced from $220V_{pk}$ to around $80V_{pk}$ which corresponds to the reduction in modulation index. Meanwhile, other low order frequency harmonics still remain very high. However, since the amplitude of each harmonic component is a function of output modulation index and the load displacement angle [pp.313, 1], some of them, such as the 150Hz, 295Hz, are obviously increased whilst some other ones such as the 140Hz, 160Hz are actually reduced. One thing which may be noticed is that, unlike the 0.8 output modulation index situation where the output voltage is a 4-level voltage waveform as shown in Fig. 4.18, the output voltage in circulating current mode with 0.3 output modulation index looks like a 2-level voltage waveform as shown in Fig. 4.84.
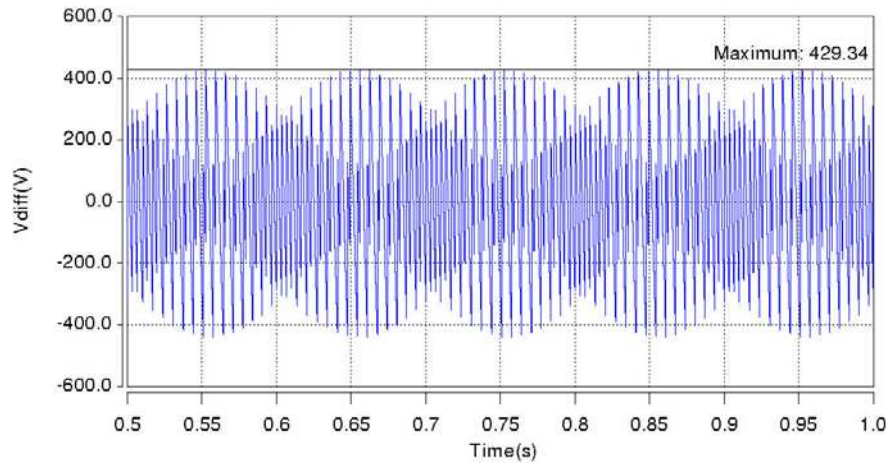
Fig. 4.80: Differential mode voltage waveform seen between the two thyristor half bridge outputs in CCM with an output modulation index of 0.3
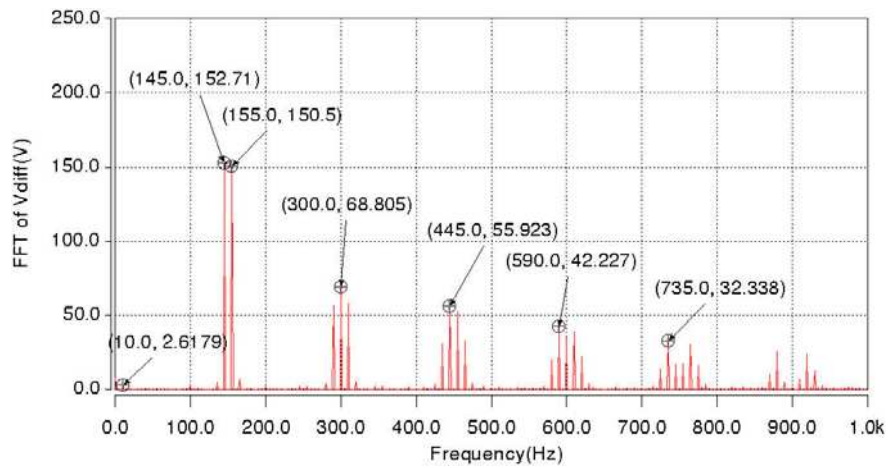
Fig. 4.81: Spectrum of the differential mode voltage seen between the two thyristor half bridge outputs in CCM with an output modulation index of 0.3
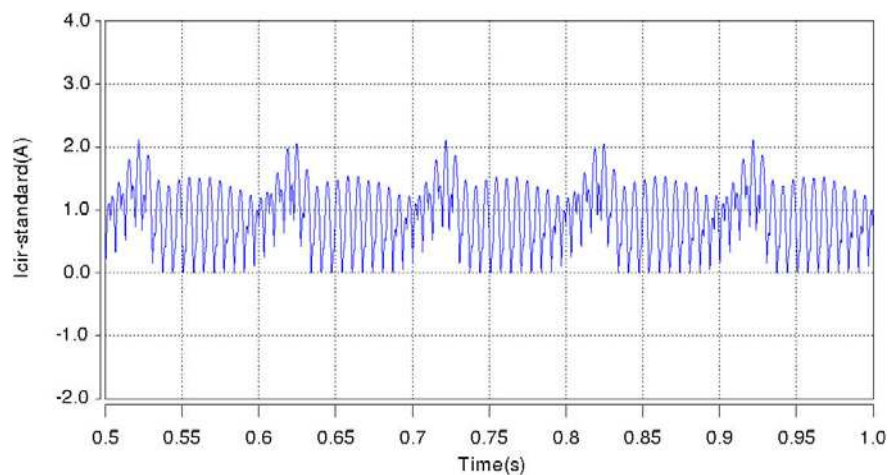
Fig. 4.82: Circulating current waveform of the standard cycloconverter in CCM with an output modulation index of 0.3
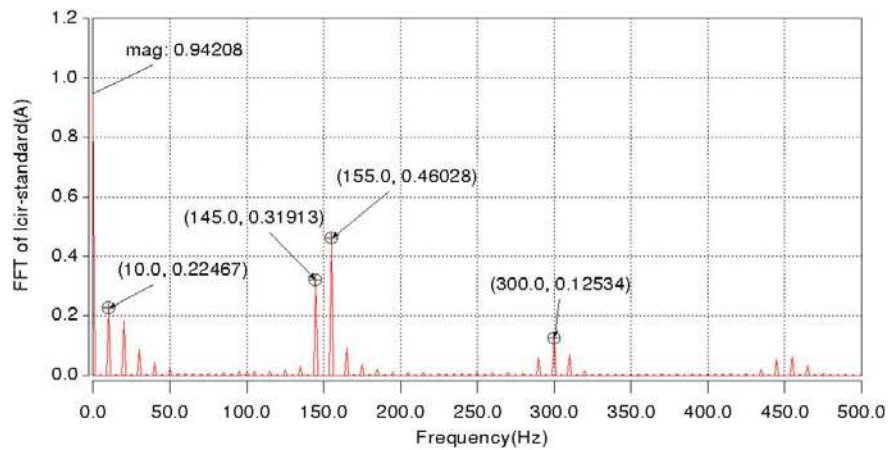
Fig. 4.83: Spectrum of the circulating current of the standard cycloconverter in CCM with an output modulation index of 0.3
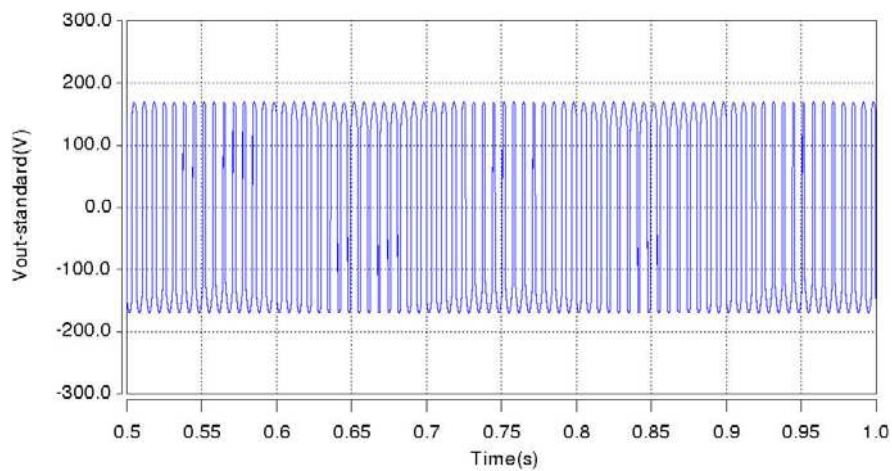
Fig. 4.84: Phase-to-supply neutral output voltage waveform of the standard cycloconverter in CCM with an output modulation index of 0.3
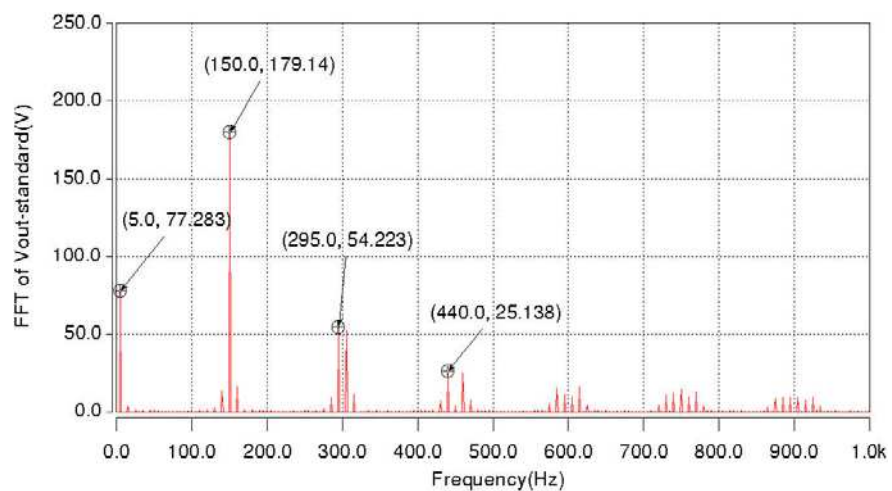
Fig. 4.85: Spectrum of the phase-to-supply neutral output voltage of the standard cycloconverter in CCM with an output modulation index of 0.3
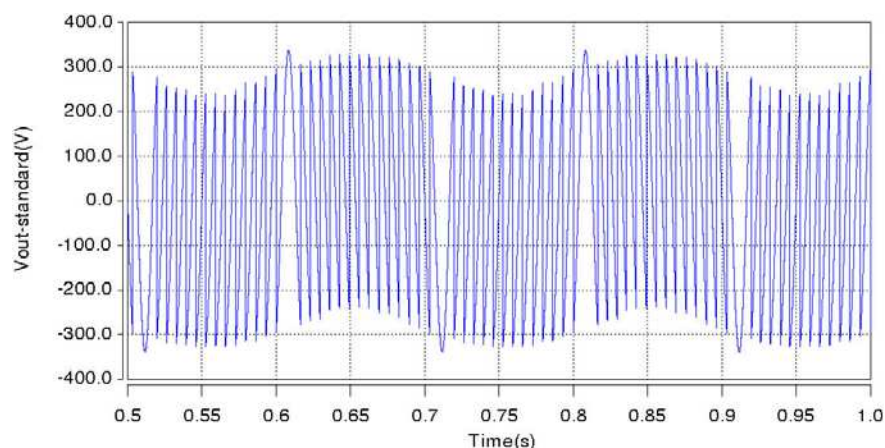
Fig. 4.86: Phase-to-supply neutral output voltage waveform of the standard cycloconverter in CCFM with an output modulation index of 0.3
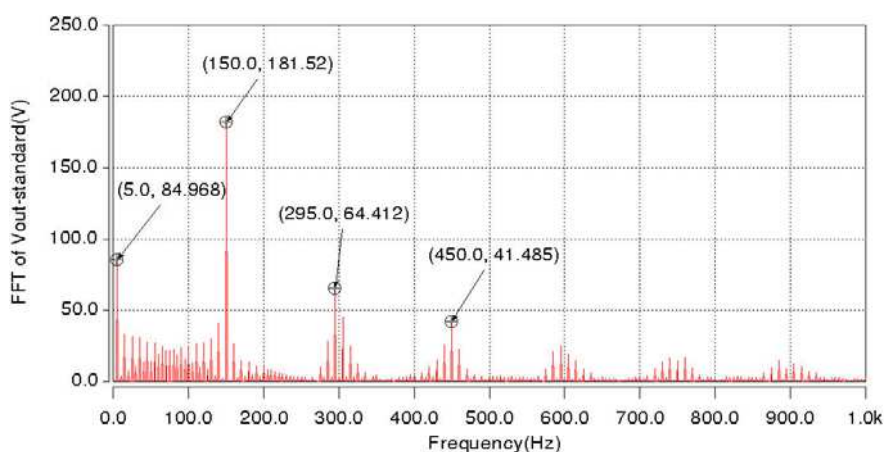
Fig. 4.87: Spectrum of the phase-to-supply neutral output voltage of the standard cycloconverter in CCFM with an output modulation index of 0.3

4.6.2.2 The Hybrid Cycloconverter with an Output Modulation Index of 0.3

Fig. 4.88 to 4.93 show the waveform of the circulating current (only for CCM), the phase-to-supply neutral output voltage and their corresponding spectrum of the hybrid cycloconverter operating in circulating current mode and circulating current-free mode when the output modulation index is 0.3.

As the peak value of the differential mode voltage is a bit smaller for the small output modulation index compared to the high one, the DC-link capacitor voltage of the auxiliary inverter used for the latter situation should be sufficient to handle this case as

well. As can be seen from the spectrum of the circulating current as shown in Fig. 4.34, the DC component of the circulating current is controlled at around 1.5A whilst the other harmonics have also been reduced compared to the standard cycloconverter. From the spectra of the output voltages in both the circulating current and circulating current-free mode, it can be seen that with the same settings of the hybrid cycloconverter as for the high output modulation index situation, the low order harmonics are significantly reduced. For example, the $179V_{pk}$ at 150Hz in circulating current mode is reduced to $17V_{pk}$ or the $181V_{pk}$ in circulating current-free mode is reduced to $1.9V_{pk}$. Furthermore, the high frequency components are still placed in clusters around multiples of the switching frequency (5kHz).
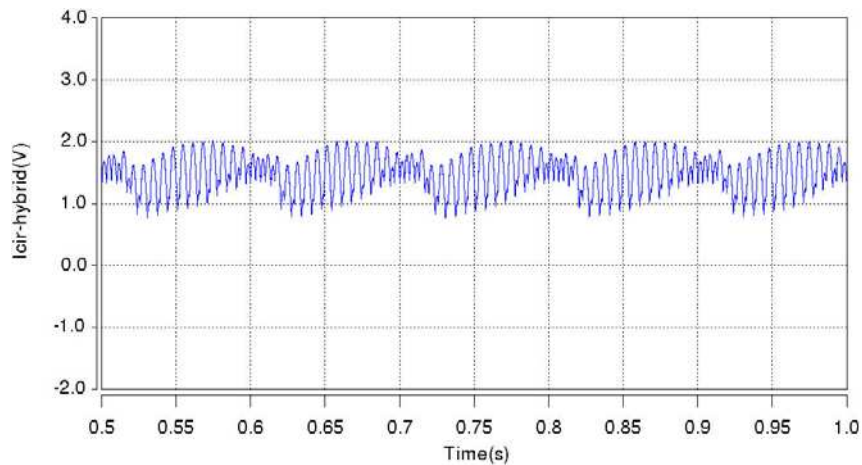
Fig. 4.88: Circulating current waveform of the hybrid cycloconverter in CCM with an output modulation index of 0.3
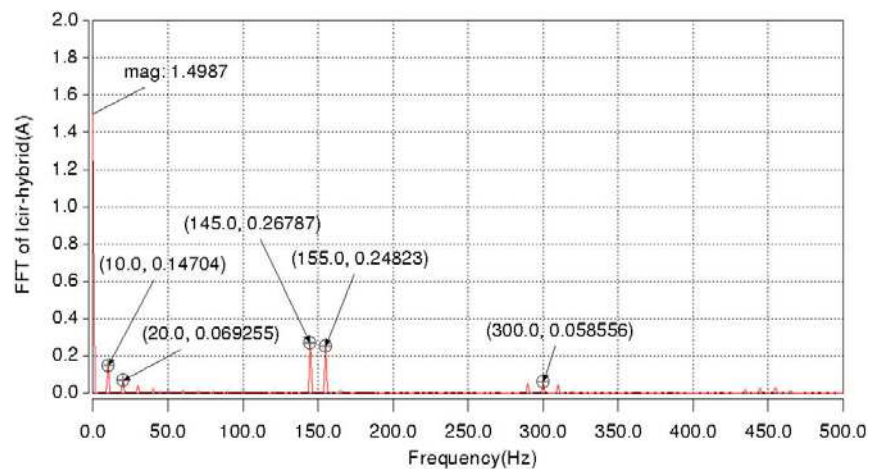
Fig. 4.89: Spectrum of the circulating current of the hybrid cycloconverter in CCM with an output modulation index of 0.3
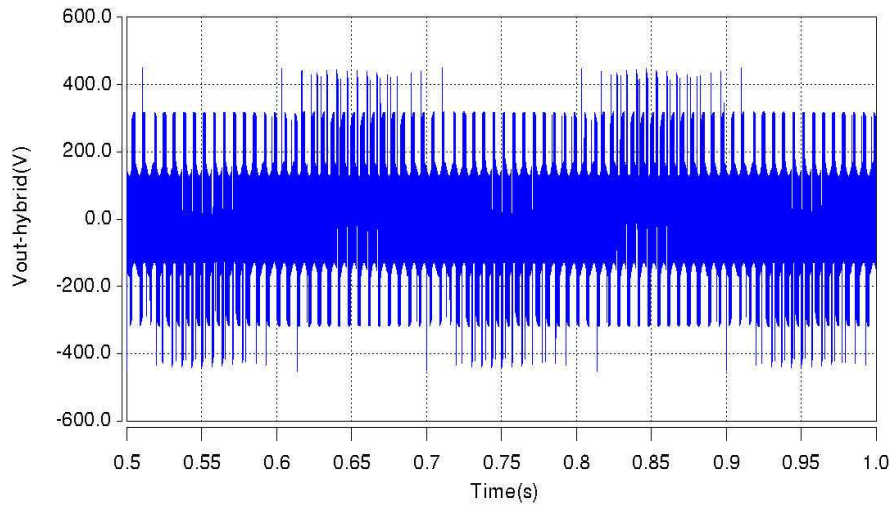
Fig. 4.90: Phase-to-supply neutral output voltage waveform of the hybrid cycloconverter in CCM with an output modulation index of 0.3
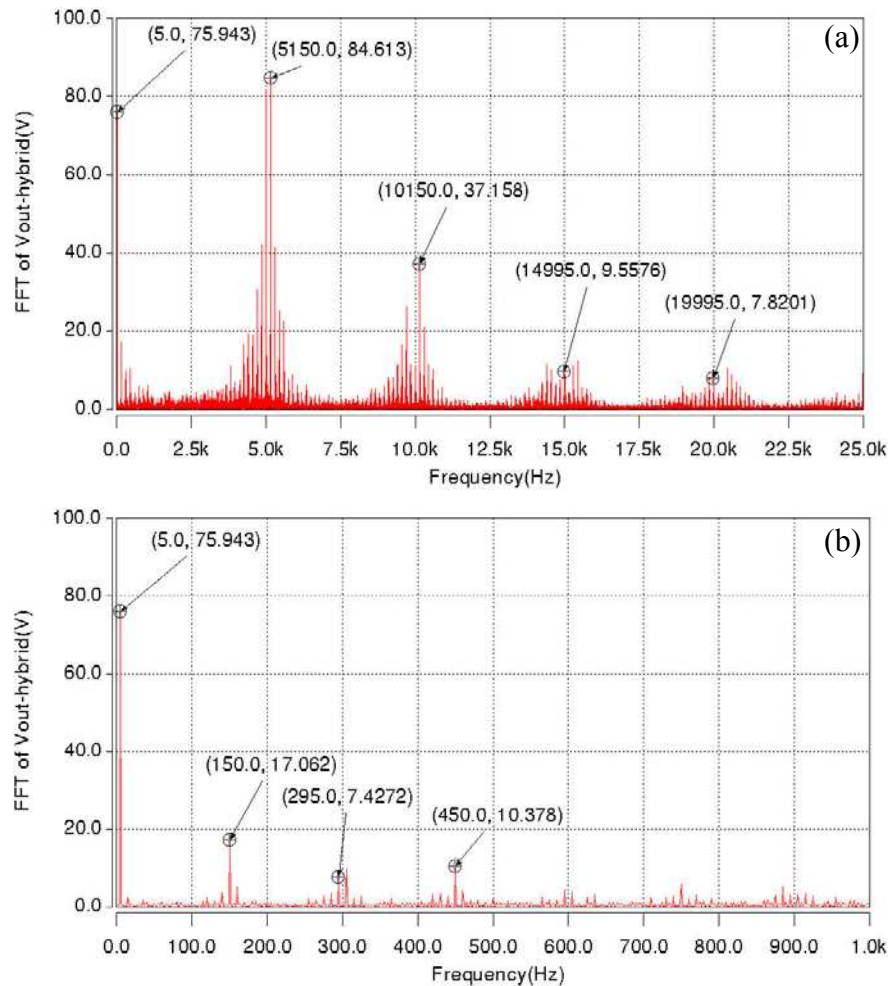
Fig. 4.91: Spectrum of the phase-to-supply neutral output voltage of the hybrid cycloconverter in CCM with an output modulation index of 0.3: a) 0-25kHz spectrum b) 0-1kHz spectrum
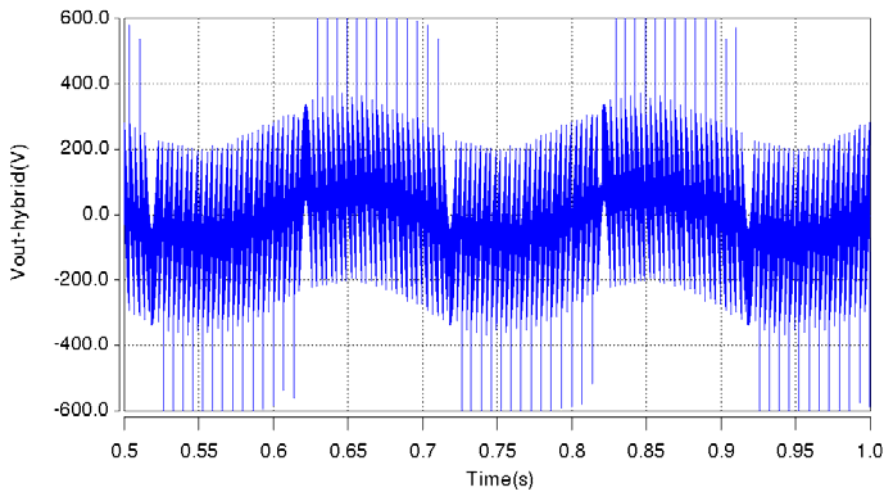
Fig. 4.92: Phase-to-supply neutral output voltage waveform of the hybrid cycloconverter in CCFM with an output modulation index of 0.3
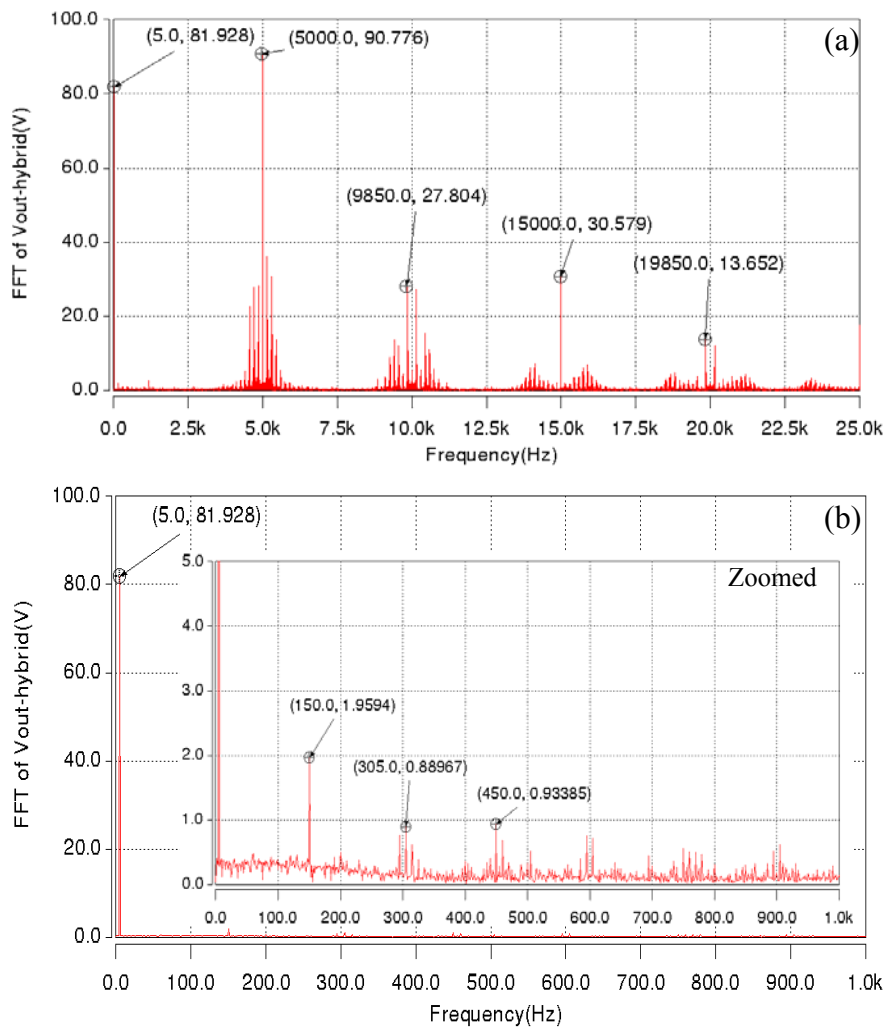
Fig. 4.93: Spectrum of the phase-to-supply neutral output voltage of the hybrid cycloconverter in CCFM with an output modulation index of 0.3: a) 0-25kHz spectrum b) 0-1kHz spectrum

From the above analysis it can be concluded that a hybrid cycloconverter is able to handle the different operating points, such as different output frequency and/or different output modulation index. Therefore, the results obtained in this section prove the general improvement on the cycloconverter via the hybrid solution. By slightly altering the parameters of the hybrid cycloconverter to match each specific situation, such as the DC-link capacitor voltage or the speed of the PI controller, the hybrid cycloconverter may achieve even better performance.

4.7 Summary of a Comparison of the Standard and the Hybrid Cycloconverter based on the Simulation Results

Based on the previous simulation results and also taking into consideration the theoretical aspects related to cycloconverters introduced in Chapter 2 and Chapter 3, a full comparison between the standard and hybrid cycloconverter in terms of converter performance, cost and complexity will be discussed in this section. Additionally, as the traditional way to improve the performance of a cycloconverter is by increasing the pulse number of the cycloconverter, this section will also consider the 6-pulse (12-pulse in CCM) and 12-pulse (24-pulse in CCM) standard cycloconverter in order to include in this comparison not only the hybrid solution to improve the performance, but also the "standard" solution (increasing the number of pulses). For simplicity, the simulation waveforms or spectrums in regard to the cycloconverter with higher number of pulses will not be displayed in this section and the relevant values or results corresponding to each aspects described below will be presented directly. The comparison will make it much easier to understand both the advantages and disadvantages of each topology and the analysis below is summarized in Table. 4.6 which can be found at the end of this section.

4.7.1 The Performance of the Cycloconverters

The performance of cycloconverters is typically compared by analyzing three parameters: the output voltage, the input current, and the circulating current if the

cycloconverter operates in circulating current mode. With the simulation results displayed in the previous sections of this chapter as well as some other results obtained for higher pulse number topologies, it is straightforward to compare different topologies on these three aspects.

Output Voltage

The number of the significant harmonic lines in the spectrum will be much reduced when the pulse number of the cycloconverter is increased as mentioned in [pp.307-313, 1] (see Equation (2.13) to (2.16) in Chapter 2). On the other hand, with a given number of thyristors, the output voltage of the standard cycloconverter in circulating current mode has a better waveform quality than when it operates in circulating current-free mode due to additional harmonic cancellation between the two outputs of the thyristor half bridges. When the auxiliary inverter is connected to the standard cycloconverter to constitute a hybrid assembly, the output voltage is clearly improved, as has been shown in Section 4.4-4.6. In order to compare the improvement obtained by increasing the number of pulses against the improvement resulting from adding an auxiliary inverter, the following distortion indices can be used: the Total Harmonic Distortion (THD) and the Weighted Total Harmonic Distortion (WTHD). The THD, as defined by Equation (4.16), is used to define the degree of distortion present in the output voltage waveform whilst the WTHD, as defined by Equation (4.17), is used to weight the output voltage harmonics inversely with the harmonic frequency, in order to approximate the potential harmonic impact on an inductive load current. However, from the 0-25kHz spectrum of the output voltages generated by the hybrid cycloconverters as shown in the previous sections, it can be seen that the amplitudes of the high frequency harmonics occurring in clusters around multiples of 5kHz are high enough to influence the THD of the output voltage, therefore it is more appropriate to use WTHD to evaluate the improvement of the hybrid cycloconverter rather than THD.

$$THD = \sqrt{\sum_{h=2,3,...}^{\infty} (\frac{V_{h,RMS}}{V_{1.RMS}})^2} \qquad (4.16)$$

$$WTHD = \frac{\sqrt{\sum_{h=2,3,\ldots}^{\infty} \left(\frac{V_{h,RMS}}{h}\right)^2}}{V_{1.RMS}} \tag{4.17}$$

Fig. 4.94 summarizes the line-to-line output voltage performance (WTHD) of all the topologies in circulating current mode: the standard and hybrid cycloconverter when operating with 6, 12, 24-pulse. As significant improvement in performance is achieved when changing from the standard to the hybrid cycloconverter both in the circulating current and circulating current-free modes, the following bars are only determined using the data collected in circulating current mode and generalize the findings.
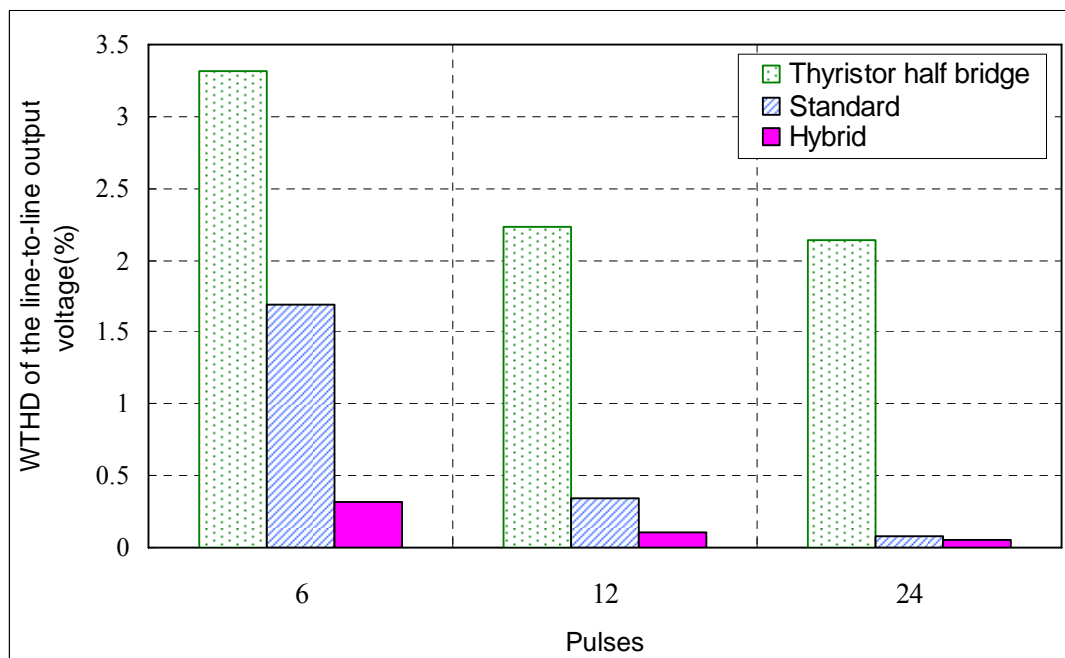
Fig. 4.94: WTHD of the line-to-line output voltage of the standard and hybrid cycloconverter in CCM depending on the number of pulses

From the Fig. 4.94 it can be seen that the additional improvement of the output voltage waveform is superior in the standard cycloconverter than the hybrid cycloconverter when the number of pulses is increased. This is because the hybrid cycloconverter is an active solution aiming to always eliminate the harmonics and has already improved the output waveform performance close to its theoretical potential and no further improvement is possible although the installed power in the auxiliary inverter (and therefore its cost) used in conjunction to cycloconverters with higher

number of pulses may also be reduced. It can also be seen that the 6-pulse hybrid cycloconverter is able to match the quality of the output voltage waveform of a 12-pulse standard cycloconverter. This means that the hybrid cycloconverter can produce the same improving effect of the output voltage whilst requiring power switches with smaller voltage (and therefore power) rating in the converter. Although some marginal improvement can still be obtained by employing the hybrid approach in conjunction with increasing the number of pulses of the cycloconverter, it may not be worthwhile increasing the complexity of the converter for a very small improvement.

Circulating Current

The circulating current is not a problem that needs to be considered if the cycloconverter operates in circulating current-free mode. In circulating current mode, the hybrid cycloconverter has the ability to control the circulating current around a given DC level (the lowest allowable value) and this means that the negative impact of the circulating current on the performance of the converter is minimized. Therefore, the circulating current is only extremely harmful to the standard cycloconverter. Even if a bulky inductance is used, the circulating current still contains many low order harmonics including a large DC component. Although increasing the number of pulses of the cycloconverter may reduce the circulating current due to the reduction of the differential mode voltage (from $506V_{pk}$ at 6-pulse to $338V_{pk}$ at 12-pulse or $170V_{pk}$ at 24-pulse), the circulating current is still poorly controlled. This means that a large DC component that degrades further the input displacement power factor still needs to be maintained in order to provide enough reserve for potential current ripple.

Input Current

In Subsection 4.5.3, it has been shown that the displacement power factor of the input side is influenced heavily by the level of the circulating current. Hence, the 6-pulse standard cycloconverter in circulating current mode has a poor input side performance, especially when the size of the circulating current reactor is not that large. Since the circulating current can be reduced by increasing the number of pulses or controlled by

the proposed hybrid cycloconverter, less reactive power can be drawn from the input side in circulating current mode and the displacement power factor can therefore be further improved. This is shown in Fig. 4.95, which illustrates the displacement power factor for both the standard and the hybrid cycloconverter in circulating current mode with different number of pulses. From these bars, it can also be seen that the most distinct improvement of the displacement power factor between the standard and the hybrid topology occurs at 6-pulse situation, which is a similar tendency to the WTHD of the line-to-line output voltage, as shown in Fig. 4.94.
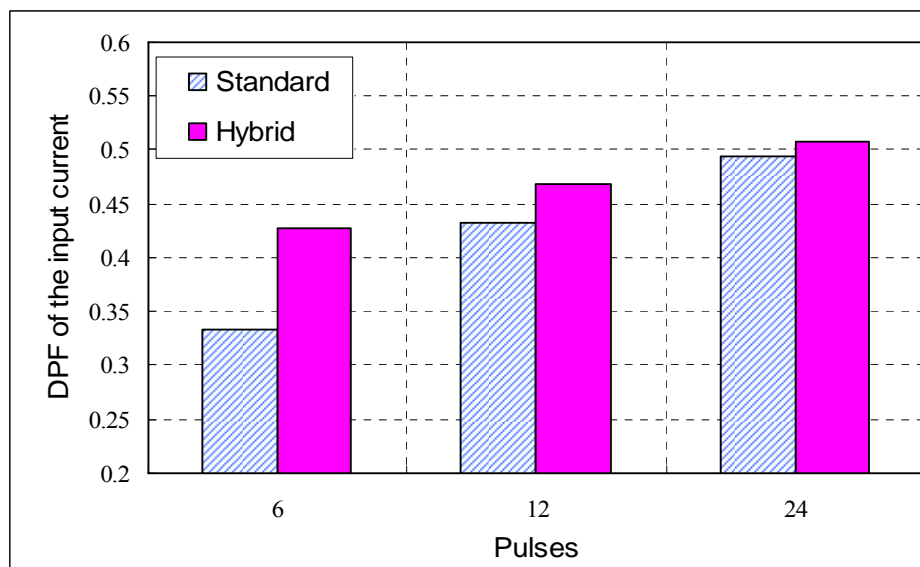
Fig. 4.95: DPF of the input current of the standard and hybrid cycloconverter in CCM depending on the number of pulses

According to [pp.359-368, 1], the number of harmonics as well as their corresponding amplitude in the input current will be reduced by increasing the number of pulses of the cycloconverter. This was also verified by Equation (2.17) to (2.20) presented in Chapter 2. Therefore, as shown in Fig. 4.96, which illustrates the distortion power factor of the standard and hybrid cycloconverter in circulating current-free mode with different number of pulses, the distortion power factor of the input current can be improved by increasing the cycloconverter pulse number. The quality of the input current cannot be obviously improved via the hybrid cycloconverter since the input power ripple remains almost the same compared to that of the standard cycloconverter. Hence, from Fig. 4.96 it can be seen that the differences between the distortion power factors for both the standard and the hybrid topologies are very small.
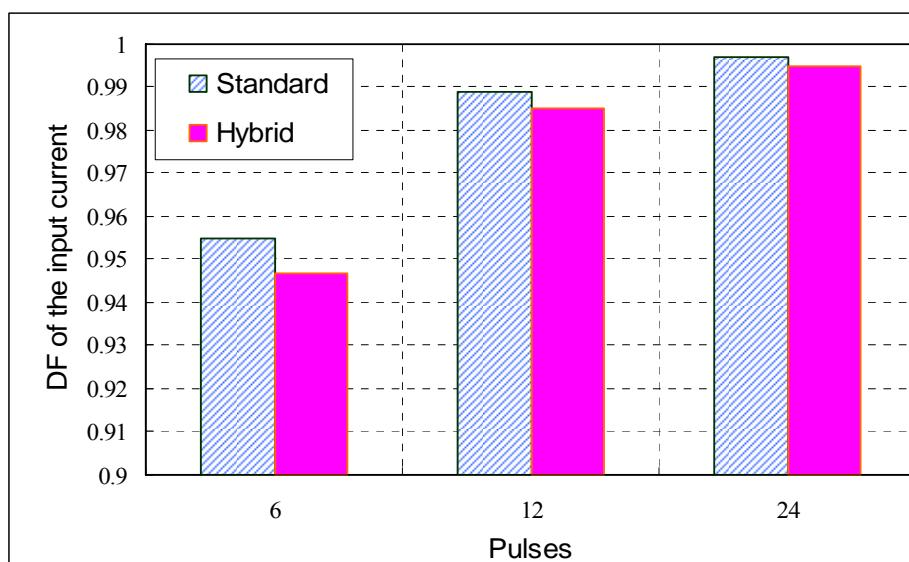
Fig. 4.96: DF of the input current of the standard and hybrid cycloconverter in
CCFM depending on the number of pulses

Therefore, from the above analysis it can be concluded that, compared with the proposed hybrid solution, increasing the number of pulses is still the most effect way on improving the input side performance of the cycloconverter when taking both the displacement power factor as well as the distortion power factor into consideration.

4.7.2 The Cost and Complexity

A comparison for the cost of all the possible cycloconverter topologies as well as the complexity of the control requirements in different topologies is presented in this subsection.

<u>The Cost</u>

For this study, real production cost would depend heavily on the volumes, and since manufacturing costs of the components were not available, the cost of the cycloconverter was evaluated in terms of the number of power switches and passive devices (for example reactors, capacitors or the input phase shift transformers). Moreover, the size reflected by the voltage and current (therefore power) rating of switches and the capability to store energy in capacitors or circulating current reactors, if it is needed, will also be taken into consideration.

The number of thyristors will normally increase in proportion to the number of pulses of the cycloconverter, for example, 6 thyristors are needed for a 3-pulse (or 6-pulse in CCM) cycloconverter, 12 thyristors are needed for a 6-pulse (or 12-pulse in CCM) cycloconverter and 24 thyristors are needed for a 12-pulse (or 24-pulse in CCM) cycloconverter. Additionally, two IGBTs and two diodes will be needed if an auxiliary two-leg H-bridge inverter is required whilst four IGBTs (two of them with anti-parallel diodes) and two diodes will be needed if a three-leg bridge inverter is required in the hybrid arrangement. Meanwhile, the higher the number of the controlled power devices is required, the higher the number of the gate drives is needed as well.

By assuming the currents flowing through the thyristor bridge and the auxiliary inverter are the same, the factor of the current can be ignored when the installed power (kVA = kilo VA) of the auxiliary inverter is compared with that of the thyristor bridge. Therefore, the kVA of the thyristor bridge is proportional to the number of thyristors and the input line-to-line voltage. The kVA of the auxiliary inverter depends on the number of power devices assembled in the auxiliary inverter and the DC-link capacitor voltage. The Equation (4.18) and (4.19) are used to calculate the installed power for the thyristor bridge and the auxiliary inverter respectively. In the equations, n_{thy} represents the number of the thyristors in a thyristor bridge, for example, n_{thy} is 6 if the thyristor bridge is 3-pulse in CCFM or 6-pulse in CCM; n_{IGBT} represents the number of the IGBTs in the auxiliary inverter, for example, n_{IGBT} is 6 if the inverter is three-leg bridge or 4 if the inverter is two-leg H-bridge. Therefore, it is not difficult to calculate the ratio of the installed power between the auxiliary inverter and the thyristor bridge according to Equation (4.20).

$$P_{thy} = n_{thy} \times \sqrt{2} \times V_{in-line} \times (\sqrt{2} \times I_{Load} + I_{cir}) \tag{4.18}$$

$$P_{inv} = n_{IGBT} \times V_c \times (\sqrt{2} \times I_{Load} + I_{cir}) \tag{4.19}$$

$$r_{kVA} = \frac{P_{inv}}{P_{thy}} = \frac{n_{IGBT} \times V_c \times (\sqrt{2} \times I_{Load} + I_{cir})}{n_{thy} \times \sqrt{2} \times V_{in-line} \times (\sqrt{2} \times I_{Load} + I_{cir})} = \frac{n_{IGBT} \times V_c}{n_{thy} \times \sqrt{2} \times V_{in-line}} \tag{4.20}$$

As mentioned in Section 4.4, a compromise needs to be made in order to achieve improved performance of the hybrid cycloconverter whilst keeping the cost as low as possible. Fig. 4.97 shows the interdependence between the WTHD of the line-to-line output voltage of the 3-pulse hybrid cycloconverter that uses the three-leg bridge inverter in circulating current-free mode versus the relative kVA (Equation (4.20)) of the auxiliary inverter to that of the thyristor bridge. The best performance of the output voltage is achieved at the ratio of around 0.35. This means that to achieve the best balance between the cost and the performance of the hybrid cycloconverter, the DC-link capacitor voltage in the auxiliary inverter has to be set at around half of the voltage seen across the thyristors according to Equation (4.21). This is also why most of the simulation results presented in this chapter have been obtained with the 295V DC-link capacitor voltage.

$$V_c = \frac{r_{kVA} \times n_{thy} \times \sqrt{2} \times V_{in-line}}{n_{IGBT}} = \frac{0.34 \times 6 \times \sqrt{2} \times 415}{4} \approx 295V \tag{4.21}$$

If the auxiliary inverter is changed to a two-leg H-bridge inverter topology, the optimal kVA ratio remains around 0.35 since the number of the IGBTs in the auxiliary inverter is reduced from four to two but the DC-link capacitor voltage is doubled.
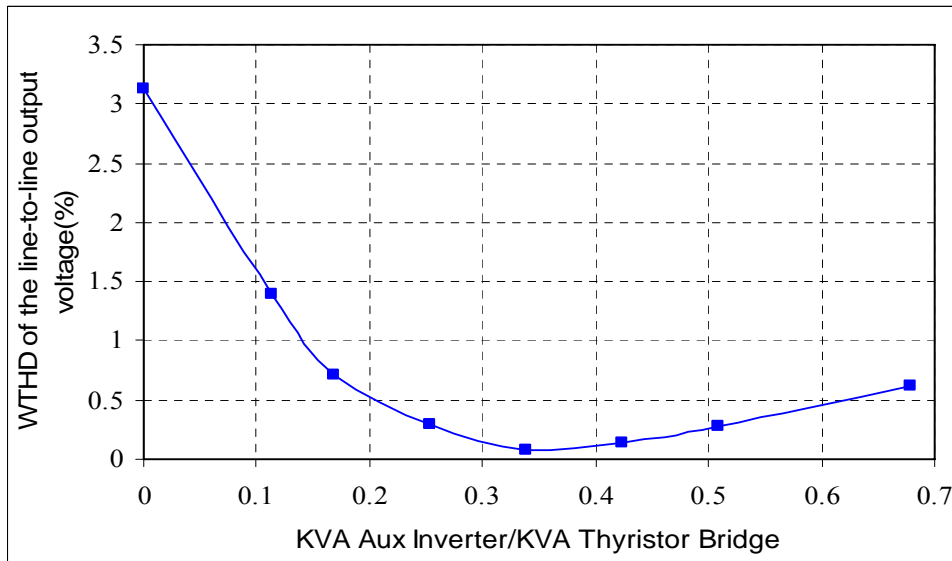
Fig. 4.97: WTHD of the line-to-line output voltage of the 3-pulse hybrid cycloconverter in circulating current-free mode depending on the ratio of the kVA between the auxiliary inverter and the thyristor bridge

By increasing of the pulse number, the auxiliary inverter's optimal DC-link capacitor voltage can be reduced from 295V at 6-pulse to 180V at 12-pulse or 105V at 24-pulse as less of the common mode voltage and differential mode voltage need to be compensated by the auxiliary inverter and therefore will result in a reduced kVA of the auxiliary inverter. However, since the number of thyristors is proportional to the pulse number, the kVA of the thyristor bridge becomes higher and higher with the increasing of the pulses, which will also lead to an overall higher kVA of the hybrid cycloconverter.

The bulky input phase shift transformer is needed only when the number of pulses is increased from a 3-pulse (6-pulse in CCM) to a 6-pulse (12-pulse in CCM) or a 12-pulse (24-pulse in CCM) solution (or even higher number).

The DC-link capacitor is only required for hybrid cycloconverters. Two DC-link (split) capacitors of larger size (AC current of the output frequency passing through) are needed in a two-leg H-bridge inverter whilst only a single DC-link capacitor that handles only a fraction of the load current amplitude at much higher frequency is needed in the three-leg bridge inverter.

The last factor used to assess the cost of the cycloconverter is the circulating current reactor, which is obviously only needed in circulating current mode. As the circulating current in the hybrid cycloconverter is controlled by the added auxiliary inverter, the size of the circulating current reactor can be further reduced compared with that in a standard cycloconverter, since not only the inductance, but also the peak current squared (much smaller for the hybrid approach) influences its size. Moreover, with the increasing of the number of pulses, the reduction of the peak value of the differential mode voltage as well as the increasing of the frequencies of the significant low order harmonics present in the differential mode voltage, will both be helpful to reduce the size of the circulating current reactors

The Complexity

As the power stage of the cycloconverter has been evaluated in previous section "The

Cost", the complexity here means how complicated degrees of the control requirements (circuits, transducers, computational power) are. For the cycloconverter without circulating current, an additional control strategy is required to handle the "voltage distortion" and the "bank selection" problems [pp.186-206, 1] which have been mentioned in Chapter 2. For a cyclcoconverter operating with circulating current, an additional control circuit is needed to help the auxiliary inverter to reduce the low order distortion present in the differential mode voltage in order to improve the waveform of circulating current whilst reducing the impact on the reactive power consumption.

Based on the previous evaluation and analysis of both the standard and hybrid cycloconverter concepts, a summary comparison in terms of converter performance, cost and complexity, is produced in Table. 4.6. The topologies for comparsion include the standard cylcoconverter in circulating current-free mode with different pulses (3-,6-,12-pluse), the 6-pulse standard cycloconverter in circulating current mode as well as the 3-pulse hybrid cycloconverter in circulating current-free mode, the 6-pulse hybrid cycloconverter in circulating current mode. Five score ratings ranging from "++" to "--" are used to indicate the comparative performance of the different topologies from the very best to the worst, in all the aspects mentioned above. The total marks are therefore derived from summing all the marks in each corresponding column. It can be seen from this table that the converter performance can be much improved by increasing the pulse number or employing the proposed hybrid cycloconverter solution no matter in circulating current mode or circulating current-free mode. However, the 3-pulse hybrid cycloconverter in circulating current-free mode topology reveals the potential to achieve the best performance among all the possible cycloconverter topologies, as overall it obtains the highest number of points. In order to make a further comparison, an experimental prototype was built to evaluate the performance of the 3-pulse hybrid and standard cycloconverter in circulating current-free mode as well as the 6-pulse hybrid and standard cycloconverter in circulating current mode.

Comparison between standard and hybrid cycloconverters		Standard cycloconverter				Hybrid cyclconverter		
		Circulating current-free Mode			Circulating current Mode (6-pulse)	Circulating current-free mode (3-pulse, 3 inverter legs)	Circulating current mode (6-pulse)	
		3-pulse	6-pulse	12-pulse			3 inverter legs	2 inverter legs
Converter performance	Output voltage	--	0	++	-	++	+	+
	Circulating current	++	++	++	--	++	+	+
	Input current	--	0	++	--	--	--	--
Cost	Number of power devices	+ (3*6)	0 (3*12)	- (3*24)	+ (3*6)	0 3*(6+6)	0 3*(6+6)	0 3*(6+4)
	kVA	++	0	--	++	+	+	+
	Phase shift input transformer	++	0	--	++	++	++	++
	Number of capacitors	+ 0	+ 0	+ 0	+ 0	0 1	0 1	- 2
	CCR	++	++	++	--	++	0	0
Complexity	Control function	-	-	-	++	-	0	0
Total Marks		**5**	**4**	**3**	**1**	**6**	**3**	**2**

Table. 4.6: Comparison summary of various standard cycloconverter and hybrid arrangements

4.8   Summary

In this chapter, the input and output performance revealed by simulation results of three-phase input to single-phase output and three-phase input to three-phase output standard and hybrid cycloconverters obtained from Saber models, has been analyzed. In the last section, additional aspects are discussed and summarized in a comprehensive comparison made among different cycloconverter topologies in terms of converter performance, cost and complexity in order to give a broad understanding of the advantages and disadvantages of the proposed and existing cycloconverter solution. The chapter concludes with a recommendation of which topologies should be experimentally evaluated.

Chapter 5

Hybrid Cycloconverter Prototype Implementation and Assembly

5.1 Introduction

The principle of the hybrid cycloconverter has already been illustrated in Chapter 3 and the simulation results based on the Saber simulation models have been analyzed in Chapter 4. The next step is to experimentally verify the improvements which the hybrid cycloconverter is able to achieve, compared to the standard cycloconverter, by building a prototype of the hybrid cycloconverter to produce the experimental results. This chapter will present the design and hardware implementation of both the power circuit and the control platform of the prototype. The overall structure of the prototype converter system is presented in Fig. 5.1.
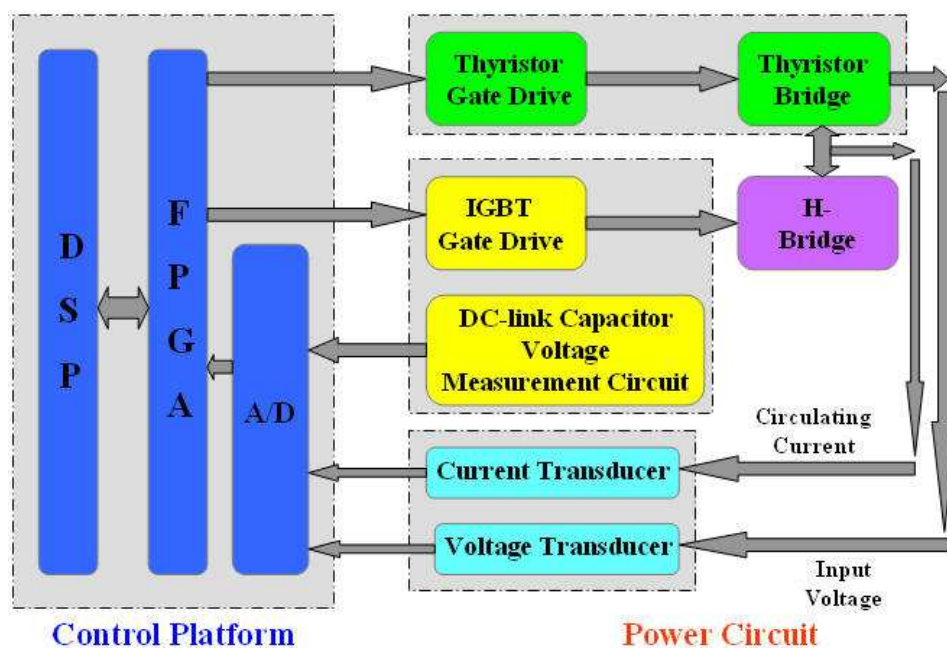
Fig. 5.1: Structure of the prototype hybrid cycloconverter system

In the power circuit section, the detailed design and parameters of the different parts, such as the thryristor bridge, the auxiliary inverter, the gate drive circuits, the transducer circuits, the circulating current reactors, will be given. All the specifications in the power stage are derived based on a target output apparent power which is around 4.5kVA (220Vrms, 7Arms). The control platform, including the characteristics of the DSP and the FPGA boards, and how the different control methods are implemented in the software code is discussed. For test purposes, a programmable AC source manufactured by Chroma was used to provide the input power for the prototype. Some photos corresponding to each part of the prototype are presented.

5.2   The Design of the Power Circuit

In this section the design of the subcircuits for the power stage are presented and the parameters related to each sub-circuit are listed.

5.2.1 The Power Switches Reutilization and Selection

There are two main components in the power stage of a hybrid cycloconverter: the thyristor bridge and the auxiliary three-leg inverter bridge. The hardware of the thyristor bridge used in the prototype is modified from a cycloconverter module that had already been built by someone else and thus only some rewiring work needed to be done to make it fit for this work. However, the auxiliary inverter in the power stage was designed and built to match the power rating of this prototype. In the following description it will be noticed that the specifications (such as voltage rating, current rating) of the IGBTs and diodes are much lower than that of the thyristors.

5.2.1.1 Thyristor Bridge

The most important characteristic of a naturally commutated thyristor is that the switch will turn on when a firing pulse is applied to the gate but will not be able to turn off on command (when the firing pulse is removed) unless the forward anode current is zero and a reverse voltage is applied on the thyristor for a given time t_q

(turn-off time) [p.6-8, 1, pp.19, 2, 57, 58]. In practice, the forward anode current should exceed a minimum current, called "latching" current, to ensure the thyristor is kept conducting after the gate signal is removed. Furthermore, as long as the anode remains positively biased, the thyristor cannot be switched off until the anode current falls below another relatively low level, called the "holding" current. Normally, the latching current of a thyristor is higher than its holding current, although both of them can be regarded as being zero in an ideal device model. Therefore, unlike a forced commutated device such as an IGBT or MOSFET, the turn off process of the thyristor limits the application of this device to the low frequency range. However, as mentioned in Chapter 1, the thyristor is available in a variety of ratings, especially competitive in the high voltage and high current region. Nowadays, thyristors are capable of blocking voltages (in both forward and reverse directions), from 50V up to 8500V and current ratings range from 5A up to 9600Arms. Thus the thyristor is naturally found to be widely used in the high power range, particularly where several thousands of kilowatts are required.

In the cycloconverter prototype the anode of each thyristor placed in the positive half bridge has to be connected to the same AC input line as the cathode of the corresponding thyristor in the negative half bridge. Therefore, the existing thyristor modules consisting of two series connected devices, as shown in Fig. 5.2, are used to build the thyristor bridge. The part number of the thyristor module used in the prototype is MCC 90-16io8, manufactured by ABB. Some important data in regard to this component, as extracted from the device datasheet [59], are shown in the Table. 5.1.
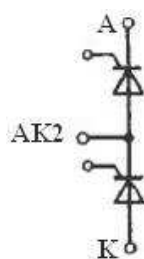
Fig. 5.2: The schematic of the thyristor module used in the prototype

In the prototype, based on the schematics shown in Fig. 5.3, the thyristors are connected as positive and negative half bridges in each phase as shown in Fig. 5.4.

Parameters	ABB MCC 90-16io8
Repetitive peak reverse voltage V_{RRM}	1600V
Mean forward (on state) current I_{TAVM}	96A
RMS forward (on state) current I_{TRMS}	140A
Direct forward (on state) voltage V_T	1.55V
Gate trigger voltage V_{GT}	1.5V
Gate trigger current I_{GT}	150mA
Latching current I_L	400mA
Holding current I_H	200mA
Turn-off time t_q	100μs

Table 5.1: Technical specifications of MCC 90-16io8
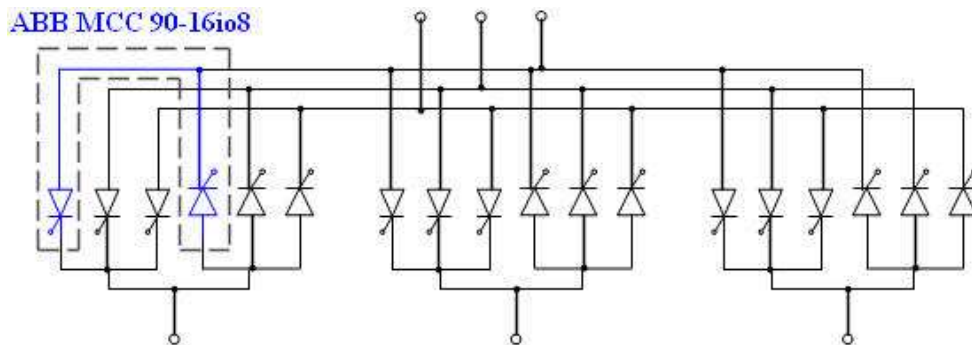
Fig. 5.3: Schematic of the three-phase input to three-phase output thyristor bridges
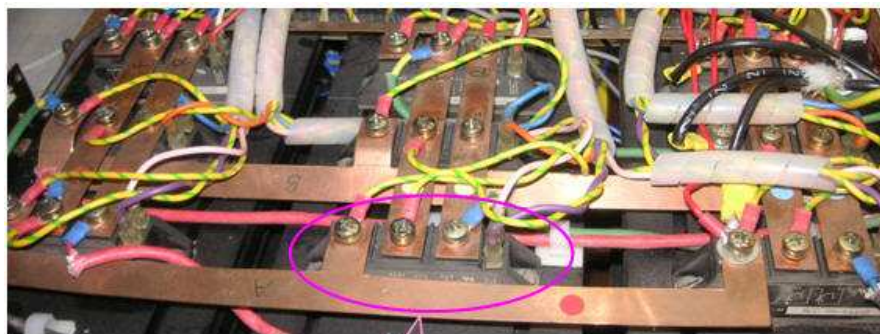
ABB MCC 90-16io8

Fig. 5.4: Photograph of the three-phase thyistor bridges

5.2.1.2 IGBT and Diode Selection

IGBTs and fast recovery diodes were chosen to form the switches for the auxiliary inverter. The three-leg bridge inverter, as shown in Fig. 3.8 or Fig. 3.9, consists of four IGBTs and two diodes. As the two IGBTs in the middle symmetric full leg connected to the load need to be able to carry reverse current in the freewheeling state, they need to have an anti-parallel diode. If the circulating current needs to be under control all the time, the DC-link capacitor voltage should be greater than 506V, which is the peak of the differential mode voltage under rated input voltage conditions (415Vrms). However, the experimental results in this work are only obtained with the reduced DC-link capacitor voltage which is 295V. Therefore, the voltage rating of both IGBTs and diodes in the auxiliary inverter should be at least higher than 295V. Furthermore, the current rating of the IGBTs and diodes should be higher than 11.5A if the load current and circulating current are set around 10Apk (7Arms) and 1.5A (DC) respectively. In practice, the fault conditions may cause over-voltage or over-current problems for IGBTs. For example, when the hybrid cycloconverter operates in circulating current mode, the DC-link capacitor could be charged to a voltage level which is equal or even higher than the amplitude of the input line-to-line voltage (around 600V) if the gating circuits for IGBTs failed to generate pulses. More discussions in regard to the hybrid cycloconverter operating under fault conditions and the corresponding protections will be presented in Subsection 5.3.2.3. Therefore, some margin needs to be left between the actual voltage/current stress applied to the devices and the maximum voltage/current rating of the switch that is given in the datasheet, to be able to handle the fault situations.

To ensure that all the power switches in the auxiliary inverter can work safely and also taking the cost into consideration, single IGBT devices per capsule type IXDR30N120, IXER35N120D1 (IGBT with anti-parallel diode) and the fast recovery diode type DSEP 30-12AR are used in the prototype. These devices are all manufactured by IXYS. The main technical specifications of the two IGBTs and one diode used in the prototype, including the maximum ratings and the switching characteristics, are presented in Table 5.2 [60 – 62].

The IXER35120D1 is the device chosen to be used in the middle leg of the auxiliary inverter as it already has an integrated anti-parallel diode. Both types of IGBT have the features of low saturation voltage, high switching speed and low switching losses. The anti-parallel diode with the IGBT has fast reverse recovery, low operating forward voltage and low leakage current. The single diode device per capsule is ultrafast with a soft recovery. One advantage which all these selected switches have in common is that they are all built in an ISOPLUS package which means that they have an isolated back surface (certified to withstand 2500V), which is typically used for cooling. This characteristic saves time and decreases the complexity of the assembly when having to isolate the power switch terminals from the heatsink.

Parameters		IXDR30N120	IXER35N120D1	DSEP 30-12AR
I G B T	Collector-to-emitter voltage rating V_{CES}	1200V	1200V	n/a
	Base-to-emitter voltage rating V_{GES}	±20V	±20V	n/a
	Maximum continuous collector current I_C	30A	32A	n/a
	Collector-to-emitter saturation voltage $V_{CE(SAT)}$	2.4V	2.6V	n/a
	Turn-on delay time $t_{d(on)}$	100ns	85ns	n/a
	Turn-on rise time t_r	70ns	50ns	n/a
	Turn-off delay time $t_{d(off)}$	500ns	440ns	n/a
	Turn-off fall time t_f	70ns	50ns	n/a
	Turn on swithing loss E_{on}	4.6mJ	5.4mJ	n/a
	Turn off swithing loss E_{off}	3.4mJ	2.6mJ	n/a
D I O D E	Forward current rating I_{FRMS}	n/a	25A	70A
	Instantaneous forward voltage V_F	n/a	1.9V	1.79V
	Peak Repetitive Reverse Voltage V_{RRM}	n/a	n/a	1200V
	Reverse Current I_R	n/a	n/a	1mA
	Reverse recovery time t_{rr}	n/a	80ns	40ns

Table 5.2: Main technical specifications of IXDR30N120, IXER35N120D1 and DSEP 30-12AR

Fig. 5.5 shows the schematic of a typical three-leg bridge inverter structure. Fig. 5.6 shows the three-phase auxiliary inverter prototype where all the IGBTs and diodes are mounted side by side on the two parallel heatsinks and connected via short 1mm² wires to constitute the auxiliary inverter. The DC-link electrolytic capacitors are connected to the auxiliary inverter by wires instead of placing them on the top of the inverter because of their large size. Each of the three decoupling film capacitors is connected across the corresponding DC-link of each inverter, as shown in the photo in Fig. 5.6. These decoupling capacitors are used to reduce the effect of induced voltage spikes due to the high frequency switching of the IGBTs and the long connections to the DC-link capacitors. A snubber circuit can be designed to reduce these spikes as well.
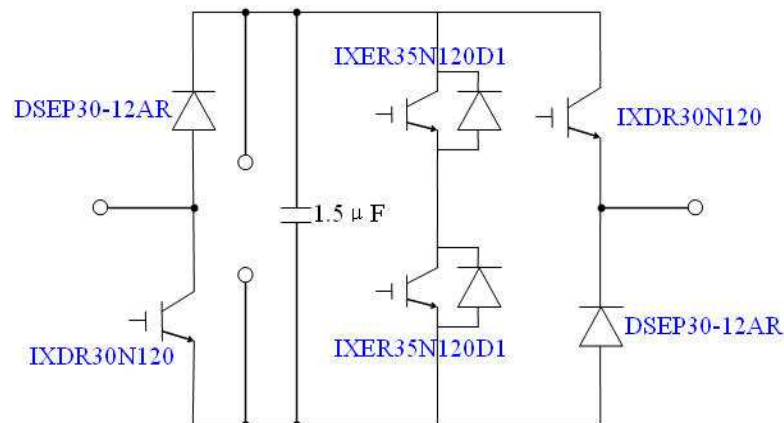
Fig. 5.5: Schematic of the three-leg bridge inverter
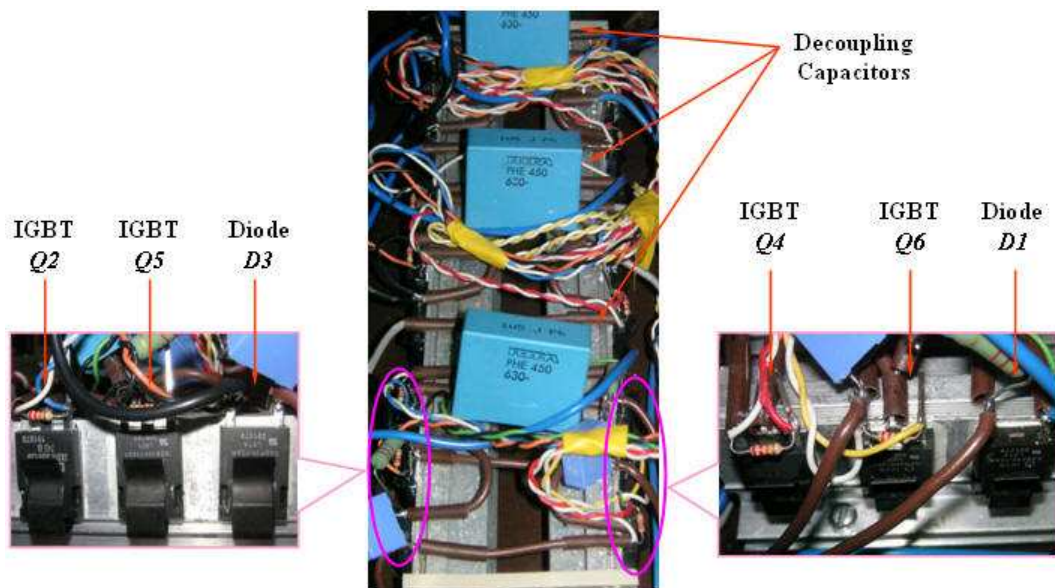
Fig. 5.6: Photograph of the three-phase auxiliary three-leg bridge inverters

5.2.2 Gate Drives and DC-link Capacitor Voltage Detection Circuits

The output pulses generated by the FPGA board are delivered to both the thyristors and IGBTs but cannot be applied directly to the power semiconductors since the FPGA does not have enough current drawing ability to drive these power devices, nor does it provide the necessary isolation. Therefore, a gate drive board is needed between the FGPA and the control terminals of the power semiconductors to provide the required current and isolation.

5.2.2.1 Thyristor Bridge Gate Drive

Fig. 5.7 shows the schematic of the thyristor gate drive circuit contained in the gate drive board used in this prototype.
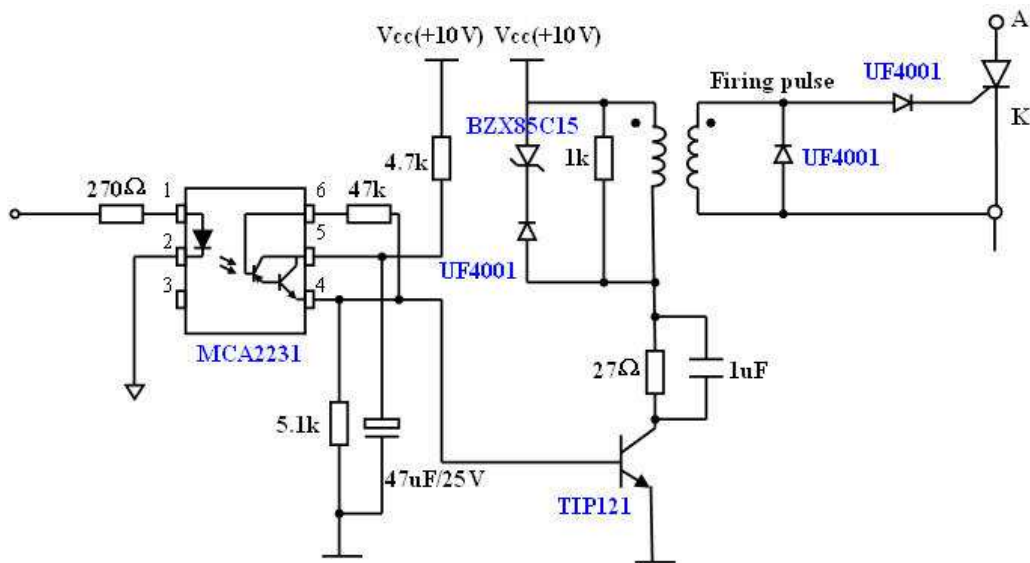
Fig. 5.7: Schematic of the thyristor gate drive

The optocoupler MCA 2231 provides the isolation between the FPGA and the gate circuit. As the MCA2231 does not have enough current ability to drive a thyristor, an isolated forward converter is used as an amplifier and is connected at the output of the optocoupler. Every time when the NPN transistor TIP121 is switched on, the voltage across the primary and secondary transformer are both 10V since the transfer ratio is

1:1. This 10V is applied to the gate of thyristors through UF4001. Meanwhile, the load current and the magnetizing current will flow through the accelerating capacitor (1μF) and as it charges more current will be diverted to the parallel 27Ω resistor, which will cause the voltage across the primary transformer to decrease gradually. Therefore, the width of each trigger pulse depends on the parameters of the resistor and capacitor. As will be seen in Subsection 5.3.2.1, the width of each thyristor firing pulse produced by the FPGA is fixed at 100μs, with a 200μs switching period, which means that the actual width of the pulse applied at the thyristor gate will be around 50μs with the gate circuit parameters of 27Ω resistor and 1μF capacitor. In order to make sure that the thyristor is fully switched on, ten identical short pulses are applied on the gate of the thyristor every time a turn on command is triggered. Therefore the total width of the pulse trigger train is 2ms (200μs × 10). Every time the transistor TIP121 is switched off, the magnetizing current is removed by the 1kΩ resistor which is in parallel with the primary transformer. The freewheeling diode on the secondary side is used to clamp the reverse voltage across the transformer so that it will not exceed -1V. The series arrangement of UF4001 and BZX85C15 are also connected in parallel with the transformer to prevent any over-voltage since it may destroy the transistor TIP121. Fig. 5.8 shows the pictures of the thyristor gate drive board and a zoom into one of the gate drive units.
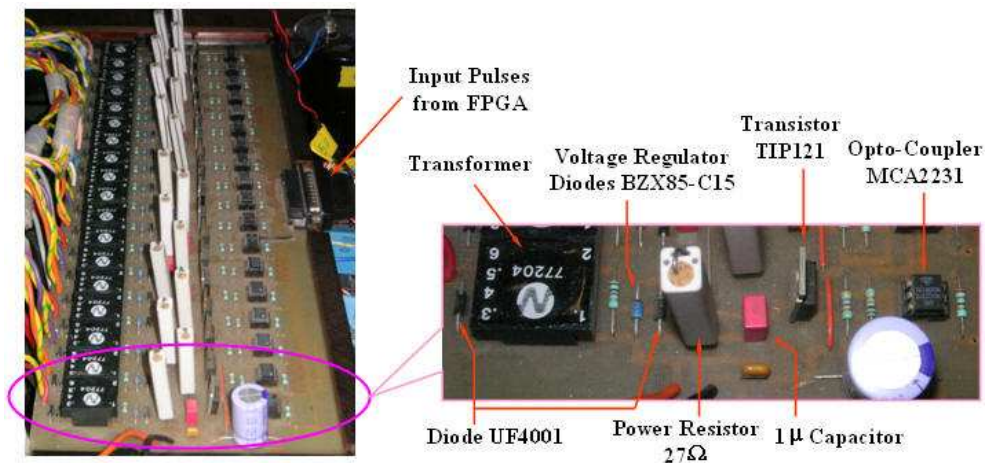
Fig. 5.8: Photographs of the thyristor gate drives and the detail of one of its cells

5.2.2.2 Three-leg Bridge Inverter Gate Drive

The schematic of a single switch gate drive for one IGBT device in the auxiliary

inverter is shown in Fig. 5.9. The optocoupler HCPL-3120 is used to provide isolation between the control circuit and the gate drive. Since the output stage of HCPL-3120 is capable of providing pulses of current up to 2.5A peak no additional amplifiers are required. The TTL buffer, SN74LS245, is used to drive the optocoupler since the LED of optocoupler requires at least 10mA of forward current. The input of the buffer uses the logic signals generated by the DSP/FPGA board. From the output side of the optocoupler, it can be seen that the IGBT is driven by ±15V through a gate resistor of 15Ω. The ±15V power supply used here is generated from NMA0515SC (not on the schematic), which is a 1W DC/DC power supply and can ensure that the input and output of the optocoupler are isolated since they are supplied from separated power supplies. Moreover, in order to prevent the IGBT from being destroyed if the gate drive encounters any failure in operation, a 22k resistor is connected as shown in the schematic to discharge the gate capacitance. Two 18V zener diodes are connected in anti-series between the gate and emitter of each IGBT to make sure the gate will not be damaged by over voltage.
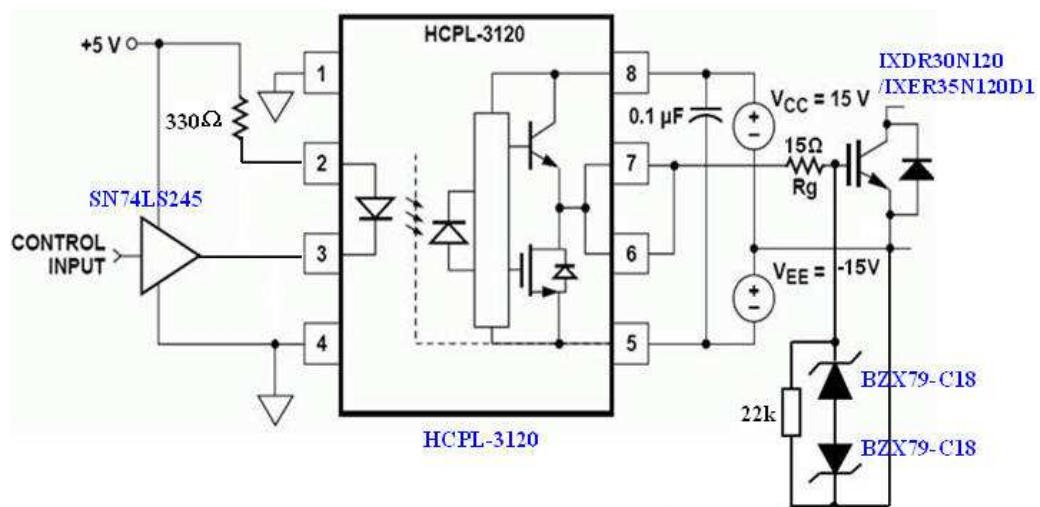
Fig. 5.9: Schematic of the three-leg bridge inverter gate drive

As shown in Fig. 5.11, the gate drive circuits of the auxiliary inverter have been implemented on one printed circuit board (PCB) and one bread board. The PCB contains eight gate drives for the auxiliary inverters in two phases whilst the bread board contains four gate drive circuits for the other one phase. Each gate drive is used to drive one of the IGBT switches mentioned previously.

5.2.2.3 DC-link Capacitor Voltage Measurement Circuit

Fig. 5.10 shows the schematic of the DC-link capacitor voltage measurement circuit. The layout of this circuit for each phase is placed on the same PCB or bread board as those gate drives for the corresponding auxiliary inverter. In this circuit, the high CMR (common mode rejection) isolation amplifier HCPL-7800 is used because it can not only be used for general analog signal isolation applications requiring high accuracy, stability and linearity but also be able to provide precise monitoring of the high voltage power source. The power supply of the input side of HCPL-7800 is +5V which is converted from the +15V supply used in the gate drive circuit, through a positive voltage regulator (μA78L05). Since the ground point of the input side of the HCPL-7800 should be the same with the negative point of the DC-link capacitor, the input of μA78L05 can only be the +15V used by the gate drives of the IGBT Q2 or Q6 (Fig. 3.8 or 3.9). Some resistors are connected as voltage dividers in order to generate a 0.2V reference for the HCPL-7800 from the +5V power supply as well as to reduce the measured DC-link capacitor voltage from 0-450V (the voltage rating of the chosen DC-link capacitor) to 0-0.4V which is the linear conversion region of HCPL-7800.
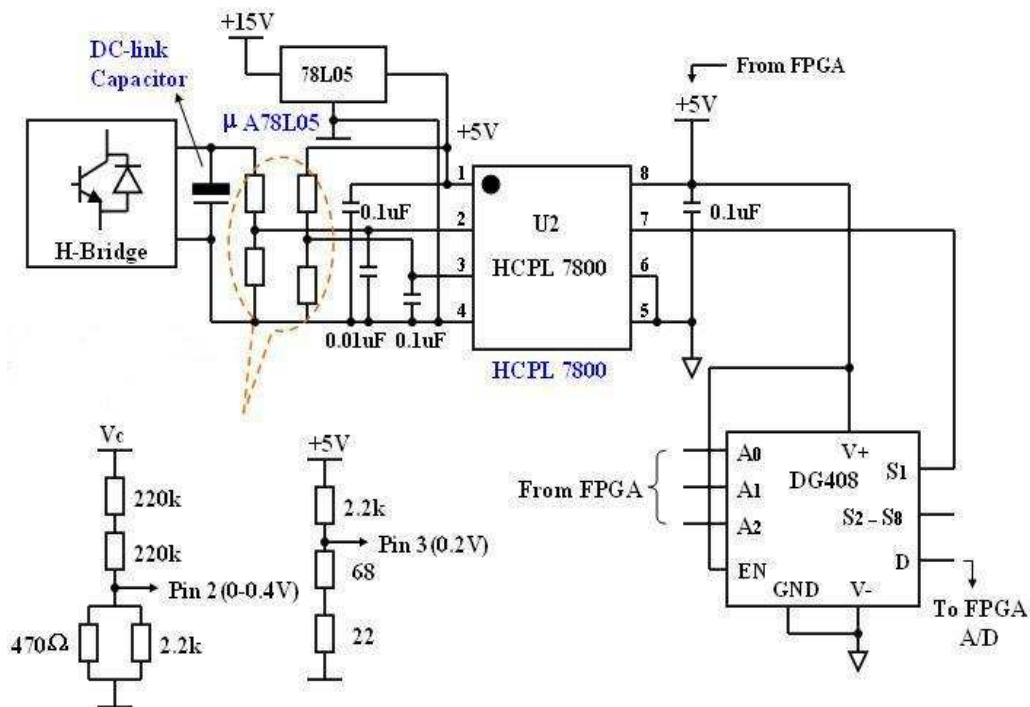
Fig. 5.10: Schematic of the DC-link capacitor voltage measurement circuit

There are ten A/D conversion circuits on the FPGA board, which will be introduced in the next section. Nine of these A/D circuits will be used for the input voltages and circulating currents measurement, so only one channel is left to measure the three DC-link capacitor voltages of the three auxiliary inverters. Because the control speed of these DC-link capacitor voltages is relatively slow, a multiplexer is used to sequentially select one of the three capacitor voltages in every switching period. The multiplexer is selected because it has the features of low signal ON resistance and fast switching transition time. The +5V power supply, which is connected to the FPGA and the buffer SN74LS245 in the gate drive circuit, is also used to provide the power supply for both the output side of HCPL-7800 and the multiplexer.

Fig. 5.11 below shows the practical implementation of the gate drive circuits and the DC-link capacitor voltage measurement circuits. The measurement circuit in each phase is fitted within the gate drive of Q6 (Fig. 3.8 or 3.9) in the middle leg of the auxiliary inverter of each phase, as the negative point of the DC-link capacitor is always connected to the emitter of that switch.
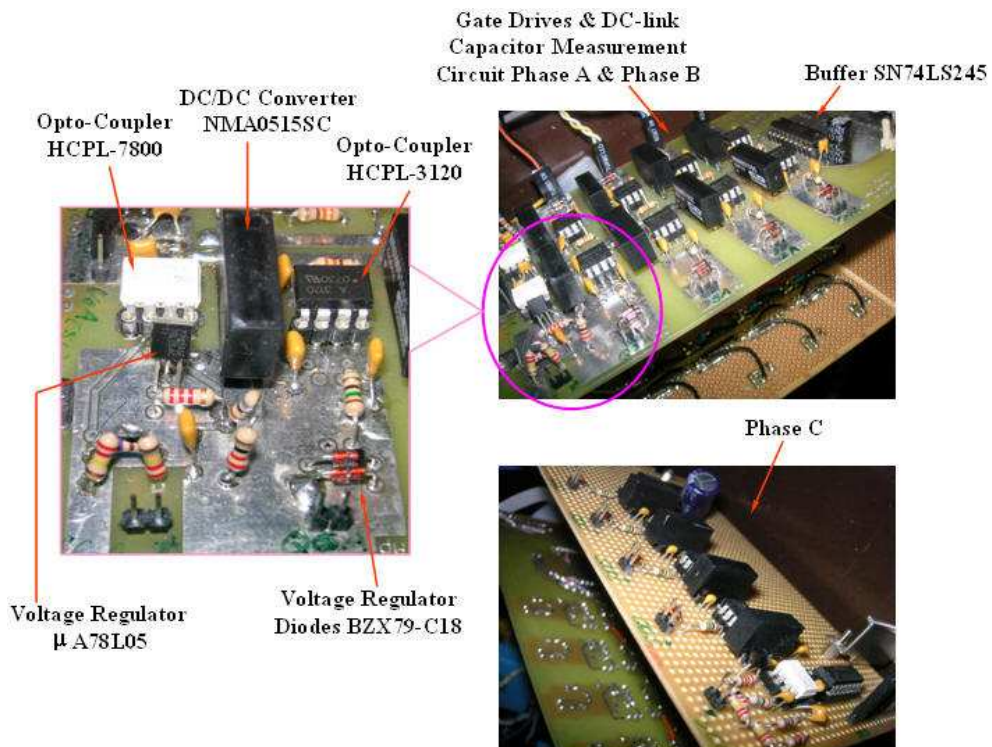
Fig. 5.11: Photographs of the auxiliary inverter gate drives, DC-link capacitor measurement circuits and one of their circuits in detail

5.2.3 Voltage and Current Transducer Circuits

As can be seen from Fig. 3.12 or 3.13, the control structure of the hybrid cycloconverter relies on the knowledge of the value of the input supply voltage, the circulating current and the load current. As both the circulating current and the load current can be obtained from the value of the currents in the two circulating current reactors, the transducer circuits of the input voltages and reactor currents have been implemented as follows.

Fig. 5.12 shows the circuit which is used to provide a linear conversion of the input voltages as well as the isolation between the input power supply and the control platform. As can be seen from the schematic, three identical groups of circuits are connected to the three input phases, a, b, c, respectively in order to measure V_{inA}, V_{inB}, and V_{inC}. The voltage transducer, LV 25-P manufactured by LEM, is used to implement the transducer circuit. A 25kΩ resistor is connected in each phase between the input power supply and the voltage transducer in order to generate a proportional current used for measurement as well as to ensure that the transducer is able to measure the full region of the rated input phase-to-supply neutral voltage (240Vrms). In practice, two 50kΩ, 10W resistors are connected in parallel to act as a 25kΩ to provide sufficient power dissipation capability. The secondary side of the voltage transducer is supplied by ±15V which is different from the one supplying the gate drives of the auxiliary inverter. The transducer output current, also in proportion to the input phase-to-supply neutral voltage, flows through the 140Ω measuring resistor. The value of this measuring resistor is calculated by ensuring that the maximum voltage across it will always remain within the A/D conversion range. The measurement circuit has been calibrated after the circuit was built in order to generate an algorithm by which the program is able to eliminate the offset, gain variation and extract the correct voltage value from the data accessible to the DSP. Fig. 5.14 shows the voltage tranducer circuits used in the prototype and one enlarged section of the circuit containing one of the channels.
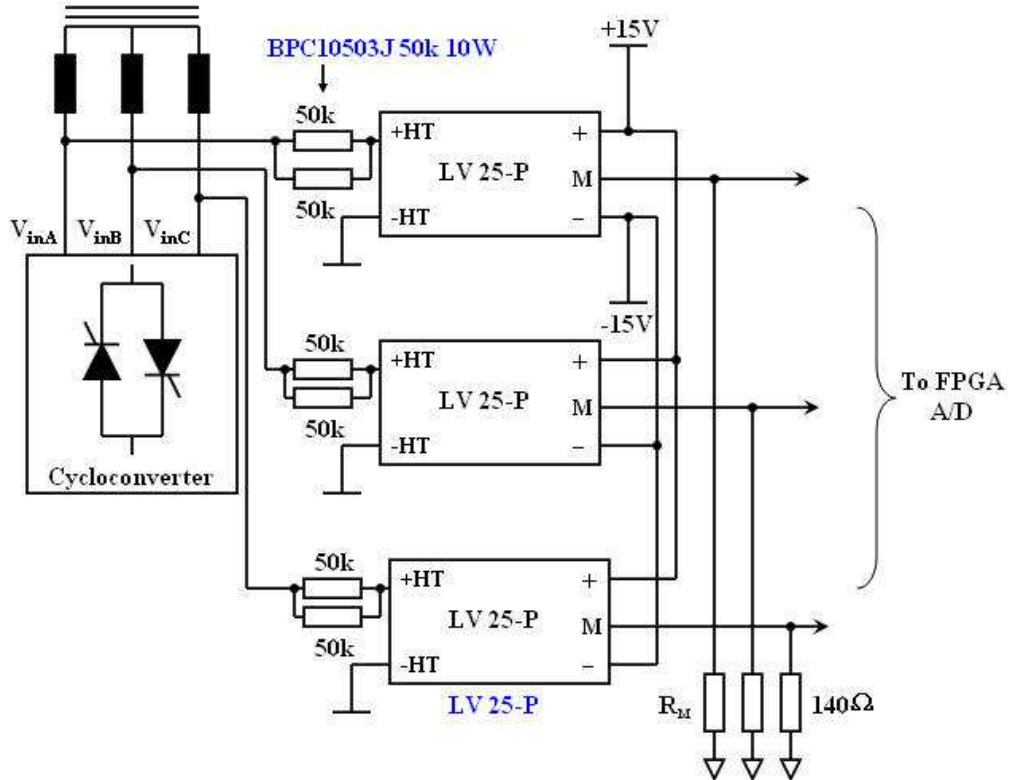
Fig. 5.12: Schematic of input voltage transducer circuits

As all current transducer circuits are identical, only the schematic of one circuit is shown in Fig. 5.13. In this circuit, the LEM LA55-P current transducer is employed to measure the current. As the primary side nominated RMS current of the LA55-P is 50A and less current is expected in the circuit, the wires are winded through the hole of the transducer a few times to increase the measurement gain and resolution, especially at light load. However, due to the size of the wires and the limitation of the hole area on the transducer, the maximum achievable was three turns, as shown in Fig. 5.14, where the current transducers and a zoom in one phase have been shown. Therefore, around 25.5A (rms) is measured by LA55-P if the load current and circulating current are 7A (rms) and 1.5A (dc) respectively. The secondary side of the transducer is supplied by the same ±15V power supply used for the voltage transducers. Similar to the voltage transducer, a 150Ω resistor, which is able to generate a voltage proportional to the current measured in the primary side of the transducer, is connected at the secondary side. The value of the resistor is to ensure that the output always remains within the conversion region of A/D converters on FPGA board. Finally, the circuit was also calibrated to ensure that the correct current value can be retrieved by the program.
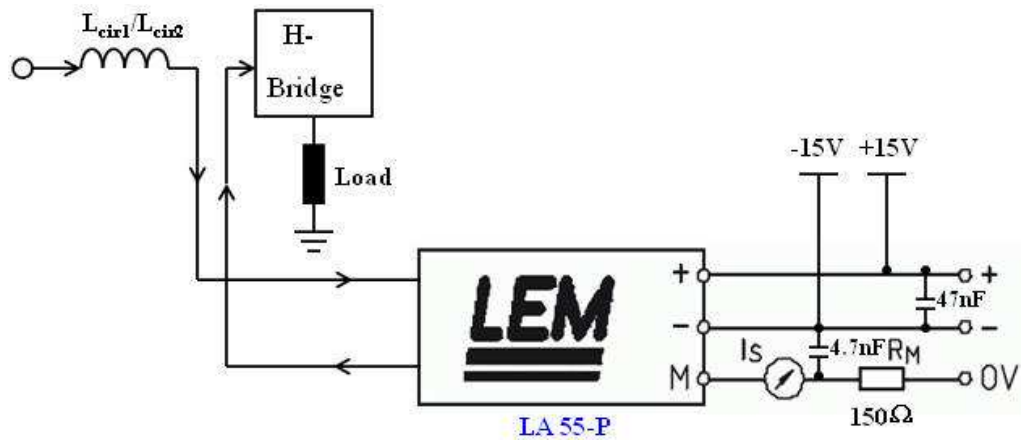
Fig. 5.13: Schematic of inductor current transducer circuit
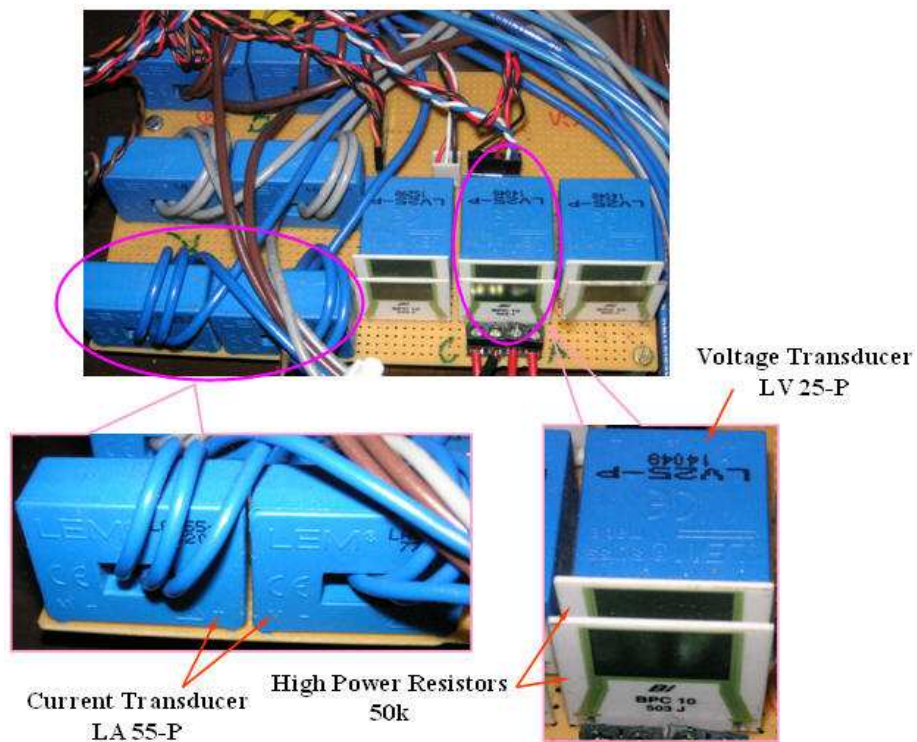
Fig. 5.14: Photographs of the voltage and current transducer circuits and their circuit in detail

As described in Chapter 4, in each phase, it is not difficult to calculate the circulating current and the load current after the two reactor currents are measured by the current transducers. Suppose that the two currents are I_{THY1} and I_{THY2}, the load current I_{Load} and the circulating current I_{cir} are calculated according to Equation (5.1) and (5.2). These equations are implemented in the DSP program which will be discussed in the Subsection 5.3.2.

$$I_{Load} = I_{THY1} - I_{THY2} \tag{5.1}$$

$$I_{cir} = \frac{(I_{THY1} + I_{THY2}) - |(I_{THY1} - I_{THY2})|}{2} \tag{5.2}$$

5.2.4 Inductor Design and DC-link Capacitor Selection

Since an off the shelf inductance to match the requirement was not available, a full design of the circulating current reactor was undertaken. This took into account a full range of factors such as the optimum inductance value, the load and the circulating currents, the restrictions for the physical size due to limited bench space and the cost. Since the peak of the circulating current in the standard cycloconverter is much larger than that in the hybrid cycloconverter, the design of the circulating current reactor is based on the requirements of the standard cycloconverter with circulating current. The whole inductor design is detailed in Appendix F, which is similar to [63], [64].

The inductors used in the prototype are manufactured by JMS Transformers, as shown in Fig. 5.15, and in order to test the prototype with different values of the circulating current reactor, the reactor was built using three windings made of the same copper wire coupled together, with the ratio of turns 1:1:2. The total number of turns that JMS was able to wind on the coli former was 480, which means 120 turns for the two smaller windings and 240 turns for the third winding. All the three windings are insulated from each other. As the total number of turns is a bit less than what has been designed, the airgap in this inductor has been reduced to around 3mm to ensure that the value of the total inductance still remains to be around 400mH, if all the windings are connected in series. For the same reason, the diameter of the copper wires winded in the inductors is around 2mm which is also a bit thicker than the upper limitation produced by Equation (F.20) in Appendix F. The thickness of the lamination stack is around 3inch (76mm) since size E35 is selected for the E+I core. Although there are some deviations from the design which are a consequence of the manufacturing process, the value of the inductors are still very close to what was expected, as listed in Table 5.3 (A,B,C,D,E,F represent different terminals at the end of each winding).
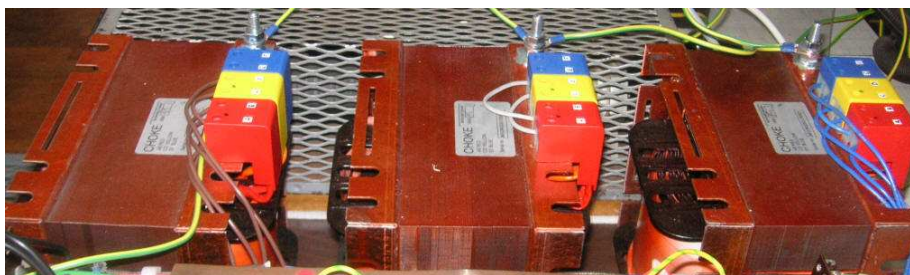
Fig. 5.15: Photograph of the three-phase inductors

	Phase A CCR	Phase B CCR	Phase C CCR
AB	24.190mH	24.527mH	23.672mH
EF	23.974mH	24.790mH	24.013mH
AF	96.58mH	97.97mH	95.48mH
CD	96.04mH	98.28mH	95.82mH
AD	384.32mH	391.95mH	380.37mH

Table. 5.3: The measured values of the inductances between different terminals when all the three windings of the inductors are connected in series

The smaller the voltage ripple across the DC-link capacitor, the smaller the voltage margin and the better the utilization of the auxiliary inverter components will be in the control of both the differential and the common mode voltage. Therefore, as shown in Fig. 5.16, three 8200μF capacitors are selected for the auxiliary inverters in three phase to ensure that the DC-link capacitor voltage will remain around the reference without having large ripple on it. As the DC-link capacitor voltage will be only set around half (295V) of the peak voltage seen across the thyristors, the voltage rating of the capacitor is selected as 450V. Some protections, which are presented in Section 5.3, have been added in the circuit in case of over-voltage under fault conditions.

Fig. 5.16: Photograph of three-phase DC-link capacitors

- 181 -

5.2.5 The Switch Box Design

There are four converter topologies that need to be experimentally evaluated with the same prototype in order to make a comparison between them and also to obtain the experimental results for them. These four topologies are the standard cycloconverter in circulating current mode (Fig. 2.8) and circulating current-free mode (Fig. 2.9), the hybrid cycloconverter in circulating current mode (Fig. 3.8) and circulating current-free mode (Fig. 3.9). Since it is unrealistic to rewire the prototype every time in the process of debugging and testing, a switch box, as shown in Fig. 5.17, is used to realize the topology alterations quickly. Fig. 5.18 shows the resulting converter topologies marked with the number 1 to 11 to reflect the nodes which correspond to the connectors on the switch box. S1 to S13 in the schematic are wire bridges instead of real switches or contacts since they cannot be found in the box. Therefore, if a wire bridge is ON, it means that the two nodes in the schematic are shorted with a wire. For example, for the topologies in circulating current-free mode, S1 has to be ON by connecting the nodes "1" and "2" directly through a wire. The description of which switches should be ON or OFF in order to configure the different topologies is shown in Table. 5.4.

Fig. 5.17: Photograph of the switch box showing the interconnecting nodes and the
bridge wires
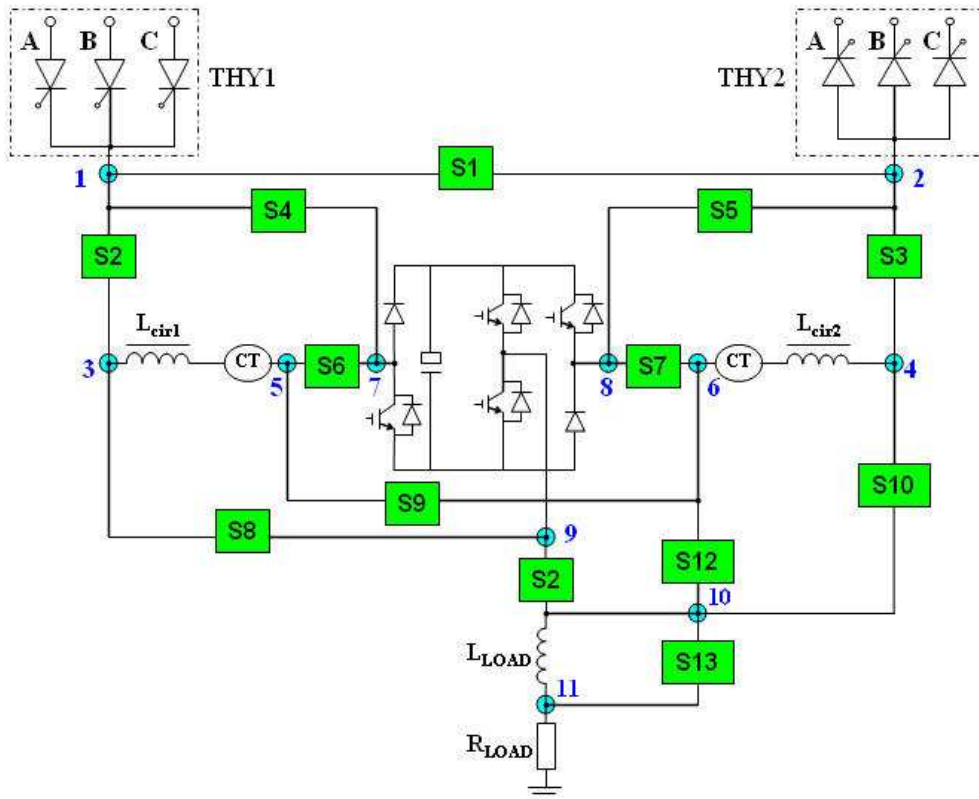
Fig. 5.18: The schematic of the universal prototype including the position of the reconfiguring bridge wires and the corresponding connecting nodes

	Standard Cycloconverter		Hybrid Cycloconverter	
	CCM	CCFM	CCM	CCFM
S1	OFF	**ON**	OFF	**ON**
S2	**ON**	**ON**	**ON**	OFF
S3	**ON**	OFF	**ON**	OFF
S4	OFF	OFF	OFF	**ON**
S5	OFF	OFF	OFF	**ON**
S6	OFF	OFF	**ON**	OFF
S7	OFF	OFF	**ON**	OFF
S8	OFF	OFF	OFF	**ON**
S9	**ON**	**ON**	OFF	**ON**
S10	OFF	**ON**	OFF	**ON**
S11	OFF	OFF	**ON**	OFF
S12	**ON**	OFF	OFF	OFF
S13	OFF	**ON**	OFF	**ON**

Table. 5.4: The table with the state of all the wire bridges in four separate cycloconverter topologies

5.3   The Cycloconverter Control Platform

The control platform for the cycloconverter uses a DSP evaluation board and a FPGA custom designed board. The DSP/FPGA system is responsible for reading the analog data, performing the calculations based on the control algorithms already described and then generating the corresponding gate driving pulses. In this section an introduction to the DSP/FPGA system used in this project as well as the principle of implementing the control methods using the software C code is presented.

5.3.1 Introduction to the TI-C6713 DSP/FPGA

The DSP used in this project is a C6713 floating point DSP, which is manufactured by Texas Instruments and offered for evaluation as a Starter Kit (DSK). With an on board parallel port, the DSP can be programmed by connecting the controller to a computer via a standard USB cable. The C6713 is a high performance floating-point DSP operating at 225MHz. The C6713 DSK is a low-cost standalone development platform that enables users to evaluate and develop applications for the DSP.

The DSP interfaces to the on-board peripherals of the C6713 DSK through a 32-bit wide External Memory Interface (EMIF), which not only allows 16Mb of on board synchronous DRAM memory, Flash Rom, CPLD, but also expands the memory interface through an expansion memory interface connector for a daughter card. Furthermore, the EMIF has four separate addressable regions called chip enable spaces (CE0 –CE3) for both the on-board devices as well as the expansion memory interfaces, and this can be helpful for selection without causing any conflict. The CE0 is allocated to SDRAM and CE1 is shared by the Flash and CPLD. The rest of the regions, CE2 and CE3 are generally reserved for daughtercards. In this project, only one of CE2 and CE3 is normally in use as just one daughter board is connected, which is the FPGA board.

The C6713 DSK also has a host port interface (HPI) connection with the DSP. The HPI port is a high speed data port which allows a bi-directional data transfer between the host PC and the DSP. Therefore, the PC can be used to control the converter as

well as download the value of the sampled variables. Therefore, it is possible to monitor the operation of the whole prototype, which is beneficial in debugging.

The FPGA board expands the functionality of the DSP by using the memory mapped interface of the FPGA and more important gives the DSK more interface circuitry and implements fast and accurate analog to digital conversion channels for measuring the desired analog signals. The FPGA board was originally developed by Dr. Lee Empringham from the PEMC group at the University of Nottingham [65]. The board has ten, 12 bit A/D channels with synchronized sampling which are used in following configuration for this application:

    3 analog inputs = Input Voltages

    6 analog inputs = Currents in all the windings of the circulating current reactors

    1 analog input = the DC-link capacitor voltage measurements (multiplexed)

The FPGA board also provides four D/A conversion channels, hardware comparators for protection and digital I/O capabilities for outputting or inputting fault trip information, as well as event triggering. Fig. 5.19 shows a photograph of the FPGA board which illustrates the physical circuitry that implements different functions used in this project.
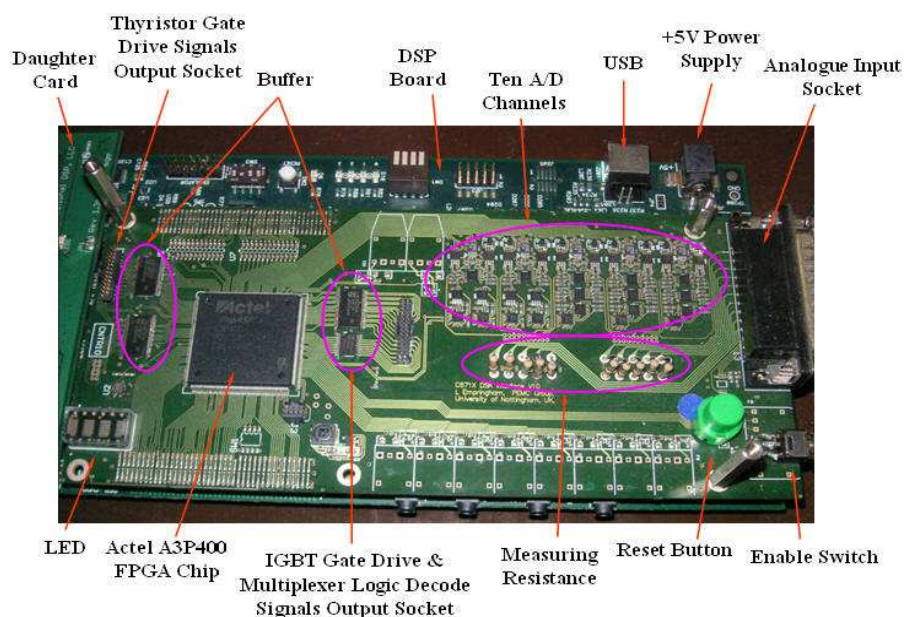
Fig. 5.19: Photograph of the FPGA board and its subcircuit functionality

The main function of the FPGA is to implement the PWM generator unit and the three state machines. The logic diagram of the FPGA was originally designed for a matrix converter system and the state machine was used there to correctly commutate the current between the bidirectional switches depending on the direction of the load current and the demanded switch state. Necessary modifications have been made on that schematic to fulfill the requirements of the various cycloconverter systems. Now both the PWM generator units and the state machines have been extended to six. If it is assumed that each of the PWM generators and each of the state machines form a pair, three of these six pairs are designed to generate trigger pulses for thyristor bridges whilst the other three pairs are used for the auxiliary inverters. In each switching period, the switching states and their corresponding duty times generated by the DSP are transferred to the PWM generator within the FPGA and the pulses generated by the PWM generator will then be transferred to the state machines, of which the output is the final digital pulses used to drive the corresponding thyristors or IGBTs.

The FPGA also provides a watchdog timer, trip monitor, trip information interface and temperature sensor interface. The A/D information is gathered by the interface and transferred into registers within the FPGA which are memory mapped to the DSP's memory interface. The trip monitor can disable the output of the state machines if any of the hardware or software trips based on the A/D information collected. A maximum of twenty-four hardware trips and eight software trips can be used. In this project, the hardware trips used are the watchdog trip, the FIFO (first in, first out the PWM generator) empty trip and the FIFO full trip. The output of the watchdog timer is connected directly to the trip monitor. Therefore a hardware trip will be generated if the watchdog timer is not serviced at the beginning of each control interrupt which may happen when the DSP program crashes or does not function properly or when any other problems arises requiring the converter to be disabled. Only two software trips, which are the overcurrent protection for the circulating currents and load current and the over-voltage protection for the DC-link capacitor voltage, are used in this project. Some more details regarding the implementation of these two software protections are explained in Subsection 5.3.2.3.

5.3.2 Implementation of the Control

The software code executed by the DSP to control the cycloconverter prototype was originally developed by Maurice Apap for the TIMES project and has been modified for this application [65]. In the main routine, all the configuration variables are set at the very beginning to prepare the external memory interface, the FPGA configuration registers and the PWM generator period. All the parameters which were defined in the program are then initialized. After all the initialization is completed, the main routine of the DSP enables the PWM interrupt and then waits for the interrupt to occur after the timer is started. As the switching frequency of the hybrid cycloconverter is 5kHz, the sampling frequency of the DSP/FPGA is set at 5kHz as well. In the following subsections, some important functions of the interrupt program will be introduced.

5.3.2.1 Trigger Pulse Generation

The program for pulse generation is one of the most important parts in the interrupt routine. Due to the different characteristics of the cycloconverter in different operating modes (circulating current mode and circulating current-free mode), the algorithms for generating the firing pulses, not only for the thyristor bridge but also for the auxiliary inverter, need to be different for each topology.

For the thyristor bridge, the delay angle equation, which is an important factor that decides the exact time to commutate from one thyristor to another, is generated by calculating the output reference equations at the beginning of the interrupt routine. In the control of the thyristor bridges, another important factor which decides the start of each delay angle is the line-to-line input voltage, because every intersection of two input phase-to-supply neutral voltage waveforms is the start of a firing delay. Obviously, if the cycloconverter is operating in circulating current-free mode, the load current is an important factor to determine the commutation between the positive and the negative thyristor half bridges. Therefore, the delay angles as well as the scaled input voltages and the load currents calculated from the two scaled reactor currents are used in the thyristor pulse generation program to decide when the commutation should take place.

As the 3-pulse thyristor half bridge is operating at 150Hz commutation frequency between any two of three thyristors, the width of the thyristor gating pulse is set at 2ms, which is long enough for triggering the thyristors without causing any overlap between any two consecutive gating pulses. In order to increase the likelihood that a thyrsitor is fully turned on, the trigger pulse is divided into ten 200μs short pulses (50% duty cycle) instead of just a 2ms single long pulse. Hence, in every interrupt of the program, the DSP generates the short pulses to the corresponding thyristors that need to be turned on.

In circulating current mode, the program enables both the positive and negative thyristor half bridges in the whole output period. However, in circulating current-free mode, one thyristor half bridge is disabled whilst the other one is conducting, depending on the direction of the load current. However, there is one exception that occurs each time the load current changes polarity. During this period of time, two thyristors connected to the same input phase but in complementary half bridges must be gated. This is to ensure the safe commutation of the load current from one thyristor half bridge to the other one without causing any short circuit of the inputs or distortion of the output voltage.

The principle of pulse generation for the IGBTs is similar for the circulating current mode and circulating current-free mode. In circulating current mode, the output of the circulating current PI controller is used as the digital modulating wave to generate pulses for the auxiliary inverter which implements the differential mode voltage control. However, the circulating current will have some low frequency components, especially when the speed of the PI controller is slow as mentioned in Chapter 3. Hence, the feedforward compensation method is used in conjunction with the PI controller by adding an estimated differential voltage to the output of the PI controller to produce the pulses for the differential voltage control. After the duty cycle D_{active} is obtained, which effects the differential mode voltage control, another part of the code is used to realize the common mode voltage control. The generation of the D_{zero} has been explained in detail in Subsection 3.4.4 of Chapter 3 and the written codes are also based on those equations presented in Chapter 3. Since only the common mode voltage needs to be controlled, the code for generating the pulses for the IGBTs in circulating current-free mode can easily be realized by disabling the code for the

differential mode voltage control and substituting 0 for D_{active} in the code for the common mode voltage control.

5.3.2.2 Current and Voltage PI Controller

As mentioned in Chapter 3, the circulating current and DC-link capacitor voltage need to be monitored and controlled, which are both realized by using PI controllers. The design of both controllers for the prototype is similar to that for the simulation models, which can be found in Chapter 4.

In the prototype implementation, the PI controller is realized in DSP software code and the pole designed for the controller in Chapter 4 is ignored as it would be very complicated to build the digital PI controller by taking the pole into consideration. The equation used to realize the function of the digital PI controller is:

$$PI_k = PI_{k-1} + K_{P-CCPI} \times (error_k - error_{k-1}) - \frac{K_{I-CCPI}}{f_S} \times error_{k-1} \qquad (5.3)$$

Where the PI_{k-1} and $error_{k-1}$ are the output and the error of the PI controller in the previous switching period; the PI_k and $error_{k-1}$ are the output and the error of the PI controller in the current switching period; f_S is the switching frequency of 5kHz; K_{P-CCPI} and K_{I-CCPI} are the proportional gain and the integral gain of the circulating current PI controller as introduced in Chapter 4.

The equation used in the code for the DC-link capacitor voltage controller is:

$$PI_k = PI_{k-1} + \frac{K_{I-DCPI}}{f_S} \times error_{k-1} \qquad (5.4)$$

Where the integral gain K_{I-DCPI} is 1.0 as designed for simulation models, which is enough for ensuring the stability of the DC-link capacitor voltage.

5.3.2.3 Software Protection

In practice, over-voltage or over-current which may destroy the devices of the prototype may occur under fault conditions. As the voltage and current rating of the thyristors assembled in the prototype are both higher than those of the IGBTs, the auxiliary inverter is more frangible compared to the thyristor half bridges. One of the most serious situations happens if the gating circuits for IGBTs fail to deliver the corresponding pulses due to the circuit disconnection or any fault generated by the DSP or FPGA. If the IGBTs in the both asymmetric legs cannot be switched on, the DC-link capacitor will be charged by the circulating current (only for circulating current mode) until the voltage of the capacitor is equal to the amplitude of the input line-to-line voltage. The DC-link capacitor may also be charged by the load current until the current reaches zero if the two IGBTs in the middle leg cannot work as well. Apart from the over-voltage, the devices can be destroyed by over-current caused by any sudden increase of the load current. The circulating current reactors may also be saturated with the increasing of the load current and causes even higher circulating current current due to the dramatic decrease in inductance. Fig. 5.20 shows the waveforms of the DC-link capacitor voltage and the circulating current of the hybrid cycloconverter obtained by simulation by assuming that the converter operates under both of the fault conditions mentioned above. From this figure it can be seen that the DC-link capacitor voltage is continuously charged by the circulating current if the IGBTs in both side leg cannot be turned on. Although the speed of charging becomes slower with the increasing of the DC-link capacitor voltage, the voltage has the possibility to be charged to a level which is equal to or even above the amplitude of the input line-to-line voltage if the gating pulses are applied on the thyristors all the time. The circulating current shown in Fig. 5.20 has the amplitude of up to around 200A due to the saturation of the circulating current reactors. This high circulating current can also speed up the charging of the DC-link capacitor.

In order to ensure the safe operation of the hardware and prevent any over-current or over-voltage from causing damage to the prototype under fault conditions, two software trips have been defined in the code for the cycloconverter prototype. One of them is specifically designed for monitoring the current through the circulating current

reactors (the circulating current and the absolute value of the positive or negative load current half wave) as this current will also flow through the circulating current reactors and all the power devices such as thyristors, IGBTs and diodes. By monitoring this current, it is possible to ensure that the current always stays below the rated saturation current of the inductors and the current ratings of the devices. Another software trip is set for the DC-link capacitor voltage. Since the DC-link capacitor voltage cannot exceed the voltage rating of the IGBTs and diodes in the auxiliary inverter as well as the voltage rating of the electrolytic capacitors, the voltage is monitored to prevent the power switches and the DC-link capacitors from damage by over-voltage. As soon as any software trip is detected, the trip monitor will disable the output of the state machines and this means none of the output pulses for the thyristor bridges and the auxiliary inverters will be produced.
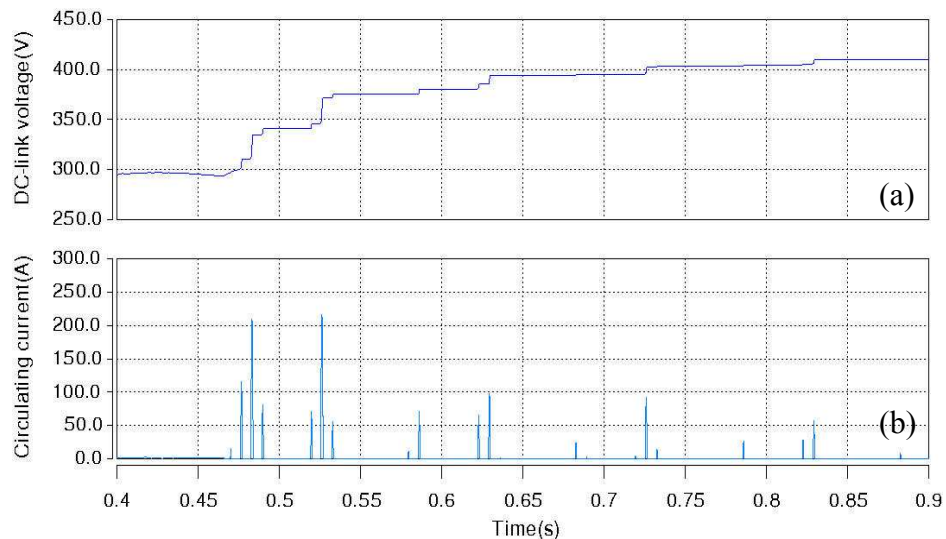
Fig. 5.20: The a) DC-link capacitor voltage b) circulating current waveform generated by the hybrid cycloconverter under fault conditions

In the prototype, due to the large value of the passive components (DC-link capacitor and circulating current reactors), only the software protection is used since it is fast enough to ensure the safe operation of the whole system based on the proper configuration of the circuit parameters. However, it would be better to implement some additional hardware protection circuits if a prototype which is required to handle all the possible fault conditions is built in the future. This is because the thyristor bridge may still be in conduction even if the gating circuits are disabled by the software protection unless the anode current is reduced below the holding current.

5.4   Summary

The design of the whole prototype, including both the power circuit and the control platform has been described in this chapter. All the schematics and photographs related to each part of the circuit have been presented. After all these parts are assembled together, the prototype of the hybrid cycloconverter is completed as shown in Fig. 5.21. Experimental results will be presented in the next chapter.
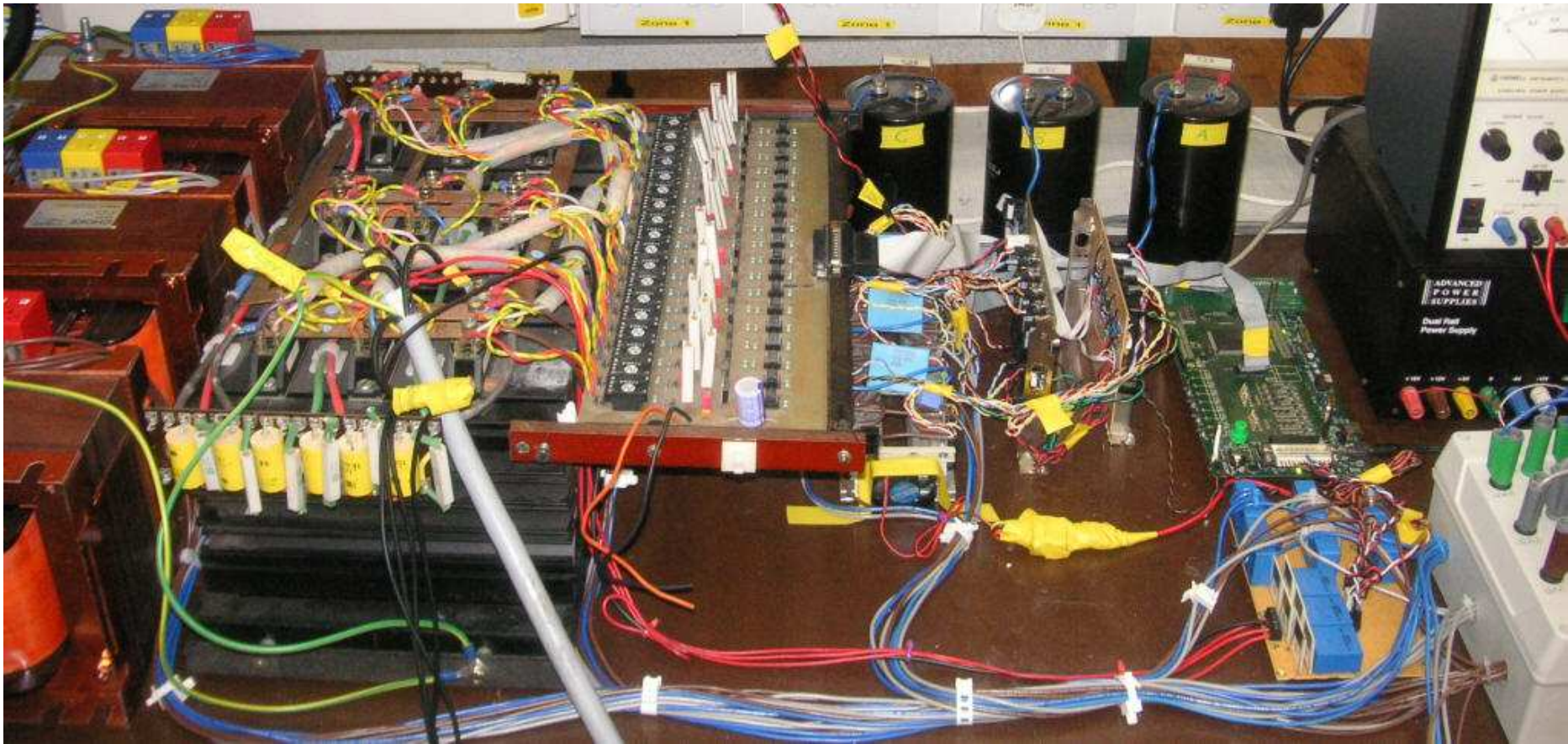
Fig. 5.21: Photograph of final hybrid cycloconverter prototype

Chapter 6

Experimental Results of the Prototype

6.1　Introduction

In Chapter 4, simulation results for both the standard and the hybrid cycloconverter in two operating modes, circulating current mode and circulating current-free mode, were presented. However, the operation of the proposed hybrid cycloconverter cannot just be verified by SABER as there are still some differences which cannot be ignored between the real experimental environment and the computer simulation environment. Therefore, a cycloconverter prototype was built as described in Chapter 5. In order to verify the hybrid cycloconverter performance both by simulation and experiment, the parameters used in the experimental setup and in the simulation model are identical. The value of each parameter is given in Table. 4.2 in Chapter 4. With those values, the estimated total output active power of the three-phase experimental prototype is around 2.1kW and the total input apparent power is up to 7kVA. The total loss in the circuit is up to 180W, depending on the topologies. For example, the standard cycloconverter in circulating current-free mode should have the highest effiency among all the cycloconverter topologies without considering the loss cuased by both the circulating current and the auxiliary inverter.

In this chapter, experimental results corresponding to most of the simulation results in Chapter 4 will be presented. The tools which were used to capture the experimental results are: the LeCroy WaveSurfer 424 oscilloscope, the LeCroy ADP300 voltage probes and the LeCroy CP150 current probes. To make it easier to compare these results with the simulation results, the structure of this chapter is similar to that of Chapter 4. Conclusions will be drawn at the end of this chapter to summarize the improvement of the hybrid cycloconverter over the standard cycloconverter.

6.2 Experimental Results of the Three-Phase Input to Single-Phase Output Standard Cycloconverter Prototype`

The experimental results of the standard cycloconverter in both the circulating current and the circulating current-free mode are presented in this section.

6.2.1 The Standard Cycloconverter Prototype in Circulating Current Mode

Fig. 6.1(a) and 6.1(b) show the output voltage waveforms generated by the positive and negative thyristor half bridge of the standard cycloconverter prototype. Similar to the simulation results, the low pass filtered components of these two output voltages have the same output frequency as well as the same phase shift. The spectrum of the above two thyristor half bridge output voltages are shown in Fig. 6.2(a) and 6.2(b), revealing that the fundamental components of both output voltages are the same ($225V_{pk}$ at 5Hz), and this matches very well with the results obtained in simulation as shown in Fig. 4.13(a) and 4.2(b). Furthermore, as the standard cycloconverter in the prototype is a 3-pulse topology and the input frequency is 50Hz, the harmonics of the output voltage of the thyristor half bridges are multiples of 150Hz, such as the 150Hz, 300Hz, 450Hz, as expected.

As the instantaneous output voltages between the positive and negative thyristor half bridge are not identical, a differential mode voltage between the two thyristor half bridges appears as shown in Fig. 6.3. Fig. 6.4 shows the spectrum of the differential mode voltage obtained from the prototype. The frequency characteristic of the experimental results is similar to the simulation results in Fig. 4.15, where the most significant harmonics are grouped in clusters around multiples of 150Hz, such as 150Hz, 300Hz, 450Hz. There is a 10Hz harmonic with about $25V_{pk}$ amplitude in the differential mode voltage of the prototype, which has also a similar level to the result obtained in the simulation. As the same reason described in Chapter 4, this 10Hz

harmonic is caused by the basic mechanism of the converter and can hardly be removed by modifications on the control method.
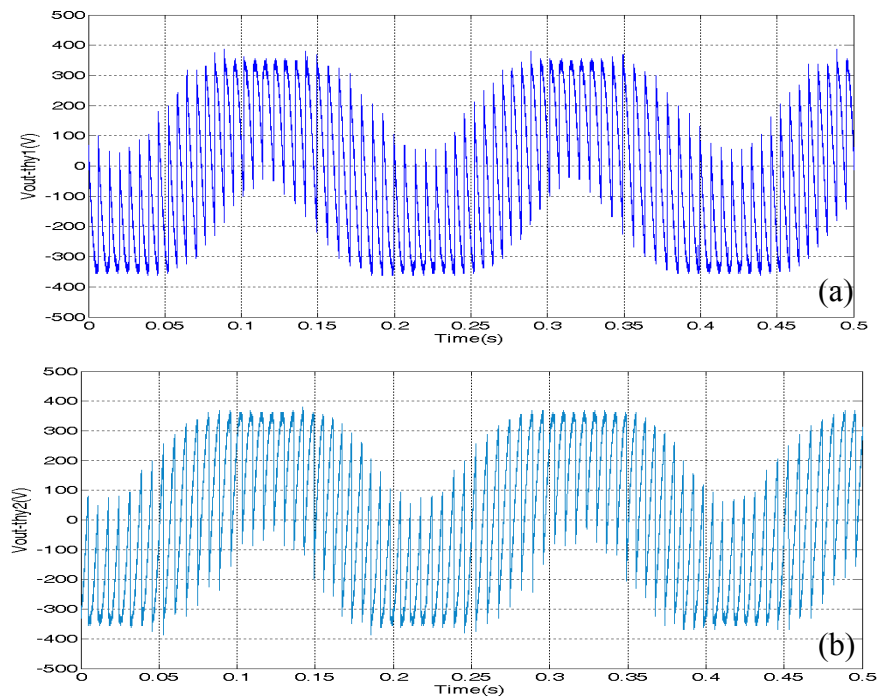
Fig. 6.1: Output voltage waveform generated by a) the positive and b) the negative thyristor half bridge of the prototype in CCM
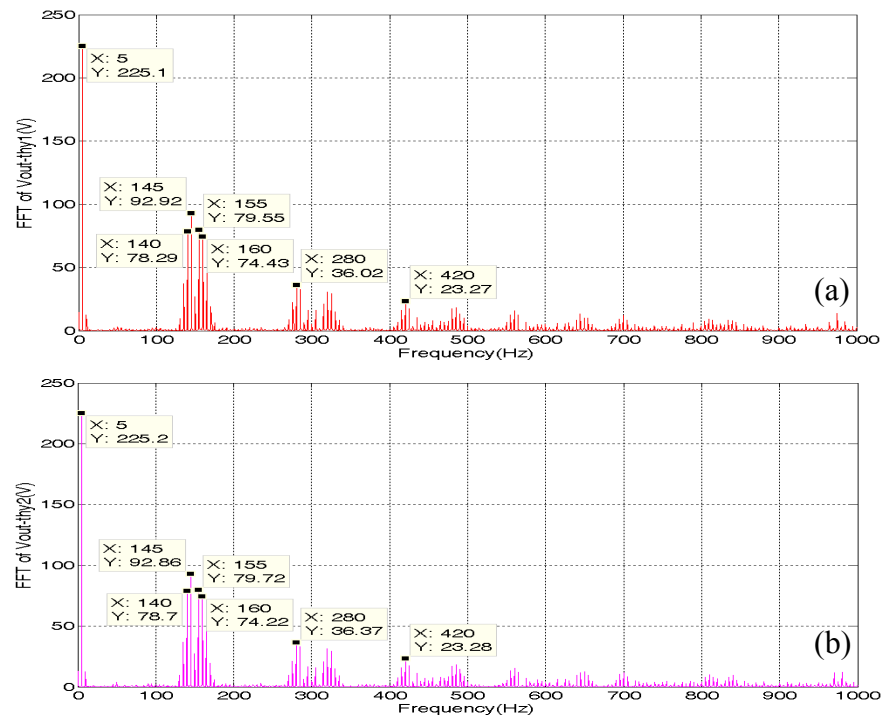
Fig. 6.2: Spectrum of the output voltage generated by a) the positive and b) the negative thyristor half bridge of the prototype in CCM
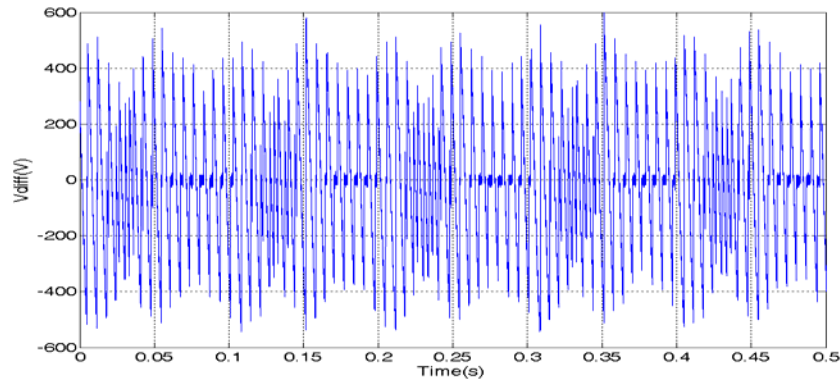
Fig. 6.3: Differential mode voltage waveform seen between the two thyristor half
bridge outputs of the prototype in CCM
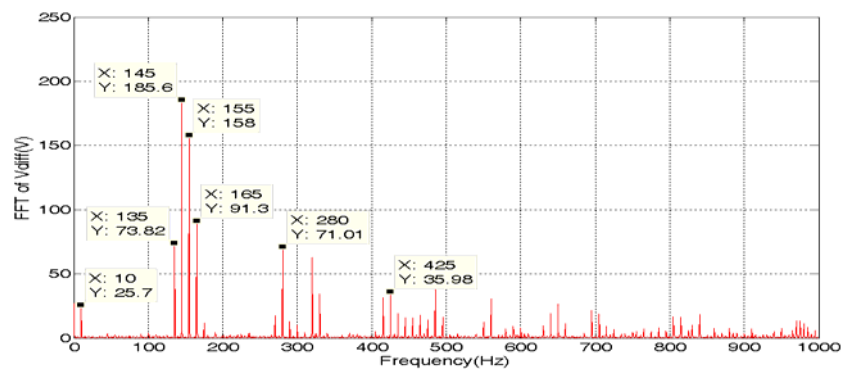
Fig. 6.4: Spectrum of the differential mode voltage seen between the two thyristor half
bridge outputs of the prototype in CCM

Fig. 6.5 shows the circulating current waveform of the standard cycloconverter prototype. Although the mutual inductance of the two circulating current reactors is very large (around 400mH), the circulating current waveform still contains very low frequency harmonics and even a DC component due to the large amount of low frequency harmonics present in the differential mode voltage previously mentioned. The spectrum of the circulating current waveform is shown in Fig. 6.6, which contains not only a DC component (1.6A), but also some low frequency harmonics such as $0.96A_{pk}$ at 10Hz, $0.56A_{pk}$ at 145Hz, $0.44A_{pk}$ at 155Hz. The amplitudes of the DC component and also the 10Hz harmonic in the experimental results are a bit smaller than those in simulation, which is probably caused by a larger impedance of the circulating current reactor and its associated circuit loop. However, as has been mentioned in Chapter 4, the DC component and the 10Hz harmonic are the disadvantage of limiting the circulating current using a reactor since the size of the reactor may become very large to achieve the desired results.
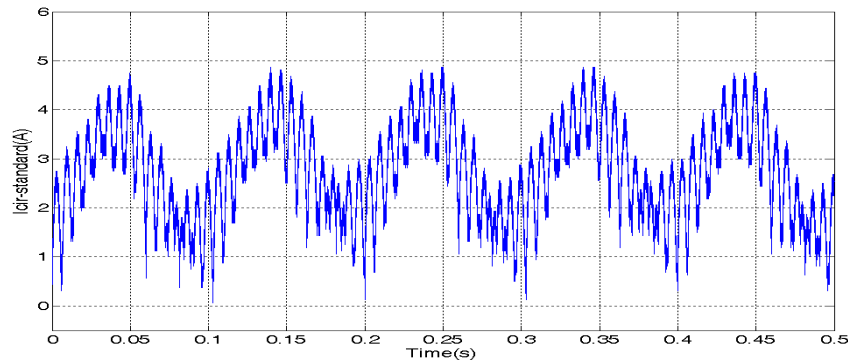
Fig. 6.5: Circulating current waveform of the standard cycloconverter prototype in CCM
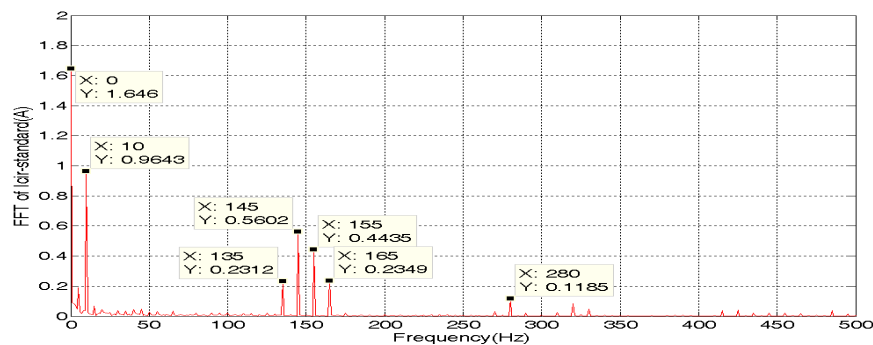
Fig. 6.6: Spectrum of the circulating current of the standard cycloconverter prototype in CCM

As the output of the standard cycloconverter operating in circulating current mode is the mid-point of the two coupled circulating current reactors, the phase-to-supply neutral output voltage is the average of the two thyristor half bridge output voltages. This output voltage is also known as the common mode voltage which needs to be improved by the auxiliary inverter. The experimental waveform of the standard cycloconverter is shown in Fig. 6.7 which is very similar to the simulation result shown in Fig. 4.18. The spectrum of the phase-to-supply neutral output voltage obtained from the prototype is shown in Fig. 6.8, from which it can be seen that some major harmonics which are anti-phase between two thyristor half bridge outputs, such as the 145Hz and 155Hz, have been cancelled at the mid-point when compared to Fig. 6.2 whilst the fundamental component (221V_{pk} at 5Hz) and some other harmonics that are in phase such as the 140Hz, 160Hz, remain almost the same as the output of the thyristor bridges. Therefore, as indicated by the simulation results, the output voltage of the standard cycloconverter prototype is able to achieve better harmonic performance than the output voltage of each thyristor half bridge.
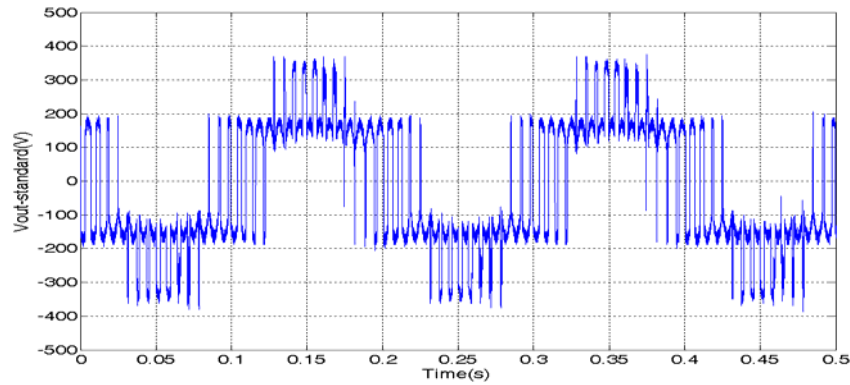
Fig. 6.7: Phase-to-supply neutral output voltage waveform of the standard cycloconverter prototype in CCM
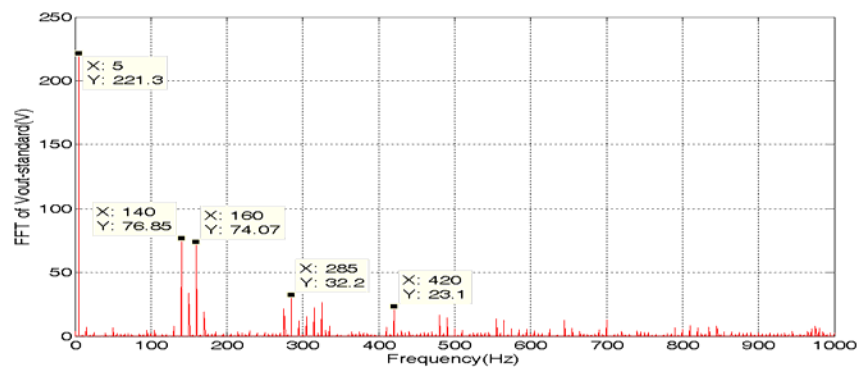
Fig. 6.8: Spectrum of the phase-to-supply neutral output voltage of the standard cycloconverter prototype in CCM

The load current waveform of the standard cycloconverter shown in Fig. 6.9 is similar to the simulated waveform in Fig. 4.20. For the same reason mentioned for the simulation result, the typical highly inductive load, the harmonics present in the output voltage will have a smaller impact on the corresponding load current especially when the order of the harmonics is high.
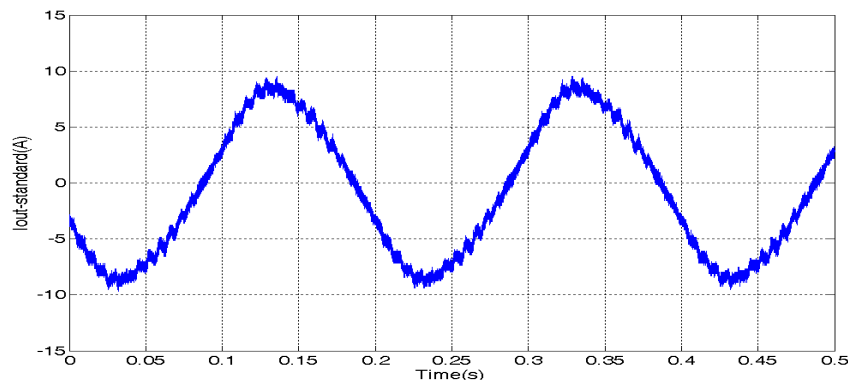
Fig. 6.9: Load current waveform of the standard cycloconverter prototype in CCM

6.2.2 The Standard Cycloconverter Prototype in Circulating Current-Free Mode

By altering the connections on the switch box mentioned in Chapter 5, it is easy to change the standard cycloconverter prototype from the circulating current mode topology to the circulating current-free mode topology, where the output of the positive and negative half bridges are connected directly without any inductors connected between them. The control method applied in the prototype is the same as has been used in the simulation as described in Chapter 4 so as to ensure safe commutation between the two thyristor bridges without causing a short circuit between any two input power lines or any over-voltage due to the disconnection of the load current.

Fig. 6.10 shows the phase-to-supply neutral output voltage generated by the standard cycloconverter prototype which compares well with the waveform obtained by simulation as shown in Fig. 4.21. From this output voltage waveform it can be seen that there is no obvious over-voltage or short circuit occurring during the instant of the commutation since the segment that appears twice per period on the waveform due to the commutation between the two thyristor half bridges shows no undesirable behaviour. This demonstrates that it is feasible to apply the control method designed for the simulation model to the real circuit. From the spectrum of the phase-to-supply neutral output voltage of the standard cycloconverter prototype shown in Fig. 6.11, it can be noted that the value of the 5Hz fundamental component is $216V_{pk}$ which is similar to that obtained in simulation. The majority of the harmonics, such as the $108V_{pk}$ at 140Hz, $101V_{pk}$ at 150Hz, $45V_{pk}$ at 285Hz, occur in clusters centered on multiples of 150Hz as expected.

Fig. 6.12 shows the waveform of the load current of the standard cycloconverter prototype. Since the load is highly inductive, the load current is predominately sinusoidal despite the important voltage distortion although it is not difficult to perceive the extra ripple superimposed on the fundamental component of the current due to the worse distortion of the output voltage compared to the circulating current mode.

Fig. 6.10: Phase-to-supply neutral output voltage waveform of the standard cycloconverter prototype in CCFM
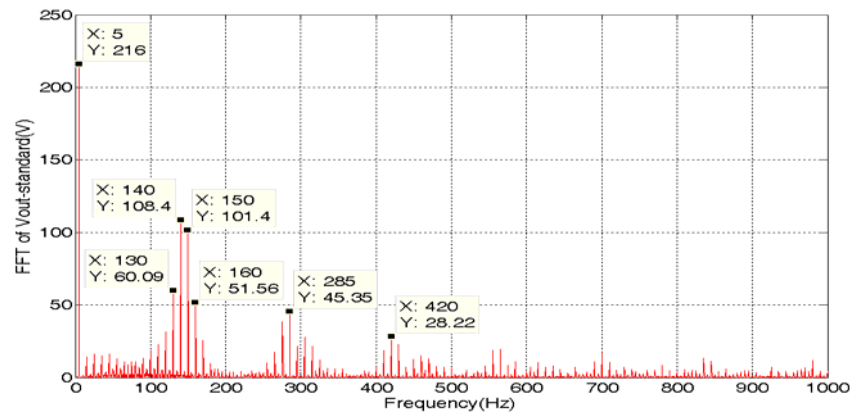
Fig. 6.11: Spectrum of the phase-to-supply neutral output voltage of the standard cycloconverter prototype in CCFM

Fig. 6.12: Load current waveform of the standard cycloconverte prototype in CCFM

6.3 Experimental Results of the Three-Phase Input to Single-Phase Output Hybrid Cycloconverter Prototype

In this section, all the relevant waveforms and their corresponding spectra for both circulating current and circulating current-free mode with the hybrid topology will be presented.

6.3.1 The Hybrid Cycloconverter Prototype in Circulating Current Mode

In order to improve the input displacement power factor, the circulating current in the standard cycloconverter needs to be controlled by the auxiliary inverter by reducing the low order harmonics present in the differential mode voltage. As already mentioned in Chapter 4, the choice for the DC-link capacitor voltage is a result of a compromise between cost and performance. Therefore, as explained in Chapter 4, the following results are only obtained for the case of 295V DC-link capacitor voltage across the auxiliary inverter. Moreover, as also was explained in Chapter 4, in order to ensure that the duty cycle of the zero switching state used to improve the common mode voltage is always above zero, the PI controller of the circulating current is only designed to eliminate the 10Hz harmonic of the differential mode voltage. Hence, the reduction of the 150Hz and other higher frequency harmonics depends solely on the feedforward of the differential mode voltage.

Fig. 6.13 shows the circulating current waveform with a fast PI controller. Compared with the circulating current generated by the standard cycloconverter prototype shown in Fig. 6.5, the circulating current waveform in the hybrid cycloconverter is also much improved although the voltage rating and the installed power is reduced by 50% from what is expected in auxiliary inverter, with only around 1A peak-to-peak ripple superposed on the a DC component. The spectrum of the circulating current shown in Fig. 6.14 further verifies the improvement of the circulating current since the DC

component is controlled to around 1.5A and other low frequency harmonics are obviously reduced compared with Fig. 6.6.
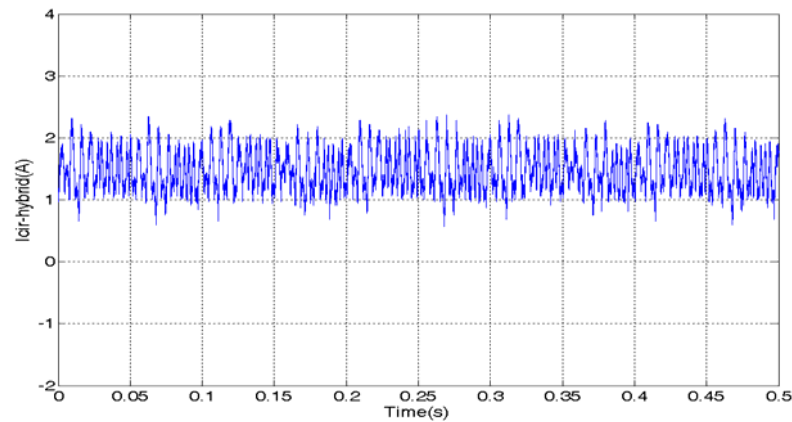
Fig. 6.13: Circulating current waveform of the hybrid cycloconverter prototype when using a fast PI controller and reduced DC-link capacitor voltage in CCM
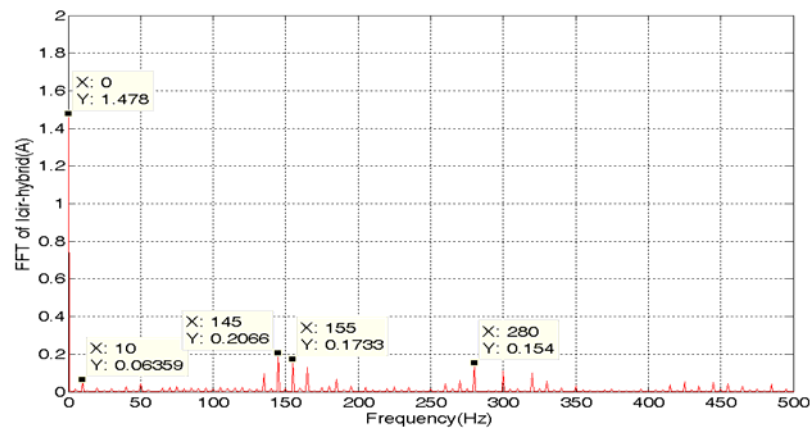
Fig. 6.14: Spectrum of the circulating current of the hybrid cycloconverter prototype when using a fast PI controller and reduced DC-link capacitor voltage in CCM

Fig. 6.15 shows the circulating current waveform with a slower PI controller. Although this circulating current waveform is not as good as the one shown in Fig. 6.13, it is still maintained around the 1.5A set-point with also apparently reduced ripple compared with the circulating current waveform of the standard cycloconverter shown in Fig. 6.5. The spectrum of this circulating current shown in Fig. 6.16 further validates the improvement over the circulating current in Fig. 6.5, where the 10Hz harmonic has been reduced by 2/3 and the 145Hz and 155Hz harmonics have been reduced by more than half of the original.
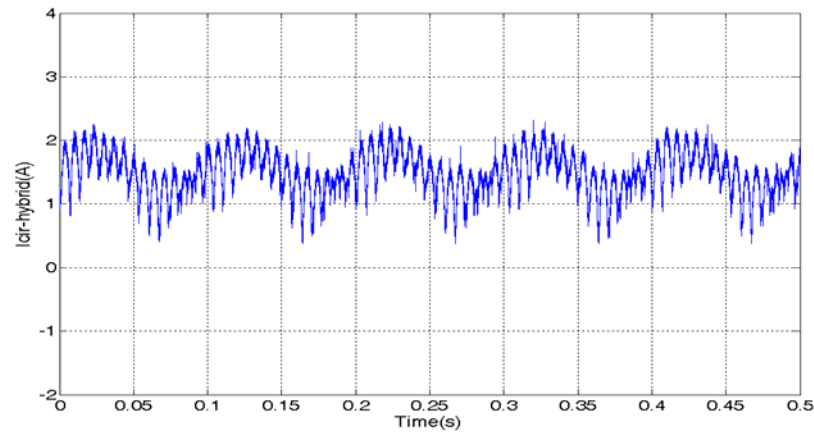
Fig. 6.15: Circulating current waveform of the hybrid cycloconverter prototype when using a slow PI controller and reduced DC-link capacitor voltage in CCM
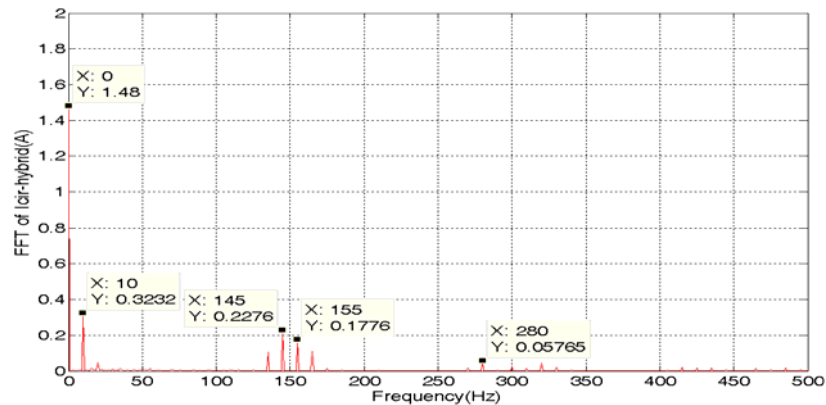
Fig. 6.16: Spectrum of the circulating current of the hybrid cycloconverter prototype when using a slow PI controller and reduced DC-link capacitor voltage in CCM

Fig. 6.17 shows the phase-to-supply neutral output voltage of the hybrid cycloconverter prototype in circulating current mode. Similar to the simulation result, the output voltage is modulated by a 5kHz PWM common mode voltage injected by the auxiliary inverter in order to compensate the difference between the actual output voltage of the standard cycloconverter and its reference. Fig. 6.18(a) shows that the harmonics between 0-25kHz of the hybrid cycloconverter phase-to-supply neutral output voltage occur in clusters around multiples of 5kHz, which is the switching frequency of the auxiliary inverter. Also it can be seen from the low frequency (0-1kHz) spectrum of the output voltage, as shown in Fig. 6.18(b), that the low order harmonics of the output voltage have been significantly reduced, such as from $76V_{pk}$ to $19V_{pk}$ at 140Hz, from $74V_{pk}$ to $20V_{pk}$ at 160Hz. This obvious improvement in the

results from the prototype validates the beneficial effect of the auxiliary inverter identified in the simulation study.
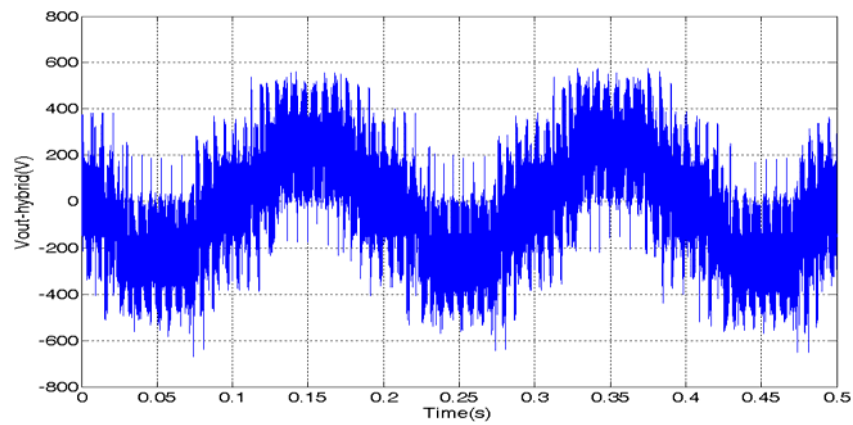
Fig. 6.17: Phase-to-supply neutral output voltage waveform of the hybrid cycloconverter prototype when using a slow PI controller and reduced DC-link capacitor voltage in CCM
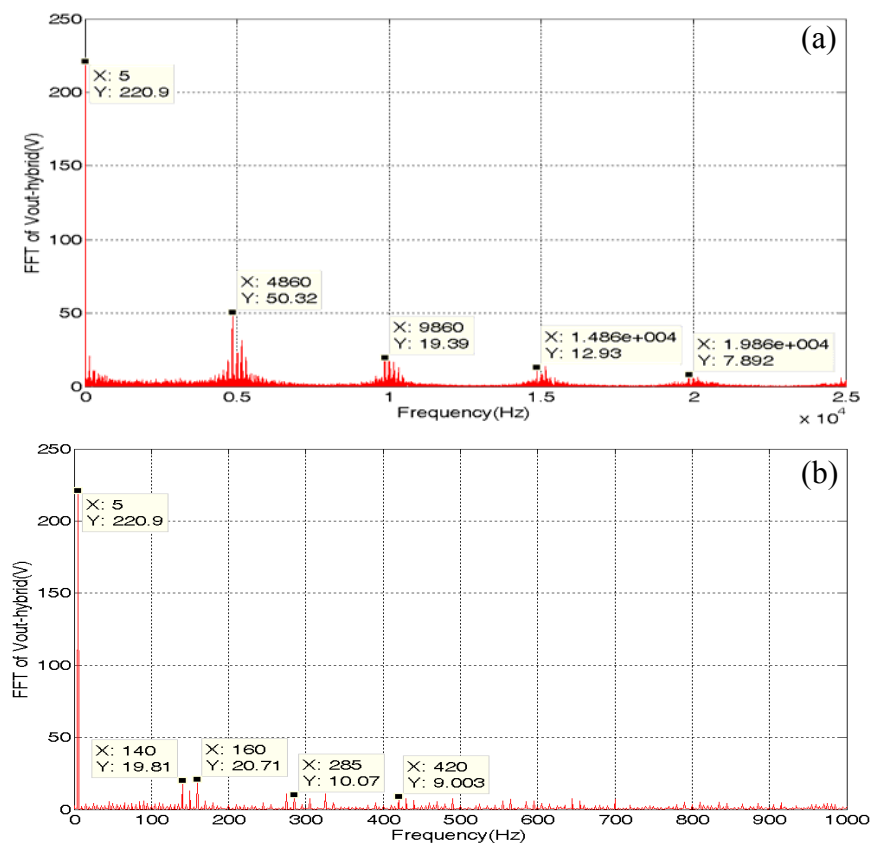
Fig. 6.18: Spectrum of the phase-to-supply neutral output voltage of the hybrid cycloconverter prototype when using a fast PI controller and reduced DC-link capacitor voltage in CCM: a) 0-25kHz spectrum b) 0-1kHz spectrum

Fig. 6.17 shows the load current waveform of the hybrid cycloconverter prototype. Although the load is highly inductive, it can be seen that the load current is improved compared to the waveform generated by the standard cycloconverter shown in Fig. 6.9.
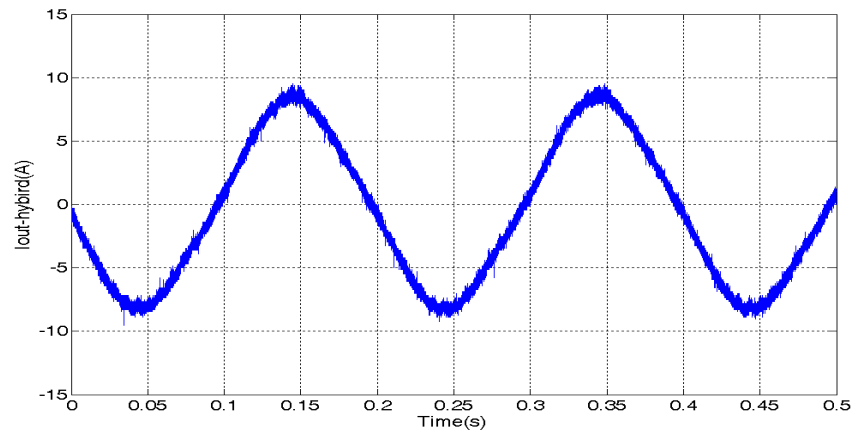
Fig. 6.19: Load current waveform of the hybrid cycloconverter prototype when using a slow PI controller and reduced DC-link capacitor voltage in CCM

Fig. 6.20(a) and (b) show the voltages injected by the auxiliary inverter between each of the asymmetric legs and the middle leg. As was explained in Chapter 3, the voltage injected by the auxiliary inverter is used to reduce the low frequency harmonics present in both the differential mode voltage as well as the common mode voltage. As when the simulation results were presented, each figure shows not only the high frequency PWM injected voltage but also the corresponding low-pass filtered components. Furthermore, the amplitude of the injected voltage, which is around 295V, is also equal to the level of the DC-link capacitor voltage. This means that the DC-link capacitor voltage has been fully utilized to exploit the hybrid cycloconverter. Fig. 6.21(a) and (b) show the spectrum of the two voltages injected by the auxiliary inverter. As expected from the simulation, the spectra of both voltages are clustered around multiples of 150Hz, corresponding to the frequencies of the harmonics in both the common mode and differential mode voltage.
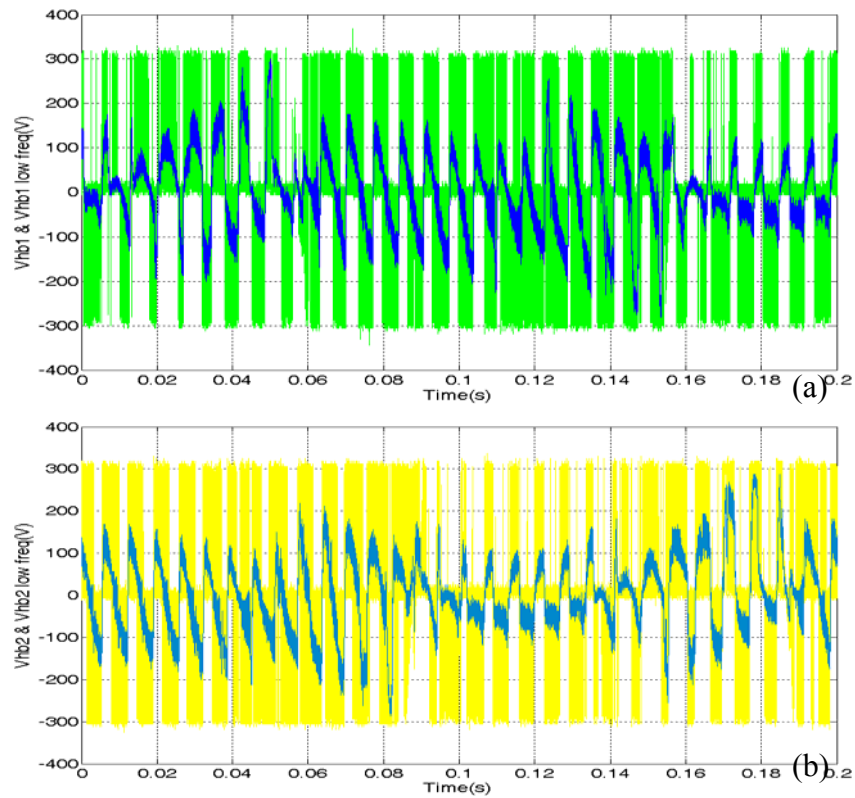
Fig. 6.20: PWM voltage and the corresponding low-pass filtered component injected by the auxiliary inverter in CCM: the voltage between the a) left b) right asymmetric leg and the full leg.
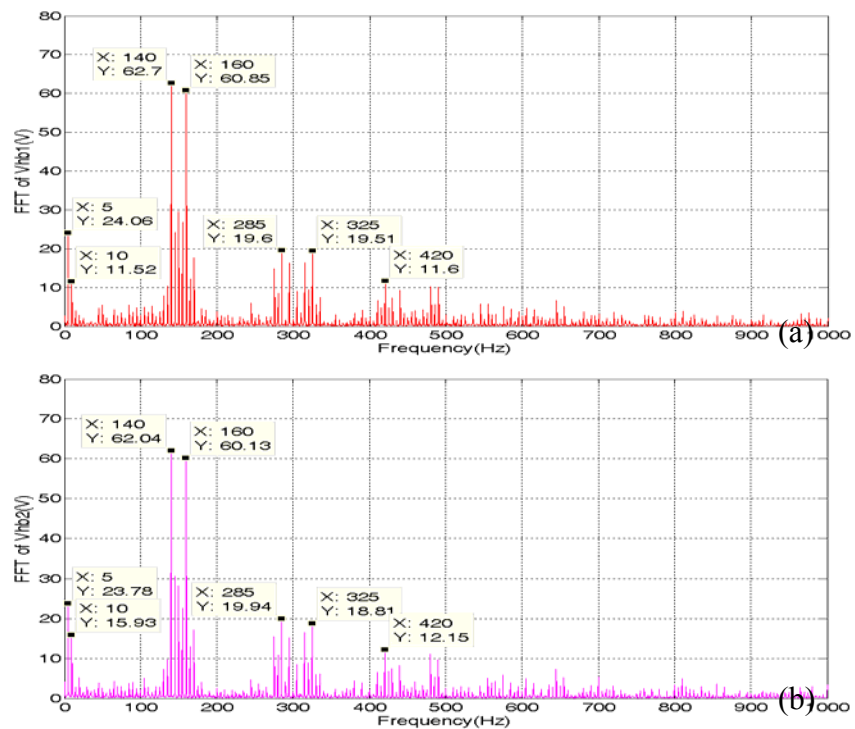
Fig. 6.21: Spectrum of the PWM voltage injected by the auxiliary inverter in CCM: the voltage between the a) left b) right asymmetric leg and the full leg.

6.3.2 The Hybrid Cycloconverter Prototype in Circulating Current-Free Mode

Similar to Chapter 4, the study in this subsection for the circulating current-free mode starts with the load side performance. Fig. 6.22 shows the phase-to-supply neutral output voltage waveform of the hybrid cycloconverter prototype in circulating current-free mode. In the prototype, the output voltage is improved by injecting a high frequency PWM common mode voltage by using the auxiliary inverter to cancel the low order harmonics contained in output voltage. The spectrum of the phase-to-supply neutral output voltage of the prototype is shown in Fig. 6.23. Compared with the spectrum of the standard cycloconverter prototype as shown in Fig. 6.11, it is apparent that the harmonics around 150Hz, 300Hz, 450Hz, have all been reduced. For example, the 140Hz and 150Hz harmonics are reduced respectively from $108V_{pk}$ to only $10.3V_{pk}$ and from $101V_{pk}$ to only $27.5V_{pk}$, whereas the 130Hz, 160Hz, and other frequencies have been reduced to a negligible level. The improvement in the hybrid cycloconverter prototype validates again the compensation effect of the auxiliary inverter as expected from the simulation results, although the prototype has not eliminated the harmonics completely as demonstrated by simulation results, which may be caused by the slight over-modulation of the auxiliary inverter. The improvement is also verified by the load current waveform shown in Fig. 6.24, where there is no obvious ripple superimposed on the fundamental component.
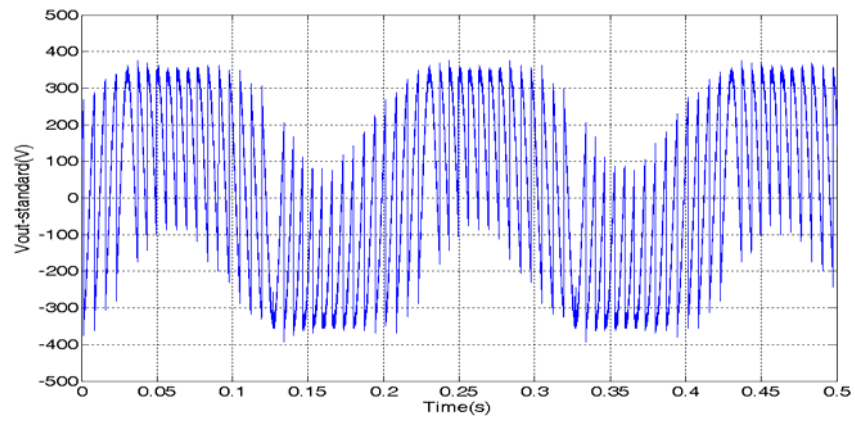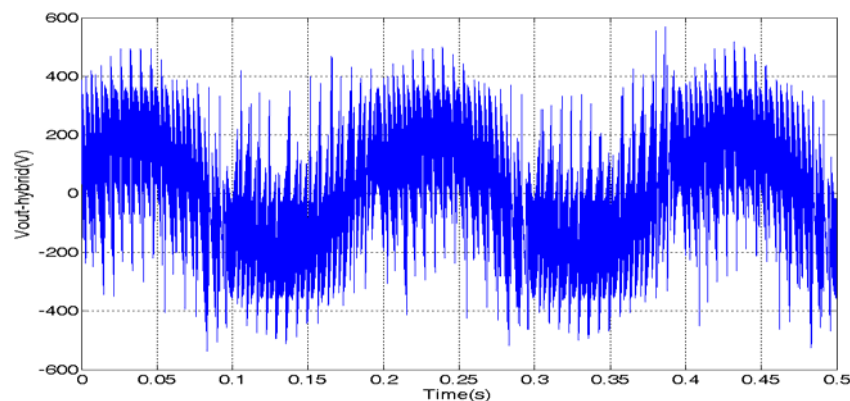

Fig. 6.22: Phase-to-supply neutral output voltage waveform of the hybrid cycloconverter prototype in CCFM
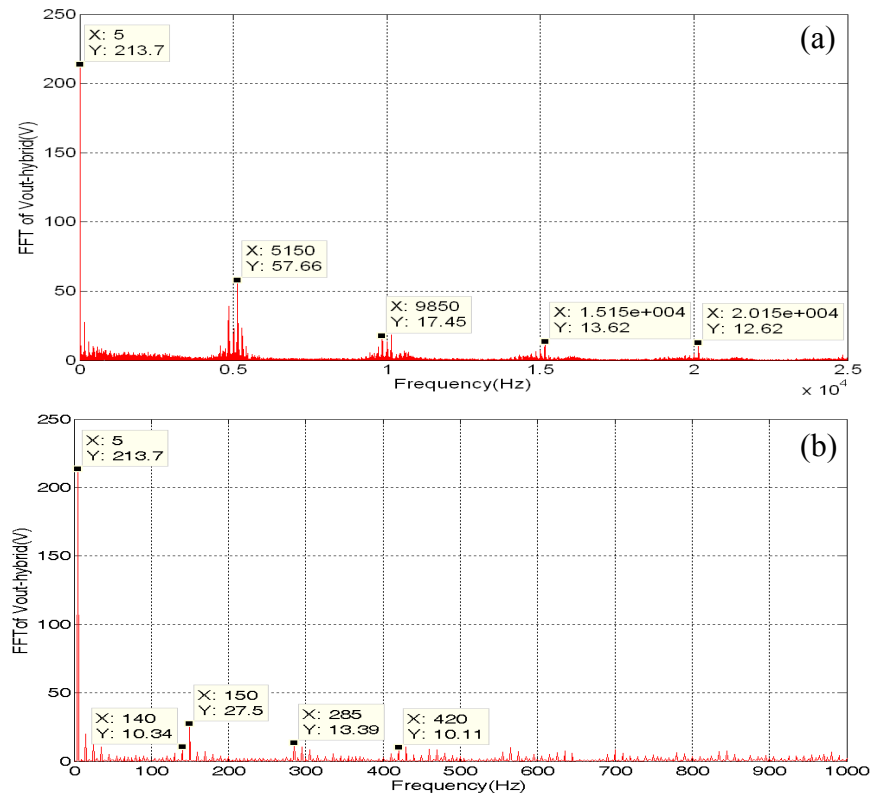
Fig. 6.23: Spectrum of the phase-to-supply neutral output voltage of the hybrid
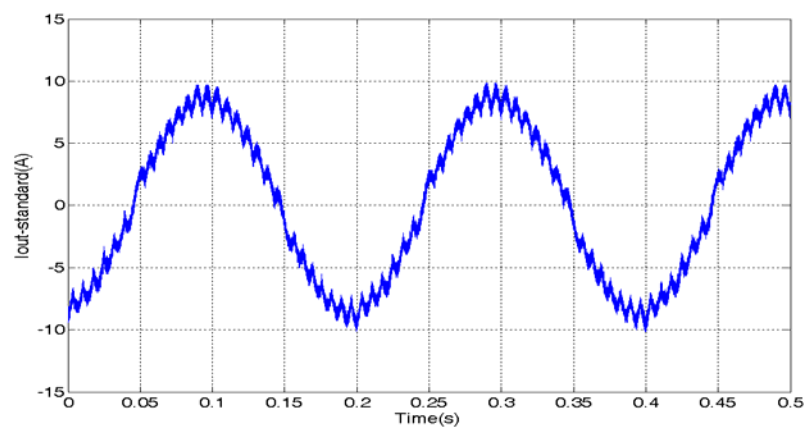cycloconverter prototype in CCFM: a) 0-25kHz range b) 0-1kHz range
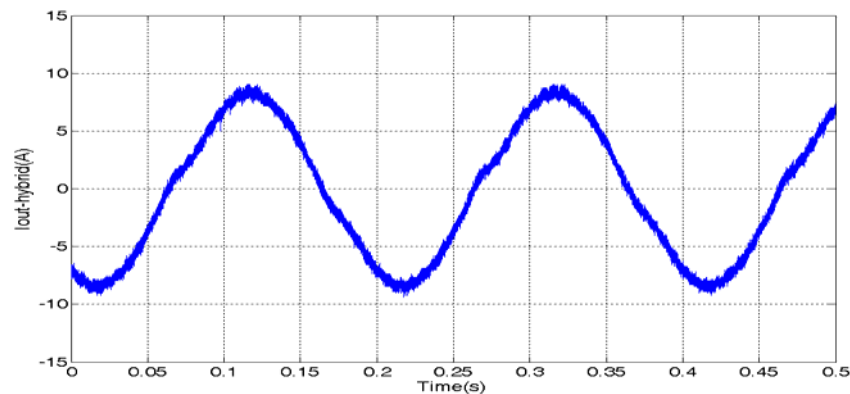
Fig. 6.24: Load current waveform of the hybrid cycloconverter prototype in CCFM

The voltage waveforms shown in Fig. 6.25 are the common mode voltage and its
low-pass filtered equivalent injected by the auxiliary inverter to cancel the harmonics
present in the output voltage of the standard cycloconverter prototype. The result is
very similar to the waveform obtained from the simulation as shown in Fig. 4.43,
although from the waveform of the low-pass filtered component it seems like a slight
over-modulation occurs, which is not as good as that in the simulation results. The
DC-link capacitor voltage in the auxiliary inverter is again at the same level as the

amplitude of the voltage injected, which for this situation is around 295V. The spectrum of the injected voltage shown in Fig. 6.26 is also very similar to the spectrum obtained in simulation. As this voltage is used to cancel the output voltage harmonics generated by the standard cycloconverter prototype, the spectrum distribution of this voltage is similar to the spectrum shown in Fig. 6.11 except for the fundamental component.
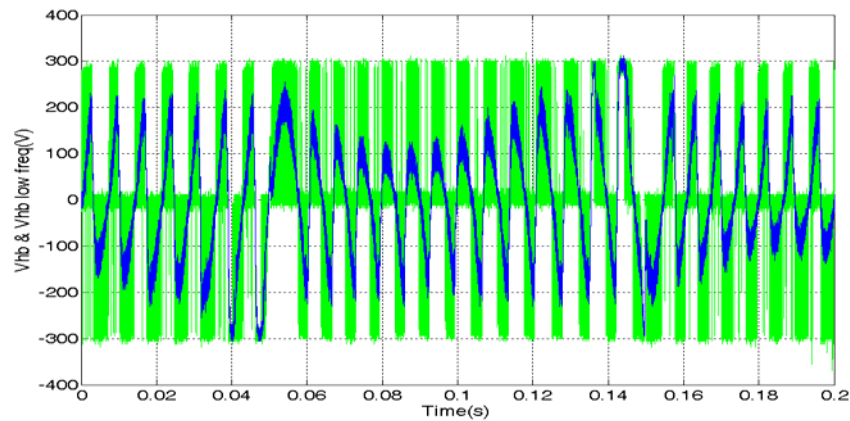
Fig. 6.25: PWM voltage waveform and the corresponding low-pass filtered component injected by the auxiliary inverter in CCFM
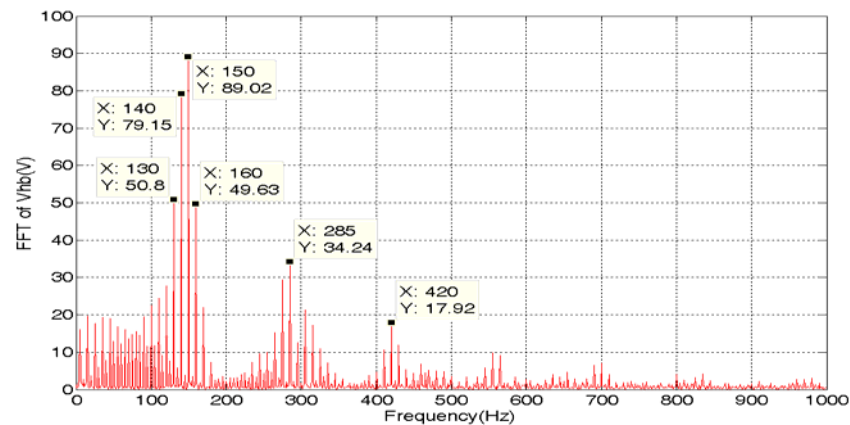
Fig. 6.26: Spectrum of the PWM voltage injected by the auxiliary inverter in CCFM

6.4   Experimental Results of the Three-Phase Input to Three-Phase Output Cycloconverter Prototype

In this section the experimental results related to the three-phase input to three-phase output cycloconverter prototype are presented. The waveforms of the line-to-line

output voltage, the load current and the input current of the three-phase output system are presented and analyzed in the same sequence as that in Chapter 4.

6.4.1 The Line-to-Line Output Voltage Evaluation of the Prototype

Fig. 6.27 shows the line-to-line output voltage waveform of the standard cycloconverter prototype in circulating current mode. Similar to the simulation result, the line-to-line output voltage a 5-level voltage waveform. From the spectrum of the voltage waveform shown in Fig. 6.28 it can be seen that, compared with the spectrum of the phase-to-supply neutral output voltage shown in Fig. 6.8, some harmonics such as the 150Hz, 285Hz, 420Hz, have been almost eliminated, whilst the amplitude of the 5Hz fundamental component and other harmonics still remain approximately 1.7 times of the corresponding harmonics present in phase-to-supply neutral output voltage, as expected. The reason for this harmonic cancelation/reduction in the line-to-line voltage waveform compared with the phase-to-supply neutral output voltage has already been discussed in Chapter 4. Also, in agreement with the simulation results, the reduction/cancelation of certain harmonics in line-to-line output voltage, such as the 150Hz, 285Hz, 420Hz, occurs in the other situations studied as well. This characteristic is helpful to not only obtaining a better load current waveform, but also in further reducing the DC-link capacitor voltage if only the performance of the line-to-line output voltage is taken into consideration.

Fig. 6.27: Line-to-line output voltage waveform of the three-phase to three-phase standard cycloconverter prototype in CCM
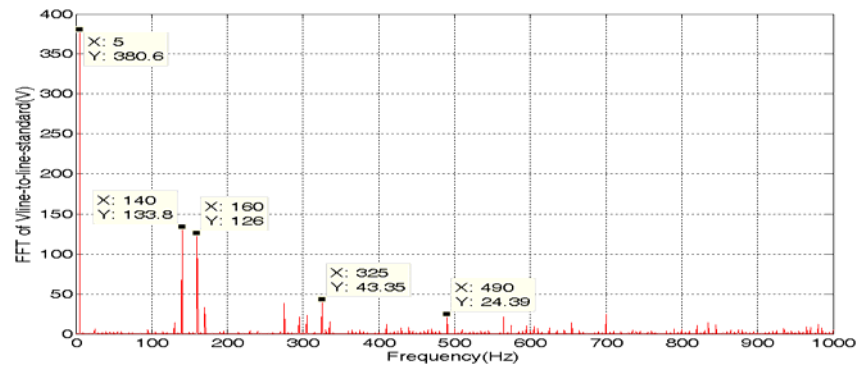
Fig. 6.28: Spectrum of the line-to-line output voltage of the three-phase to three-phase standard cycloconverter prototype in CCM

The line-to-line output voltage waveform of the hybrid cycloconverter prototype in circulating current mode is shown in Fig. 6.29. Fig. 6.30(a) shows the wide frequency spectrum of the line-to-line voltage and illustrates the significant high frequency voltage harmonics present around multiples of the 5kHz switching frequency, just like the phase-to-supply neutral output voltage of the hybrid cycloconverter. Compared with the spectrum of the line-to-line output voltage generated by the standard cycloconverter shown in Fig. 6.28, the significant low frequency harmonics have all been significantly reduced by the hybrid cycloconverter, such as from $133V_{pk}$ to $33V_{pk}$ at 140Hz or from $126V_{pk}$ to $34V_{pk}$ at 160Hz, as shown in Fig. 6.30(b). Moreover, similar to the line-to-line output voltage of the standard cycloconverter prototype, some harmonics, such as the 150Hz, 285Hz, 420Hz, are in phase and completely cancelled in the line-to-line output voltage of the hybrid cycloconverter prototype, as shown in Fig. 6.30(b).

Fig. 6.29: Line-to-line output voltage waveform of the three-phase to three-phase hybrid cycloconverter prototype in CCM
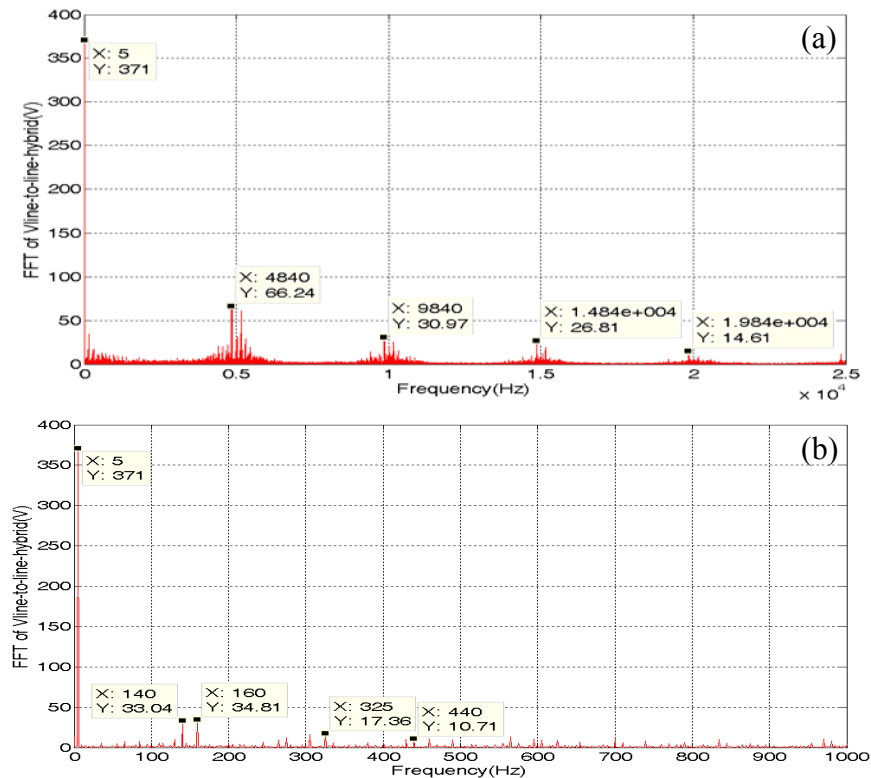
Fig. 6.30: Spectrum of the line-to-line output voltage of the three-phase to three-phase hybrid cycloconverter prototype in CCM: a) 0-25kHz range b) 0-1kHz range

Fig. 6.31 shows the line-to-line voltage waveform of the standard cycloconverter prototype in circulating current-free mode. Again, compared with the corresponding phase-to-supply neutral output voltage as shown in Fig. 6.22, some harmonics which are in phase have cancelled in the line-to-line output, as shown in Fig. 6.32, whilst other harmonic components have increased by the $\sqrt{3}$ ratio, as expected.
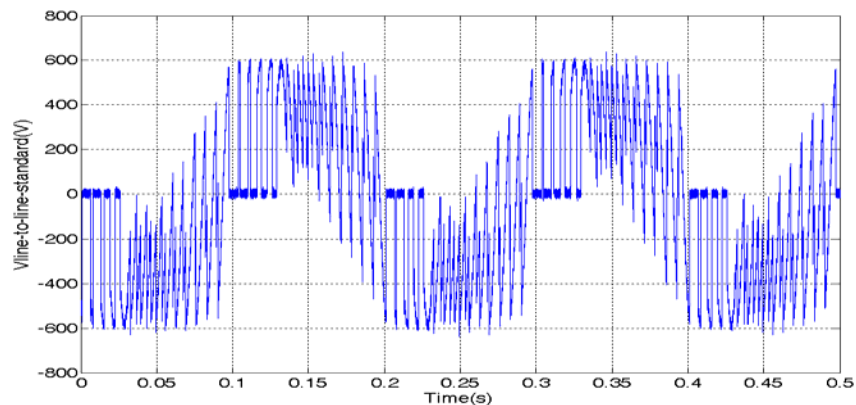
Fig. 6.31: Line-to-line output voltage waveform of the three-phase to three-phase standard cycloconverter prototype in CCFM
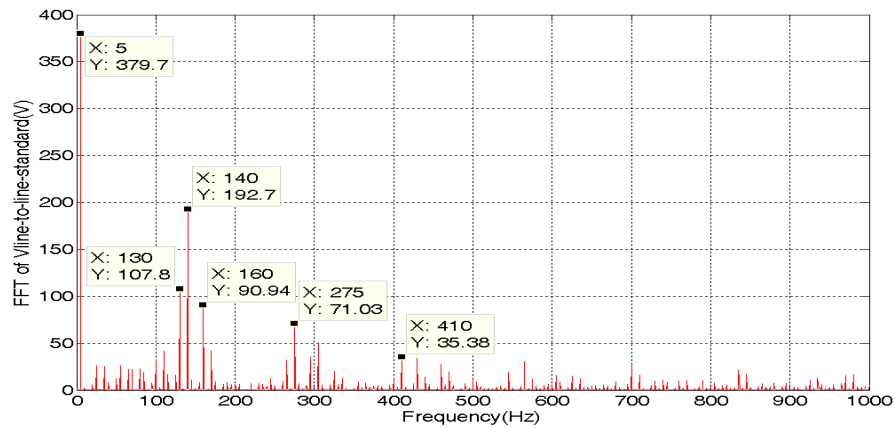
Fig. 6.32: Spectrum of the line-to-line output voltage of the three-phase to three-phase standard cycloconverter prototype in CCFM

The line-to-line output voltage waveform and its spectrum of the hybrid cycloconverter prototype in circulating current-free mode, as shown in Fig. 6.33 and 6.34, have the same characteristics mentioned above for the other three situations. Compared with the spectrum of the line-to-line output voltage of the standard cycloconverter shown in Fig. 6.32, all the low frequency harmonics are drastically reduced, such as from $192V_{pk}$ to $21V_{pk}$ at 140Hz or from $90V_{pk}$ to $17V_{pk}$ at 160Hz, as shown in Fig. 6.34(b)..
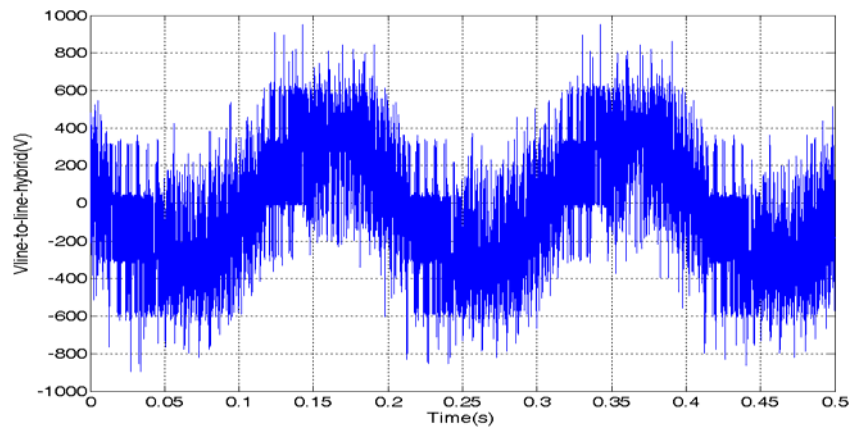
Fig. 6.33: Line-to-line output voltage waveform of the three-phase to three-phase hybrid cycloconverter prototype in CCFM
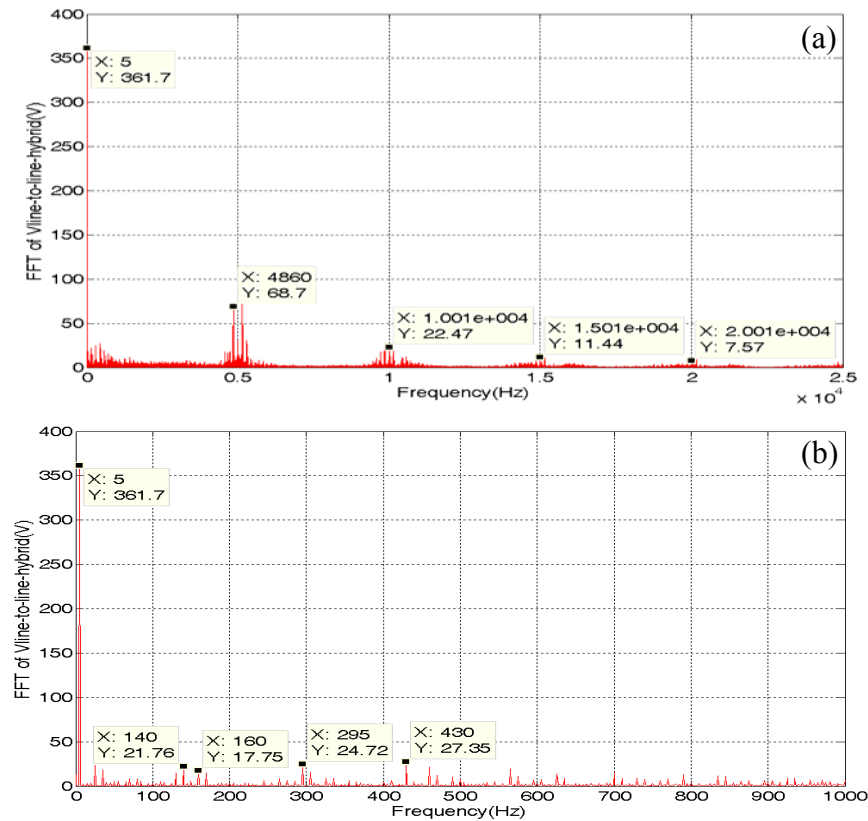
Fig. 6.34: Spectrum of the line-to-line output voltage of the three-phase to three-phase hybrid cycloconverter prototype in CCFM: a) 0-25kHz range b) 0-1kHz range

6.4.2 Three-Phase Load Current Evaluation of the Prototype

Fig. 6.35 to Fig. 6.38 present the load current waveforms of the three-phase input to three-phase output standard and hybrid cycloconverter prototype in both the circulating current and circulating current-free mode. As expected, the three-phase load currents are 120° phase displaced with respect to each other and are reasonably balanced waveforms, although there is some noise on the waveforms due to the high frequency switching operation of the IGBTs, especially on the output current waveforms of the hybrid topologies.
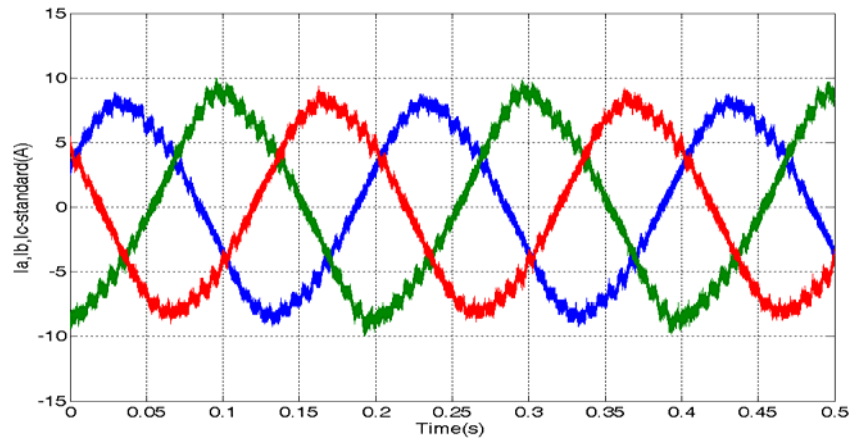
Fig. 6.35: Load currents waveform of the three-phase to three-phase standard
cycloconverter prototype in CCM
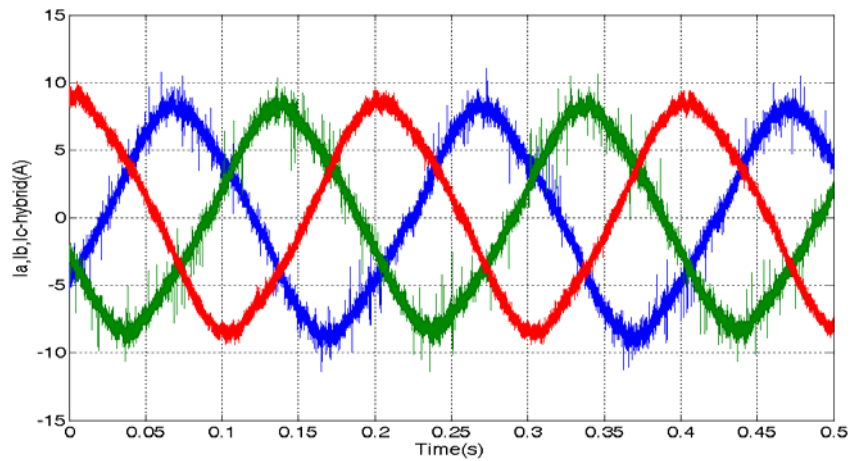
Fig. 6.36: Load currents waveform of the three-phase to three-phase hybrid
cycloconverter prototype in CCM
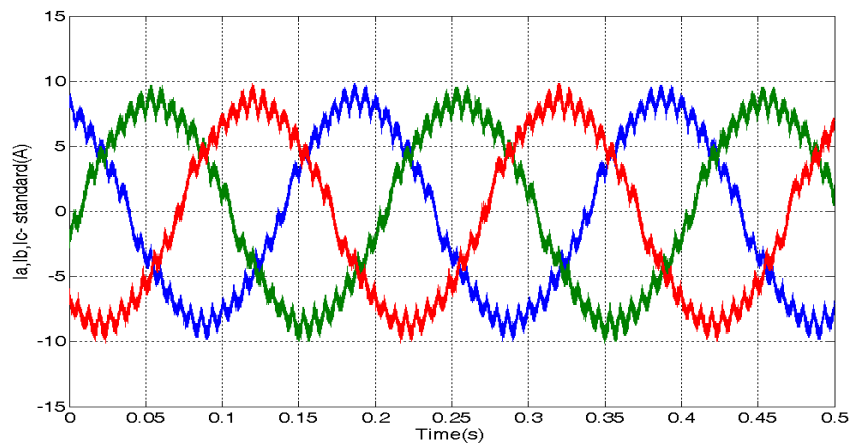
Fig. 6.37: Load currents waveform of the three-phase to three-phase standard
cycloconverter prototype in CCFM
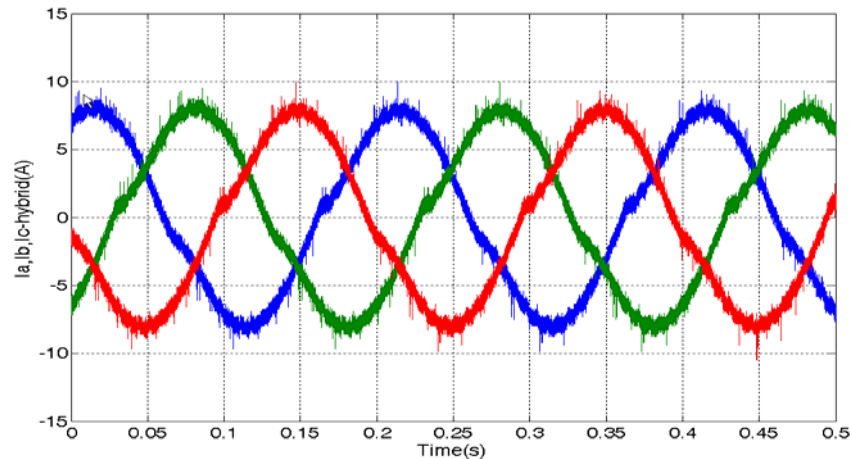
Fig. 6.38: Load currents waveform of the three-phase to three-phase hybrid
cycloconverter prototype in CCFM

6.4.3 The Input Current Evaluation of the Prototype

As mentioned in Chapter 4, the input side quality primarily depends on the pulse number of the cycloconverter, the load side performance as well as how large the circulating current is. If, similar to the simulation model, a highly inductive load is connected to the output of the prototype, and all the prototyped topologies are 3-pulse cycloconverter (or 6-pulse in CCM, but with the same number of thyristors in each half bridge), the circulating current will be the most important factor in determining the input power quality. The relevant power quality measures which are determined for the input side evaluation of the prototype are presented in Table. 6.3. The displacement power factors displayed in Table. 6.3 are all calculated by assuming that the output active power is equal to the input active power without taking any power losses of the prototype into consideration. This is why the displacement power factors of the prototype are slightly smaller than those found in the simulation results.

Fig. 6.39 shows the input current waveform of the standard cycloconverter prototype in circulating current mode. As seen from the spectrum of the input current waveform shown in Fig. 6.40, the amplitude of the fundamental component (50Hz) is around $13A_{pk}$, which is a bit smaller than the value obtained in simulation and all other significant harmonics, inter-harmonics or even sub-harmonics, such as the 85Hz, 115Hz, 185Hz, 250Hz, have more or less the same amplitude as in the simulation results.
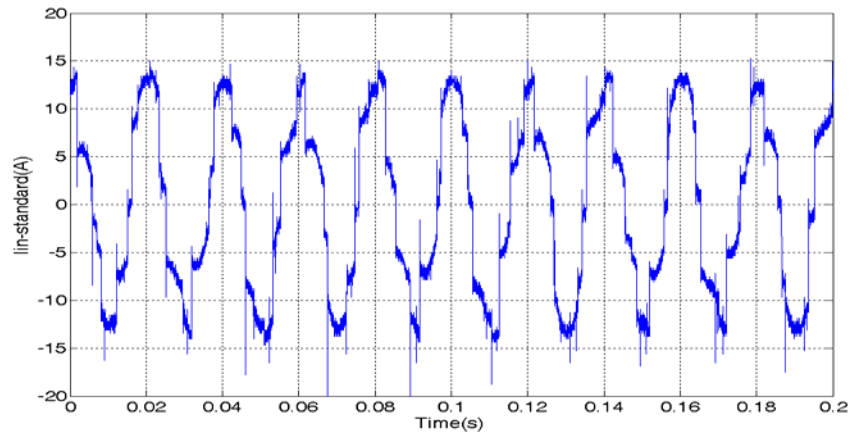
Fig. 6.39: Input current waveform of the three-phase to three-phase standard cycloconverter prototype in CCM
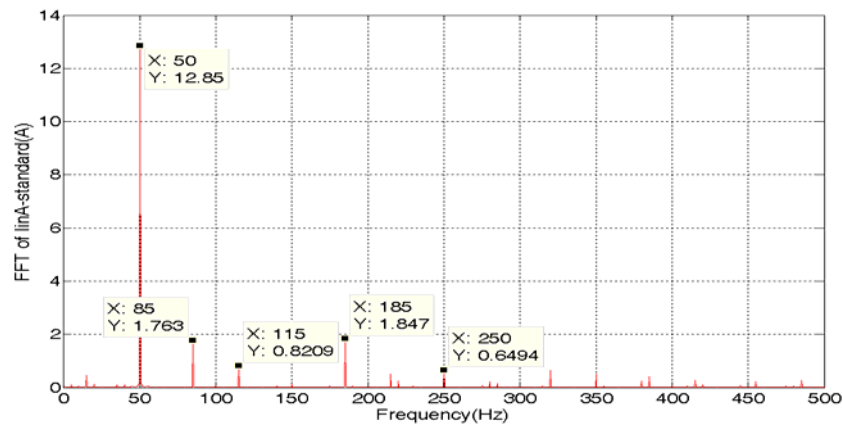
Fig. 6.40: Spectrum of the input current of the three-phase to three-phase standard cycloconverter prototype in CCM

The input current waveform and its spectrum for the hybrid cycloconverter prototype in circulating current mode are shown in Fig. 6.41 and Fig. 6.42 respectively. Compared with the standard cycloconverter, the fundamental component of the input current is reduced from $12.85A_{pk}$ to $11.18A_{pk}$, as shown in Fig. 6.42. Therefore, in conjunction with the results displayed in Table. 6.3, the experimental results further validate that in circulating current mode the hybrid cycloconverter is able to improve the input displacement power factor (from 0.309 to 0.395) by drawing less reactive power from the input side compared with the standard cycloconverter. As mentioned in Chapter 4, this achievement is all owed to the successfully control of the circulating current around a given DC reference, although a better achievement may be obtained by further improving the circulating current without considering the compensation of the output voltage. The input current quality of the hybrid cycloconverter prototype

remains similar to that of the standard cycloconverter prototype due to the similar input power harmonics. This similarity is also verified by comparing the significant input current harmonics (inter-harmonics and sub-harmonics) of the standard and the hybrid prototype, as shown in Table. 6.1, where the amplitudes of most of the frequency components are similar to each other; also the distortion power factors or the total harmonics distortion factors displayed in Table. 6.3 show that the value corresponding to the standard and the hybrid cycloconverter prototypes are very similar to each other. Therefore, by taking both the displacement power factor and the distortion power factor into consideration, it can be concluded that the hybrid cycloconverter prototype in circulating current mode is able to improve the input power factor through the achievement of a better displacement power factor.
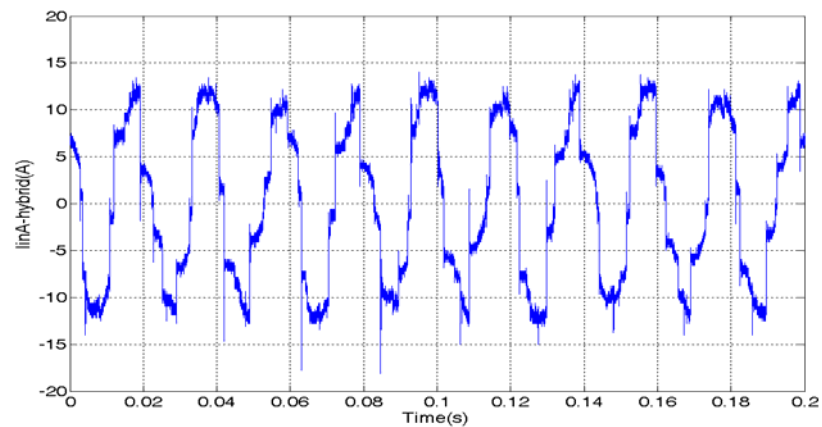
Fig. 6.41: Input current waveform of the three-phase to three-phase hybrid cycloconverter prototype in CCM
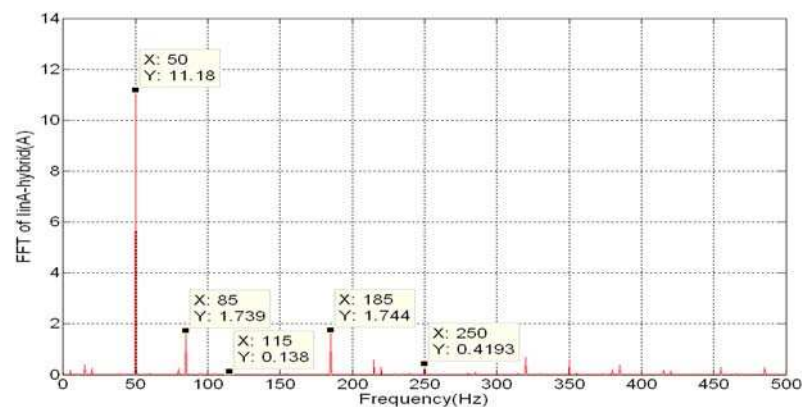
Fig. 6.42: Spectrum of the input current of the three-phase to three-phase hybrid cycloconverter prototype in CCM

	85Hz	115Hz	185Hz	250Hz
Standard	1.76A$_{pk}$	0.82A$_{pk}$	1.84A$_{pk}$	0.64A$_{pk}$
Hybrid	1.73A$_{pk}$	0.13A$_{pk}$	1.74A$_{pk}$	0.41A$_{pk}$

Table. 6.1: Comparison of the amplitudes of significant harmonics present in the input current for both the standard and hybrid cycloconverter prototype in CCM

Fig. 6.43 and 6.44 show the input current waveform and its spectrum of the standard cycloconverter prototype in circulating current-free mode. Without any circulating current, the cycloconverter draws only 8.7A$_{pk}$ fundamental input current, which is less than the two situations above. Therefore, the cycloconverter in circulating current-free mode is able to obtain a better input displacement power factor than that of the cycloconverter in circulating current mode, as summarized in Table. 6.3.
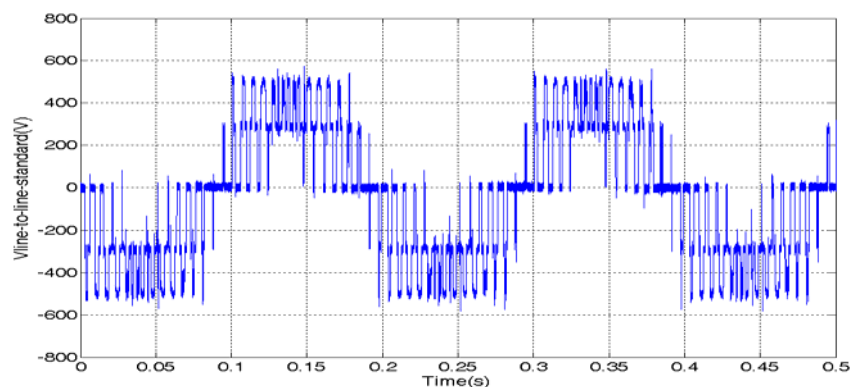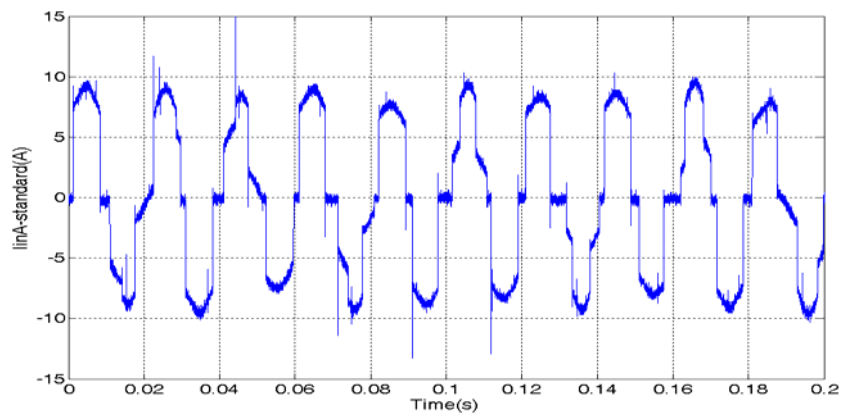

Fig. 6.43: Input current waveform of the three-phase to three-phase standard cycloconverter prototype in CCFM
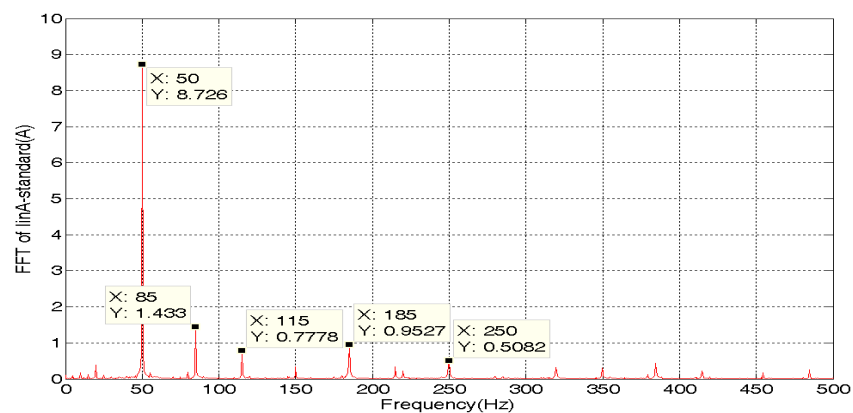
Fig. 6.44: Spectrum of the input current of the three-phase to three-phase standard cycloconverter prototype in CCFM

Fig. 6.45 and Fig. 6.46 show the waveform and its corresponding spectrum of the input current in hybrid cycloconverter operating in circulating current-free mode. Similar to the circulating current mode, with almost the same harmonics in the input power, the amplitudes of all the significant harmonics present in the input current are not much different from those in the standard cycloconverter, as summarized in Table. 6.2. This is also verified by the distortion power factors (or THD) shown in Table. 6.3, where the values in corresponding to both the standard and the hybrid topology are very close to each other. As shown in Table. 6.3, the displacement power factor that corresponds to the hybrid cycloconverter topology in circulating current-free mode is also very similar to that of the standard cycloconverter in circulating current-free mode.
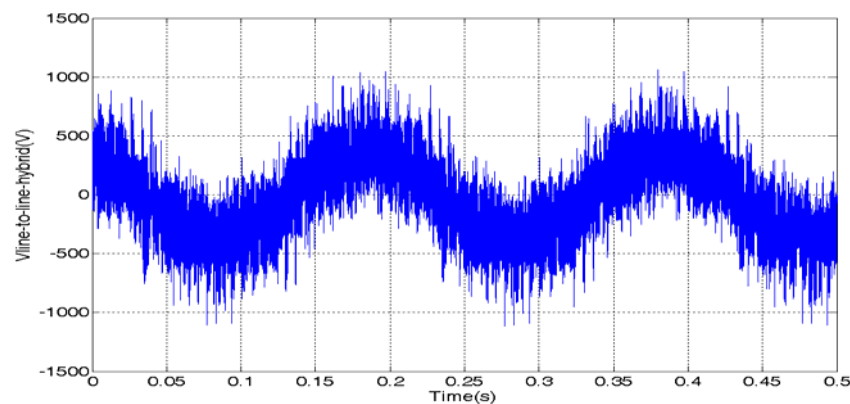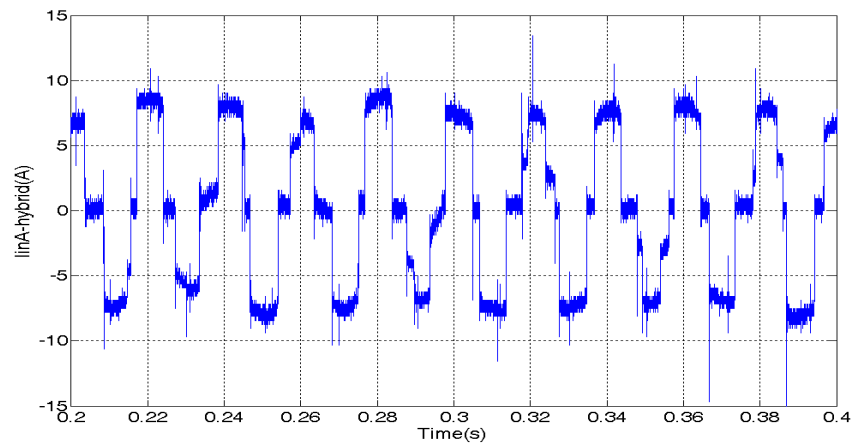

Fig. 6.45: Input current waveform of the three-phase to three-phase hybrid cycloconverter prototype in CCFM
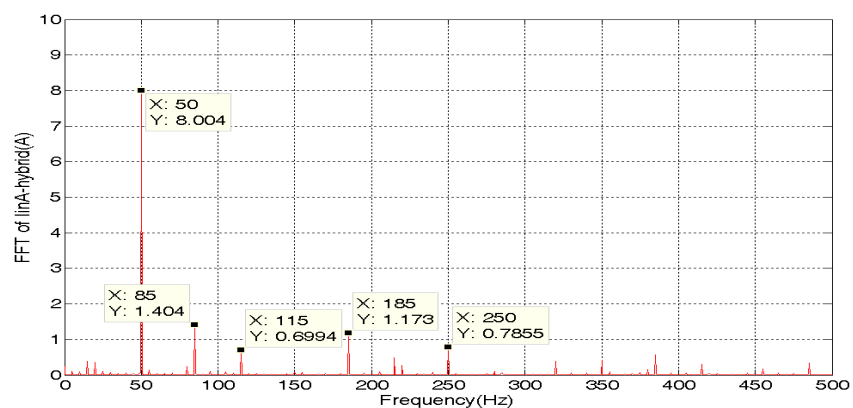

Fig. 6.46: Spectrum of the input current of the three-phase to three-phase hybrid cycloconverter prototype in CCFM

	85Hz	115Hz	185Hz	250Hz
Standard	$1.43A_{pk}$	$0.77A_{pk}$	$0.95A_{pk}$	$0.50A_{pk}$
Hybrid	$1.40A_{pk}$	$0.69A_{pk}$	$1.17A_{pk}$	$0.78A_{pk}$

Table. 6.2: Comparison of the amplitudes of significant harmonics present in the input current for both the standard and hybrid cycloconverter prototype in CCFM

From the above comparisons of the input current for the different topologies considered, it can be concluded that similar to the results obtained from the simulation, more input current is drawn by the standard cycloconverter prototype in circulating current mode than any other topology. This is as a result of more current circulating and this fact can also lead to a worse input displacement power factor. The input distortion factor remains more or less the same for all the topologies due to the similarities in the harmonic profile of the input power. Therefore, similar to the conclusions drawn for the simulation results, it is confirmed that the cycloconverter prototypes without circulating current are able to obtain the best input power factor.

Operating Mode	Topology	DPF	DF	THD	PF
CCM	**Standard**	0.309	0.9654	0.2703	0.298
	Hybrid	0.395	0.963	0.280	0.380
CCFM	**Standard**	0.490	0.954	0.314	0.467
	Hybrid	0.502	0.945	0.346	0.474

Table. 6.3: A summary of input side evaluation for both the standard and hybrid cycloconverter prototype in CCM and CCFM

6.5 Summary

In this chapter, the experimental results of both the standard and hybrid cycloconverter prototype in circulating current and circulating current-free mode are presented. By comparing the experimental results presented in this chapter with the corresponding simulation results presented in Chapter 4, it can be concluded that the experimental results match very well with the simulation results. This coincidence not only validates the simulation models developed, but also further verifies the improvement in performance of the hybrid cycloconverter. Table. 6.4 below summarizes the WTHD

of the output voltage (phase-to-supply neutral and line-to-line) generated by different topologies. According to this table, the hybrid cycloconverters are able to obtain the best performance in both operating modes.

Operating Mode	Topology	Output Voltage Types	WTHD (%)	Performance
CCM	Thyristor Bridge	Phase-to-supply neutral	3.64	Worst
		Line-to-line	N/A	
	Standard Cycloconverter	Phase-to-supply neutral	2.18	Better
		Line-to-line	1.74	
	Hybrid Cycloconverter	Phase-to-supply neutral	0.82	Best
		Line-to-line	0.61	
CCFM	Standard Cycloconverter	Ph-to-neutral	4.34	Worst
		Line-to-line	3.19	
	Hybrid Cycloconverter	Phase-to-supply neutral	0.73	Best
		Line-to-line	0.56	

Table. 6.4: WTHD comparison between output voltages in different topologies

Chapter 7

Conclusions

Up to now, forced commutated semiconductors such as the IGBT, BJT and MOSFET, have generally only be applied in the medium and low voltage and current range. Therefore, as has been discussed at the beginning of this thesis, the line-commutated cycloconverter, which is a direct AC-AC converter, is hard to replace with any other type of converter in the high voltage and high current region due to the high kVA of the semiconductors – thyristors - used in the circuit. Although the GTOs or IGCTs can be used to consist forced-commutated cycloconverters with higher output frequency, their applications are still limited compared to the line-commutated cycloconverter in the high power region. This is because the power capacity of GTOs or IGCTs is still relatively lower than the thyristors. However, the line-commutated cycloconverter also has some major deficiencies which limit its application. Although it is possible to reduce the impact of the disadvantages of the cycloconverter by increasing the number of pulses, this is often achieved at the expense of increasing the complexity of the whole circuit as a result of using more semiconductors and a bulky input transformer. Hence, the work presented in this thesis was intended to first investigate the performance of the existing topologies of cycloconverter and then to investigate a new method of improving the cycloconverter performance without significantly increasing the size of the converter.

Since there are two operating modes for the cycloconverter – circulating current mode and circulating current-free mode, there are two corresponding types of topologies, as introduced in Chapter 2. These two topologies are mainly distinguished by the need for a circulating current reactor to be connected between the positive and negative thyristor half bridges to limit the circulating current. Therefore, one of the major advantages of the circulating current-free mode is that it is a less bulky circuit, although, compared with the circulating current mode, a more demanding control is

needed to ensure the safe commutation between the two thyrsitor half bridges when the load current changes polarity. Another advantage of the circulating current-free mode is that it has a better input power factor, since unlike the circulating current mode, no circulating current is needed by the circuit that demands a large amount of reactive power from the supply. On the other hand, the advantage of the circulating current mode is that, since the output voltage is generated at the mid-point of the circulating current reactors, the anti-phase harmonics that appear at certain frequencies generated by the two thyristor half bridges will reduce/cancel each other at the mid-point and this will produce a better output waveform than that of the circulating current-free mode.

In this research, the concept of a new hybrid cycloconverter, as has been presented in Chapter 3, is proposed to improve the performance of the standard cycloconverter. To validate the feasibility of the hybrid cycloconverter approach, the new cycloconverter topologies operating in both the circulating current and circulating current-free mode have been modelled in SABER. In order to verify the improved performance of the new approach, the hybrid cycloconverter has been experimentally evaluated by building a laboratory prototype. The new topologies consist of a 3-pulse (or 6-pulse in CCM) standard cycloconverter and an auxiliary inverter (two-leg H-bridge inverter or three-leg bridge inverter). The two-leg H-bridge inverter is composed of two diodes and two IGBTs whilst the three-leg bridge inverter is composed of two diodes and four IGBTs (two of the IGBTs have the anti-parallel diode built in). Therefore, by properly controlling these IGBTs in a high switching frequency range, the auxiliary inverter can be used like an active filter to improve the output performance of the cycloconverter. In this project, the three-leg bridge inverter is the chosen topology for the auxiliary inverter for both the implementation of the computer simulation model and the prototyped system in the lab. Furthermore, by modifying the control method, this auxiliary inverter can be applied not only to improve the performance of the circulating current-free mode but also the circulating current mode.

In the circulating current-free mode, the auxiliary inverter is just connected between the common point of the thyristor half bridges and the load. The auxiliary inverter in this mode can generate a high frequency PWM voltage by employing a common mode voltage reference, which is the difference between the output voltage of the thyristor

half bridges and the output voltage reference. Therefore, the low frequency distortions present in the output voltage of the thyristor bridge can be drastically reduced or even completely eliminated following the injection of this high frequency PWM voltage using the auxiliary inverter. In this way, as has already been proved by both the simulation and experimental results presented in Chapter 4 and Chapter 6, the output voltage waveform of the hybrid cycloconverter can achieve a much better quality than that of the standard cycloconverter although it has been proved that the input power quality remains more or less the same even with a better output performance.

In the circulating current mode, the auxiliary inverter is connected between the two outputs of the positive and negative thyristor half bridges which means that each of the asymmetrical legs of the auxiliary inverter is connected with one of the thyristor half bridge outputs through one branch of the circulating current reactor. The output of the hybrid cycloconverter is connected to the mid-point of the third leg of the auxiliary inverter. The function of the auxiliary inverter in this mode is not only to improve the common mode voltage (output voltage) waveform by reducing/cancelling its low frequency distortions, but also to regulate the circulating current to a given DC reference. This is achieved by reducing the low frequency harmonics present in the differential mode voltage that can also lead to the reduction of the circulating current reactors size. Therefore, the auxiliary inverter will have two references, which are the differential mode voltage reference and the common mode voltage reference, for generating a high frequency PWM voltage. Furthermore, each switching period of the auxiliary inverter has to be divided into two parts which are used to handle the control of the differential mode voltage and the common mode voltage injected by the auxiliary inverter respectively. Some compromise needs to be made to ensure that the improvement on both control objectives are acceptable, as has been demonstrated in the results produced by both the simulation models and the experimental prototype. According to the results, the input power quality can also be improved in this operating mode due to the reduced level of the circulating current.

Both the simulation and the experimental results have indicated that the performance of the cycloconverter can obviously be enhanced by the hybrid cycloconverter solution compared to their standard cycloconverter counterparts. Compared with the method of improving the output side performance by increasing the number of pulses

of the thyristor bridge as shown in the last section of Chapter 4, the hybrid cycloconverter has been shown to require fewer semiconductors as well as reduced voltage rating for the auxiliary inverter's power devices due to a much lower DC-link capacitor voltage. Although increasing the number of pulses is considered as the most effective way to improve the input quality of the cycloconverter as described in Chapter 4, the hybrid solution is also helpful to achieving better input power factor. This is because the input displacement power factor in circulating current mode can be improved after the introduction of the hybrid solution since there is less reactive power drawn from the supply when accurate control of the circulating current is achieved. By considering the electrical performance in conjunction with the cost and the complexity of the control requirements as presented in Chapter 4 and Chapter 6, it can be concluded that, compared with all the other possible cycloconverter topologies, the 3-pulse hybrid cycloconverter in circulating current-free mode is the one which has the potential to achieve the best overall performance.

This PhD thesis on the new hybrid approach is a step forward towards better solutions to eliminate the deficiencies of the cycloconverter and broaden its range of applications.

7.1 Future Work

Although the concept of the hybrid cycloconverter has been shown to be able to achieve better performance than the standard cycloconverter, there is still work to be done to further improve the converter performance.

Firstly, if only the improvement of the line-to-line output voltage of the cycloconverter is taken into consideration, the auxiliary inverter does not have to compensate for the common mode harmonics present in all the phase-to-supply neutral output voltages. Therefore, the DC-link capacitor voltage may be further reduced that can lead to a lower semiconductor rated voltage. The control methods discussed in the thesis can also be further modified to make sure that an even smaller DC-link capacitor voltage in the auxiliary inverter is able to achieve the same improving effect of the line-to-line output voltage. This feature could be helpful to

further reduce the size and the cost of the auxiliary converter.

Secondly, instead of connecting the auxiliary inverter after the thyristor bridge, the inverter can also be connected between the input power supply and the thyristor bridge. In this way, the auxiliary inverter will have the function of improving the input current directly. Up to now, increasing the number of pulses is still the only most effective way to improve the input performance as explained in Chapter 4. However, it is worth seeing if the auxiliary inverter is able to achieve the same or even better improvement than increasing number of pulses.

Thirdly, a 6-pulse or even 12-pulse hybrid cycloconverter can be developed in the lab to get more relevant results if an alternative strategy needs to be considered by taking all the factors into consideration, especially the performance at the input side. Although the 3-pulse hybrid approach has already achieved great improvements particularly at the output side, there is still much to be improved on the input side. Furthermore, when the number of pulses is increased, it is possible to get better performance with a smaller and lower power rating auxiliary inverter.

Finally, this research would be more complete by taking the factors of both the efficiency and the EMC (electromagnetic compatibility) into consideration, especially when any further experimental hybrid cycloconverter prototype is built. Although the hybrid solution may be able to reduce winding loss of the circulating current reactors due to the accurately control of the circulating current, more switching loss and core loss may be generated due to the added auxiliary inverter operating in high switching frequency. For the same reason, the hybrid cycloconverter may generate much higher emissions, which is different from the standard counterpart which is normally used for low speed application. Therefore, if these two factors are concerned, it would be helpful to enhance the whole performance assessment of the hybrid cycloconverter and broaden its industrial interest after.

References:

[1]   B.R. Pelly, "Thyristor Phase-Controlled Converters and Cycloconverters", *Wiley Interscience,* 1971.

[2]   N.Moham, T.M.Undeland and W.P.Robbins (Wiley), "Power Electronics: Converters, Application and Design(3rd)"，*John Wiley & Sons, Inc.*

[3]   J. Murphy, F.G. Turnbull, "Power Electronic Control of AC Motors", *Franklin Book Co,* 1988.

[4]   W. McMurray, "The Theory and Design of Cycloconverters", *Massachusetts Inst. of Tech. Press,* Cambridge, MA, 1972.

[5]   G. Möltgen, "Line Commutated Thyristor Converters", *Pitman, London, 1972.*

[6]   D.C. Griffith, R.M. Ulmer, "A semiconductor variable-speed AC motor drive", *Electr. Eng.* (New York), 80, May 1961, pp. 350-353.

[7]   R.Heck, M. Meyer, "A static-frequency-changer-fed squirrel-cage motor drive for variable speed and reversing", *Siemens Rev.,* 30, Nov. 1963, pp. 401-405.

[8]   J.C. Guyeska, H.E. Jordan, "Static AC variable frequency drive", *Proc. IEEE Nat. Electron. Conf.,* 20, 1964, pp. 358-365.

[9]   P. Bowler, "The application of a cycloconverter to the control of induction motors", *IEE Conf. Publ. No. 17, Power Applications of Controllable Semiconductor Devices,* 1965, pp. 137 -145.

[10] W. Slabiak, L.J. Lawson, "Precise control of a three-phase squirrel-cage induction motor using a practical cycloconverter", *IEEE Trans. Ind. Gen. Appl.,* IGA-2, 4, July/Aug. 1966, pp. 274 -280.

[11] R. A. Hamilton, G.R. Lezan, "Thyristor adjustable frequency power supplies for hot strip mill run-out tables", *IEEE Trans. Ind. Appl.,* IGA-3, 2, Mar./Apr. 1967, pp. 168-175.

[12] H. Stemmler, "Drive systems and electronic control equipment of the gearless tube mill", *Brown Boveri Rev.,* 57, 3, Mar. 1970, pp. 121 -129.

[13] T. Maeno, M. Kobata, "AC commutatorless and brushless motor", *IEEE Trans. Power Appar. Syst.,* PAS – 91, 4, July/Aug. 1972, pp. 1476 -1484.

[14] L. Terens, J. Bommeli, K. Peters, "The cycloconverter-fed synchronous motor",*Brown Boveri Rev.,* 69, 4/5, Apr./May 1982, pp. 122 -132.

[15] K. Sugi, Y. Naito, R. Kurosawa, Y. Kano, S. Katayama, T. Yoshida, "A microcomputer-based high capacity cycloconverter drive for main rolling mill", *Int. Power Electron. Conf.,* Tokyo. 1983, pp. 744 – 755.

[16] R. Hagmann, "AC-cycloconverter drives for cold and hot rolling mill applications", *IEEE Proc. of IAS'91,* Vol.2, pp. 1134-1140, 1991.

[17] J. Trautner and A. Wick, "DC Link converter and cyclo-converter-fed AC motors: The concepts and properties of large variable-speed drives," *Siemens Rev. (Energy&Automation -Issue on Large Electric Motor&VSD),* vol. 1, pp. 16–31, 1988.

[18] J.R. Rodriguez, J.Pontt, P. Newman, R. Musalem, H. Miranda, L.Moran, "Technical Evaluation and Practical Experience of High-power Grinding Mill Drives in Mining Applications", *IEEE Trans. on Ind. App.,* Vol. 41, No. 3, pp. 866-874, 2005.

[19] L. Terens, J. Bommeli, K. Peters, "The cycloconverter fed synchronous motor", *Brown Boveri Rev.,* pp. 122-132, Apr/May 1982.

[20] T. Nakano, H. Ohsawa, K. Endoh, "A high performance cycloconverter-fed

synchronous machine drive system", *IEEE Trans. Ind. Appl.,* Vol. IA-20, no. 5, pp. 1278-1284, Sep./Oct. 1984.

[21] W.A. Hill, R.A. Turton, R.J. Duncan and C.L. Schwalm, "A vector-controlled cycloconverter drive for an icebreaker", *IEEE Trans. Ind. Appl.,* Vol. IA-23, no. 6, pp. 1036-1042, 1987.

[22] R. Hagmann, "AC-cycloconverter drives for cold and hot rolling mill applications", *IEEE IAS Conf.*, 1991, pp. 1134-1140. Vol. 2.

[23] Y. Tamura, S. Tanaka, S. Tadakuma, "Control method and upper limit of output frequency in circulating-current type cycloconverter", *IEEE Int. Semicond. Power Converter Conf.,* 1982, pp, 313-323.

[24] P. Syam, P.K. Nandi, A.K. Chattopadhyay, "Effect of output current ripple on the input supply current and the power quality for a cycloconverter-fed drive", *Proc. IEE Part-B, EPA*, Vol.151, No. 04, pp.425-433, July 2004.

[25] R. Chu, J. Burns, "Impacts of cycloconverter harmonics", *IEEE Trans. On Ind. Appl.,* Vol. 25, Nr. 3, May/June, 1989, pp. 427-435.

[26] H. Hosada, S. Tatara, R. Kurosawa, H. Hakata and K. Doi, "A high-performance cross-current type cycloconverter fed induction motor drive system", *IEEE Trans, Ind. Appl.,* Vol. IA-24, No. 3, pp. 479-486, May/June 1988.

[27] R. Ueda, T. Sonoda, T. Mochizuki, S. Takata, "Stabilization of bank selection in no circulating cycloconverter by means of reliable current-zero and current-polarity detection", *Conf. Rec. IEEE Ind. Appl. Soc. Annual Meeting,* 1982, pp. 651-656.

[28] P.Syam, P.K. Nandi, A.K. Chattopadhyay, "Improvement in power quality and a simple method of subharmonic suppression for a cycloconverter-fed synchronous motor drive," *Proc. Inst. Electr. Eng. – Electr. Power Appl.,* vol. 149, no. 4, pp. 292-303, Jul. 2002. *Trans, Ind. Appl.,* Vol. IA-24, No. 3, pp. 479-486, May/June

1988.

[29] C.J. Amato, "Sub-ripple distortion components in practical cycloconverters", *IEEE Trans. Aerosp. (Suppl.),* AS-3, June 1965, pp. 98 -106.

[30] F.C. Ronnie, J.J. Burns, "Impact of cycloconverter harmonics", *IEEE Transactions on Industrial Application*, Vol. 25. No. 3. May/June, 1989.

[31] R. Balasubramanyam, V.I. John, J.P. Tamby, "Harmonic performance of cycloconverter synchronous motor marine propulsion systems", *IEEE,* 1993, 496 – 502.

[32] Z.Wang, Y. Liu, "Modeling and simulation of a cycloconverter drive system for harmonic studies", *IEEE Transactions on Industrial Electronics*, Vol. 47, No. 3, June 2000.

[33] J. Pontt, J. Rodriguez, J. San Martin, R. Aguilera, J. Rebolledo, E. Caceres, I. Illanes, P. Newman, "Interharmonic currents assessment in high-power cycloconverter-fed drives", *37th IEEE Power Electronics Specialists Conference,* June 18 – 22, 2006, Jeju, Korea.

[34] M. Meyer, G. Möltgen, "Kreisströme bei Umkehrstromrichtern", *Siemens-Z.,* 37, 5, May 1963, pp. 375-379.

[35] R.A. Vaneck, "Frequency changer systems using the cycloconverter principle", *IEEE Trans. Appl. and Ind.,* 82, May 1963, pp. 163-168.

[36] G.P. Hunter, "Low Cost Cycloconverter Induction Motor Drives using New Modulation Techniques", *PhD thesis,* University of Technology, Sydney, 2007.

[37] B.M. Bird and J.S. Ford, "Improvements in phase-controlled circulating-current cycloconverter using communication principles", *IEE Proc.,* Vol. 121, No. 10, pp. 1146-1149, 1974.

[38] L. Gyugyi, B.R. Pelly, "Static power frequency changers", *Wiley-Interscience,* 1976.

[39] G.P. Smith(now Hunter), "Line commutated frequency changers for speed control of electrical machines", *Masters thesis*, University of Technology, Sydney, 1983.

[40] L. Gyugyi, J. Rosa, B.R.Pelly, "Novel integral firing angle control for converters", *U.S. Patent,* No. 3,585,485, 1971.

[41] E.J. Stacey, R.D. Jessee, "Method and apparatus for stabilized integral control of static power frequency changers", *U.S. Patent*, No. 4,307,444, 1981.

[42] M. Nakano, Y. Matsuo, "Output feedback-type firing control scheme for phase-controlled devices", *Elect. Eng. in Japan,* Vol. 103B, No. 4, pp. 259-266, April, 1983.

[43] G.P. Hunter, V. Ramsden, "A mill motor inching drive using a three pulse cycloconverter with double integral phase control", *Power Electronics Drives and Energy Systems for Industrial Growth,* Dec 1-3, 1998, Vol. 1, pp. 447-451.

[44] T.M. Hamblin, T.H. Barton, "Cycloconverter control circuits", *IEEE Trans,* Ind. Appl., Vol. IA-8, No. 4, pp. 443-453, July/Aug. 1972.

[45] S. Valiviita, "Zero-crossing detection of distorted line voltages using 1-b measurements", *IEEE Trans on Industrial Electronics,* Vol. 46, No. 5, Oct. 1999.

[46] L. Juby, R. Bucknall, N.A. Haines, "A harmonic reduction technique for cycloconverter propulsion drives", *Electrical Machine and Drives Conference,* 11-13 Sep 1995, IEE Conf. Pub. No. 412. pp. 333-337.

[47] D. Basic, V.S. Ramsden, P. Muttik, P.T. Griffiths, W.H. Zhu, "Harmonic compensation of high-power cycloconverter drives", *12th Conference on the Electronic Power Supply Industry,* Nov 1998, Pattaya, Thailand, pp. 48-56.

[48] D. Basic, V.S. Ramsden, P. Muttik, "Performance of combined power filters in harmonic compensation of high-power cycloconverter drives", *7th IEE Power Electronics and Variable Speed Drives Conference,* PEVSD'98, London, Sep.1998. pp. 674-679.

[49] D.Basic, V.S. Ramsden, P. Muttik, "Hybrid filter control system with adaptive filters for selective elimination of harmonics and interharmonics", *IEE Proceeding-Electric Power Application,* in press.

[50] S. Bhattacharya, D. Divan, "Synchronous frame based controller implementation for a hybrid series active filter", *30th IEEE Industry Applications Conference IAS'95, Oct. 1995,* Vol. 3, pp. 2531-2540.

[51] T. Nakajima, E. Masada, Y. Ogihara, "Compensation of the cycloconverter input current harmonics using active power filter", *2nd European Conference on Power Electronics and Applications,* EPE'87, 1987, pp. 1227-1232.

[52] C. Klumpner, T. Xu, J. Clare, "A New Hybrid Cycloconverter with Smooth Output Voltage Generation Capability and Accurate Control of the Circulating Current", *IEEE Proc. of IECON,* pp. 2291-2296, 2006.

[53] T. Xu, C. Klumpner, J. Clare, "Hybrid Cycloconverters: An Exploration of Benefits", *Proc. of EPE 2007,* paper #479, 2007.

[54] C. Klumpner, T. Xu, J. Clare, "Experimental Evaluation of Hybrid Cycloconverters", *APEC,* Session. 19, pp. 196-700.

[55] C. Klumpner, T. Wijekoon, P. Wheeler, "A New Hybrid AC/AC Power Converter", *IEEE Proc of IAS'05,* Vol. 4, pp. 2374-2381, 2005.

[56] L. Dixon, "Average current mode control of switching power supplies", *Unitrode Application Note*, U-140,
http://www.ti.com/sc/docs/psheets/abstract/apps/slua079.htm

[57] V. Benda, D.A. Grant, J. Gowar, "Power Semiconductor Devices: Theory and Application", *John Wiley & Sons,* 1999.

[58] B.J. Baliga, "Power Semiconductor Devices", *PWS Pub. Co.; 1ˢᵗ edition,* 1995.

[59] Netz-Thyristor-Module, "Phase Control Thyristor-Modules MCC Series", http://www.datasheet.in/datasheet-html/M/C/C/MCC90-xx_ABBSemiconductors .pdf.html

[60] IXYS, "Datasheet of IXDR30N120 – High Voltage IGBT with optional Diode ISOPLUS package", http://pdf1.alldatasheet.com/datasheet-pdf/view/97957/IXYS/IXDR30N120.html

[61] IXYS, "Datasheet of IXDR35N120D1 – NPT3 IGBT with Diode", http://pdf1.alldatasheet.com/datasheet-pdf/view/102222/IXYS/IXER35N120D1. html

[62] IXYS, "Datasheet of DSEP30-12AR – HiperFREDTM Epitaxial Diode with soft revovery", http://pdf1.alldatasheet.com/datasheet-pdf/view/142321/IXYS/DSEP30-12AR.ht ml

[63] C.Wm.T. Mclyman, "Transformer and inductor design handbook", 416 pages, ISBN: 08247-7828-6, *Marcel Dekker Inc.*, New York, USA, 1988.

[64] Honneywell Metglas, "Power factor correction – Inductor design for switched mode power supplies using metglas powerlite C-cores", http://www.metglas.com/downloads/apps/pfc.pdf, N/A

[65] D.L. Liliana, "A matrix converter drive system for an aircraft rudder electro-mechanical actuator", *PhD thesis,* University of Nottingham, Nottingham, 2006.

Nomenclature

V_{inA}	phase A input power supply
V_{inB}	phase B input power supply
V_{inC}	phase C input power supply
$V_{in\text{-}line}$	line-to-line input voltage
V_{N_pk}	peak value of the input phase-to-supply neutral voltage
V_{o_ref}	reference for the output voltage of the standard or the hybrid cycloconverter
V_{max}	average output voltage of cycloconverter with zero firing delay
$V_{o\_ref\_pk}$	peak value of the reference for the output voltage
V_{THY1_ref}	reference for the output voltage of the positive thyristor half bridge
V_{THY1}, $V_{out\text{-}thy1}$	output voltage of the positive thyristor half bridge in CCM
V_{THY2_ref}	reference for the output voltage of the negative thyristor half bridge
V_{THY2}, $V_{out\text{-}thy2}$	output voltage of the negative thyristor half bridge in CCM
V_{THY}	output voltage of the standard cycloconverter in CCFM
V_{diff}	differential mode voltage between the positive and negative thyristor half bridge
V_{diff_pk}	peak value of the differential mode voltage between the positive and negative thyristor half bridge
$V_{out(\text{-}standard)}$	output voltage of the standard cycloconverter (or common mode voltage of the positive and negative thyristor half bridges in CCM)
V_o, $V_{out\text{-}hybrid}$	output voltage of the hybrid cycloconverter
$V_{line\text{-}to\text{-}line\ \text{-}standard\ (\text{-}hybrid)}$	line-to-line output voltage of a three-phase output cycloconverter
V_{cap_ref}	the DC-link capacitor voltage reference

V_{cap1}	upper DC-link capacitor voltage of the two-leg H-bridge inverter
V_{cap2}	lower DC-link capacitor voltage of the two-leg H-bridge inverter
V_{cap}	DC-link capacitor voltage of the three-leg bridge inverter
V_c	DC-link capacitor voltage in the auxiliary inverter
V_{HC}	output of the DC-link capacitor voltage controller
V_{cir}	Output of the circulating current PI controller
V_{DM}	differential mode voltage reference of the auxiliary inverter
V_{CM}	common mode voltage reference of the auxiliary inverter
V_{HB1_ref}	reference for the voltage between one of two asymmetric legs in the auxiliary inverter and the output of the hybrid cycloconverter
V_{HB2_ref}	reference for the voltage between the other one of two asymmetric legs in the auxiliary inverter and the output of hybrid cycloconverter
V_S	the peak to peak voltage of the PWM oscillator
V_s	the voltage source applied to the stator of the induction machine
V_{hb1}, V_{hb2}	The voltage between one of two asymmetric legs in the auxiliary inverter and the output of the hybrid cycloconverter in CCM
V_{hb}	The voltage between one asymmetric leg in the auxiliary inverter and the output of the hybrid cycloconverter in CCFM
V_O	output voltage of the boost converter
i_A	input current of single-phase output cycloconverter
$I_{inA(-standard\ -hybrid)}$	input current of a three-phase output cycloconverter
I_{THY1}	current across one of the coupled circulating current reactor
I_{THY2}	current across the other one of the coupled circulating current reactor
I_{rms}	maximum rms value of the current flowing through the windings
I_{Load}	load current of the hybrid cycloconverter
$I_{out-standard,\ (-hybrid)}$	load current of the standard or hybrid cycloconverter

$I_{a,b,c\text{-}standard,}$ $_{(\text{-}hybrid)}$	load currents of a three-phase to three-phase cycloconverter
I_{o_pk}	peak value of the load current
I_{cir_ref}	circulating current reference in hybrid cycloconverter
$I_{cir(\text{-}standard,}$ $_{\text{-}hybrid)}$	circulating current of the cycloconverter
$I_{cir\text{-}pk}$	peak value of the circulating current
ΔI_{cir}	circulating current ripple
I_{thy_h}	thyristor's holding (or latching) current
I_f, I_h	fundamental and harmonic components of the stator current
P_{thy}	installed power of the thyristor bridge
P_{inv}	installed power of the auxiliary inverter
L_{cir1}	inductance of one of the coupled circulating current reactor
L_{cir2}	inductance of the other one of the coupled circulating current reactor
L_{cir}	the value of a single circulating current reactor
L_{Load}	inductance of the load
L_s, L_r	leakage inductance of the stator and rotor
L_o	magnetizing inductance of the motor
M	mutual inductance of the two coupled circulating current reactors
$C1$	upper DC-link capacitor of the two-leg H-bridge inverter
$C2$	lower DC-link capacitor of the two-leg H-bridge inverter
C	DC-link capacitor of the three-leg bridge inverter
C_{FZ}, C_{FP}	the value of capacitors in the circulating current PI controller
C_D	the value of capacitors in the DC-link capacitor voltage controller
R_{Load}	resistance of the load
R_{CCR}	resistance of the circulating current reactor

R_S	sense resistance of the circulating current
R_F, R_I	the value of resistors in the circulating current PI controller
R_D	the value of resistor in the DC-link capacitor voltage controller
R_s, R_r	stator and rotor resistance
f_{in}	input supply frequency
f_{out}	output load frequency
f_S	switching frequency of the auxiliary inverter
f_H, f_{H1}, f_{H2}, f_{H3}	harmonic frequencies
f_{ch}	characteristic cycloconverter harmonics of the input current
α	firing delay angle for the thyristor in cycloconverter
α_{THY1}	firing delay angle for the thyristor in the positive thyristor bridge
α_{THY2}	firing delay angle for the thyristor in the negative thyristor bridge
D_{zero}	duty cycle of the zero state of the auxiliary inverter
D_{active}	duty cycle of the active state of the auxiliary inverter
D_+	duty cycle in which the output voltage of the hybrid cycloconverter is generated by adding the DC-link capacitor voltage to the output voltage of the standard cycloconverter
D_-	duty cycle in which the output voltage of the hybrid cycloconverter is generated by subtracting the DC-link capacitor voltage from output voltage of the standard cycloconverter
D_0	duty cycle in which the DC-link capacitor voltage is bypassed between the output of the hybrid cycloconverter and output of the standard cycloconverter
D_{Q}, D_{Q4}, D_{Q5}, D_{Q6}	Duty cycle of the firing pulses for IGBTs in the auxiliary inverter
K_d	voltage transfer ratio for the differential mode voltage feedforward compensation
K_c	voltage ratio between the fundamental output voltage of the standard cycloconverter and its reference

$K_{P\text{-}CCPI}$	proportional gain of the circulating current PI-controller
$K_{I\text{-}CCPI}$	integral gain of the circulating current PI-controller
$K_{I\text{-}DCPI}$	integral gain of the DC-link voltage PI-controller
θ_i	$2\pi f_{in}t$
θ_o	$2\pi f_{out}t$
r	output to input modulation index
r_{kVA}	the relative kVA of the auxiliary inverter to that of the thyristor bridge
n_{thy}	number of the thyristors in a thyristor bridge
n_{IGBT}	number of the IGBTs in the auxiliary inverter
s_f, s_h	slip at the fundamental frequency and harmonic frequency
ω_{diff}	frequency of the differential mode voltage
Φ_o	load displacement angle
M	coupling coefficient of the CCR
E_{tot}	total energy stored in the whole circulating current reactor
k_{window}	filling factor of the core window
j_{co}	current density of the core
B_{max}	saturation magnetic flux of the circulating current reactor
A_p	core area product
A_c	product of core cross section
W_a	window area
l_m	magnetic path length of the core
μ	permeability
N_{tot}	total turns of the whole circulating current reactor
l_g	airgap
F	the amount of fringing flux

d_{co}	diameter of the copper conductor
G_{CA_max}	the maximum current amplifier gain
PI_{k-1}	output of the PI controller in previous switching period
PI_k	output of the PI controller in current switching period
$error_{k-1}$	error of the PI controller in previous switching period
$error_k$	error of the PI controller in current switching period

Appendix A

Papers Publised

C. Klumpner, T. Xu, J. Clare, "A New Hybrid Cycloconverter with Smooth Output Voltage Generation Capability and Accurate Control of the Circulating Current", *IEEE Proc. of IECON'06 (THE 32th Annual Conference of the IEEE Industrial Electronics Society),* pp. 2291-2296, 2006.

T. Xu, C. Klumpner, J. Clare, "Hybrid Cycloconverters: An Exploration of Benefits", *Proc. of EPE 2007 (12th European Conference on Power Electronics an Applications),* paper #479, 2007.

C. Klumpner, T. Xu, J. Clare, "Experimental Evaluation of Hybrid Cycloconverters", *APEC'09 (The Applied Power Electronics Conference and Exposition),* Session. 19, pp. 196-700 (on CD-ROM).

Appendix B

Derivation of Input Current General Equations

In this appendix, the input current harmonic equation is derived for a single-phase, 3-pulse cycloconverter in circulating current-free mode.

According to the [pp.331, 1], the input current of a single-phase, 3-pulse cycloconverter in circulating current-free mode can be expressed as:

$$
\begin{aligned}
i_A = I_{o\_pk} \sin(\theta_i + \phi_0) \{ \frac{1}{3} + \frac{\sqrt{3}}{\pi} [\sin\theta_i \sin f(\theta_o) + \frac{1}{2}\cos 2\theta_i \cos 2 f(\theta_o) - \frac{1}{4}\cos 4\theta_i \cos 4 f(\theta_o) \\
- \frac{1}{5}\sin 5\theta_i \sin 5 f(\theta_o) + \frac{1}{7}\sin 7\theta_i \sin 7 f(\theta_o) \cdots] + \frac{4\sqrt{3}}{\pi^2}[-\cos\theta_i \cos f(\theta_o) - \frac{1}{2}\sin 2\theta_i \sin 2 f(\theta_o) \\
+ \frac{1}{4}\sin 4\theta_i \sin 4 f(\theta_o) + \frac{1}{5}\cos 5\theta_i \cos 5 f(\theta_o) - \frac{1}{7}\cos 7\theta_i \cos 7 f(\theta_o) \cdots] \times [\sin(\theta_o + \phi_0) + \frac{1}{3}\sin 3(\theta_o + \phi_0) \\
+ \frac{1}{5}\sin 5(\theta_o + \phi_0) + \frac{1}{7}\sin 7(\theta_o + \phi_0) \cdots] \}
\end{aligned}
$$

(B.1)

According to Equation (2.10), the firing angle phase modulating function is represented mathematically by:

$$ f(\theta_o) = \sin^{-1} r \sin\theta_o $$

(B.2)

If Equation (B.2) is substituted into Equation (B.1), the equation for the input current in circulating current-free mode can be derived. As the equation after the substitution of $f(\theta_o)$ is extremely complicated, the equation presented here is the one which assumes $r = 1.0$ and $\Phi_o = 90°$, the full equation can be found in [pp.334, 1].

$$i_A = \frac{-\sqrt{3}I_{o\_pk}}{2\pi}\cos\theta_i + \frac{1}{3}I_{o\_pk}\cos\theta_o + \frac{\sqrt{3}I_{o\_pk}}{2\pi}\{-\cos(\theta_i + 2\theta_o) + \frac{1}{2}[\cos(2\theta_i + \theta_o) + \cos(2\theta_i + 3\theta_o)]$$

$$-\frac{1}{4}[\cos(4\theta_i + 3\theta_o) + \cos(4\theta_i + 5\theta_o)] + \frac{1}{5}[\cos(5\theta_i + 4\theta_o) + \cos(5\theta_i + 6\theta_o)]$$

$$-\frac{1}{7}[\cos(7\theta_i + 6\theta_o) + \cos(7\theta_i + 8\theta_o)] \cdots\}$$

$$(B.3)$$

Where i_A is the input current; I_{o_pk} is the peak value of the load current;

$$i_A = \frac{-\sqrt{3}I_{o\_pk}}{2\pi}\cos\theta_i + \frac{1}{3}I_{o\_pk}\cos\theta_o + \frac{\sqrt{3}I_{o\_pk}}{2\pi}\{-\cos(\theta_i + 2\theta_o) + \frac{1}{2}[\cos(2\theta_i + \theta_o) + \cos(2\theta_i + 3\theta_o)]$$

$$-\frac{1}{4}[\cos(4\theta_i + 3\theta_o) + \cos(4\theta_i + 5\theta_o)] + \frac{1}{5}[\cos(5\theta_i + 4\theta_o) + \cos(5\theta_i + 6\theta_o)]$$

Appendix C

Switching States Analysis of the Auxiliary Inverters

V_{diff}	I_{Load}	Duty		$Q2$	$Q4$	C1	C2	Output Voltage(V_o)
1	1	D_{active}		0	0	Charge(I_{cir}, I_{Load})	Charge(I_{cir})	$V_o = (V_{THY1} + V_{THY2})/2$
1	1	D_{zero}	D_-	0	1	Charge(I_{Load})	constant	$V_o = (V_{THY1} + V_{THY2})/2 - V_c$
1	1		D_+	1	0	constant	Discharge(I_{Load})	$V_o = (V_{THY1} + V_{THY2})/2 + V_c$
1	0	D_{active}		0	0	Charge(I_{cir})	Charge(Icir, I_{Load})	$V_o = (V_{THY1} + V_{THY2})/2$
1	0	D_{zero}	D_-	0	1	Discharge(I_{Load})	constant	$V_o = (V_{THY1} + V_{THY2})/2 - V_c$
1	0		D_+	1	0	constant	Charge(I_{Load})	$V_o = (V_{THY1} + V_{THY2})/2 + V_c$
0	1	D_{active}		1	1	Discharge(I_{cir})	Discharge(I_{cir}, I_{Load})	$V_o = (V_{THY1} + V_{THY2})/2$
0	1	D_{zero}	D_-	0	1	Charge(I_{Load})	constant	$V_o = (V_{THY1} + V_{THY2})/2 - V_c$
0	1		D_+	1	0	constant	Discharge(I_{Load})	$V_o = (V_{THY1} + V_{THY2})/2 + V_c$
0	0	D_{active}		1	1	Discharge(I_{cir}, I_{Load})	Discharge(I_{cir})	$V_o = (V_{THY1} + V_{THY2})/2$
0	0	D_{zero}	D_-	0	1	Discharge(I_{Load})	constant	$V_o = (V_{THY1} + V_{THY2})/2 - V_c$
0	0		D_+	1	0	constant	Charge(I_{Load})	$V_o = (V_{THY1} + V_{THY2})/2 + V_c$

Table C.1: The switching states for two-leg H-bridge inverter in CCM

I_{Load}	Duty		Q2	Q4	C1	C2	Output Voltage(V_o)
1	D_{zero}	D_-	0	0	Charge(I_{Load})	constant	$V_o = V_{THY} - V_c$
1		D_+	1	0	constant	Discharge(I_{Load})	$V_o = V_{THY} + V_c$
0		D_-	0	1	Discharge(I_{Load})	constant	$V_o = V_{THY} - V_c$
0		D_+	0	0	constant	Charge(I_{Load})	$V_o = V_{THY} + V_c$

Table C.2: The switching states for two-leg H-bridge inverter in CCFM

V_{CM}	V_{diff}	I_{Load}	Duty		Q2	Q4	Q5	Q6	C	Output Voltage(V_o)
1	1	1	D_{active}		0	0	1	0	Charge(I_{cir})	$V_o =(V_{THY1}+V_{THY2})/2+V_c/2$
1	1	1	D_{zero}	D_-	0	1	0	0	Charge(I_{Load})	$V_o = (V_{THY1}+ V_{THY2})/2- V_c$
1	1	1		D_0	1	0	0	0	Constant	$V_o = (V_{THY1}+ V_{THY2})/2$
0	1	1	D_{active}		0	0	1	0	Charge(I_{cir})	$V_o =(V_{THY1}+V_{THY2})/2+V_c/2$
0	1	1	D_{zero}	D_+	1	0	1	0	Discharge(I_{Load})	$V_o = (V_{THY1}+ V_{THY2})/2+ V_c$
0	1	1		D_0	1	0	0	0	Constant	$V_o = (V_{THY1}+ V_{THY2})/2$
1	1	0	D_{active}		0	0	0	1	Charge(I_{cir})	$V_o =(V_{THY1}+ V_{THY2})/2-V_c/2$
1	1	0	D_{zero}	D_-	0	1	0	1	Discharge(I_{Load})	$V_o = (V_{THY1}+ V_{THY2})/2- V_c$
1	1	0		D_0	0	1	0	0	Constant	$V_o = (V_{THY1}+ V_{THY2})/2$
0	1	0	D_{active}		0	0	0	1	Charge(I_{cir})	$V_o =(V_{THY1}+ V_{THY2})/2-V_c/2$

									State	V_o
0	1	0	D_{zero}	D_+	1	0	0	0	Charge(I_{Load})	$V_o = (V_{THY1}+ V_{THY2})/2+ V_c$
0	1	0		D_0	0	1	0	0	Constant	$V_o = (V_{THY1}+ V_{THY2})/2$
1	0	1	D_{active}		1	1	0	0	Discharge(I_{cir})	$V_o =(V_{THY1}+ V_{THY2})/2-V_c/2$
1	0	1	D_{zero}	D_-	0	1	0	0	Charge(I_{Load})	$V_o = (V_{THY1}+ V_{THY2})/2- V_c$
1	0	1		D_0	1	0	0	0	Constant	$V_o = (V_{THY1}+ V_{THY2})/2$
0	0	1	D_{active}		1	1	0	0	Discharge(I_{cir})	$V_o =(V_{THY1}+ V_{THY2})/2-V_c/2$
0	0	1	D_{zero}	D_+	1	0	1	0	Discharge(I_{Load})	$V_o = (V_{THY1}+ V_{THY2})/2+ V_c$
0	0	1		D_0	1	0	0	0	Constant	$V_o = (V_{THY1}+ V_{THY2})/2$
1	0	0	D_{active}		1	1	0	0	Discharge(I_{cir})	$V_o =(V_{THY1}+V_{THY2})/2+V_c/2$
1	0	0	D_{zero}	D_-	0	1	0	1	Discharge(I_{Load})	$V_o = (V_{THY1}+ V_{THY2})/2- V_c$
1	0	0		D_0	0	1	0	0	Constant	$V_o = (V_{THY1}+ V_{THY2})/2$
0	0	0	D_{active}		1	1	0	0	Discharge(I_{cir})	$V_o =(V_{THY1}+V_{THY2})/2+V_c/2$
0	0	0	D_{zero}	D_+	1	0	0	0	Charge(I_{Load})	$V_o = (V_{THY1}+ V_{THY2})/2+ V_c$
0	0	0		D_0	0	1	0	0	Constant	$V_o = (V_{THY1}+ V_{THY2})/2$

Table C.3: The switching states for three-leg bridge inverter in CCM

V_{CM}	V_{diff}	I_{Load}	Duty		Q2	Q4	Q5	Q6	C	Output Voltage(V_o)
1	1	1	D_{zero}	D_-	0	0	0	0	Charge(I_{Load})	$V_o = V_{THY} - V_c$
1	1	1		D_0	1	0	0	0	constant	$V_o = V_{THY}$
0	0	1	D_{zero}	D_+	1	0	1	0	Discharge(I_{Load})	$V_o = V_{THY} + V_c$
0	0	1		D_0	1	0	0	0	constant	$V_o = V_{THY}$
1	1	0	D_{zero}	D_-	0	1	0	1	Discharge(I_{Load})	$V_o = V_{THY} - V_c$
1	1	0		D_0	0	1	0	0	constant	$V_o = V_{THY}$
0	0	0	D_{zero}	D_+	0	0	0	0	Charge(I_{Load})	$V_o = V_{THY} + V_c$
0	0	0		D_0	0	1	0	0	constant	$V_o = V_{THY}$

Table C.4: The switching states for three-leg bridge inverter in CCFM

Appendix D

Circuit Diagrams of the Simulated Standard and Hybrid Cycloconverter Saber Models

In this appendix, the circuit diagrams of the standard and hybrid cycloconverters operating in both the circulating current mode and the circulating current-free mode that have been implemented in the simulation software, SABER, are presented.

In every schematic, all the circuits and functional blocks have been marked. The red colored words and lines have been used to designate the power stage whilst the blue colored words and lines ware used for control stage. The annotation of some circuits or blocks will appear only once if these circuits or blocks are common for the rest and have been used more than one time in the following figures. An example is the "positive thyristor half bridge" and "negative thyristor half bridge" which appear first and being marked accordingly only in Fig. D.1 and Fig. D.2; later they have been merged as "Thyristor bridge" in Fig. D.3 and Fig. D.4, although they are describing the same circuit.

In these schematics, all the devices and control blocks are obtained from the SABER parts gallery, except the thyristor bridge firing pulse generator, the bridge selection block and the PWM generator for the auxiliary inverter IGBTs, which are all written in MAST modelling language.
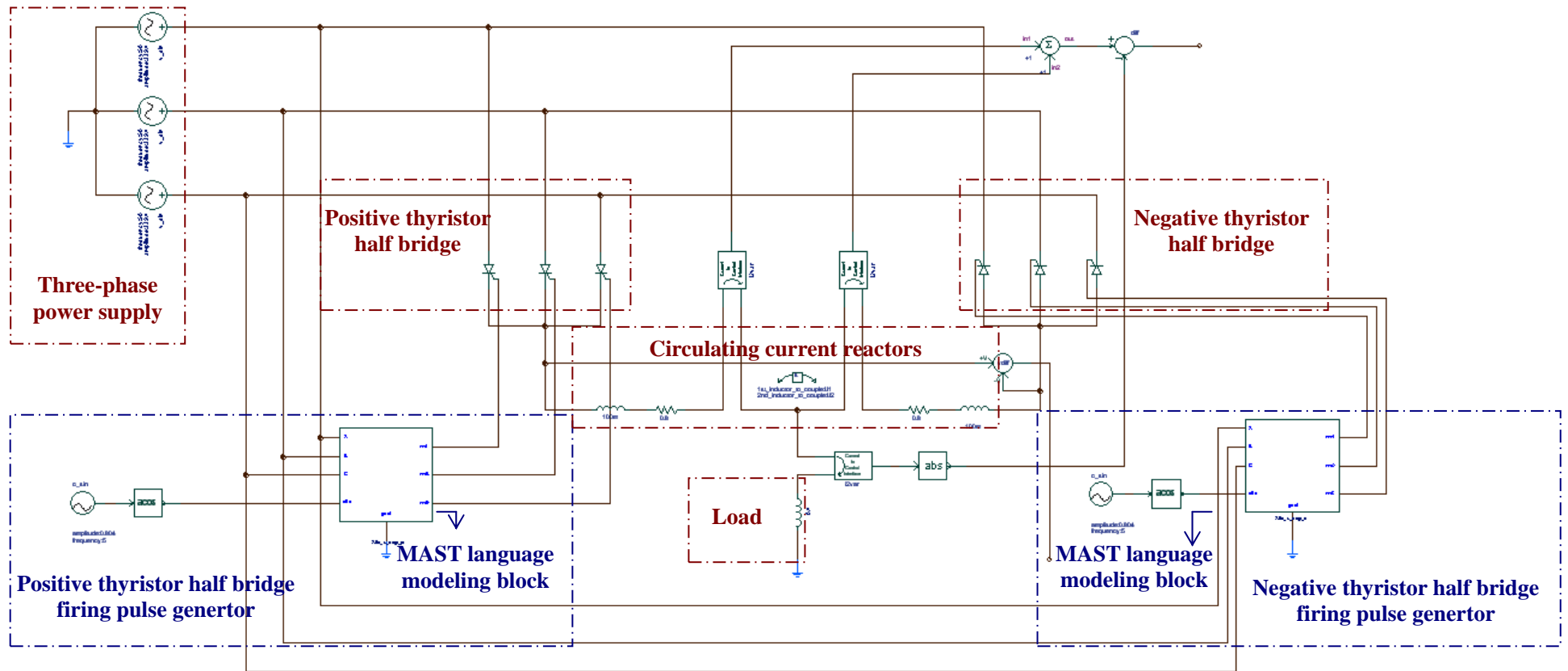
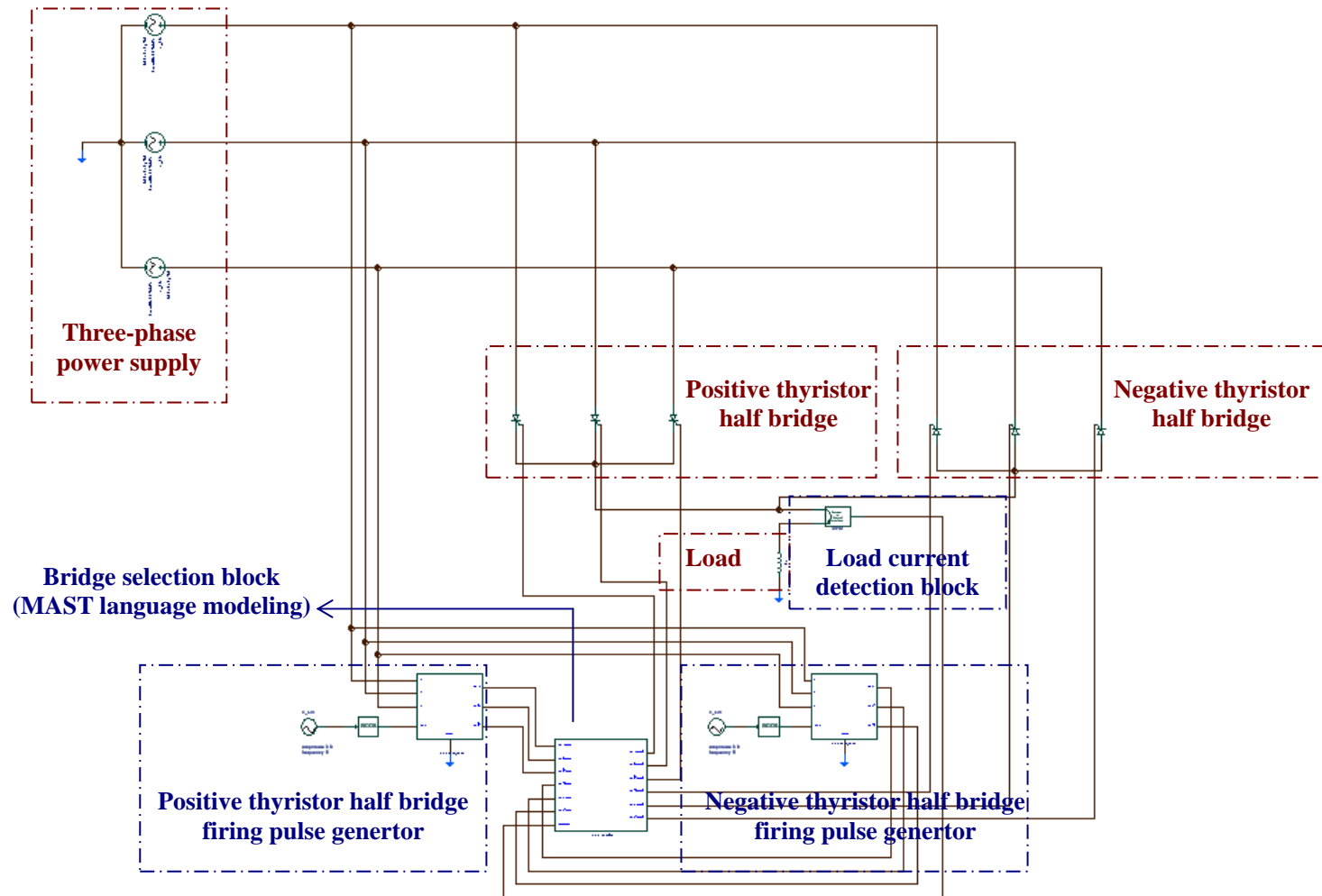Fig. D.1: Simulation circuit of the standard cycloconverter in CCM

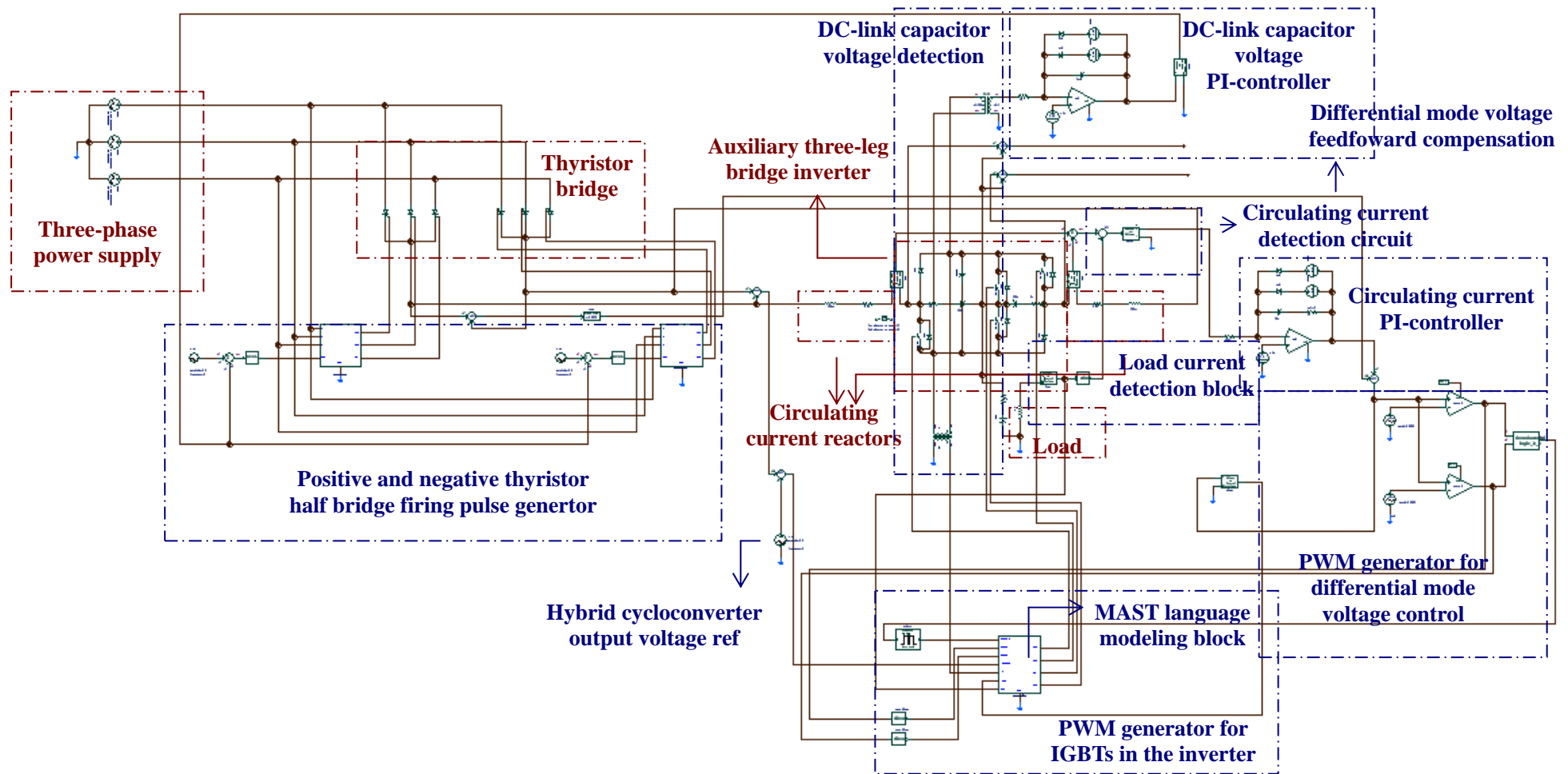Fig. D.2: Simulation circuit of the standard cycloconverter in CCFM

Fig. D.3: Simulation circuit of the hybrid cycloconverter in CCM
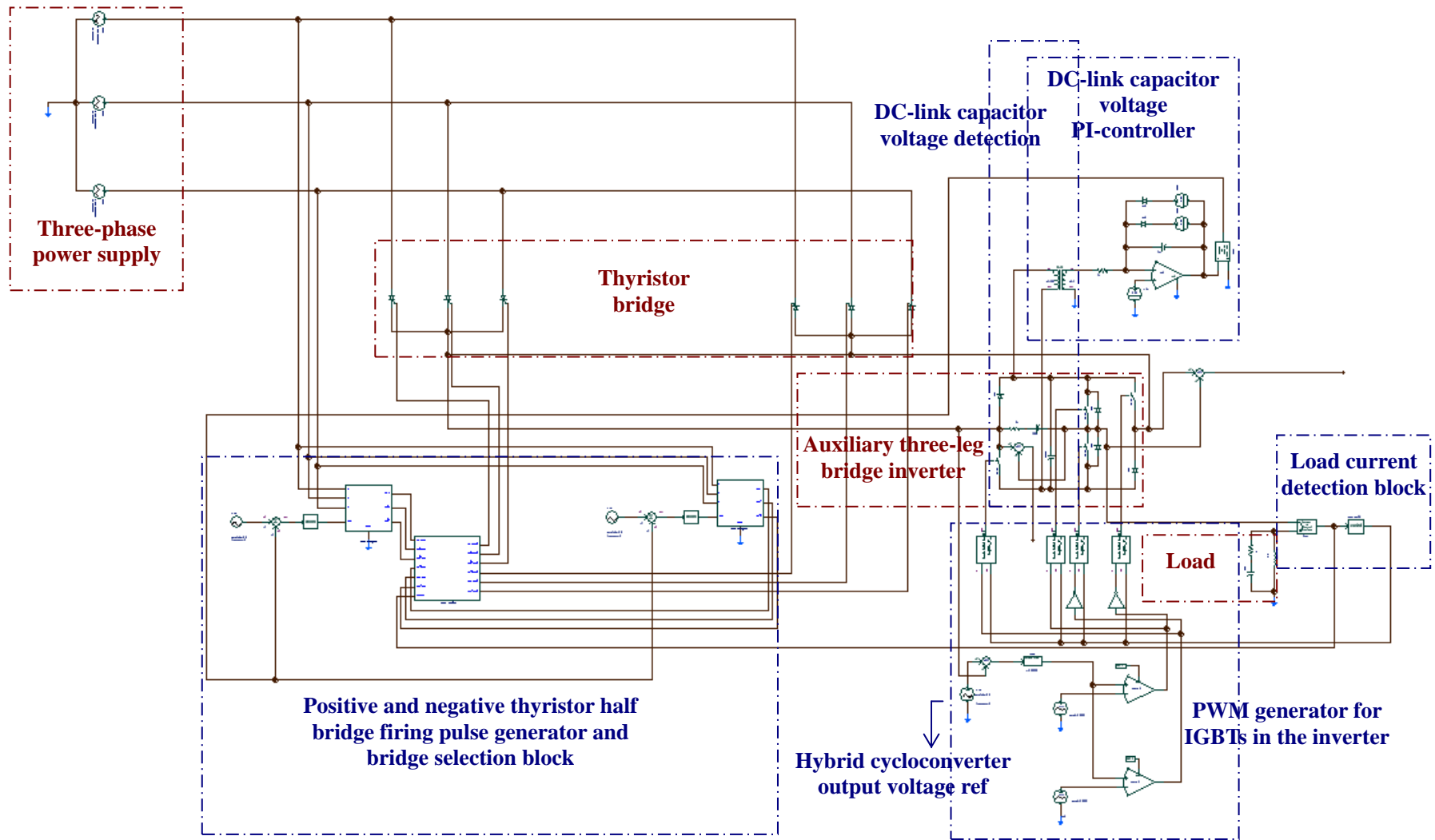
Fig. D.4: Simulation circuit of the hybrid cycloconverter in CCFM

Appendix E

Theoretical FFT of the Output Voltage and Input Current in Standard Cycloconverter

According to equation 2.6 or 2.8, when the modulation index r is 1.0, the amplitude of the fundamental output voltage is:

$$V_{max} = \frac{3\sqrt{3} \cdot V_{N\_pk}}{2\pi} = \frac{3\sqrt{3} \cdot 339.4}{2\pi} = 280.8V \qquad (E.1)$$

The load displacement angle Φ_o can also be calculated with the load parameters given in Table. 4.1:

$$\phi_o = tg^{-1} \frac{2\pi \cdot f_{out} \cdot L_{load}}{R_{load}} = tg^{-1} \frac{6.28 \cdot 5 \cdot 0.4}{20} = 32° \approx 30° \qquad (E.2)$$

Therefore, according to the harmonic analysis in Chapter 2 and the Table.11.3 – 11.6 in [pp.318-322, 1], the frequencies in the output voltage harmonics and their corresponding amplitude can be calculated for the simulation model and the experimental work with the parameters defined in Table. 4.2. In order to compare them, the significant harmonics frequency and their corresponding amplitude are displayed as the figures obtained in simulation and experiment. The theoretical FFT of the output voltage in circulating current mode and circulating current-free mode are shown in Fig. E.1 and E.2 respectively.

The theoretical FFT of the cumulated input current in circulating current-free mode, as shown in Fig. E.3, is generated according to the Table. 12.1 – 12.3 in [pp.369-371, 1] and under the assumption of that the peak load current is 10A.
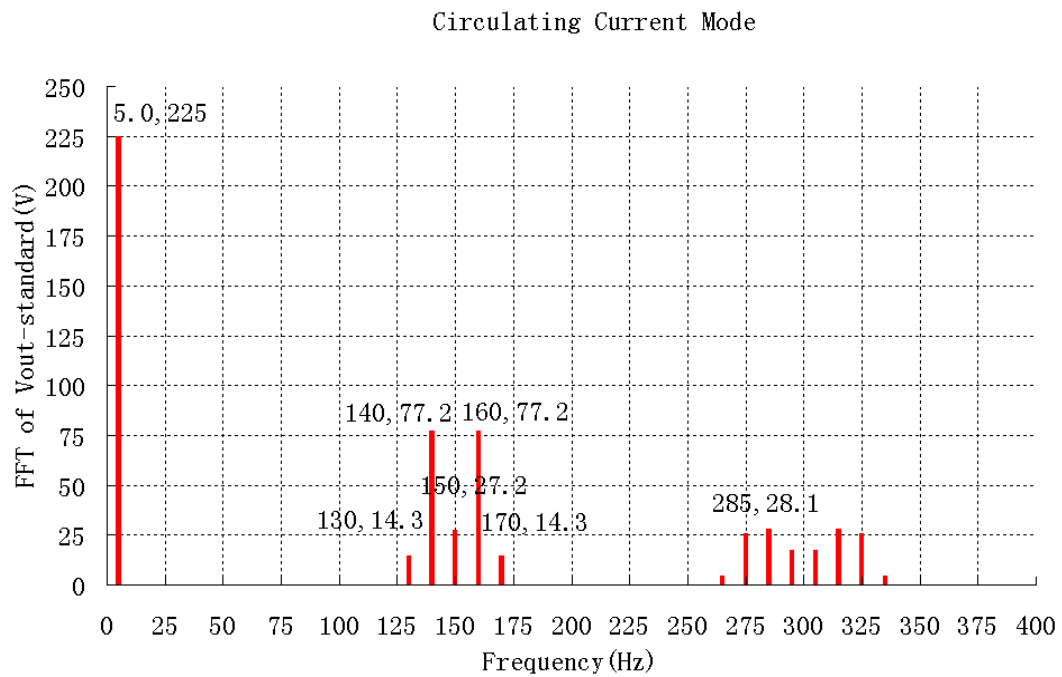
Fig. E.1: Theoretical FFT of the standard cycloconverter output voltage in CCM determined as specified in [pp.322, 1]
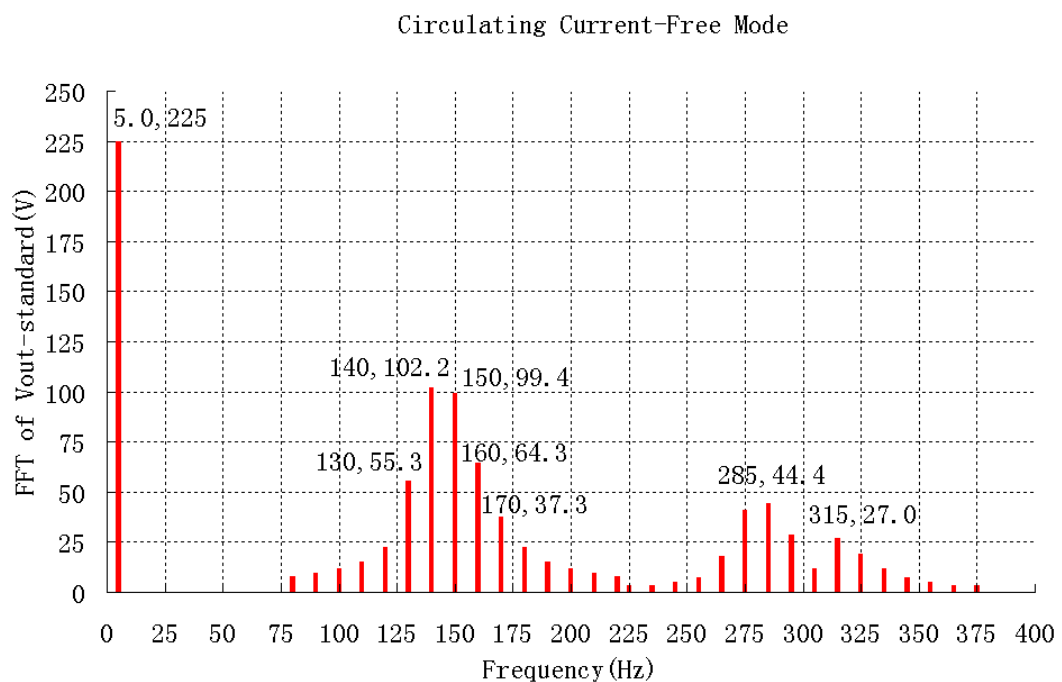

Fig. E.2: Theoretical FFT of the standard cycloconverter output voltage in CCFM determined as specified in [pp.318-320, 1]
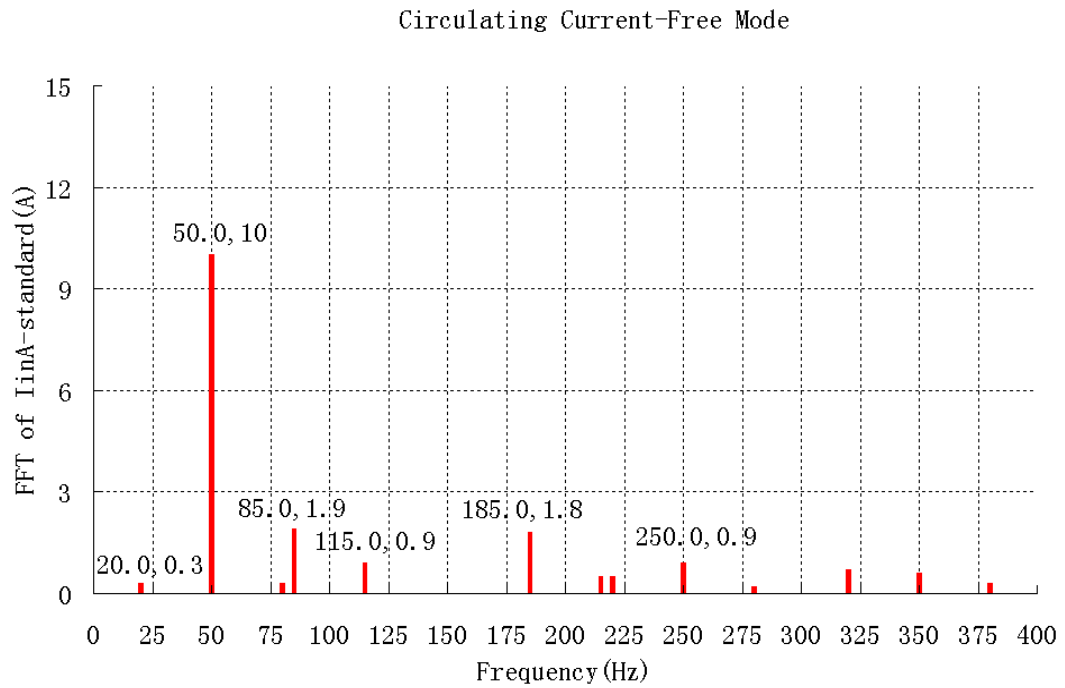
Fig. E.3: Theoretical FFT of the standard cycloconverter input current in CCFM
determined as specified in [pp.369-371, 1]

Appendix F

Circulating Current Inductors Design

The design of the circulating current reactors is based on the design procedure suggested in [57], [58]. The steps of carrying out the inductor design include identifying the technical requirement, select the magnetic core and calculating the windings. All the steps are presented in detail as follows.

First of all, according to the simulation result of the circulating current in the standard cycloconverter (Fig. 4.16) obtained in Chapter 4, the value of this inductance should not be less than 400mH in order to limit the peak value of the circulating current (I_{cir_pk}) at around 5A. If the circulating current reactor is made out of two identical windings coupled together on the same core, the inductance of a single section of the current reactor (L_{cir1} or L_{cir2}) is ideally (coefficient factor is assumed to be 1.0) one quarter of the total inductance.

$$I_{cir\_pk} = 5A \tag{F.1}$$

$$L_{cir1} = L_{cir2} = L_{cir} = 100mH \tag{F.2}$$

Furthermore, some current margin should be allowed to make sure that the circulating current at its minimum level is always higher than the thyristor's holding (or latching) current which has been referred in Table. 5.1. Here, the margin is set at 0.5A.

$$I_{thy\_h} = 0.5A \tag{F.3}$$

Therefore, if it is assumed that the load current is 7Arms, the total energy stored in the circulating current reactors can be calculated according to the Equation (F.5).

$$I_{Load} = 7A \tag{F.4}$$

$$E_{tot} = 0.5 \times 4 \times L_{cir} \times [(\sqrt{2}I_{Load})^2 + 2(I_{cir\_pk} + I_{thy\_h})^2] = 31.7J \tag{F.5}$$

It is usually assumed that the filling factor of the core window k_{window} is 0.4, the current density j_{co} is 500A/cm², and the saturation magnetic flux density B_{max} is 1.4T. Therefore, the core area product A_p can be calculated according to the following equation [64]:

$$A_p = \frac{E_{tot} \times 10^4}{k_{window} \times j_{co} \times B_{max}} = \frac{31.7 \times 10^4}{0.4 \times 500 \times 1.4} = 1132cm^2 \tag{F.6}$$

Since A_p is the product of the core cross section A_c and the window area W_a, if an E+I core is selected, having a geometry shown in Fig. F.1, the A_c and W_a can be expressed as dependences of the dimension "x" of the lamination of the core:

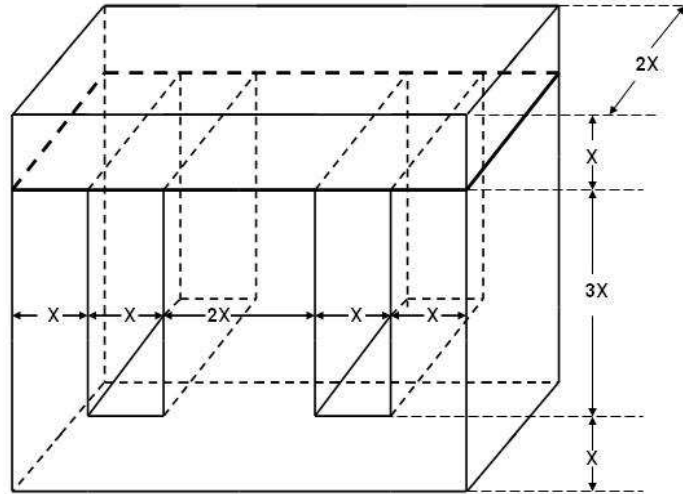$$A_c = 4x^2 \quad \text{and} \quad W_a = 3x^2 \tag{F.7}$$

Fig. F.1: The structure of an EI core

Therefore, A_p and x are:

$$A_p = A_c \times W_a = 12x^4 \tag{F.8}$$

$$x = \sqrt[4]{\frac{A_p}{12}} = 3.12cm \tag{F.9}$$

The value 31.2mm for x indicates that size E32 for the E+I core is large enough to meet the saturation magnetic flux criteria. However, as E32 was not available from the manufacturer, E35 is selected since it is close to the E32.

If an E35 EI core is selected, where x is 3.5cm, the A_p, A_c and W_a will be:

$$A_p = 12x^4 = 1.801 \times 10^3 cm^4 \tag{F.10}$$

$$A_c = 4x^2 = 49cm^2 \quad \text{and} \quad W_a = 3x^2 = 36.75cm^2 \tag{F.11}$$

The magnetic path length of the core is:

$$l_m = 12x = 42cm \tag{F.12}$$

The permeability μ is assumed at 1000:

$$\mu = 1000 \tag{F.13}$$

The total turns of the circulating current reactor is given by the Equation (F.14) [64]:

$$N_{tot} = \frac{L_{cir} \times [(\sqrt{2}I_{Load}) + 2(I_{cir} + \Delta I_{cir})] \times 2 \times 10^4}{B_{max} \times A_c} = 609 \tag{F.14}$$

Therefore, by substituting the Equation (F.11) – (F.14) into the Equation (F.15), the airgap is determined.

$$l_g = \frac{0.4\pi \times N_{tot}^2 \times A_c \times 10^{-8}}{4 \times L_{cir}} - \frac{l_m}{\mu} = 0.53cm \tag{F.15}$$

The amount of fringing flux, *F*, which is estimated through Equation (F.16) [64], will be used to re-calculate the corrected number of turns of the inductor under the required inductance value.

$$F = \frac{(2x + l_g)^2}{4x^2} = 1.157 \tag{F.16}$$

Therefore, the value of corrected turns can be re-calcuated according to Equation (F.17) [64]:

$$N_{tot} = \sqrt{\frac{4L_{cir} \times [l_g + \frac{l_m}{\mu}] \times 10^8}{0.4\pi \times A_c \times F}} = 566 \tag{F.17}$$

From the simulation, the rms current for any one of the two coupled windings is around 6A. However, since the inductors are designed for the worst case which is the standard cycloconverter in circulating current mode, they can also be used as the circulating current reactors for the hybrid cycloconverter or even as the load inductors (large value was necessary due to the low output frequencies typical for cycloconverter) in both the circulating current and circulating current-free mode. After the comparison, the maximum rms value of the current flowing through the windings should be around 7A when the inductors are used as the load. Therefore, the diameter of the copper conductor is determined by:

$$d_{co} \geq \frac{4}{\pi}\sqrt{\frac{I_{rms}}{j_{co}}} = \frac{4}{\pi}\sqrt{\frac{7}{500}} = 1.5mm \tag{F.18}$$

Meanwhile, the total cross section of the windings should not exceed the window area or a core with a higher area product should be used:

$$\frac{N_{tot} \cdot \pi \cdot d_{co}^2}{4} \leq k_{window} \cdot W_a \tag{F.19}$$

Therefore,

$$d_{co} \leq \sqrt{\frac{4 \times k_{window} \times W_a}{N_{tot} \times \pi}} = \sqrt{\frac{4 \times 0.4 \times 3 \times 35^2}{566 \times \pi}} \leq 1.8mm \qquad (F.20)$$